

UC Berkeley

UC Berkeley Electronic Theses and Dissertations

Title

The Development and Application of Homogeneous and Heterogeneous Late Metal Complexes in Catalysis

Permalink

<https://escholarship.org/uc/item/10471465>

Author

Witham, Cole

Publication Date

2010

Peer reviewed|Thesis/dissertation

**The Development and Application of Homogeneous and Heterogeneous Late Metal
Complexes in Catalysis**

by

Cole Austin Witham

A dissertation submitted in partial satisfaction of the

requirements for the degree of

Doctor of Philosophy

in

Chemistry

in the

Graduate Division

of the

University of California, Berkeley

Committee in charge:

Professor F. Dean Toste, Chair
Professor Gabor A. Somorjai
Professor Benito O. de Lumen

Spring 2010

The Development and Application of Homogeneous and Heterogeneous Late Metal

Complexes in Catalysis

© 2010

By Cole Austin Witham

ABSTRACT

The Development and Application of Homogeneous and Heterogeneous Late Metal Complexes in Catalysis

by

Cole Austin Witham

Doctor of Philosophy in Chemistry

University of California, Berkeley

Professor F. Dean Toste, Chair

In recent years, gold(I) complexes have seen increased use as catalysts for the activation of alkynes toward nucleophilic addition. Now, studies show that carbene-like intermediates are accessible, often depending on the substrates and catalyst ligands utilized. While metal carbenoid behavior for gold(I) has been proposed in other transformations, our research has expanded the reactivity of gold beyond simple electrophilic activation, based on evidence that gold can function as both a π -acid and as an electron donor. For instance, electron donation from gold d-orbitals can serve to facilitate the formation of gold carbenoid intermediates after initial cycloisomerization. The gold carbenoid species is then capable of undergoing subsequent reactivity to generate synthetically useful products that can also be further functionalized. Chapter 1 will discuss the development of new gold(I) carbenoid reactivity whereby an oxidation even results in oxygen atom transfer to the carbenoid center to generate carbonyl functional groups. The broad range of reactions for which this methodology can be applied will be discussed as will catalyst and ligand effects for the transformations.

During the course of our investigations into homogeneous gold catalysis, several relevant questions consistently arise. Among them are whether the catalyst can be recovered and recycled, what the cost is of the catalyst, and how load the catalyst loading can be. In order to address these issues, we initiated a research program focused on studying the translation of homogeneous catalytic processes to heterogeneous ones, all in the solution phase. In doing so, we could obtain catalytic activity with heterogeneous catalysts for reactions that were previously only obtained homogeneously. Chapter 2 details our efforts in pursuit of this goal and successes in developing oxidatively modified, electrophilic platinum nanoparticles that display activity for a range of π -bond activation/cyclization reactions. Our characterization studies for the designed nanoparticle system and examination of catalyst activity are presented, as are catalyst leaching investigations. Initial efforts into flow reactors and new dendrimer capping agents are also discussed. The discovery of treatments for nanoparticles that induce the desired homogeneous catalytic activity should lead to the further development of reactions previously inaccessible in heterogeneous catalysis.

The Development and Application of Homogeneous and Heterogeneous Late Metal Complexes in Catalysis

Table of Contents

Chapter 1. *Gold(I)-Catalyzed Oxidative Rearrangements*

Introduction	2
Discovery and Development of Gold(I)-Catalyzed Oxidations	4
Carbene Reactivity with Sulfoxides	16
Extension to Enantioselective Catalysis	27
Conclusion	29
Experimental	31
References	49
Appendix 1: Selected Spectral Data	53
Appendix 2: Data Acquisition Details for X-Ray Crystal Structure of Complex 1.117 .	94

Chapter 2. *Late Metal Nanoparticles in Solution-Phase Heterogeneous Catalysis*

Introduction	106
Design, Synthesis and Development of Platinum Nanoparticle Catalysts	108
Catalyst Activity Studies	112
Reaction Results and Discussion	120
Extension to Palladium and Gold Nanoparticles	125
Leaching Tests	126

EXAFS/XANES Analysis	131
Future Directions: Flow Reactor	136
Future Directions: New Dendrimer Capping Materials	139
Future Directions: Different Reactions and Metals	142
Conclusion	144
Experimental	145
References	170
Appendix: Selected Spectral Data	175

Acknowledgments

I would like to thank my advisor, Professor F. Dean Toste, for all of his excellent guidance and support during my PhD studies. His confidence in me as well as the freedom he gave me to pursue new ideas really allowed me to succeed. I will always be in debt to him for all of the encouragement, direction, more forceful encouragement and for letting me take the lead in creating a new collaboration that resulted in some new chemistry that I can only refer to as the hot sweetness. Thank you Dean! I learned so much new chemistry and developed countless useful skills while in your lab. It was totally worth it and I would definitely do it over again.

I also have to thank Professor Gabor Somorjai, who would become my co-advisor during the second half of my PhD as part of the collaboration. You are awesome. You always had great (and often entertaining) advice and suggestions and were very patient with me as I learned about the chemistry your group does. The way that you are able to quickly get to the root of an issue and address it was really inspirational. I really appreciated your kindness, guidance and gentle prodding. I can't thank you enough.

A massive thanks goes to Wenyu Huang. He was my chief collaborator during the nanoparticle project, and I really thought of us as a tag team. We worked so well together and between the two of us, we could always figure out the answer. Wenyu taught me a lot of the materials/physical chemistry that was important to the project and endured my endless series of "what does that mean?" I honestly couldn't have done it without your help, Wenyu!

I am further appreciative of the help and efforts of all those who worked with me on projects and contributed to the research that would ultimately find its way into publications. Specifically, Pablo Mauleón, Nathan Shapiro, Benjamin Sherry, Frank Tsung, John Kuhn, Jack Liu, Brett Helms, Sirine Fakra and Matthew Marcus. Obviously, I also want to thank all the members of the Toste and Somorjai groups, past and present, that have helped me in some way over the years.

There are also several people I would like to thank who have helped, provided much needed and appreciated guidance, and/or supported me in some way either at Berkeley, Harvey Mudd College or before: Iain Watson, Prof. Thomas Minehan, Prof. Gerald Van Hecke, Prof. Chih-Yung Chen, Prof. Andrew Duncan, Jeanne Noda, Russell Hilst, Gary Hughes, and Tom Gamber. Without all of you, I would never have made it this far. You believed in me, inspired me and helped me to succeed. I will never forget any of you.

Last but not least, thanks to my family. Without you I definitely wouldn't have made it this far. Your support was always there and always appreciated, even after you really stopped understanding what I was doing.

So long, and thanks for all the fish.

Chapter 1

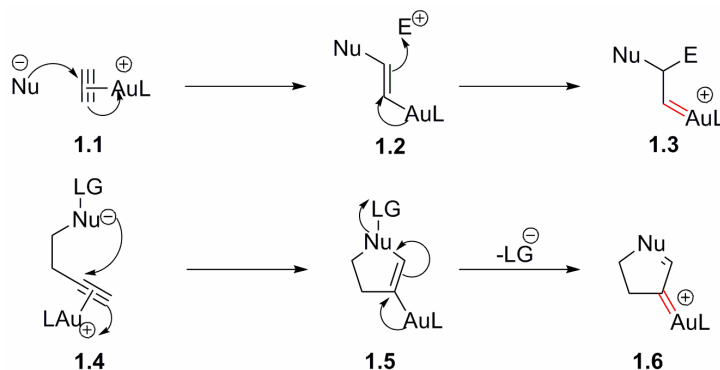
Gold(I)-Catalyzed Oxidative Rearrangements

*Portions of the work in this chapter have been published:
Witham, C. A.; Mauleón, P.; Shapiro, N. D.; Sherry, B. D.; Toste, F. D.
J. Am. Chem. Soc. 2007, 129, 5838.*

Introduction

The field of homogeneous catalysis with gold(I) complexes has rapidly grown in the last decade. Many of these gold(I) catalyzed reactions utilize gold's π -acidity to activate alkynes towards nucleophilic attack.¹⁻⁶ More recently, work in the Toste group and others has extended this reactivity to systems where gold serves as both a π -acid and an electron donor.^{4,7} In this case, a vinyl gold intermediate **1.1** formed by addition of a nucleophile to a gold-activated alkyne can react with an electrophile to generate carbocation **1.3** that is then stabilized by backbonding from gold (Scheme 1.1). This was characterized as “pull-push” reactivity in which gold would both withdraw and donate electron density over the course of a given catalytic cycle. In addition, relativistic effects provided an explanation for this electron donation, as electrons in the gold d-orbitals would be available for backbonding into cationic organic ligands.^{8,9}

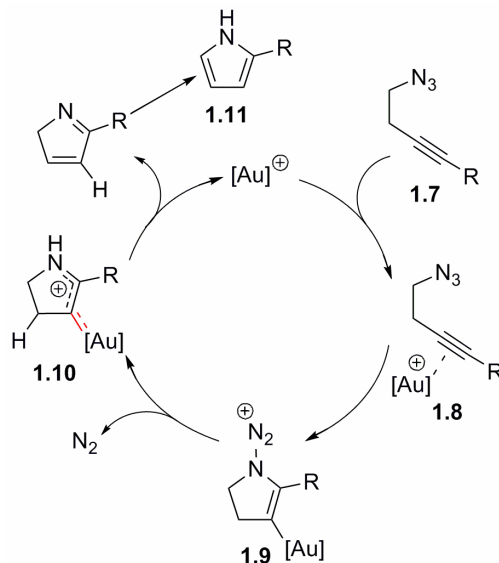
Scheme 1.1. General Reactivity Pattern to Form Gold(I) Carbenoid Species.



This backbonding can also be exploited to generate a gold carbenoid intermediate (Scheme 1.1), and several reports postulate the existence of such intermediates in gold-catalyzed rearrangements.^{2e-g,7,10} For example, if a leaving group-bearing nucleophile, **1.4**, adds to a gold(I) activated alkyne, subsequent loss of the leaving group can afford a cationic gold carbenoid species **1.6**.^{7,11} This species could then undergo further reactivity or proceed through a standard protodemetalation or hydride shift to regenerate the catalyst.

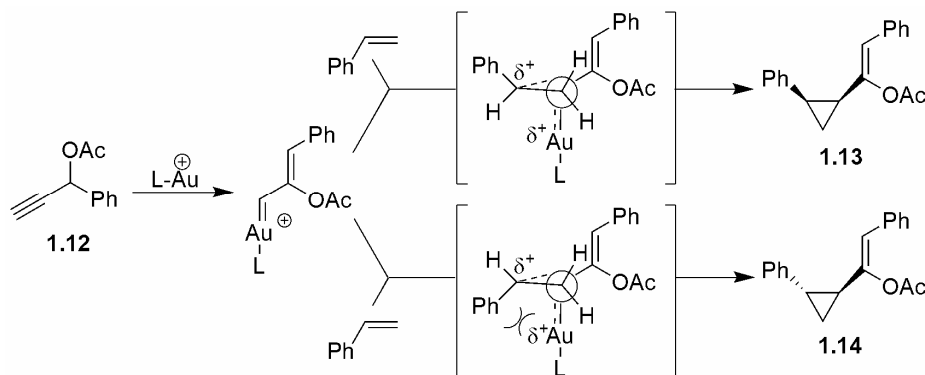
As a model for this reactivity, a modified Schmidt reaction was developed by Gorin *et al.* where the proximal nitrogen of alkyl azides acts as the nucleophile toward gold(I)-activated alkynes (**1.8**) with subsequent expulsion of N₂ (Scheme 1.2).⁷ In this case, the electron accepting ability of gold(I) led to complexation and activation of the alkyne, while electron donation facilitated the loss of the N₂ leaving group to generate the carbenoid intermediate **1.10**. Primary and secondary azides with alkyl and aryl substitution on the alkyne were well tolerated, allowing for the preparation of pyrroles with various substitution patterns. It is postulated that the cationic intermediate (**1.10**) is stabilized by electron donation from gold(I); the gold atom exhibits carbenoid character.⁷ In the final step of the catalytic cycle, a 1,2-hydride shift occurs to regenerate the catalyst and afford the observed product **1.11**.

Scheme 1.2. Intramolecular Acetylenic Schmidt Reaction Catalytic Cycle.⁷



Alternatively, the reactivity of a metal carbenoid center can be utilized to obtain further functionalized products of increased complexity. For example, it has been shown that propargyl esters can serve as carbene precursors,⁴ and, in the presence of chiral, cationic gold(I) catalysts as well as an external olefin, substrate **1.12** will undergo stereoselective cyclopropanation.^{4a,12} The *cis*-selectivity of the reaction to generate **1.13** is consistent with stereochemical models proposed for cyclopropanation reactions involving carbene transfer from a metal-carbenoid (Scheme 1.3).^{4a}

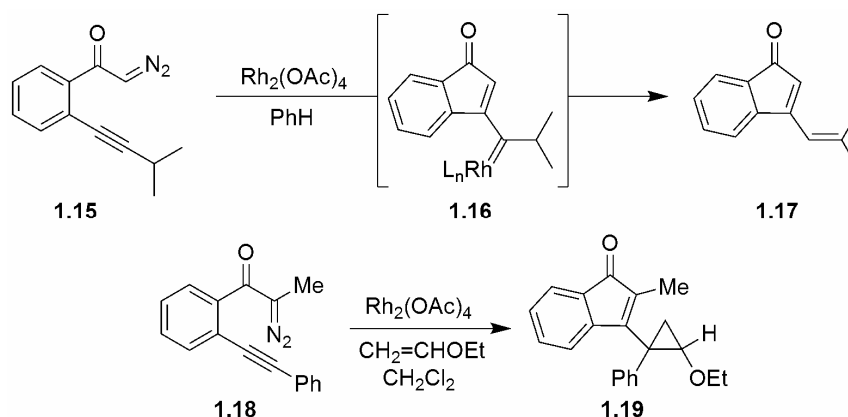
Scheme 1.3. Cyclopropanation of Propargyl Esters.^{4a}



It is important to note that in both of the above examples, the gold(I) catalyst first coordinates and activates the alkyne towards nucleophilic attack to form an intermediate gold carbenoid. With the exception of the cyclopropanation described above, a 1,2-hydrogen shift or protodemetalation typically follows to regenerate the gold catalyst.^{2-5,7,10,12} Unfortunately, this limits the reactivity of these gold intermediates. Thus, we sought to find novel ways to both generate and further functionalize the gold carbenoid species.

When considering the multiple functional groups, in addition to the alkynyl azides and propargyl acetates seen above, that can function as precursors to carbene species, among the most useful and easily accessed are the α -diazocarbonyls. Rhodium(II) is a commonly used catalyst for these types of molecules and will rapidly generate transient electrophilic metal carbenoids from α -diazoketones.^{13,14} For example, when α -diazoketones with tethered alkynes were reacted with $\text{Rh}_2(\text{OAc})_4$, the intermediate rhodium carbenoid cyclized with the alkyne to form a second rhodium carbenoid intermediate **1.16**.¹⁴ (Scheme 1.4) The reaction proceeds by addition of the rhodium-stabilized carbenoid into the acetylenic π -bond to give a vinyl carbenoid intermediate. Due to the presence of an easily accessible α - or β -hydrogen, a 1,2-hydrogen shift occurs to generate **1.17**. Alternatively, in the presence of an olefin, cyclopropanation can occur (Scheme 1.4).¹⁴

Scheme 1.4. Typical Reactions of α -Diazoketones Under Rhodium Catalysis.¹⁴

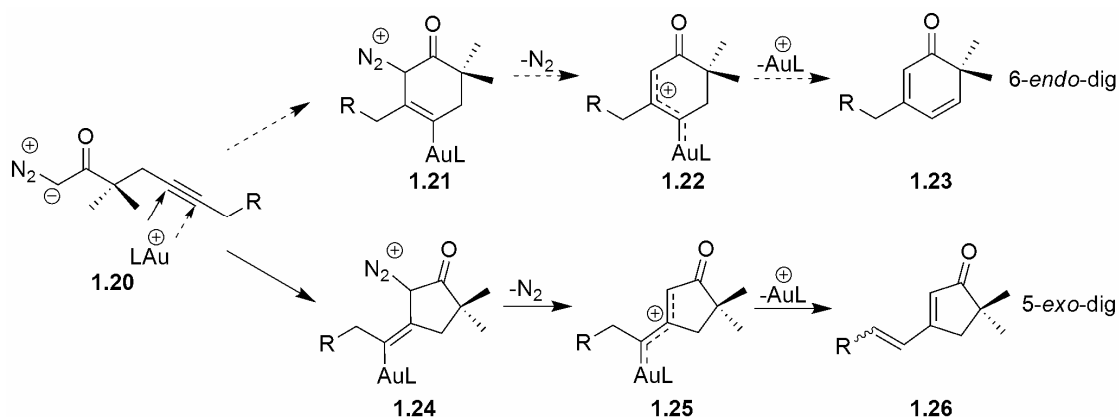


We anticipated that gold might have reactivity similar to rhodium towards α -diazocarbonyl compounds, as both are electrophilic metals capable of exhibiting carbenoid character. Subsequent investigations could then elucidate the mechanism of formation for these gold carbenes, which may be different than that for rhodium carbenes.

Discovery and Development of Gold(I)-Catalyzed Oxidations

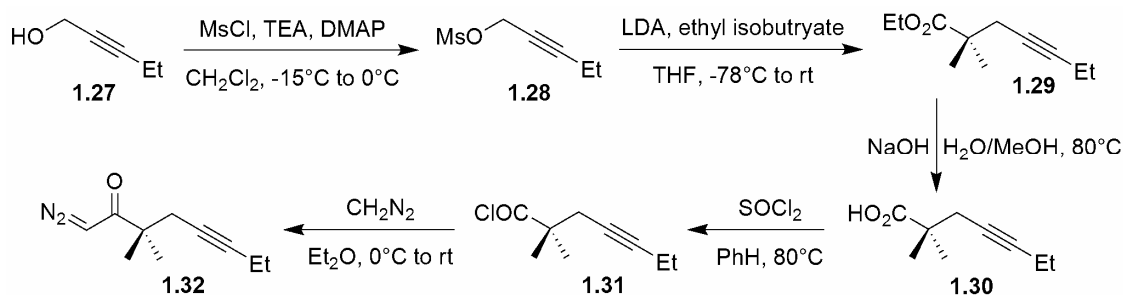
Based on the precedented reactivity of gold, we postulated that instead of the diazo-decomposition observed with rhodium catalysis,^{13,14} the nucleophilic diazocarbon might attack the electropositive, gold-activated alkyne to form a cyclic intermediate.⁷ (Scheme 1.5) In analogy to the azide reaction, subsequent loss of N_2 would create a cationic intermediate which is stabilized by electron donation from gold(I) giving the gold atom carbenoid character. Either the kinetically favored 5-*exo*-dig (**1.26**) or thermodynamic 6-*endo*-dig (**1.23**) product could be generated depending on the regiochemistry of attack by the nucleophilic center. Based on previous reactivity of gold catalysts,^{1-6,10,12} we believed that a 1,2-hydrogen shift would occur to regenerate the gold catalyst. This reaction would provide further support for the intermediacy of gold carbenes and may provide the opportunity for cyclopropanation or other functionalization. Regardless, the formation of these products would allow us to realize our goals of finding new ways to generate gold carbenoid species and discovering new reactivity for those species.

Scheme 1.5. Expected Reaction Pathways for α -Diazocarbonyl Compounds with Gold(I) Catalyst.

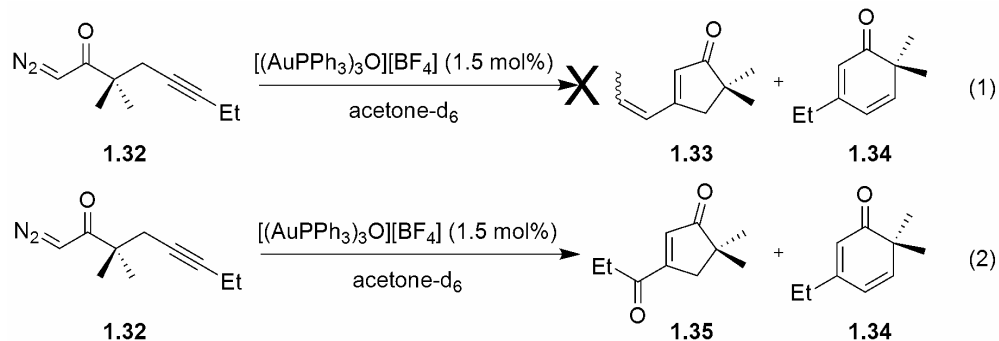


Initially, we synthesized a linear γ,δ -alkynyl- α -diazocarbonyl compound. We chose to use a substrate with a geminal-dimethyl group in hopes that the Thorpe-Ingold effect¹⁵ would further drive the reaction to the desired cyclization product. Thus, diazo compound **1.32** was prepared via a five step modular synthesis (Scheme 1.6). After an initial mesylation of the requisite 2-propynol, an S_N2 reaction coupled the mesylate with ethyl isobutyrate. Saponification gave the carboxylic acid **1.30**, and after activation to the acid chloride and reaction with diazomethane, the desired product **1.32** was obtained in good overall yield. Notably, this modular synthesis allows for variation in alkyne and α -substitution.

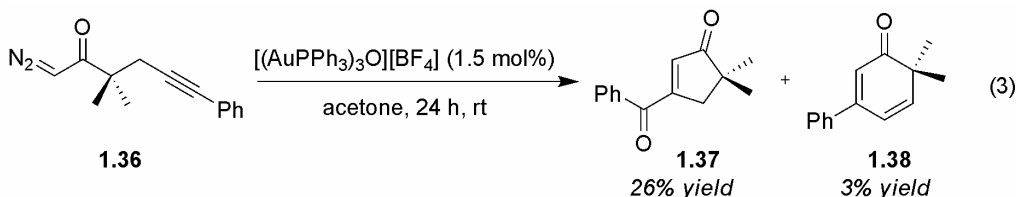
Scheme 1.6. Synthesis of α -Diazocarbonyl Compound **1.32**.



1.32 was then reacted with the triphenylphosphinegold(I) oxonium salt, $[(AuPPh_3)_3O][BF_4]$.¹⁶ We expected to see the 1,2-hydrogen shift products **1.33** or **1.34** (eq. 1) with the reaction proceeding by the mechanism detailed in Scheme 1.4. We were surprised to discover that the oxidized product **1.35** was formed along with **1.34** (eq. 2). Complete conversion of starting material was observed.



Since the 5-*exo*-dig cyclization product was the only product that resulted in the additional oxidation, we sought to increase the reaction selectivity before further studies were attempted. We synthesized substrate **1.36** with a phenyl group on the alkyne rather than an alkyl group, thus eliminating the α -proton required for the 1,2-hydrogen shift that generates the 6-*endo*-dig product. As expected, this resulted in an increased yield of the oxidized 5-*exo*-dig product **1.37** and a significantly decreased yield of the 6-*endo*-dig product **1.38** (eq. 3).



Since it is clear that oxidation must be occurring to generate **1.37**, we hypothesized that adding an oxidant to the reaction mixture would facilitate this process. Because the reaction proceeds with only gold(I) catalyst in acetone, it is possible that O₂ from air acts as the requisite oxidizing agent. As predicted, the use of an oxygen atmosphere in purged solvent seems to confirm our hypothesis by increasing the yield (Table 1.1, entry 1). This led us to continue our oxidant screen by adding one equivalent of various oxidizing agents to the reaction mixture. The oxidants chosen had varying degrees of nucleophilicity as well as differing functional groups. From this investigation, we discovered that 2,3-dichloro-5,6-dicyano-1,4-benzoquinone (DDQ) affords the highest yield observed thus far (Table 1.1, entry 4).

Table 1.1. Oxidant Effects for Gold(I) Catalytic Cyclization.

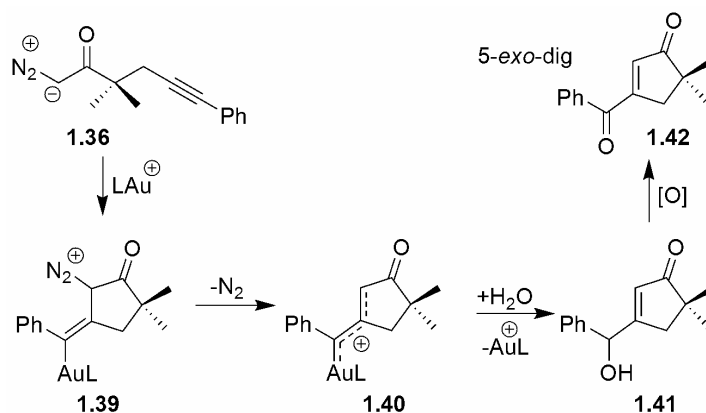
Reaction scheme: **1.36** reacts with $[(AuPPh_3)_3O][BF_4]$ (1.5 mol%) and an oxidant in acetone at room temperature for 24 hours to yield **1.37** and **1.38**.

entry ^a	oxidant	SM	1.37 ^b	1.38 ^b
1	O ₂	7%	38%	2%
2	benzoquinone	<1%	30%	23%
3	PhI(OAc) ₂	<1%	3%	-
4	DDQ	<1%	43%	-
5	mCPBA	<1%	35%	-

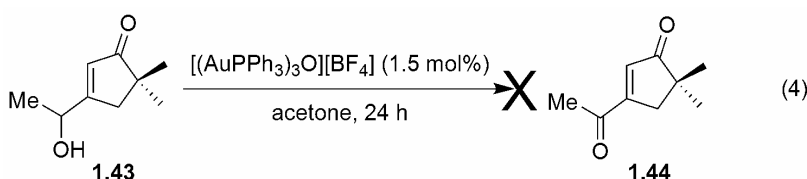
^a All reactions 0.2 M. ^b All yields NMR vs methyl benzoate internal standard unless otherwise noted. SM = Starting Material present.

With this oxidation result in hand, we revised our initial proposed mechanism. We hypothesized that the gold carbene intermediate is formed, but then is quenched by water to form the alcohol (Scheme 1.7). Oxidation follows to afford the observed product.

Scheme 1.7. Proposed Mechanism for Carbenoid Water Quench Followed by Oxidation.

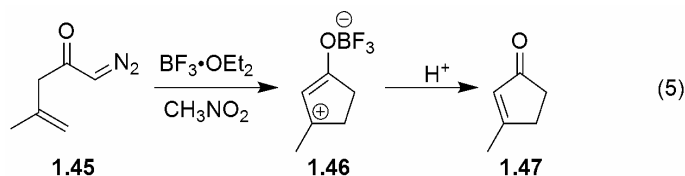


To test this, we independently synthesized alcohol **1.43**.^{17,18} When **1.43** was added to a solution of the gold(I) oxonium catalyst in acetone, however, we did not observe any oxidation of the alcohol to the ketone **1.44** after multiple days (eq. 4).



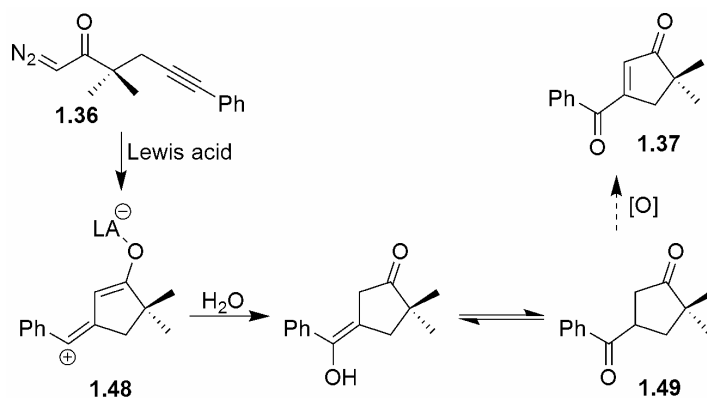
Using DDQ as an oxidant, we only observed a small amount of **1.44**, and the rate of its formation was not on the timescale of the original reaction. Thus, it seemed likely that our mechanistic hypothesis was incorrect. We then considered alternative mechanisms that could generate the observed oxidized cyclization product. It is known that gold can act as a Lewis

acid, which suggests it could coordinate carbonyl functionalities. Literature precedent also exists for Lewis acid catalyzed cyclization reactions of diazocarbonyl compounds (eq. 5).^{19,20}

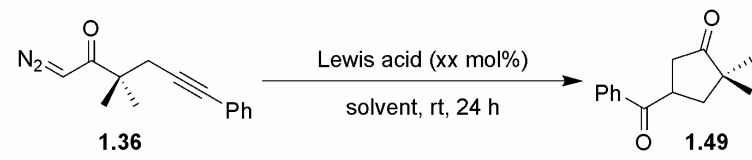


As seen in Scheme 1.8, 5-*exo*-dig cyclization could occur to generate a vinyl cation. This would be trapped by water to generate the enol-ketone intermediate, which could tautomerize to the diketone product **1.49**. A screen of Lewis acids demonstrated that the diketone could be generated, and that In(ONf)₃²¹ in acetone produced the highest yield (Table 1.2).

Scheme 1.8. Lewis Acid Catalyzed Oxidative Cyclization Mechanism.



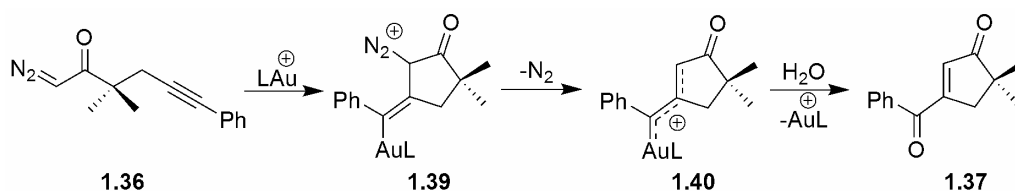
Then, we expected oxidative dehydrogenation of **1.49** would occur to afford the observed dieneone **1.37** (Scheme 1.8). However, treatment of diazocarbonyl compound **1.36** with various Lewis acids in the presence of DDQ only generated the diketone product **1.49** with no trace of the dieneone **1.37**. More importantly, isolated **1.49** subjected to gold(I) and DDQ also remained unreacted; no oxidized **1.37** was observed. This strongly suggests that this mechanism is not operative under our gold conditions.

Table 1.2. Optimization of Lewis Acid Catalyzed Cyclization of **1.36** to **1.49**.

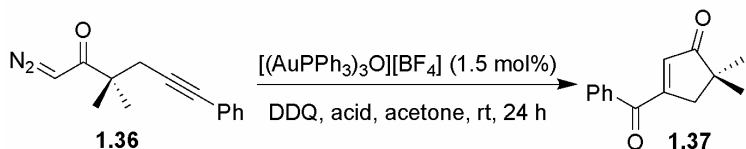
entry ^a	Lewis acid	mol%	solvent	SM	1.49 ^b
1	Sc(OTf) ₃	15	acetone	<1%	26%
2	Bi(OTf) ₃	10	acetone	<1%	28%
3	In(OTf) ₃	10	acetone	<1%	48%
4	Zn(OTf) ₃	10	acetone	<1%	0%
5	InCl ₃	15	acetone	55%	14%
6	InCl ₃ / AgBF ₄	15	acetone	<1%	45% ^c
7	InCl ₃ / 1.50 NaBARF ₂₄ ²²	15	acetone	86%	0%
8	1.51 In(ONf) ₃ ²¹	15	acetone	<1%	56%
9	In(OTf) ₃	15	DMSO	<1%	0%
10	In(OTf) ₃	15	CH ₃ CN	<1%	0%
11	In(OTf) ₃	15	CH ₂ Cl ₂	<1%	0%

^a All reactions 0.2 M. ^b All yields NMR vs methyl benzoate internal standard unless otherwise noted. ^c Isolated yield. SM = Starting Material present.

Based on these findings, we reached the significant conclusion that gold is not acting as a simple Lewis acid. Rather, the mechanism for the formation of the observed ene-dione **1.36** can be represented by the sequence seen in Scheme 1.9. Here, a gold carbene is formed and is oxidized directly to the ene-dione product. This mechanism suggests that we have not only found a new way to generate the gold carbenes but may have also discovered further functionalization of the gold carbene, the first such example in our group other than an intermolecular quench of an olefin.

Scheme 1.9. Proposed Cyclization Mechanism via Direct Oxidation of Gold(I) Carbenoid.

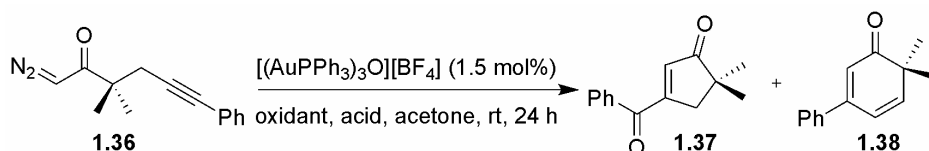
With this mechanistic hypothesis in hand, we sought to obtain additional information regarding the oxidation step. Based upon the fact that oxidants seemed necessary for the reaction, we realized that if the substrate is losing two electrons to the oxidant during the process, two protons are required to complete the reaction. Thus, if Brønsted acids were added to the reaction mixture, perhaps they would facilitate this redox chemistry. We found that the addition of acetic, pivalic and benzoic acid all gave similar results and afforded a significant increase in the reaction yield (Table 1.3, entries 2, 3 and 7). Based on these results, we concluded that the presence of a carboxylic acid facilitated the reaction with no apparent pK_a correlation or dependence on steric bulk.

Table 1.3. Acid Effects with DDQ as Oxidant for Gold Catalyzed Cyclization.


entry ^a	acid	SM	1.37 ^b
1	-	<1%	43%
2	TsOH	<1%	24%
3	AcOH	<1%	52% ^c
4	PhCOOH	<1%	55% ^c
5	3,5-ditertbutylbenzoic acid	<1%	47%
6	2,4,6-trimethylbenzoic acid	<1%	53%
7	2,6-bis(CF ₃)benzoic acid	<1%	47%
8	Pivalic acid	<1%	52%
9	Phenylboronic acid	<1%	41%

^a All reactions 0.2 M. ^b All yields NMR vs methyl benzoate internal standard unless otherwise noted. ^c Isolated yield. SM = Starting Material present.

Excited by this discovery and the resulting increase in yield, we focused our efforts on investigating the effects of different oxidants. Table 1.4 shows the results of this screen; unfortunately, none compared favorably with DDQ (Table 1.4, entry 1). Other common single electron oxidants decreased the yield of reaction, and some, such as duraquinone and cerium ammonium nitrate (CAN), lessened the selectivity for the 5-*exo*-dig product.

Table 1.4. Oxidant Effects with Acid Present for Gold Catalyzed Cyclization.


entry ^a	oxidant	acid	SM	1.37 ^b	1.38 ^b
1	DDQ	AcOH	<1%	52% ^c	-
2	C ₆ Cl ₄ O ₂	AcOH	<1%	34%	-
3	Me ₃ NO	AcOH	49%	-	-
4	mCPBA	AcOH	<2%	30%	-
5	DDQ	PhCOOH	<1%	55% ^c	-
6	Duraquinone	PhCOOH	<1%	38%	26%
7	CuCl	PhCOOH	11%	14%	-
8	PhIO	PhCOOH	11%	19%	-
9	PhNO	PhCOOH	18%	4%	-
10	CAN	PhCOOH	<1%	31% ^d	-

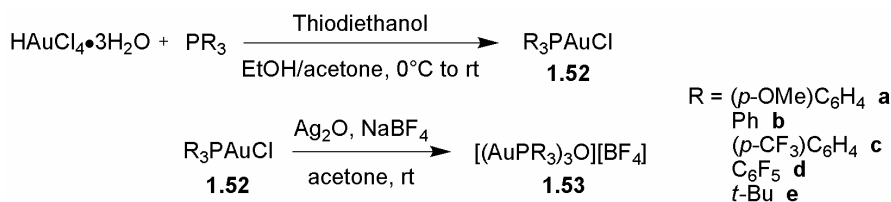
^a All reactions 0.2 M. ^b All yields NMR vs methyl benzoate internal standard unless otherwise noted. ^c Isolated yield. ^d Plus 11% unknown product. SM = Starting Material present.

We then examined the nature of the catalyst during the reaction with DDQ and benzoic acid. Interestingly, when the catalyst is monitored by ³¹P NMR, the initial signal characteristic of the gold(I) oxonium species ($\delta = 23.4$ ppm) disappears when DDQ and benzoic acid are

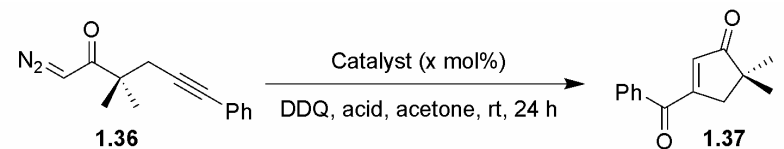
added. Two new ^{31}P NMR signals appear at $\delta = 29.2$ and 44.3 ppm. The most abundant signal at $\delta = 44.3$ ppm corresponds to $(\text{PPh}_3)_2\text{AuBF}_4$ (see Chapter 1 Appendix 1 for representative spectra). When this bistriphenylphosphine gold cation was independently synthesized and used as the catalyst, similar yields were observed (Table 1.5, entry 9). This suggests that our gold(I) oxonium catalyst is not the active catalytic species, but fragments in solution to produce one or more catalytically active species. We were not able to determine the species that corresponds to the other ^{31}P NMR signal observed.

It seems plausible that the gold(I) oxonium catalyst is generating the catalytically active species in situ, thus, we felt it prudent to investigate alternative phosphine ligands to improve the selectivity of the catalyst. Greater than 99% conversion was observed, so it seemed possible that the catalyst was not selective enough to counterbalance other side reactions that may occur. We synthesized a number of gold(I) trimers (Scheme 1.10). It should be noted that while many of the gold complexes had been previously synthesized,^{16,22-28} many of them are novel. However, the methodology utilized for the synthesis of these metal complexes was based on a common procedure for the case where the ligand on gold was a phosphine (Scheme 1.10).^{16,28,29}

Scheme 1.10. Standard Procedure for Preparation of Gold(I) Oxonium Trimer Catalysts.



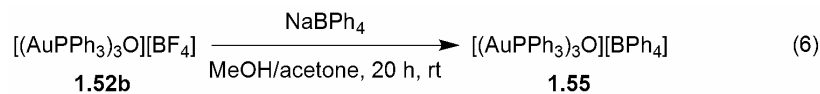
Utilizing various different phosphines gold(I) oxonium catalysts and the XANTPHOS³⁰ ligated gold(I) catalyst, no significant increase in yield was observed (Table 1.5). XANTPHOS allowed us to investigate large phosphine ligands with a stronger steric influence than simple phosphines.

Table 1.5. Gold(I) Oxonium Catalyst and Loading Screen.


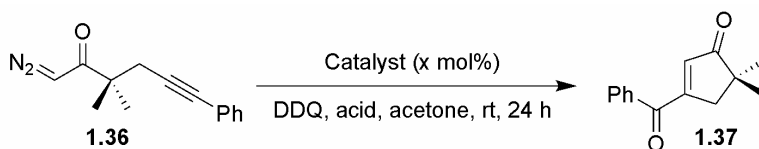
entry ^a	catalyst	mol %	acid	SM	1.37 ^b
1	1.53b [(AuPPh ₃) ₃ O][BF ₄]	1.5	AcOH	<1%	52% ^c
2	1.54 [(AuP(<i>o</i> -tolyl) ₃) ₃ O][BF ₄]	1.5	AcOH	9%	55%
3	1.53c [(AuP(<i>p</i> -CF ₃ (C ₆ H ₄) ₃) ₃ O][BF ₄]	1.5	AcOH	8%	51%
4	1.53e [(AuP(<i>t</i> -Bu) ₃) ₃ O][BF ₄]	1.5	AcOH	8%	48%
5	1.53d [(AuP(C ₆ F ₅) ₃) ₃ O][BF ₄]	1.5	AcOH	11%	25%
6	1.53a [(AuP(<i>p</i> -OMe(C ₆ H ₄) ₃) ₃ O][BF ₄]	1.5	AcOH	8%	46%
7	1.55 [(AuPPh ₃) ₃ O][BPh ₄]	1.5	AcOH	10%	23%
8	1.53b [(AuPPh ₃) ₃ O][BF ₄]	1.5	PhCOOH	<1%	55% ^c
9	1.56 (PPh ₃) ₂ AuBF ₄	1.5	PhCOOH	<1%	54%
10	1.53b [(AuPPh ₃) ₃ O][BF ₄]	0.5	PhCOOH	5%	39%
11	1.53b [(AuPPh ₃) ₃ O][BF ₄]	3.0	PhCOOH	<1%	50%
12	1.53b [(AuPPh ₃) ₃ O][BF ₄]	1.5 ^d	AcOH	<1%	53%
13	1.57 XANTPHOSAuCl ³⁰	3.0	AcOH	<1%	33%
14	1.57 XANTPHOSAuCl ³⁰ / AgBF ₄	3.0	AcOH	<1%	43%

^a All reactions 0.2 M. ^b All yields NMR vs methyl benzoate internal standard unless otherwise noted. ^c Isolated yield. ^d 1.5 mol% catalyst added every hour for total of 4.5 mol%. SM = Starting Material present.

This finding suggested that altering the steric and electronic nature of the ligands had no effect on the selectivity of the catalyst. Changing the counter-ion for the triphenylphosphine gold(I) oxonium catalyst also had detrimental effects (Table 1.5, entry 7; eq. 6). In addition, either increasing or decreasing the catalyst loading reduced the yield (Table 1.5, entries 10 and 11).



As we were not able to successfully increase the yield by altering the phosphine ligands, we then investigated gold(I) catalysts with different ligand types. Based upon our initial catalyst investigations with gold oxonium complexes, it seemed that Au—O bonds may be required for high activity of the catalyst. This was further validated by the result that nitrogen-bound ligands with Au—Cl bonds did not have significant reactivity (Table 1.6, entries 1, 2, and 5-7). The use of the *N*-heterocyclic carbene ligated gold(I) complex, IPrAuCl²⁷ **1.66**, in conjunction with AgBF₄ likewise had decreased activity (Table 1.6, entries 9 and 10). Nitrogen-bound ligand complexes with Au—O bonds also provided no improvement (Table 1.6, entries 3, 4 and 8).

Table 1.6. Gold(I) Catalyst Investigations with Au—X Bonds.

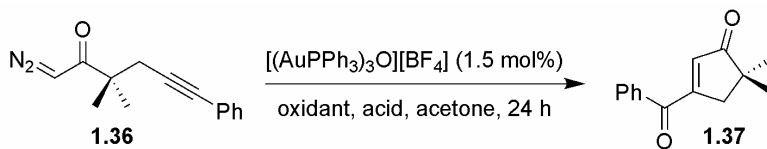
entry ^a	catalyst	mol%	acid	SM	1.37 ^b
1	1.58 [(dppm)Au] ₂ Cl ₂	1.5	AcOH	<1%	27%
2	1.59 DMSAuCl	5.0	AcOH	15%	20%
3	1.60 [Au(bpy)(OH) ₂][PF ₆] ²⁵	5.0	AcOH	6%	33%
4	1.61 [{Au(bpy)(μ-O)} ₂][PF ₆] ²⁵	4.5	AcOH	7%	30%
5	1.62 [Au(bpy)Cl ₂][PF ₆] ²⁵	5.0	AcOH	14%	26%
6	1.63 [Au(terpy)Cl]Cl ₂ •3H ₂ O ²⁶	2.0	AcOH	13%	21%
7	1.64 [Au(terpy)Cl][ClO ₄] ²⁶	2.0	AcOH	16%	25%
8	1.65 [Au(terpy)(OH)][ClO ₄] ²⁶	2.0	AcOH	13%	25%
9	1.66 IPrAuCl ²⁷ / 1.50 NaBARF ₂₄ ²²	2.0	AcOH	<1%	24%
10	1.66 IPrAuCl ²⁷ / AgBF ₄	4.0	AcOH	<1%	32%

^a All reactions 0.2 M. ^b All yields NMR vs methyl benzoate internal standard unless otherwise noted. SM = Starting Material present.

Furthermore, utilizing basic yield vs. conversion studies of the gold catalyzed reactions, we were able to show that catalyst degradation was actively occurring during the reaction. The ratio of yield:conversion remains relatively constant throughout the reaction, and a transition of active reaction pathways between that leading to the desired product and that leading to unwanted side products is not observed. These observations hold true for nearly all of the gold(I) catalysts examined, and suggest that any alternative reaction pathways are consistently active concurrent with the desired reaction. However, these results do not exclude the possibility that the initial catalyst species degrades into multiple components which independently catalyze different processes. This hypothesis would be consistent with the ³¹P NMR profile of the catalyst, as two distinct species are observed. It is also possible that the same catalytic species generates all products including undesired side products.

In an effort to minimize these side reactions and optimize the desired reaction pathway, we methodically altered the relative amounts, concentrations and temperature (Table 1.7). We found 0 °C to be ideal where a yield of 60% was obtained. Microwave radiation also did not have a significant effect (Table 1.7, entry 12). Using an excess amount of DDQ has no effect on the reaction, while excess acid also increased the yield to 60%. However, when the reaction was run at 0°C with excess of acid, the reaction still gave only 60% yield. Surprisingly, decreasing the concentration, which we predicted to decrease the relative amount of polymerization and other carbene-related side products, did not have a significant effect (Table 1.7, entries 14 and 15). In an attempt to further verify that a Lewis acid mechanism was non-operative, we rigorously dried all solvents and reagents to remove any water present that would allow this mechanism to proceed. However, the reaction proceeded in 64% yield, indicating water is not necessary for the transformation (Table 1.7, entry 16).

Table 1.7. Concentration, Temperature, and Relative Amount Variation.



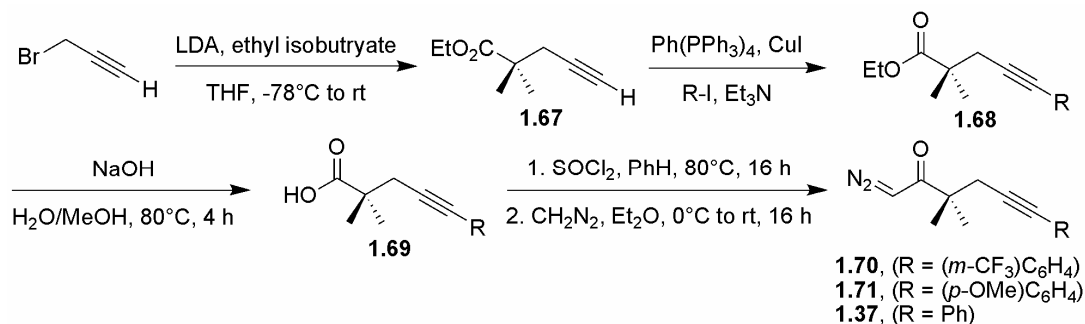
entry ^a	oxidant (equiv.)	acid (equiv.)	concentration	temp	SM	1.37 ^b
1	DDQ (1.0)	AcOH (1.0)	0.2	rt	<1%	52% ^c
2	DDQ (1.0)	PhCOOH (1.0)	0.2	rt	<1%	55% ^c
3	DDQ (0.5)	AcOH (1.0)	0.2	rt	<1%	36%
4	DDQ (2.0)	AcOH (1.0)	0.2	rt	<1%	49%
5	DDQ (1.0)	AcOH (10.0)	0.2	rt	<1%	55%
6	DDQ (3.0)	AcOH (3.0)	0.2	rt	<1%	59%
7	DDQ (1.0)	AcOH (1.0)	0.2	0°C to rt	6%	54%
8	DDQ (1.0)	AcOH (1.0)	0.2	-78°C to rt	<1%	45%
9	DDQ (1.0)	PhCOOH (1.0)	0.2	0°C to rt	<1%	60%
10	DDQ (1.0)	PhCOOH (1.0)	0.2	-25°C to rt	<1%	56%
11	DDQ (1.0)	PhCOOH (5.0)	0.2	0°C to rt	<1%	59%
12	DDQ (1.0)	AcOH (1.0)	0.2	80°C ^b	<1%	52%
13	DDQ (1.0)	AcOH (1.0)	0.2	50°C	<1%	56%
14	DDQ (1.0)	PhCOOH (1.0)	0.01	rt	<1%	58%
15	DDQ (1.0)	PhCOOH (1.0)	0.002	rt	<1%	39% ^c
16 ^d	DDQ (1.0)	PhCOOH (1.0)	0.2	rt	<1%	64% ^c

^a All yields NMR vs methyl benzoate internal standard unless otherwise noted.

^b Conducted in microwave oven for 15 min. ^c Isolated yield. ^d Solvent and reagents dried and degassed. SM = Starting Material present.

With these optimized conditions in hand, we sought to assess the scope of our reaction and determine whether this new reactivity is general for all γ,δ -alkynyl- α -diazoketones. A representative synthesis can be seen in Scheme 1.11. Both electron-donating and electron-withdrawing aryl groups were placed on the diazoketones in the hopes that varying the electronics would vary the stability of the intermediate gold carbenoid species.

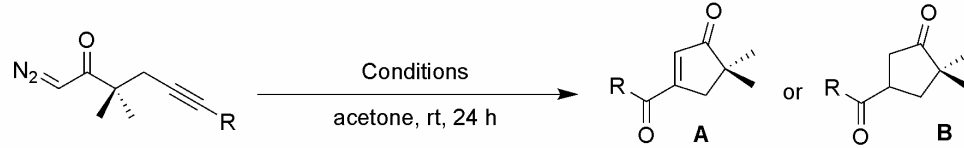
Scheme 1.11. General Synthetic Technique to γ,δ -Alkynyl- α -diazoketones.



Unfortunately, only the *p*-CF₃ substrate gave the desired gold(I) catalysis product in significantly different yield (Table 1.8, entries 1-4). The alkyl-substituted substrates were reexamined in our optimized reaction conditions, but still afforded poor yields of the desired product (Table 1.8, entries 5 and 6). Unlike before, no 1,2-hydrogen shift product was observed

for either of these substrates, however, indicating that our new conditions did improve selectivity.

Table 1.8. Gold(I) and Lewis acid Catalysis Results for Substrate Screen.



entry ^a	R	diazo-compound	conditions	SM	product	yield ^b	
						A	B
1	Ph	1.36	[(AuPPh ₃) ₃ O][BF ₄] (1.5 mol%), DDQ, PhCOOH	<1%	1.37	55% ^c	-
2	(<i>p</i> -OMe)C ₆ H ₄	1.71	[(AuPPh ₃) ₃ O][BF ₄] (1.5 mol%), DDQ, AcOH	2%	1.73	57%	-
3	Ph	1.36	[(AuPPh ₃) ₃ O][BF ₄] (1.5 mol%), DDQ, AcOH	<1%	1.37	52% ^c	-
4	(<i>m</i> -CF ₃)C ₆ H ₄	1.70	[(AuPPh ₃) ₃ O][BF ₄] (1.5 mol%), DDQ, AcOH	7%	1.74	39%	-
5	Et	1.32	[(AuPPh ₃) ₃ O][BF ₄] (1.5 mol%), DDQ, PhCOOH	<1%	1.35	29%	-
6	H	1.72	[(AuPPh ₃) ₃ O][BF ₄] (1.5 mol%), DDQ, AcOH	<1%	-	0%	-
7	(<i>p</i> -OMe)C ₆ H ₄	1.71	In(OTf) ₃ (15 mol%)	<1%	1.75	-	70% ^c
8	Ph	1.36	In(OTf) ₃ (15 mol%)	2%	1.49	-	48%
9	(<i>m</i> -CF ₃)C ₆ H ₄	1.70	In(OTf) ₃ (15 mol%)	<1%	1.76	-	31%
10	Et	1.32	In(OTf) ₃ (15 mol%)	<1%	1.77	-	43%
11	H	1.72	In(OTf) ₃ (15 mol%)	<1%	-	-	0%

^a All reactions 0.2 M. ^b All yields NMR vs methyl benzoate internal standard unless otherwise noted. ^c Isolated yield. SM = Starting Material present.

However, for the Lewis acid catalyzed reaction to the diketone, a trend in the electronic nature of the substrates was observed. Electron withdrawing aryl groups decreased the yield, while the electron donating *p*-methoxy-benzene substituent raised the yield to 70%. Based on our mechanistic hypothesis for the Lewis acid catalyzed reaction, this electronic effect was expected since a vinyl cation was forming that could be stabilized via resonance to the aryl substituent.

Due to the apparent maximum of 60% yield for the gold(I) catalyzed process, we revisited our initial mechanistic hypothesis. Perhaps our initial assumption that a single electron oxidant was required was too limiting; other types of oxidants may prove more applicable for the desired transformation. This reasoning was supported by an experiment conducted to test the atmospheric effects on reaction yield and selectivity. Using the conditions with gold trimer, DDQ and benzoic acid, we found that conducting the reaction under N₂ atmosphere in purged solvent decreased the yield by nearly 10% (Table 1.9, entry 2), while having an O₂ atmosphere in purged solvent also decreased the yield, but to a lesser extent (Table 1.9, entry 1). More importantly, adding water to the reaction compensated for the decrease in yield when run under N₂ atmosphere (Table 1.9, entry 3).

Table 1.9. Atmospheric Effects on Au(I)-catalyzed Reaction.

entry ^a	atmosphere	SM	1.37 ^b
1	O ₂ using purged solvent	<1%	46%
2	N ₂ using purged solvent	<1%	43%
3	N ₂ with 3 equiv. of H ₂ O	<1%	54%

^a All reactions at [] = 0.2 M. ^b All yields NMR vs methyl benzoate internal standard unless otherwise noted. ^c Isolated yield. SM = Starting Material present.

This suggested that water may be important to the reaction and oxygen may not be necessary because water has been present throughout our studies. Conceivably the oxidation of the gold carbene without an added oxidizing agent is the result of a reaction of gold with water with an oxygen atom transfer from water to the carbenoid center. When an added oxidizing agent, such as DDQ, is present, both processes are active. Furthermore, if an oxidant were used that is better suited than water for an oxygen atom transfer to formally oxidize the carbenoid center, higher yields and thus selectivity for the oxidation pathway might be obtained.

Carbene Reactivity with Sulfoxides

Based on literature precedent which detailed the ability of both free carbenes and metal carbenoids to react with nucleophilic oxidants,³¹⁻³³ we believed that similar reactivity would be possible for the postulated gold carbenoid intermediate in our diazoketone cyclization reaction. A preliminary investigation of common oxidants such as sulfoxides, peroxides and hypervalent iodine under the phosphine gold oxonium trimer conditions indicated that the original oxidant, DDQ, even without an acid additive still gave higher yields of 5-*exo*-dig product than the nucleophilic oxidants (Table 1.10).

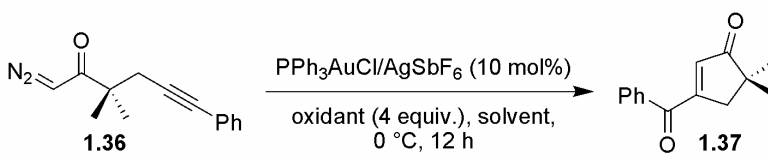
Table 1.10. Nucleophilic Oxidant Optimization for Diazoketone Cyclization.

entry ^a	oxidant	SM	1.37	1.38 ^b
1	O ₂	7%	38%	2%
2	benzoquinone	<1%	30%	23%
3	PhI(OAc) ₂	<1%	3%	-
4	DDQ	<1%	43%	-
5	mCPBA	<1%	35%	-
6	Ph ₂ SO	2%	13%	-

^a All reactions 0.2 M. ^b All yields NMR vs methyl benzoate internal standard. SM = Starting Material present.

However, as depicted in Table 1.11, after modification of the reaction parameters and solvent (dichloromethane at 0°C and 0.1 M with four equivalents of oxidant), as well as changing the catalyst to the more active phosphine gold cation and increasing its loading to 10 mol%, we found the optimal conditions where diphenyl sulfoxide in dichloromethane generated the oxidized product in 80% yield.

Table 1.11. Oxidant Screen with Optimized Conditions for Diazoketone Cyclization.

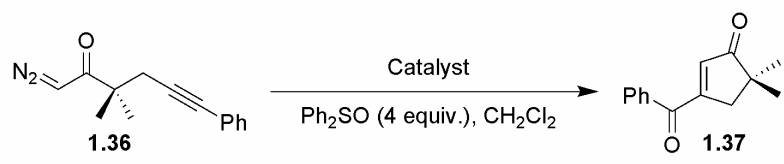


entry ^a	oxidant	solvent	1.37 ^b
1	DDQ	acetone	65%
2	DDQ	CH ₂ Cl ₂	21%
3	Ph ₂ SO	acetone	<10%
4	Ph ₂ SO	CH ₂ Cl ₂	80%
5	O ₂	CH ₂ Cl ₂	25%
6	PhI(OAc) ₂	CH ₂ Cl ₂	35%
7	DMSO	CH ₂ Cl ₂	—
8	Oxone	CH ₂ Cl ₂	10%

^a All reactions 0.1 M. ^b All yields NMR vs methyl benzoate internal standard.

The results of a limited catalyst screen also indicated that triphenylphosphine gold(I) cation with hexafluoroantimonate anion was best (Table 1.12, entry 2), with other ligands and counterions giving similar or decreased yields. A control experiment also confirmed that no silver background reaction was occurring (entry 9).

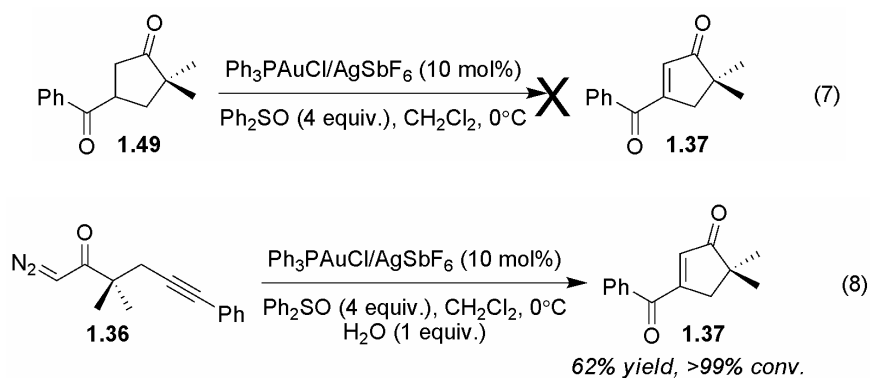
Table 1.12. Catalyst Screen with Sulfoxide Oxidant.



entry	catalyst	temp	conc.	time	SM	1.37 ^a
1	Ph ₃ PAuCl 1.52b / AgOTf	0°C	0.2 M	1.5 h	67%	10%
2	Ph ₃ PAuCl 1.52b / AgSbF ₆	0°C	0.2 M	1.5 h	<1%	80%
3	Ph ₃ PAuCl 1.52b / AgBF ₄	0°C	0.2 M	1.5 h	<1%	48%
4	Ph ₃ PAuCl 1.52b / NaBARF ₂₄ ²² 1.50	0°C	0.1 M	18 h	30%	31%
5	Ph ₃ PAuNTf ₂ 1.78	rt	0.2 M	24 h	<1%	61%
6	IPrAuCl ²⁷ 1.66 / AgSbF ₆	rt	0.2 M	5 h	<1%	56%
7	<i>t</i> -Bu ₃ PAuCl 1.52e / AgSbF ₆	0°C	0.2 M	1.5 h	<1%	71%
8	((<i>p</i> -CF ₃)C ₆ H ₄) ₃ PAuCl 1.52c / AgSbF ₆	0°C	0.2 M	1.5 h	<1%	74%
9 ^b	AgSbF ₆	0°C	0.1 M	24 h	100%	—

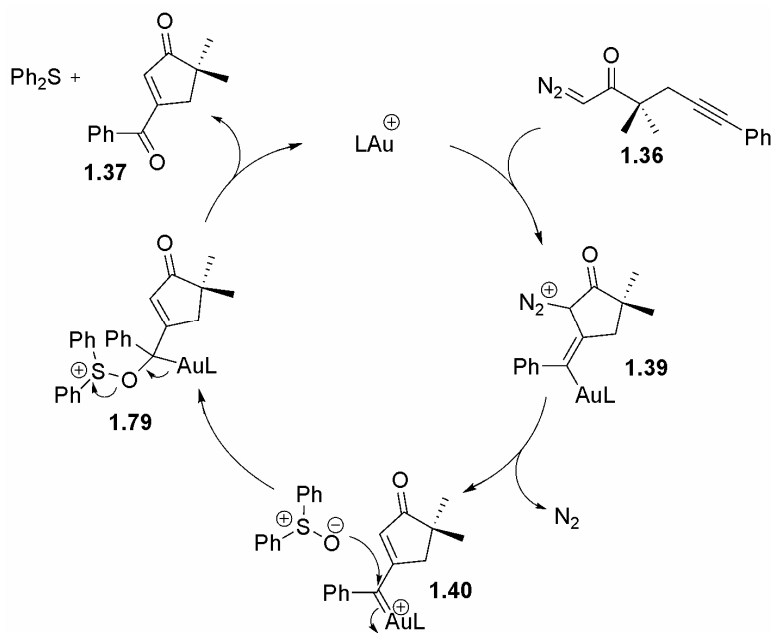
^a All yields NMR vs methyl benzoate internal standard. ^b 7 mol% catalyst. SM = Starting Material present.

While the optimized sulfoxide conditions gave the highest yield of oxidized cyclization product yet achieved, we sought further verification that the reaction was proceeding as hypothesized with nucleophilic addition of the diazocarbon to a gold(I)-activated alkyne followed by oxygen atom transfer from the oxidant. To start, we revisited the concept of a Lewis acid catalyzed process. When the diketone intermediate, **1.49**, discussed above, was subjected to the optimized conditions, no formation of the oxidized ene-dione **1.37** was observed (eq. 7). Likewise, when water was added to the oxidation reaction, which would facilitate the reaction if a Lewis acid pathway were active, a decrease in yield was observed (eq. 8).



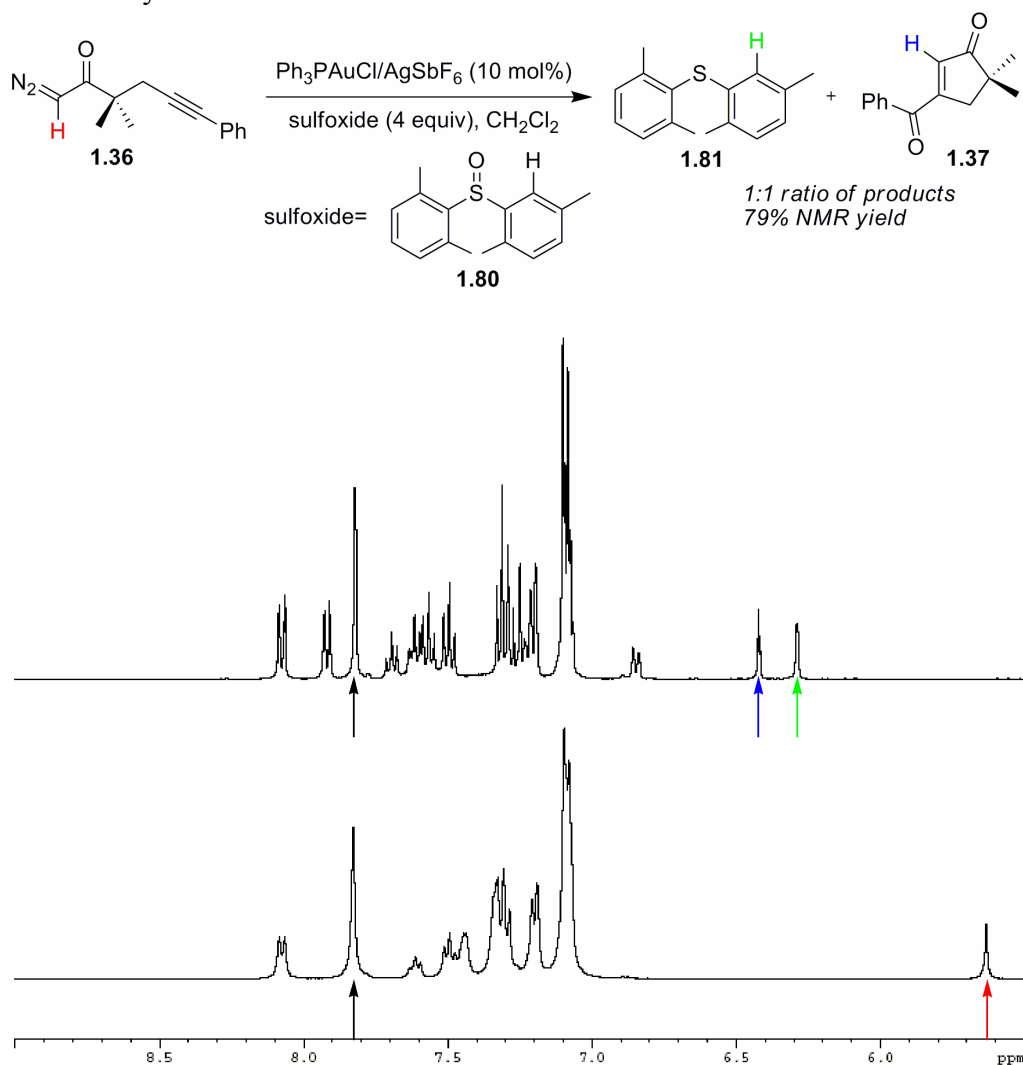
Thus, we felt increasingly confident in the proposed reaction pathway where the diazocarbon nucleophile adds to a gold(I) activated alkyne, a 5-*endo*-dig cyclization occurs with loss of N_2 to form a carbenoid intermediate and sulfoxide oxidizes the carbenoid carbon via oxygen atom transfer (Scheme 1.12).

Scheme 1.12. Proposed Catalytic Cycle for Oxidative Rearrangement of Diazocompounds.

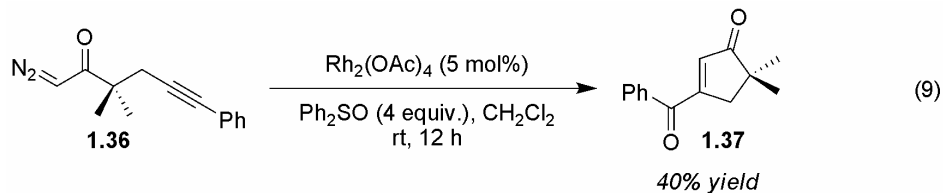


As a test for the oxygen transfer event, an asymmetric sulfoxide was synthesized and the gold catalysis monitored by Nuclear Magnetic Resonance (NMR) (Figure 1.1). We were able to observe the disappearance of a ^1H NMR signal corresponding to sulfoxide **1.80** (black arrow) and the starting material **1.36** (red arrow), and the appearance of a ^1H NMR signal corresponding to sulfide **1.81** (green arrow) and oxidized product **1.37** (blue arrow). When the reaction was complete, we observed a 1:1 integration ratio of the sulfide peak and the product peak, indicating that the oxygen was transferred from the sulfoxide to the product with concurrent formation of the sulfide.

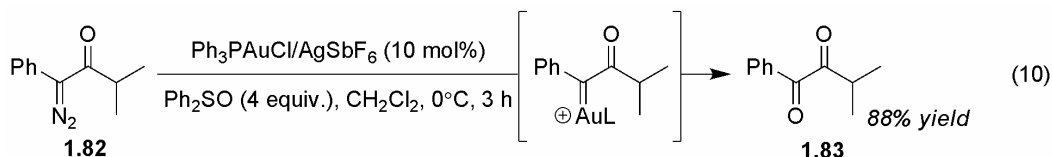
Figure 1.1. Evidence for Conversion of Sulfoxide to Sulfide by NMR for Oxidative Cyclization.



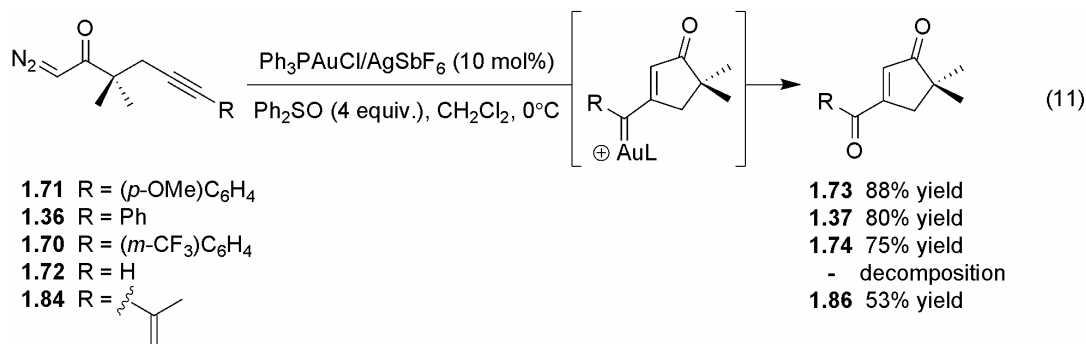
In an effort to confirm that diazo-decomposition was not occurring to generate the gold carbenoid intermediate, we utilized a common Rh catalyst for the transformation. With dirhodium tetraacetate, a significant decrease in yield was observed (eq. 9). As diazo-decomposition is known and expected to occur with Rh, these results suggested that our proposed non diazo-decomposition mechanism was indeed active.³⁴



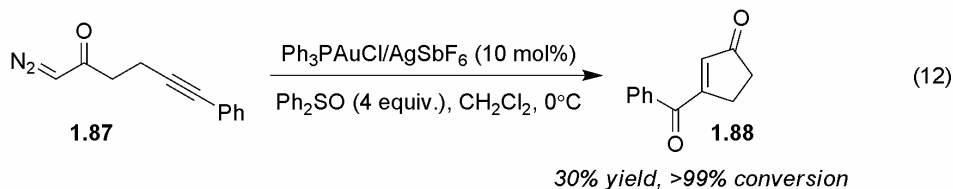
Furthermore, when gold catalyst was used, none of the ketoaldehyde product corresponding to trapping of an α -keto-carbenoid intermediate was observed. Since we were able to obtain this type of reactivity under identical conditions with a different compound (eq. 10), we believe that the diazo-decomposition pathway is not active for this transformation, and that our proposed mechanism stands as the best description of the catalytic cycle.³⁵



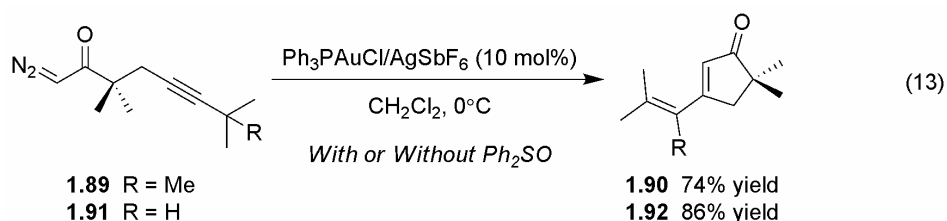
An investigation of the scope of reactivity for the diazoketone oxidative rearrangement showed that disubstituted olefins as well as electron donating and withdrawing aryl groups were tolerated on the alkyne (eq. 11). We observed a clear electronic trend for the substrates, in that electron donating groups yielded the product in significantly higher yield than electron withdrawing.



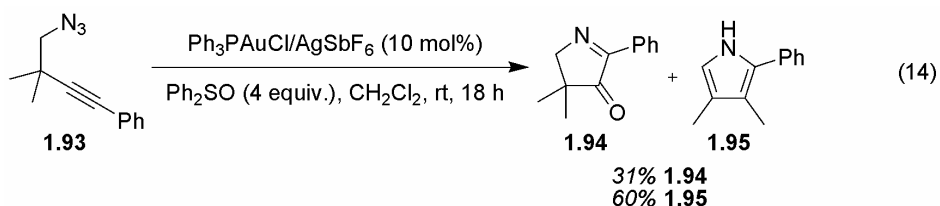
This can be easily rationalized by the stabilization imparted to the carbenoid center alpha to the aryl group in the gold-carbenoid intermediate. Thus, electron donating groups would increase the stability of the intermediate and result in an increased yield. Notably, terminal alkyne substrate **1.72** led to complete decomposition with no aldehyde product observed. It was also found that substitution on the backbone was critical, as removal of the geminal dimethyl group responsible for a Thorpe-Ingold effect¹⁵ dramatically decreased the yield of reaction (eq. 12).



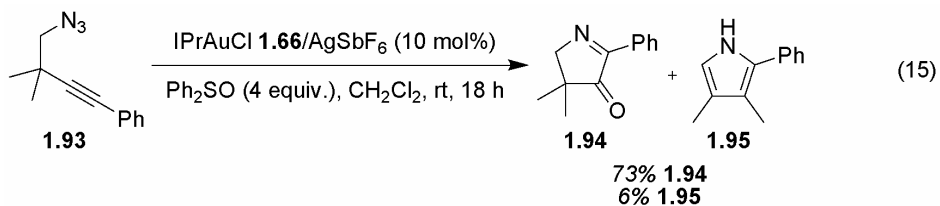
When *tert*-butyl and *iso*-propyl groups were placed on the alkyne, non-oxidized products were observed (eq. 13). In this case, the presence of an α -methyl and α -hydrogen, respectively, resulted in a 1,2-shift rather than oxidation by sulfoxide to generate the diene-one products, even in the presence of diphenyl sulfoxide. This result initially led us to believe that formation of the oxidized product was contingent on the lack of migrateable groups alpha to the carbenoid center. As a test of this hypothesis, we turned to an alternative substrate where a gold catalyzed process was believed to proceed through a carbenoid intermediate and terminated by a 1,2-shift.

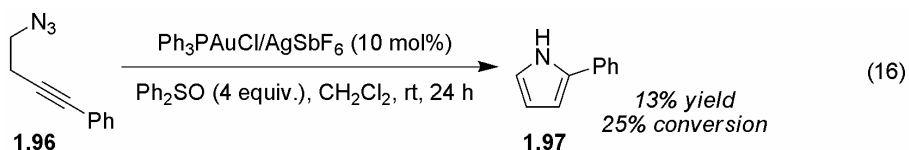


Gorin *et al.* recently published the rearrangement of homopropargyl azides,⁷ which proceed through a similar catalytic cycle where the proximal nitrogen of the azide acts as a nucleophile towards a gold(I)-activated alkyne. Cyclization occurs with loss of N_2 to give a postulated gold-carbenoid intermediate. Then, a 1,2-hydrogen shift occurs to give pyrrole products (Scheme 1.2). However, when azide **1.93** was subjected to the gold oxidation conditions, we were able to detect a mixture of the pyrrolone product **1.94**, resulting from oxidation of the carbenoid intermediate, as well as the pyrrole product **1.95** resulting from 1,2-methyl shift (eq. 14).



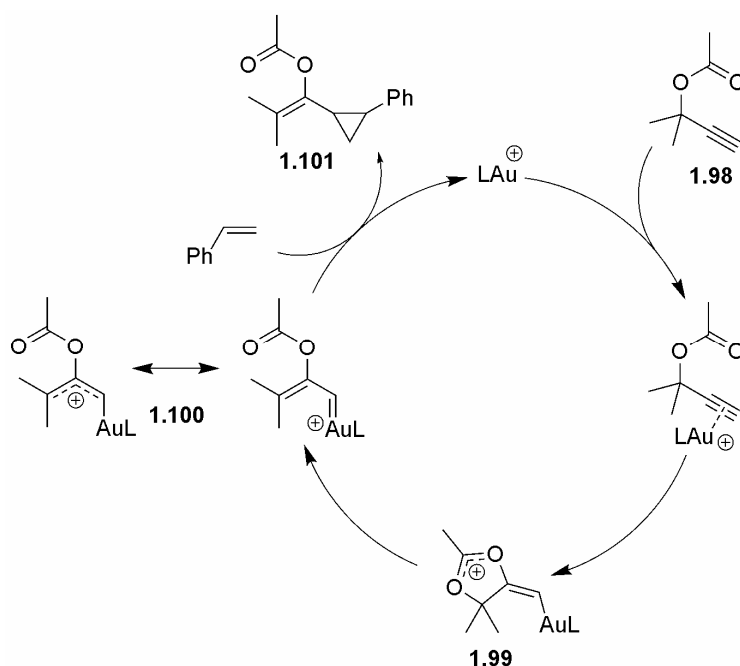
We then changed the ligand on gold from a phosphine to the 'IPr' *N*-heterocyclic carbene,²⁷ **1.66**, which we believed would stabilize the carbenoid intermediate through electron donation as well as provide a steric hindrance to the 1,2 shift. Our hypothesis was correct as we were able to effectively inhibit 1,2-methyl shift to generate the pyrrolone **1.94** in good to high yield with minimal formation of pyrrole **1.95** (eq. 15). Unfortunately, when the homopropargyl azide with no geminal dimethyl group in the propargyl position was subjected to the conditions, 1,2-hydrogen shift still occurred faster than oxidation (eq. 16).



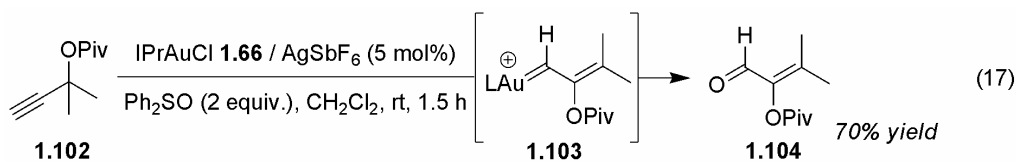


As discussed above, propargyl esters are known to undergo a reaction where gold complexes the alkyne and catalyzes a cyclization reaction involving the ester moiety.^{4,12} This generates a gold carbenoid intermediate which can react with olefins such as styrene to yield cyclopropane products (Scheme 1.13).

Scheme 1.13. Proposed Mechanism of Gold Catalyzed Cyclopropanation of Propargyl Esters.³⁶



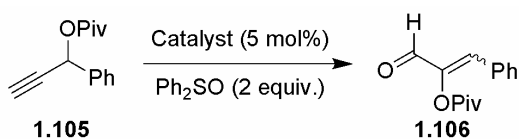
In the course of this transformation, the cationic intermediate formed after 5-*exo-dig* cyclization of the ester undergoes a bond cleavage facilitated by gold backbonding to generate a formal [2,3] migration of the propargyl ester and generate the carbenoid intermediate (Scheme 1.13). Just as it was shown these carbenoid intermediates can be used to form cyclopropane products, we were able to harness the reactivity of the carbenoid species to obtain oxidized aldehyde products (eq. 17).



A number of transition-metal complexes have been reported to catalyze olefin cyclopropanation with propargyl esters.^{4,12,37} Thus, we utilized this class of substrates to test for

the generality of oxidation of metal-carbenoid intermediates by sulfoxides. In doing so, we could also obtain additional support for the existence of a gold(I) carbenoid intermediate, rather than a simple stabilized cation. Table 1.13 shows the results of this investigation. Platinum and ruthenium, metals known to generate carbenoid species,^{4,12,37} were oxidized under our conditions (entries 4,5,8,9). Palladium also generated the enal product, albeit in lower yield (entry 7). Furthermore, all metals investigated generated only 1,2-addition products. If a stabilized cation were present for gold, 1,4-addition product would be expected. Thus, the exclusive formation of **1.106** reaffirms the potential carbenoid character of gold(I) intermediates which renders the carbon alpha to the gold center the most electrophilic and reactive to nucleophilic addition.

Table 1.13. Oxidative Rearrangement of Propargyl Esters with Late Metal Catalysts.



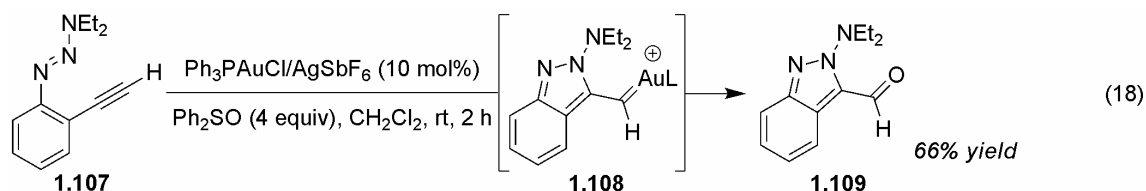
entry	catalyst	solvent	temp	time	yield ^a	Z/E
1	Ph ₃ PAuCl 1.52b / AgSbF ₆	CH ₂ Cl ₂	25 °C	1.5 h	72%	75:25
2	IPrAuCl 1.66 / AgSbF ₆	CH ₂ Cl ₂	25 °C	1.5 h	73%	99:01
3	AuCl ₃	CH ₂ Cl ₂	25 °C	1.5 h	96%	45:55
4	PtCl ₂	toluene	60 °C	17 h	72%	94:6
5	[RuCl ₂ (CO) ₃] ₂	toluene	60 °C	20 h	81%	97:3
6	AuCl ₃	toluene	25 °C	17 h	92%	15:85
7	PdBr ₂	THF	50 °C	22 h	53%	90:10
8	PtCl ₂	DCE	45 °C	40 h	79%	68:32
9	[RuCl ₂ (CO) ₃] ₂	DCE	45 °C	65 h	83%	78:22

^a All yields determined by NMR vs methyl benzoate internal standard.

Due to the substitution at the propargyl position, we were able to investigate the *Z*:*E* ratios for various catalysts. The *N*-heterocyclic carbene (NHC) gold(I)-catalyzed reaction of **1.105** in the presence of diphenylsulfoxide afforded aldehyde **1.106** in 73% yield with excellent control of olefin geometry for the *Z*-isomer (entry 2). Triphenylphosphine ligated gold gave a nearly identical yield but decreased selectivity (entry 1). As mentioned above, a similar aldehyde, **1.104**, was formed in 70% yield by NHC ligated gold(I)-catalyzed oxidative rearrangement of ester **1.103** (eq. 17). Interestingly, platinum- (entries 4 and 8), palladium- (entry 7) and ruthenium- (entries 5 and 9) carbenoid intermediates showed good to high selectivity for the *Z*-isomer, with significantly increased selectivity observed when toluene at 60 °C was used rather than dichloroethane at 45 °C. On the other hand, gold(III) chloride catalyzed the rearrangement of **1.106** to selectively furnish the *E*-isomer (entry 6). Gold(III) chloride was the only catalyst used to generate the *E*-isomer of **1.106** preferentially (entry 6). Notably, treatment of (*Z*)-**1.106** with AuCl₃ did not induce isomerization to (*E*)-**1.106**. While a good explanation for this phenomenon is unknown, there are many previous examples of different reactivity between gold(I) and gold(III) catalysts.³⁸

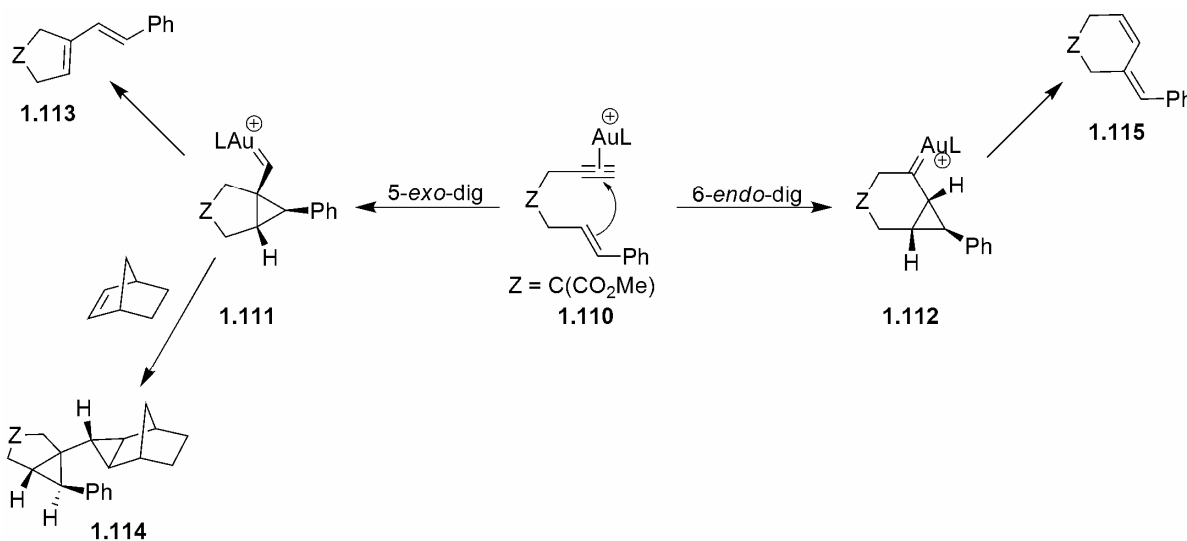
The gold carbenoid oxidation conditions were also proven to be applicable to other substrates such as triazene **1.107** known to generate copper carbenoid species and react with molecular oxygen to generate aldehydes.³⁹ Under the gold conditions, we were able to similarly

generate aldehyde product **1.108** in a yield comparable to the copper system providing further verification of a carbenoid intermediate (eq. 18).



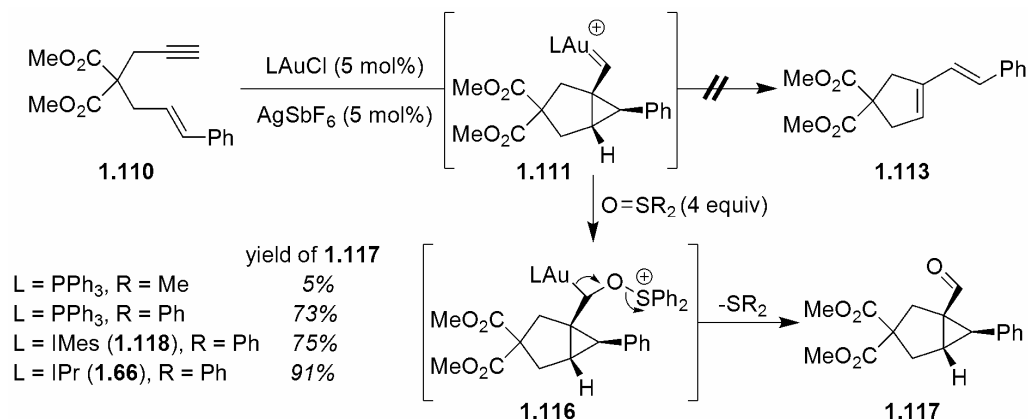
Based on a series of publications from Echavarren and others,^{2e,12b,40,41} we hypothesized that 1,6-enyne cycloisomerizations which proceed through a carbenoid intermediate could also be utilized in our gold catalytic conditions to generate new oxidized products. Depending on the conditions, Echavarren found that either 5-*exo*- or 6-*endo*-dig cyclizations of 1,6-enyne **1.110** would occur through a gold-carbenoid intermediate followed by a skeletal rearrangement to form dienes **1.113** or **1.115**.^{2e,2i,40,41} Alternatively, the addition of an olefin would result in cyclopropanation of the intermediate carbenoid species to form **1.114**^{12b} (Scheme 1.14).

Scheme 1.14. Reactivity of 1,6-Enynes under Gold Catalysis Conditions.



Our initial attempt at oxidizing the carbenoid species employed cationic triphenylphosphinegold(I) as the catalyst and diphenylsulfoxide as the oxidant generated the desired bicyclic aldehyde **1.117** in 73% yield without any competitive formation of diene **1.113**. The yield was unchanged by the use of *N*-heterocycliccarbene IMes^{2i,27} (**1.118**) as the ligand, while *N*-heterocycliccarbene IPr²⁷ (**1.66**), used in the above described azide rearrangement, improved the yield to 91% (Scheme 1.15). Under these conditions, a variety of 1,6-enynes underwent gold(I)-catalyzed oxidative cyclization to afford either cyclopropyl aldehydes (Table 1.14) or cyclopentenyl aldehyde **1.129**^{12b,40,41} (eq. 19).

Scheme 1.15. Oxidative Rearrangement of 1,6-Enynes with Sulfoxide and Gold(I) Catalyst.

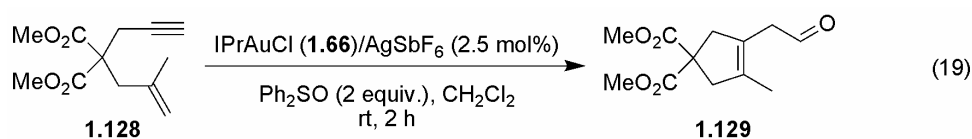


A variety of backbone tethers were tolerated in the reaction conditions (Table 1.14). Gem-diesters (entry 1 and 2), ether (entry 5 and 6) and tosylamines (entry 7) all gave the desired product in excellent yields. We were also able to form the cyclized product with a cyclopropyl olefin when a diene was present in the starting material rather than a simple substituted olefin (entry 2 and 6).

Table 1.14. Scope of 1,6-Enyne Reactivity in Gold Oxidative Conditions.

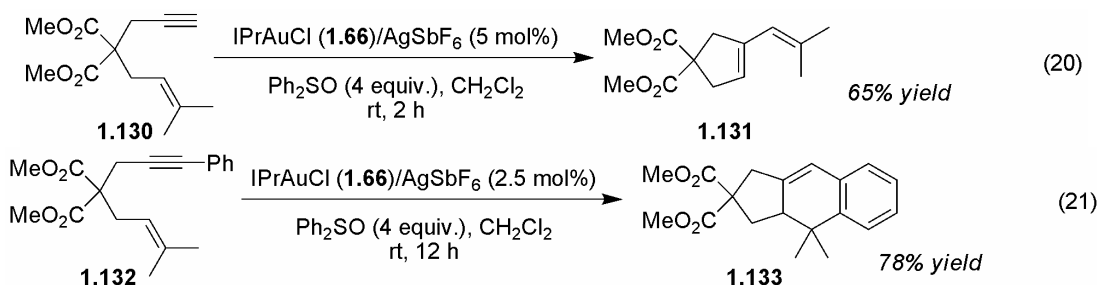
entry	1,6-enyne	X	R ¹	R ²	product	yield
1	1.110	(MeO ₂ C) ₂ C	Ph	H	1.117	91%
2	1.118	(MeO ₂ C) ₂ C	vinyl	H	1.124	75%
3 ^a	1.119	(MeO ₂ C) ₂ C	Ph	Me		<i>NR</i>
4 ^a	1.120	(MeO ₂ C) ₂ C	Ph	Ph		<i>NR</i>
5	1.121	O	Ph	H	1.125	94%
6	1.122	O	(<i>E</i>)-C ₂ H ₂ (C ₆ H ₅)	H	1.126	83%
7	1.123	NTs	Ph	H	1.127	91%

^a Reaction run for 15 h.



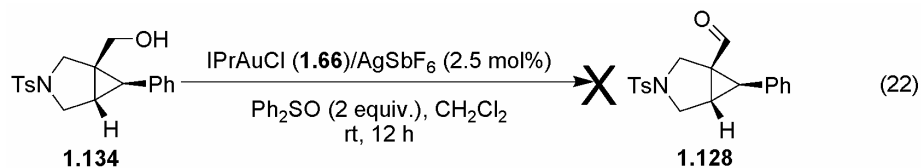
Only disubstituted olefins were tolerated; trisubstituted olefins selectively generated skeletal rearrangement product **1.131** (eq. 20). Furthermore, we found that both methyl and phenyl alkynyl substitution gave no reaction, suggesting that non-terminal alkynes were not suitable for this reaction (Table 1.14, entry 3 and 4). However, phenyl alkynyl substitution in combination with a trisubstituted olefin resulted in electrophilic aromatic substitution to generate tricyclic

product **1.133**, consistent with previously published observations²ⁱ (eq. 21). The alternative aldehyde product **1.129** was only observed when the olefin substitution pattern was adjusted to a 1,1-disubstituted manner on the starting enyne **1.128** (eq. 19). Notably, in all cases where oxidation reactivity was observed, intermolecular reaction of the gold-carbenoid intermediate with sulfoxide occurred selectively over skeletal rearrangement to the diene.



In addition, the bicyclic cyclopropyl aldehyde products were always formed diastereoselectively. Detailed DFT calculations performed by Echevarren and coworkers document the exact process by which the carbenoid is formed and skeletal rearrangement occurs.⁴¹ They indicate a concerted formation of the cyclopropyl carbenoid intermediate in which the olefin geometry translates to the observed diastereoselectivity. Under our conditions, when a *cis*-olefin was used instead of the standard *trans*-olefin in the gold oxidation conditions, only diene **1.113** resulting from a skeletal rearrangement was observed. This is possibly due to increased steric interactions between the phenyl group previously on the olefin and the gem-diester backbone linker. The end result is to decrease the stability of the carbenoid intermediate and render the intramolecular skeletal rearrangement more kinetically favorable relative to intramolecular oxygen transfer from sulfoxide.

As mentioned above in the context of diazocompound cyclizations, an alternative mechanism for the formation of the observed oxidized products would be via trapping of the vinyl cation or carbenoid species with water to give an alcohol, which would then be oxidized to the observed aldehyde or ketone. With regards to the 1,6-enyne oxidative rearrangement, this mechanistic proposal would involve the formation of a cyclopropyl alcohol which would be oxidized to the observed aldehyde product. While experiments on the diazoketone system led us to disfavor this alternative mechanistic pathway, we verified this conclusion using the 1,6-enyne substrate. As expected, when alcohol **1.134** was subjected to the gold oxidation conditions, no formation of **1.128** was observed (eq. 22).



We also investigated the use of alternative nucleophilic oxidants for the 1,6-enyne oxidative rearrangement. As seen in Table 1.15, diphenylsulfoxide was the only such oxidant to generate any product in appreciable yield. In the realm of sulfoxides, based on the failure of both DMSO and di-*t*-butylsulfoxide⁴² (entries 6 and 9), we reasoned that a bulky and strongly electron donating sulfoxide is required for reactivity. All other types of oxidants as well as a Wittig

reagent (entry 8) and a sulfoxonium chloride (entry 7) failed to react. It is unclear why the strong preference exists for diphenylsulfoxide, while other molecules of similar nucleophilicity do not add into the carbenoid.

Table 1.15. Oxidant Screen for Gold Catalyzed 1,6-Enyne Oxidative Rearrangement.

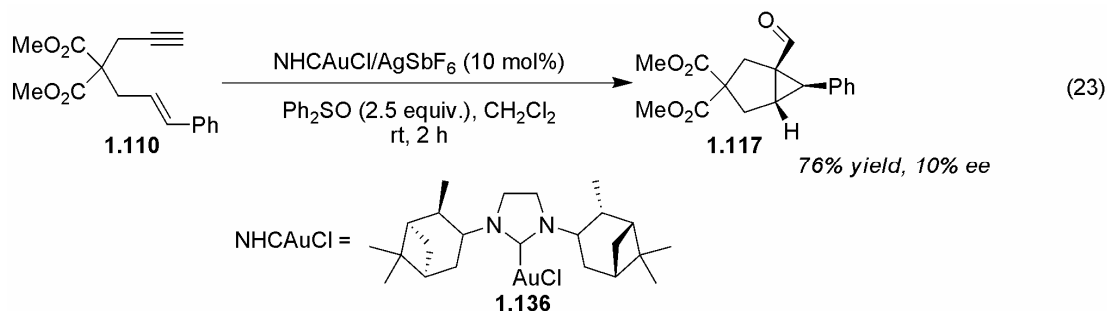
entry	oxidant	equiv. of oxidant	yield ^a	
			1.117	1.113
1	NMO	4		NR
2	O ₂	4	-	60%
3	<i>m</i> CPBA	4		decomp
4	oxone	4	-	57%
5	PhI(OAc) ₂	4		NR
6	DMSO	4	14%	-
7		2	-	10%
8		2		NR
9		2		NR

^a All yields determined by NMR vs methyl benzoate internal standard.

Extension to Enantioselective Catalysis

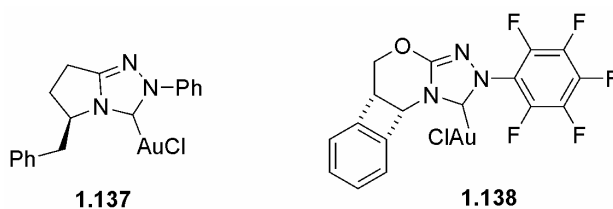
In the last five years, numerous examples of enantioselective gold catalysis have appeared in the literature,⁴³ illustrating the importance of combining gold reactivity with the synthetic utility of stereoselective transformations. The possibility of applying chiral gold catalysis to the oxidative rearrangement methodology led us to investigate the enantioselective formation of the already diastereopure bicyclic cyclopropyl aldehyde **1.117**. Based on the success of *N*-heterocycliccarbene (NHC) ligands, we initially focused on the synthesis of several known NHC salts. Once complexed to gold, they would be used in the oxidative conditions to evaluate their efficacy.

Unfortunately, the synthesis of these NHC gold(I) chloride catalysts was largely unsuccessful. Once the NHC salt was formed, complexation to gold was difficult. The result of significant synthetic efforts to a variety of chiral NHC ligands was the formation of one such NHC gold complex was synthesized (**1.136**)⁴⁴ which afforded a yield of 76% and substandard ee of 10% (eq. 23).



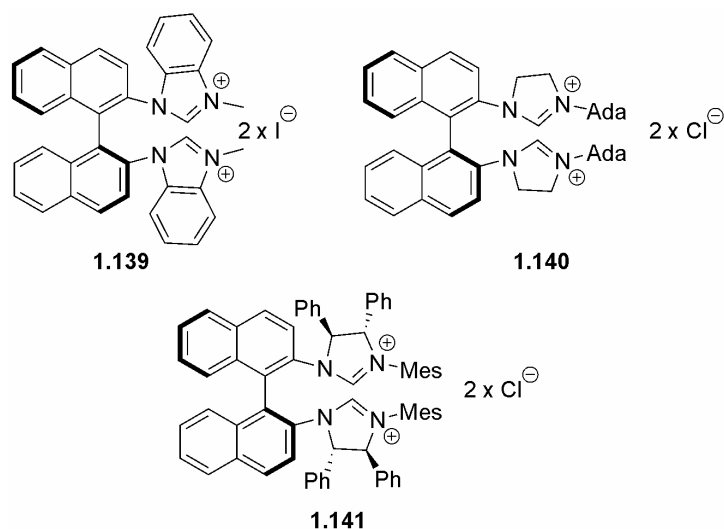
While this was a proof of principle that chiral NHCs could be used to obtain enantioselectivity, a significantly higher ee would have to be obtained for synthetic applicability. To this end, two different triazolium gold(I) chloride catalysts were utilized with limited success. The hexafluoroantimonate salt of **1.137**⁴⁵ resulted in only 22% yield of aldehyde **1.117** with 0% ee, and **1.138**⁴⁵ resulted in 34% yield of **1.117** in 12% ee (Figure 1.2).

Figure 1.2. Chiral *N*-heterocyclic Carbene Ligands for Enantioselective Gold Catalysis.



Despite these setbacks, we returned to *N*-heterocycliccarbenes inspired by recent reports that bis-NHC ligands could be synthesized.⁴⁶ We hypothesized that they could then form digold species in analogy with those recently utilized for asymmetric hydroaminations.⁴⁷ Despite considerable efforts to synthesize ligands of the types seen below utilizing a variety of conditions,⁴⁸ we were only able to obtain the bis-NHC molecule **1.139** (Figure 1.3).^{46b,c} Unfortunately, the gold chloride complex could not be formed.

Figure 1.3. Representative Examples of Bis-*N*-heterocycliccarbene Ligands.



A screen of multiple known chiral gold(I) catalysts, including SEGPHOS, BINAP, BIPHEP, relatives and derivatives met with similarly disappointing results. The best ee obtained was 32% with either SEGPHOS(AuCl)₂ or xylylBINAP(AuCl)₂ with one catalytic equivalent of AgSbF₆ in a reaction that generated the bicyclic cyclopropyl aldehyde **1.117** in 53% and 43% yield, respectively, with considerable skeletal rearrangement diene **1.113** also formed.

Conclusion

When the reactions detailed in this chapter are taken as a whole, the reactive possibilities for gold(I)-carbenoid intermediates can be discussed. Generally, a 1,2-hydrogen shift to quench the carbenoid intermediate is preferred. When this shift is not possible, due to substitution or other chemical constraints in the molecule, the carbenoid species has lifetime of sufficient duration to allow for intermolecular reaction with a sulfoxide. For the propargyl esters and diazoketones used for this methodology, no further reactive pathway other than protodemetalation is available to the carbenoid intermediate, thus oxidation is observed. Conversely, 1,6-enynes do have the capability to undergo a skeletal rearrangement, but based on our observations that oxidation occurs selectively over this process, we can conclude it is a less kinetically favorable pathway compared to sulfoxide addition and oxidation. For the azide rearrangements, if 1,2-methyl shift is a possible pathway, it can be inhibited by judicious use of ligands on gold, specifically the *N*-heterocycliccarbene IPr,²⁷ to stabilize the carbenoid intermediate and provide steric inhibition to migration.

In conclusion, these investigations have led to the discovery and development of a new method of oxidation of a gold(I)-carbenoid intermediate by a stoichiometric sulfoxide oxidant. We believe that mechanistically, this process can be described as an oxygen atom transfer from the sulfoxide to the carbenoid center. This gold oxidation chemistry, where a carbonyl group is formed where the gold carbenoid center existed allows us to probe the nature of the intermediates in many reactions and can serve as an indicator for when a gold carbenoid intermediate is present in the mechanism. Based on the chemoselectivity of the addition, the

oxygen atom transfer event provides further support for the carbenoid nature of the intermediates in these rearrangements. Furthermore, these reactions provide an entry into rearranged products containing an aldehyde or ketone moiety for further functionalization. In the case of 1,6-enynes, stereochemistry has been created in the molecule that, in the future, may be translated into an enantioselective process.

Experimental Section

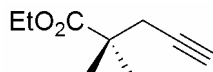
General Information. Unless otherwise noted, all commercial materials were used without further purification. All reactions other than the gold(I) and Lewis acid catalysis reactions, unless otherwise noted, were conducted using standard high-vacuum or Schlenck techniques. Unless otherwise noted, the following solvents were purified by the following methods: diethyl ether (Et₂O), methylene chloride (CH₂Cl₂), tetrahydrofuran (THF), and toluene were passed through a column of alumina under nitrogen; benzene, acetonitrile, triethylamine, *N,N'*-diisopropylethylamine and diisopropylamine were distilled from CaH₂. When used for washing or extractions, solvents were used as received.

TLC analysis of reaction mixtures was performed on Merck silica gel 60 F₂₅₄ TLC plates. Flash chromatography was carried out on MP SiliTech 32-63 D 60 Å silica gel. ¹H, ¹³C and ³¹P NMR spectra were recorded with Bruker AV-300, AVQ-400, AVB-400, AV-500 or DRX-500 spectrometers and were referenced to residual ¹H and ¹³C signals of the deuterated solvents, respectively. Unless otherwise indicated, IR spectra were recorded with a ThermoNicolette Avatar 370 FTIR as thin films on a ZnSe crystal. Enantiomeric excess was determined on a Shimadzu VP Series Chiral HPLC. Mass spectral and CHN data was obtained via the Micro-Mass/Analytical Facility operated by the College of Chemistry, University of California at Berkeley.

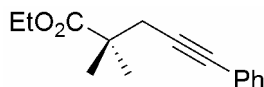
(Ph₃P)AuCl and other (R₃P)AuCl complexes were prepared by the method of Shapley *et al.*⁴⁹ Both IPrAuCl (**1.66**) and IMesAuCl (**1.118**) were prepared by the method of Echavarren *et al.* via treatment of the imidazolium salt with Ag₂O followed by DMSAuCl.²¹ DMSAuCl (**1.59**) was prepared by the method of Yamamoto *et al.*⁵⁰ [(dppm)Au]₂Cl₂ (**1.58**) was prepared by the method of Puddephatt *et al.*⁵¹ NaBARF₂₄ (**1.50**) was prepared by the method of Bergman *et al.*²² (Ph₃P)₂AuBF₄ (**1.56**) was prepared by the method of Westland *et al.*⁵² *N,N*-diethyl-*N'*-(2-ethynylphenyl)triazene (**1.107**) was prepared by the method of Haley *et al.*³⁹ 1,6-enynes **1.110**, **1.128**, **1.119**, and **1.130** were prepared by the method of Sher *et al.*^{53,54} Enynes **1.120** and **1.132** were prepared in analogy to the Sher method, utilizing (3-bromo-1-propyn-1-yl)benzene.⁵⁵ **1.118** was prepared by the method of Harvey *et al.*,⁵⁶ **1.121** and **1.122** were prepared by the method of Hosomi *et al.*,⁵⁷ and **1.123** was prepared by the method of Echavarren *et al.*⁵⁸ Propargyl pivaloate **1.102** was prepared by the method of Gulhane *et al.*⁵⁹ *t*-Butyl sulfoxide, **1.135**, was prepared by the method of Bégué *et al.*⁴² **1.122**⁶⁰ was prepared, isolated and characterized by Dr. Pablo Mauleón. Compounds **1.34**, **1.38**⁶¹ and **1.72** were prepared, isolated and characterized by Dr. Benjamin Sherry. Precursor ligand to **1.138** was purchased from Strem Chemical Company.

General Procedure for oxidative cyclization reactions catalyzed by [(AuPPh₃)₃O][BF₄]: A 0.110 mmol sample of diazoketone was dissolved in 0.5 mL of acetone in a one dram vial. If desired, one equivalent of acid (acetic or benzoic) was added, followed by addition of one equivalent of 2,3-dichloro-5,6-dicyano-1,4-benzoquinone (DDQ). Then, 1.5 mol% catalyst was added. Moderate bubbling ensued and when the bubbling had dissipated, the vial was capped and the reaction mixture was maintained at the temperature indicated for 24 h. Crude reaction mixtures were purified by flash chromatography (5% ethyl acetate/hexanes).

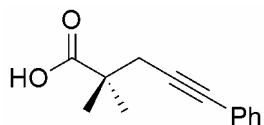
Procedure for Synthesis of Diazocarbonyl Compounds.



Preparation of 2,2-dimethyl-ethyl pentynoate (1.67): To a solution of freshly prepared LDA (39.3 mmol) in THF (35 mL) cooled to $-78\text{ }^{\circ}\text{C}$ was added a solution of ethyl isobutyrate (5.0 mL, 37.4 mmol) in THF (42 mL) by addition funnel over 1h with stirring. After addition was complete, the reaction mixture stirred for 20 min at $-78\text{ }^{\circ}\text{C}$ and then warmed to $0\text{ }^{\circ}\text{C}$ and stirred for 10 min before cooling back to $-78\text{ }^{\circ}\text{C}$. A solution of propargyl bromide (5.0 mL, 80 wt% in toluene, 44.88 mmol) in THF (21 mL) was then added dropwise. The mixture was stirred overnight and warm to room temperature. After quenching with NH_4Cl (aq. $\sim 60\text{ mL}$) the organic layer was separated and the aqueous layer extracted with Et_2O (2x20 mL). The organic layers were combined and washed with brine (20 mL), dried over MgSO_4 , filtered and concentrated to a brown oil. This oil was distilled by Kugelrohr ($65\text{ }^{\circ}\text{C}$, 0.2 mmHg) to give 4.982 g of **1.67** (86%). $^1\text{H NMR}$ (CDCl_3 , 300 MHz): δ 1.26 (s, 6H), 1.99 (t, $J = 3.6\text{ Hz}$, 1H), 2.42 (d, $J = 3.6\text{ Hz}$, 2H), 4.12 (q, $J = 9.6\text{ Hz}$, 2H). $^{13}\text{C NMR}$ (CDCl_3 , 100 MHz): δ 14.2, 24.5, 29.5, 41.9, 60.7, 70.4, 81.0, 176.5. HRMS (EI) calc. for $\text{C}_8\text{H}_{11}\text{O}_2$ ($\text{M}^+ - \text{CH}_3$) 139.0757, found 139.0759. Anal. calc. for $\text{C}_9\text{H}_{14}\text{O}_2$: C, 70.10; H, 9.15. Found: C, 70.25; H, 9.42.

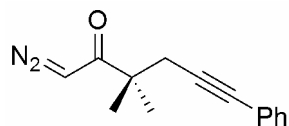


Preparation of 2,2-dimethyl-5-phenyl ethyl pentynoate: 1.67 (4.63g, 30 mmol) was added to a solution of dry, degassed triethylamine/acetonitrile (100 mL, 1:4, 0.3 M) and iodobenzene (6.71 mL, 60 mmol). After stirring at room temperature for 10 min, $\text{Pd}(\text{PPh}_3)_4$ (243 mg, 0.21 mmol, 0.7 mol%) and CuI (286 mg, 1.5 mmol, 5 mol%) were added. The reaction mixture was stirred at room temperature in the dark for 20 h. The crude mixture was then filtered through a plug of celite and concentrated to a yellow oil. The oil was purified by flash chromatography (10% ethyl acetate/hexanes) to afford the product as a colorless oil (6.13 g, 26.6 mmol, 89%). $^1\text{H NMR}$ (CDCl_3 , 400 MHz): δ 1.30 (t, $J = 6.8\text{ Hz}$, 3H), 1.33 (s, 6H), 2.70 (s, 2H), 4.21 (q, $J = 7.2\text{ Hz}$, 2H), 7.33 (m, 3H), 7.43 (m, 2H). $^{13}\text{C NMR}$ (CDCl_3 , 100 MHz): δ 14.3, 24.7, 30.6, 42.5, 60.7, 82.7, 86.8, 123.8, 127.7, 128.2, 131.6, 176.8. HRMS (EI) calc. for $\text{C}_{15}\text{H}_{18}\text{O}_2$ 230.1303, found 230.1307. Anal. calc. for $\text{C}_{15}\text{H}_{18}\text{O}_2$: C, 78.23; H, 7.88. Found: C, 77.90; H, 8.16.



Preparation of 2,2-dimethyl-5-phenyl-4-pentynoic acid: To a solution of NaOH (1.77 g, 44.4 mmol) in methanol/ H_2O (2:1, 205 mL, 0.1 M) was added the 2,2-dimethyl-5-phenyl ethyl pentynoate (5.11 g, 22.2 mmol). The mixture was heated at reflux ($80\text{ }^{\circ}\text{C}$) for 4 h. After cooling back to room temperature, the crude mixture was concentrated and then diluted with H_2O (15 mL). The aqueous mixture was extracted with Et_2O (3x10 mL). The aqueous layer was acidified to $\text{pH} = 2$ with concentrated HCl and extracted with ethyl acetate (3x20 mL). These extracts were washed with brine ($\sim 10\text{ mL}$), dried over MgSO_4 and concentrated to a white solid (4.18 g, 20.7 mmol, 93%). $^1\text{H NMR}$ (CDCl_3 , 400 MHz): δ 1.42 (s, 6H), 2.74 (s, 2H), 7.32 (m, 3H), 7.43 (m, 2H). $^{13}\text{C NMR}$ (CDCl_3 , 100 MHz): δ 24.4, 30.2, 42.3, 82.9, 86.2, 123.5, 127.7,

128.1, 131.6, 183.3. HRMS (EI) calc. for C₁₃H₁₄O₂ 202.0997, found 202.0994. Anal. calc. for C₁₃H₁₄O₂: C, 77.20; H, 6.98. Found: C, 77.09; H, 7.09.



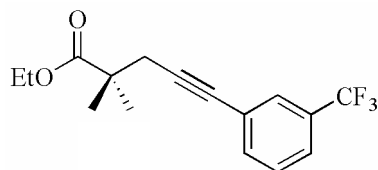
Preparation of 1.36: 2,2-dimethyl-5-phenyl-4-pentynoic acid (4.18 g, 20.7 mmol) was added to a solution of thionyl chloride (2.26 mL, 31.0 mmol) in benzene (34.6 mL, 0.6 M). The mixture was heated at reflux (80 °C) for 16 h, then cooled to room temperature. The crude mixture was concentrated using rotary evaporation then washed with benzene (4x10 mL) to remove remaining SOCl₂. A crude brown oil was obtained and immediately used in the next step.

The acid chloride intermediate was added to Et₂O (35 mL) and cooled to 0 °C. A freshly prepared ethereal solution of diazomethane⁶² at 0 °C (120 mL, 0.1 M) was added portionwise to the acid chloride mixture with stirring. The reaction mixture was then stirred at 0 °C for 1 h. The flask was warmed to room temperature and stirred for 16 h. The reaction mixture was quenched with 1 mL of acetic acid and concentrated using rotary evaporation. The crude yellow oil was purified by flash chromatography (5% ethyl acetate/hexanes) to afford the product as a yellow oil (2.67 g, 12.5 mmol, 60% over two steps). IR: 2099, 1625, 1345 cm⁻¹. ¹H NMR (CDCl₃, 400 MHz): δ 1.27 (s, 6H), 2.82 (s, 2H), 5.52 (s, 1H), 7.26 (m, 3H), 7.38 (m, 2H). ¹³C NMR (CDCl₃, 100 MHz): δ 24.9, 30.5, 46.0, 53.1, 83.3, 86.9, 123.8, 128.1, 128.5, 131.9, 199.6. HRMS (EI) calc. for C₁₄H₁₄ON (M⁺-N) 214.0995, found 214.0994. Anal. calc. for C₁₄H₁₄N₂O: C, 74.31; H, 6.14; N, 12.38. Found: C, 74.02; H, 6.32; N, 12.45.

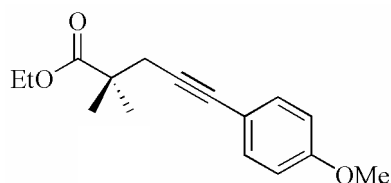
Compounds **1.32**, **1.70-2**, **1.84**, **1.89** and **1.91** were prepared by a method similar to that used for compound **1.36**. For compounds **1.32**, **1.89**, **1.91** and **1.84** the following method was used to generate the intermediate ester:

To a solution of freshly prepared LDA (1.05 equiv) in THF (1.1 M) cooled to -78 °C was added a solution of ethyl isobutyrate in THF (0.9 M) by addition funnel over 1 h with stirring. After addition was complete, the reaction mixture stirred for 20 min at -78 °C and then warmed to 0 °C and stirred for 10 min before cooling back to -78 °C. A solution of the appropriate propargyl mesylate (1.2 equiv; 1-bromo-2-pentyne for **1.32**, 4,4-dimethylpent-2-ynyl methanesulfonate⁶³ for **1.89**, 4-methylpent-4-en-2-ynyl methanesulfonate⁶⁴ for **1.91** and 4-methylpent-2-ynyl methanesulfonate⁶⁴ for **1.84**) in THF (2.1 M) was then added dropwise. The mixture was stirred overnight and warm to room temperature. After quenching with NH₄Cl, the organic layer was separated and the aqueous layer extracted with Et₂O. The organic layers were combined and washed with brine, dried over MgSO₄, filtered and concentrated to a brown oil. This oil was purified by flash chromatography (5% ethyl acetate/hexanes).

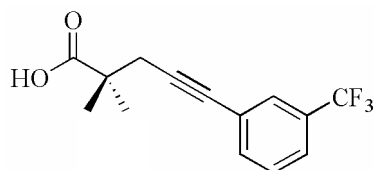
Characterization data for selected intermediate compounds along this synthetic pathway are listed below:



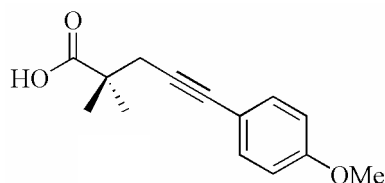
Ethyl 2,2-dimethyl-5-(3-(trifluoromethyl)phenyl)pent-4-ynoate. Pale yellow oil (91%). ^1H NMR (CDCl_3 , 400 MHz): δ 1.28 (t, 3H, $J = 7.2$ Hz), 1.36 (s, 6H), 2.69 (s, 2H), 4.18 (q, 2H, $J = 6.8$ Hz), 7.42 (m, 1H), 7.53 (m, 2H), 7.65 (s, 1H). ^{13}C NMR (CDCl_3 , 100 MHz): δ 14.0, 24.5, 30.4, 42.3, 60.6, 81.2, 88.6, 124.2, 124.6, 128.2, 128.6, 130 (q, $J = 33.0$ Hz), 134.6, 176.4. ^{19}F NMR (CDCl_3 , 339 MHz): δ -62.0. HRMS (EI) calcd for $\text{C}_{16}\text{H}_{17}\text{F}_3\text{O}_2$ 298.117319 found 298.118065; Anal. Calcd for $\text{C}_{16}\text{H}_{17}\text{F}_3\text{O}_2$: C, 64.42; H, 5.74. Found: C, 64.24; H, 5.81.



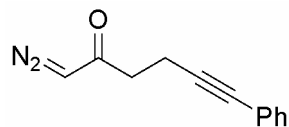
Ethyl 5-(4-methoxyphenyl)-2,2-dimethylpent-4-ynoate. Yellow oil (68%). ^1H NMR (CDCl_3 , 400 MHz): δ 1.29 (t, 3H, $J = 7.2$ Hz), 1.36 (s, 6H), 2.67 (s, 2H), 3.81 (s, 3H), 4.20 (q, 2H, $J = 7.2$ Hz), 6.84 (d, 2H, $J = 9.6$ Hz), 7.45 (d, 2H, $J = 9.6$ Hz). ^{13}C NMR (CDCl_3 , 100 MHz): δ 14.2, 24.6, 30.6, 42.5, 55.2, 60.6, 82.4, 85.1, 113.8, 115.9, 132.9, 159.2, 176.8. HRMS (EI) calcd for $\text{C}_{16}\text{H}_{20}\text{O}_3$ 260.14120 found 260.14125; Anal. Calcd for $\text{C}_{16}\text{H}_{20}\text{O}_3$: C, 73.82; H, 7.74. Found: C, 73.61; H, 8.02.



2,2-Dimethyl-5-(3-(trifluoromethyl)phenyl)pent-4-ynoic acid. White solid (86%). ^1H NMR (CDCl_3 , 400 MHz): δ 1.39 (s, 6H), 2.71 (s, 2H), 7.40 (m, 1H), 7.54 (m, 2H), 7.64 (s, 1H). ^{13}C NMR (CDCl_3 , 100 MHz): δ 24.4, 30.2, 42.3, 81.5, 88.1, 124.3, 125.1, 128.3, 128.7, 130.5 (q, $J = 33.0$ Hz), 134.7, 183.0. HRMS (EI) calcd for $\text{C}_{14}\text{H}_{13}\text{F}_3\text{O}_2$ 270.08677 found 230.08677; Anal. Calcd for $\text{C}_{14}\text{H}_{13}\text{F}_3\text{O}_2$: C, 62.22; H, 4.85. Found: C, 61.91; H, 4.83.

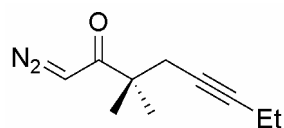


5-(4-Methoxyphenyl)-2,2-dimethylpent-4-ynoic acid. Peach solid (80%). ^1H NMR (CDCl_3 , 400 MHz): δ 1.41 (s, 6H), 2.71 (s, 2H), 3.84 (s, 3H), 6.84 (d, 2H, $J = 8.8$ Hz), 7.37 (d, 2H, $J = 8.8$ Hz). ^{13}C NMR (CDCl_3 , 100 MHz): δ 24.5, 30.3, 42.4, 55.3, 82.7, 84.6, 113.9, 115.8, 133.0, 159.2, 183.2. HRMS (EI) calcd for $\text{C}_{14}\text{H}_{16}\text{O}_3$ 232.10982 found 232.10995; Anal. Calcd for $\text{C}_{14}\text{H}_{16}\text{O}_3$: C, 72.39; H, 6.94. Found: C, 72.08; H, 7.29.

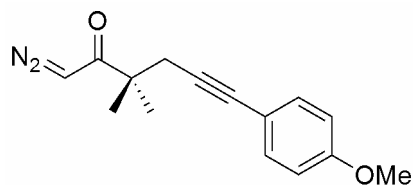


1.87. Yellow oil. ^1H NMR (CDCl_3 , 600 MHz): δ 2.62 (br s, 2H), 2.74 (t, $J = 7.2$ Hz, 2H), 5.36 (br s, 1H), 7.26 (m, 3H), 7.38 (m, 2H). ^{13}C NMR (CDCl_3 , 100 MHz): δ 15.1, 39.6, 54.7, 81.3, 88.2, 123.4, 127.8, 128.2, 131.6, 192.7. LRMS (EI): $m/z = 171$ ($\text{M}^+ - \text{N}_2$). Note: the ester precursor to compound **1.87** was prepared by the method of Uemura *et al.*⁶⁵ All subsequent synthetic steps followed the same method detailed above.

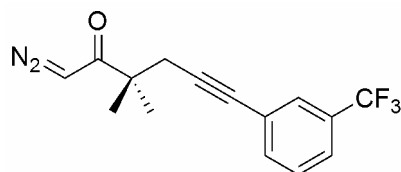
Characterization Data for All End-Product Diazo Compounds



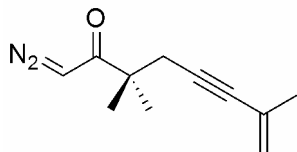
1.32. Yellow oil. ^1H NMR (CDCl_3 , 400 MHz): δ 1.08 (t, $J = 7.6$ Hz, 3H), 1.17 (s, 6H), 2.13 (qt, $J = 2.4$ and 7.6, 2H), 2.30 (t, $J = 2.4$ Hz, 2H). ^{13}C NMR (CDCl_3 , 100 MHz): δ 12.4, 14.2, 24.5, 29.7, 45.6, 52.6, 75.6, 84.3, 199.6. This compound was prepared, isolated and characterized by Dr. Benjamin Sherry.



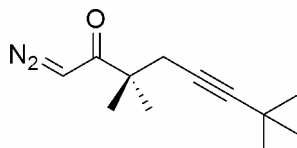
1.71. Yellow oil. IR: 2100, 1606, 1508, 1346, 1245 cm^{-1} . ^1H NMR (CDCl_3 , 400 MHz): δ 1.26 (s, 6H), 2.02 (s, 2H), 2.58 (s, 2H), 3.79 (s, 3H), 5.53 (s, 1H), 6.79 (d, $J = 8.8$ Hz, 2H), 7.28 (d, $J = 8.8$ Hz, 2H). ^{13}C NMR (CDCl_3 , 100 MHz): δ 14.1, 24.6, 45.7, 52.7, 55.2, 82.7, 84.9, 113.8, 115.6, 132.9, 159.2, 199.4. HRMS (EI) calc. for $\text{C}_{15}\text{H}_{16}\text{O}_2$ ($\text{M}^+ - \text{N}_2$) 228.1144, found 228.1150.



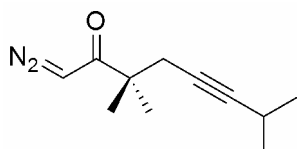
1.70. Yellow oil. IR: 2102, 1627, 1332, 1124 cm^{-1} . ^1H NMR (CDCl_3 , 400 MHz): δ 1.28 (s, 6H), 2.66 (s, 2H), 5.53 (s, 1H), 7.39 (m, 1H), 7.52 (m, 2H), 7.62 (s, 1H). ^{13}C NMR (CDCl_3 , 100 MHz): δ 24.6, 30.3, 45.6, 52.8, 81.6, 88.5, 124.3, 124.5, 127.8, 128.3, 130 (q, $J = 33.0$ Hz), 134.7, 199.0. LRMS (EI): $m/z = 294$ (M^+). Anal. calc. for $\text{C}_{15}\text{H}_{13}\text{N}_2\text{OF}_3$: C, 61.22; H, 4.45; N, 9.52. Found: C, 60.97; H, 4.44; N, 9.20.



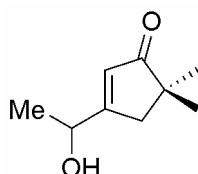
1.84. Yellow oil. IR: 2010, 1737, 1626, 1349, 1241, 1150 cm^{-1} . ^1H NMR (CDCl_3 , 400 MHz): δ 1.27 (s, 6H), 1.91 (s, 3H), 2.54 (s, 2H), 5.20 (s, 1H), 5.25 (s, 1H), 5.53 (s, 1H). ^{13}C NMR (CDCl_3 , 125 MHz): δ 24.1, 25.0, 30.5, 46.1, 53.1, 84.8, 86.1, 121.3, 127.4, 199.7. HRMS (EI) calc. for $\text{C}_{11}\text{H}_{14}\text{N}_2\text{O}$ 190.1109, found 190.1106.



1.89. Yellow oil. IR: 2099, 1625, 1468, 1348, 1266, 1150 cm^{-1} . ^1H NMR (CDCl_3 , 400 MHz): δ 1.24 (s, 15H), 1.61 (s, 2H), 2.36 (s, 2H), 5.54 (s, 1H). ^{13}C NMR (CDCl_3 , 125 MHz): δ 24.3, 27.3, 29.6, 31.2, 45.6, 52.5, 91.7, 199.7. HRMS (EI) calc. for $\text{C}_{12}\text{H}_{18}\text{N}_2\text{O}$ 206.1417, found 206.1419.

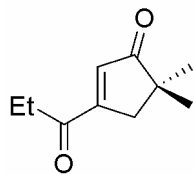


1.91. Yellow oil. IR: 2094, 1598, 1308, 1276 cm^{-1} . ^1H NMR (CDCl_3 , 400 MHz): δ 1.17 (s, 3H), 1.19 (s, 3H), 1.24 (s, 6H), 2.37 (d, $J = 2.4$ Hz, 2H), 2.56 (septet, $J = 2.4$ Hz, 1H), 5.53 (s, 1H). ^{13}C NMR (CDCl_3 , 100 MHz): δ 20.6, 23.3, 24.5, 29.7, 45.7, 52.6, 75.7, 88.8, 199.7. HRMS (EI) calc. for $\text{C}_{11}\text{H}_{16}\text{N}_2\text{O}$ 192.1266, found 192.1263.

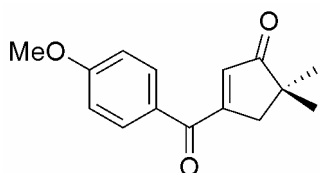


Preparation of 3-(1-hydroxyethyl)cyclopent-2-enone (1.43): The compound was prepared according to the published procedure.¹⁷ IR: 3403, 1692, 1613 cm^{-1} . ^1H NMR (CDCl_3 , 500 MHz): δ 1.44 (d, 3H, $J = 6.5$ Hz), 2.45 (t, 2H, $J = 5.0$ Hz), 2.64 (m, 2H), 4.65 (q, 1H, $J = 6.5$ Hz), 6.13 (s, 1H). ^{13}C NMR (CDCl_3 , 125 MHz): δ 22.0, 27.8, 35.2, 67.7, 127.9, 184.0, 209.6. Spectral data was consistent with the values previously reported.^{17b}

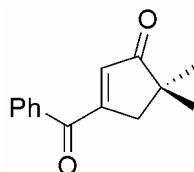
General Procedure for Diazocompound Oxidative Rearrangements Catalyzed by $\text{Ph}_3\text{PAuCl/AgSbF}_6$: A 0.10 mmol sample of starting material was dissolved in 1.0 mL of CH_2Cl_2 (0.1 M) in a scintillation vial. Four equivalents of diphenyl sulfoxide were added and the reaction mixture was cooled to 0 $^\circ\text{C}$. Then, 10 mol% of premixed catalyst in 0.1 mL CH_2Cl_2 was added. Moderate bubbling ensued and when the bubbling had dissipated, the vial was sealed and the reaction mixture was maintained at 0 $^\circ\text{C}$ for 2 h. Crude reaction mixtures were purified by flash chromatography (5% ethyl acetate/hexanes).



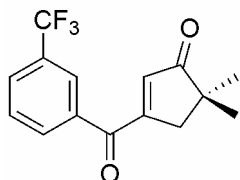
1.35. Pale yellow solid (29%): IR: 3062, 2978, 2937, 1703, 1681, 1467, 1376, 1178, 1120 cm^{-1} . ^1H NMR (CDCl_3 , 400 MHz): δ 1.13 (s, 6H), 1.15 (t, $J = 7.2$ Hz, 3H), 2.64 (d, $J = 2.0$ Hz, 2H), 2.82 (q, $J = 7.2$ Hz, 2H). ^{13}C NMR (CDCl_3 , 100 MHz): δ 7.6, 24.9, 33.5, 43.0, 44.5, 133.5, 165.8, 200.2, 215.0. RMS (EI) calc. for $\text{C}_{10}\text{H}_{14}\text{O}_2$ 166.0992, found 166.0994. Anal. calc. for $\text{C}_{10}\text{H}_{14}\text{O}_2$: C, 72.26; H, 8.49. Found: C, 71.07; H, 8.53.



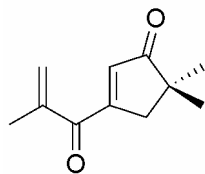
1.73. Pale yellow solid (88%): ^1H NMR (CDCl_3 , 400 MHz): δ 1.26 (s, 6H), 2.89 (s, 2H), 3.92 (s, 3H), 6.35 (s, 1H), 6.99 (d, $J = 7.2$ Hz, 2H), 7.92 (d, $J = 6.8$ Hz, 2H). ^{13}C NMR (CDCl_3 , 125 MHz): δ 24.9, 44.2, 45.2, 55.6, 114.1, 128.4, 128.6, 130.1, 131.7, 133.1, 164.3, 167.7, 192.4, 214.1. HRMS (EI) calc. for $\text{C}_{15}\text{H}_{16}\text{O}_3$ 244.1098, found 244.1099.



1.37. Pale yellow oil (80%): IR: 1710, 1655, 1234 cm^{-1} . ^1H NMR (CDCl_3 , 400 MHz): δ 1.22 (s, 6H), 2.86 (s, 2H), 6.37 (s, 1H), 7.50 (t, $J = 8.0$ Hz, 2H), 7.63 (t, $J = 7.2$ Hz, 1H), 7.84 (d, $J = 7.2$ Hz, 2H). ^{13}C NMR (CDCl_3 , 100 MHz): δ 25.0, 44.4, 44.8, 128.9, 129.3, 133.9, 134.4, 136.1, 166.7, 193.9, 214.1. HRMS (EI) calc. for $\text{C}_{14}\text{H}_{14}\text{O}_2$ 214.0997, found 214.0994.

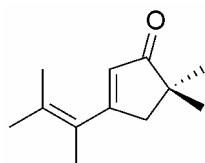


1.74. Pale yellow solid (65%): ^1H NMR (CDCl_3 , 400 MHz): δ 1.28 (s, 6H), 2.94 (s, 2H), 6.46 (s, 1H), 7.71 (t, $J = 7.6$ Hz, 1H), 7.94 (d, $J = 7.6$ Hz, 1H), 8.07 (d, $J = 7.6$ Hz, 1H), 8.15 (s, 1H). ^{13}C NMR (CDCl_3 , 100 MHz): δ 24.9, 44.5, 125.7, 129.5, 130.1, 132.3, 135.2, 136.7, 165.3, 192.2, 213.4. HRMS (EI) calc. for $\text{C}_{15}\text{H}_{13}\text{F}_3\text{O}_2$ 282.0867, found 282.0868. Anal. calc. for $\text{C}_{15}\text{H}_{13}\text{F}_3\text{O}_2$: C, 63.83; H, 4.64. Found: C, 63.83; H, 4.79.

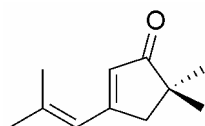


1.86. Pale yellow solid (53%): ^1H NMR (CDCl_3 , 500 MHz): δ 1.16 (s, 9H), 1.98 (s, 3H), 2.75 (s, 2H), 5.91 (s, 1H), 6.02 (s, 1H), 6.28 (s, 1H). ^{13}C NMR (CDCl_3 , 125 MHz): δ 17.0, 24.6, 43.9, 44.8, 128.5, 132.9, 166.9, 195.6, 213.4. HRMS (EI) calc. for $\text{C}_{11}\text{H}_{14}\text{O}_2$ 178.0996, found 178.0994.

General Procedure for Diazocompound Cyclization Reactions Catalyzed by $\text{Ph}_3\text{PAuCl/AgSbF}_6$: A 0.10 mmol sample of starting material was dissolved in 1.0 mL of CH_2Cl_2 (0.1 M) in a scintillation vial. Then, 10 mol% of premixed catalyst in 0.1 mL CH_2Cl_2 was added. Moderate bubbling ensued and when the bubbling had dissipated, the vial was sealed and the reaction mixture was maintained room temperature for 2h. Crude reaction mixtures were purified by flash chromatography (5% ethyl acetate/hexanes).

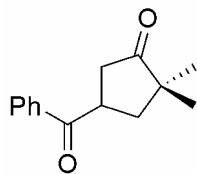


1.90. Pale yellow oil (74%): ^1H (CDCl_3 , 400 MHz): δ 1.15 (s, 6H), 1.80 (s, 3H), 1.82 (s, 6H), 2.58 (d, $J = 2.0$ Hz, 2H), 5.85 (s, 1H). ^{13}C NMR (CDCl_3 , 100 MHz): δ 17.2, 21.6, 22.7, 25.2, 43.6, 48.1, 125.9, 127.9, 133.6, 176.6, 214.6. HRMS (EI) calc. for $\text{C}_{12}\text{H}_{18}\text{O}$ 178.1356, found 178.1358.

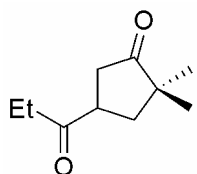


1.92. Pale yellow oil (86%): ^1H (CDCl_3 , 500 MHz): δ 1.12 (s, 6H), 1.95 (s, 3H), 1.97 (s, 3H), 2.18 (s, 2H), 5.93 (s, 1H), 6.03 (s, 1H). ^{13}C NMR (CDCl_3 , 125 MHz): δ 20.9, 25.2, 28.3, 43.5, 48.7, 121.9, 126.9, 147.4, 169.8, 214.4. HRMS (EI) calc. for $\text{C}_{11}\text{H}_{16}\text{O}$ 164.1202, found 164.1201.

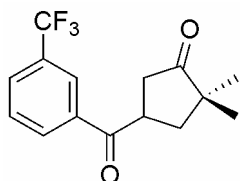
General Procedure for Lewis acid catalyzed cyclization reaction: A 0.110 mmol sample of diazoketone was dissolved in 1.1 mL (0.1 M) acetone in a scintillation vial and 15 mol % $\text{In}(\text{OTf})_3$ was added. Moderate bubbling ensued and when the bubbling had dissipated, the vial was capped and the reaction mixture was maintained at room temperature for 24 h. Crude reaction mixtures were purified by flash chromatography (5% ethyl acetate/hexanes).



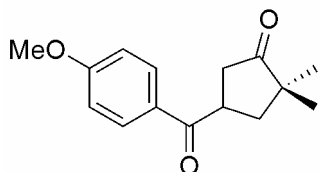
1.49. Pale yellow oil (48%): ^1H NMR (CDCl_3 , 400 MHz): δ 1.16 (s, 3H), 1.20 (s, 3H), 2.00 (dd, $J = 10.8$ and 12.8 Hz, 1H), 2.27 (dd, $J = 7.2$ and 12.8 Hz, 1H), 2.62 (dd, $J = 7.2$ and 18.8 Hz, 1H), 2.90 (dd, $J = 10.0$ and 18.8 Hz, 1H), 4.11 (quintet, $J = 2.4$ Hz, 1H), 7.55 (t, $J = 8.0$ Hz, 2H), 7.65 (t, $J = 7.6$ Hz, 1H), 8.03 (d, $J = 7.6$ Hz, 2H). ^{13}C NMR (CDCl_3 , 100 MHz): δ 24.0, 24.5, 39.7, 40.0, 42.8, 46.3, 128.4, 128.9, 133.5, 136.1, 200.3, 220.2. HRMS (EI) calcd for $\text{C}_{14}\text{H}_{16}\text{O}_2$ 216.1154 found 216.1150; Anal. Calcd for $\text{C}_{14}\text{H}_{16}\text{O}_2$: C, 77.75; H, 7.46. Found: C, 77.43; H, 7.68.



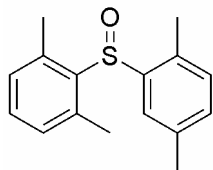
1.77. Pale yellow oil (43%): ^1H NMR (CDCl_3 , 400 MHz): δ 1.08 (s, 3H), 1.14 (s, 3H), 1.15 (t, 3H, $J = 8.0$ Hz), 1.83 (t, 1H, $J = 10.2$ Hz), 2.18 (m, 2H), 2.4-2.75 (m, 4H), 3.25 (quintet, 1H, $J = 3.2$ Hz). ^{13}C NMR (CDCl_3 , 100 MHz): δ 7.74, 23.8, 24.3, 35.0, 38.9, 41.7, 44.2, 46.3, 211.2, 220.1. HRMS (EI) calcd for $\text{C}_{10}\text{H}_{16}\text{O}_2$ 168.11505 found 168.11503.



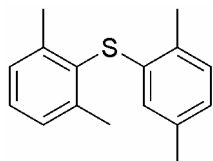
1.76. Pale yellow oil (31%): ^1H NMR (CDCl_3 , 400 MHz): δ 1.18 (s, 3H), 1.24 (s, 3H), 2.00 (dd, 1H, $J = 12.8$ Hz, 10.4 Hz), 2.27 (dd, 1H, $J = 7.2$ Hz, 13.2 Hz), 2.62 (dd, 1H, $J = 10.8$ Hz, 18.8 Hz), 2.90 (dd, 1H, $J = 9.6$ Hz, 18.8 Hz), 4.11 (quintet, 1H, $J = 7.6$ Hz), 7.71 (t, 1H, $J = 8.0$ Hz), 7.91 (d, 1H, $J = 7.6$ Hz), 8.21 (d, 1H, $J = 7.6$ Hz), 8.36 (s, 1H). ^{13}C NMR (CDCl_3 , 125 MHz): δ 24.0, 24.4, 39.4, 40.0, 42.5, 46.2, 125.2, 129.5, 129.8, 131.5, 136.5, 199.0, 219.5. HRMS (EI) calcd for $\text{C}_{15}\text{H}_{15}\text{F}_3\text{O}_2$ 284.10289 found 284.10242.



1.75. Pale yellow solid (70%): ^1H NMR (CDCl_3 , 400 MHz): δ 1.15 (s, 3H), 1.19 (s, 3H), 2.02 (m, 2H), 2.23 (m, 2H), 3.93 (s, 3H), 7.01 (d, 2H, $J = 9.6$ Hz), 8.02 (d, 2H, $J = 9.6$ Hz). ^{13}C NMR (CDCl_3 , 125 MHz): δ 24.0, 24.5, 39.4, 39.7, 42.8, 46.2, 55.5, 114.0, 128.9, 130.7, 163.8, 198.7, 220.6. LRMS (EI): $m/z = 248$ ($\text{M}^+ + 2$).



1.80. White solid. ^1H NMR (CDCl_3 , 600 MHz): δ 1.97 (s, 3H), 2.40 (s, 3H), 2.47 (s, 6H), 7.01 (m, 3H), 7.13 (d, $J = 7.2$ Hz, 1H), 7.24 (t, $J = 7.6$ Hz, 1H), 7.80 (s, 1H). ^{13}C NMR (CDCl_3 , 150 MHz): δ 18.4, 19.5, 21.1, 126.8, 130.1, 130.7, 131.0, 131.7, 135.8, 140.3. HRMS (EI) calcd for $\text{C}_{16}\text{H}_{18}\text{SO}$ 258.1082 found 258.1078. The material was synthesized by Nathan Shapiro.



1.81. White solid. ^1H NMR (CDCl_3 , 600 MHz): δ 2.12 (s, 3H), 2.42 (s, 9H), 6.24 (s, 1H), 6.81 (d, $J = 7.2$ Hz, 1H), 7.04 (d, $J = 7.2$ Hz), 7.20 (d, $J = 7.8$ Hz, 2H), 7.26 (m, 1H). ^{13}C NMR (CDCl_3 , 150 MHz): δ 19.5, 21.1, 21.8, 124.8, 125.3, 128.4, 129.0, 129.8, 130.7, 131.8, 135.9, 136.6, 143.9. HRMS (EI) calcd for $\text{C}_{16}\text{H}_{18}\text{S}$ 242.1135 found 242.1129. The material was synthesized by Nathan Shapiro.

Preparation of Triphenylphosphinegold(I) oxonium tetrafluoroborate (1.53b): The compound was prepared from $\text{Ph}_3\text{PAuCl}^{29,49}$ according to the published procedure.¹⁶ ^1H NMR (CDCl_3 , 400 MHz): δ 7.32-7.36 (m, 6H), 7.45-7.54 (m, 9H). ^{13}C NMR (CDCl_3 , 100 MHz): δ 128.8, 129.1, 129.3, 132.1, 133.8, 134.0. ^{31}P NMR (CDCl_3 , 162 MHz): δ 23.8. LRMS (FAB): $m/z = 1393$ ($\text{M}^+ - \text{BF}_4$). Spectral data was consistent with the values previously reported.¹⁶

Preparation of $[\text{Au}(\text{bpy})(\text{OH})_2][\text{PF}_6]$ (1.60): The compound was prepared according to the published procedure.²⁵ ^1H NMR ($(\text{CD}_3)_2\text{CO}$, 400 MHz): δ 4.15 (s, 2H), 8.25 (t, 2H, $J = 8.8$ Hz), 8.76 (t, 2H, $J = 10.0$ Hz), 8.92 (d, 2H, $J = 10.8$ Hz), 9.14 (d, 2H, $J = 7.2$ Hz). Spectral data was consistent with the values previously reported.²⁵

Preparation of $[\{\text{Au}(\text{bpy})(\mu\text{-O})\}_2][\text{PF}_6]$ (1.61): The compound was prepared according to the published procedure.²⁵ ^1H NMR (CD_3CN , 300 MHz): δ 8.08 (m, 2H), 8.48-8.53 (m, 4H), 8.64 (d, 2H, $J = 7.6$ Hz). Spectral data was consistent with the values previously reported.²⁵

Preparation of $[\text{Au}(\text{bpy})\text{Cl}_2][\text{PF}_6]$ (1.62): The compound was prepared according to the published procedure.²⁵ ^1H NMR ($(\text{CD}_3)_2\text{CO}$, 400 MHz): δ 8.31 (m, 2H), 8.84 (t, 2H, $J = 8.0$ Hz), 9.00 (d, 2H, $J = 8.0$ Hz), 9.62 (d, 2H, $J = 5.6$ Hz). Spectral data was consistent with the values previously reported.²⁵

Preparation of $[\text{Au}(\text{terpy})\text{Cl}]\text{Cl}_2 \cdot 3\text{H}_2\text{O}$ (1.63): The compound was prepared according to the published procedure.²⁶ ^1H NMR ($(\text{CD}_3)_2\text{CO}$, 300 MHz): δ 7.41-7.46 (m, 2H), 7.94-8.09 (m, 3H), 8.51 (m, 2H), 8.68 (m, 4H). Spectral data was consistent with the values previously reported.²⁶

Preparation of [Au(terpy)Cl][ClO₄] (1.64): The compound was prepared according to the published procedure.²⁶ ¹H NMR (D₂O, 300 MHz): δ 8.03 (m 2H), 8.69 (m 7H), 9.17 (d, 2H, J = 8.0 Hz). Spectral data was consistent with the values previously reported.²⁶

Preparation of [Au(terpy)(OH)][ClO₄] (1.65): The compound was prepared according to the published procedure.²⁶ ¹H NMR (D₂O, 300 MHz): δ 8.10 (m, 2H), 8.61 (m, 7H), 8.88 (d, 2H, J = 7.6 Hz). Spectral data was consistent with the values previously reported.²⁶

Preparation of IPrAuCl (1.66): The compound was prepared according to the published procedure.²⁷ ¹H NMR (CD₂Cl₂, 400 MHz): δ 1.26 (d, 12 H, J = 6.8 Hz), 1.37 (d, 12 H, J = 6.8 Hz), 2.60 (septet, 4H, J = 6.8 Hz), 7.27 (s, 2H), 7.38 (d, 4H, J = 7.6 Hz), 7.60 (t, 2H, J = 8.0 Hz). ¹³C NMR (CD₂Cl₂, 100 MHz): δ 23.7, 24.1, 28.7, 123.2, 124.2, 130.6, 134.0, 145.7, 175.1. Spectral data was consistent with the values previously reported.²⁷

Preparation of [(AuP(*o*-tolyl)₃)₃O][BF₄] (1.54): To a solution of (*o*-tolyl)₃PAuCl¹⁶ (915 mg, 1.71 mmol) in acetone (170 mL), freshly prepared silver(I) oxide (1.42 g, 6.14 mmol) and NaBF₄ (1.00 g, 9.11 mmol) were added. The resulting brown heterogeneous mixture was stirred at room temperature for two hours in the dark. The crude mixture was then concentrated to dryness and the black solid extracted with CH₂Cl₂ (3 x 9 mL). The extracts were filtered to give a colorless liquid. Et₂O was added to precipitate a white solid which was filtered under suction, washed with Et₂O (2 x 10 mL), and dried in vacuo to give 710 mg of a white solid (78%). ¹H NMR (CD₂Cl₂, 400 MHz): δ 2.37 (s, 9H), 6.86 (m, 3H), 7.19 (d, 6H, J = 6.0 Hz), 7.51 (t, 3H, J = 7.2 Hz). ¹³C NMR (CD₂Cl₂, 100 MHz): δ 22.5, 124.1, 124.7, 126.8, 132.2, 133.3, 142.4. ³¹P (CD₂Cl₂, 162 MHz): -1.67. LRMS (FAB): *m/z* = 1520 ((M⁺+1)-BF₄) (MW too large for HRMS); Anal. Calcd for C₆₃H₆₃Au₃BF₄OP₃: C, 47.09; H, 3.95. Found: C, 46.65; H, 3.98.

Preparation of [(AuP(*p*-CF₃)C₆H₄)₃)₃O][BF₄] (1.53c): To a solution of ((*p*-CF₃)C₆H₄)₃PAuCl^{28b} (603 mg, 0.86 mmol) in acetone (86 mL), freshly prepared silver(I) oxide (721 mg, 3.11 mmol) and NaBF₄ (474 mg, 4.315 mmol) were added. The resulting brown heterogeneous mixture was stirred at room temperature for two hours in the dark. The crude mixture was then concentrated to dryness and the black solid extracted with CH₂Cl₂ (3 x 9 mL). The extracts were filtered to give a colorless liquid. Pentane was added to precipitate a white solid which was filtered under suction, washed with pentane (2 x 10 mL), and dried in vacuo to give 395 mg of a white solid (66%). ¹H NMR (CDCl₃, 400 MHz): δ 7.66-7.73 (m, 36H). ³¹P (CD₂Cl₂, 162 MHz): 24.4. LRMS (FAB): *m/z* = 2005.5 (M⁺-BF₄) (MW too large for HRMS); Anal. Calcd for C₆₃H₃₅Au₃BF₃₁OP₃B: C, 36.12; H, 1.73. Found: C, 36.12; H, 1.57.

Preparation of [(AuP(*t*-Bu)₃)₃O][BF₄] (1.53e): To a solution of ((*t*-Bu)₃PAuCl^{28e} (225 mg, 0.52 mmol) in acetone (52 mL), freshly prepared silver(I) oxide (432 mg, 1.865 mmol) and NaBF₄ (318 mg, 2.90 mmol) were added. The resulting brown heterogeneous mixture was stirred at room temperature for two hours in the dark. The crude mixture was then concentrated to dryness and the black solid extracted with CH₂Cl₂ (3 x 9 mL). The extracts were filtered to give a colorless liquid. This liquid was then concentrated to dryness to give 203 mg of a brown solid (90%). ¹H NMR (CDCl₃, 400 MHz): δ 1.51 (s, J = 14.0 Hz). ¹³C NMR (CD₂Cl₂, 100 MHz): δ 30.0, 31.9. ³¹P (CD₂Cl₂, 162 MHz): 82.7. HRMS (FAB) calcd for C₃₆H₈₁Au₃OP₃ 1213.4465 found 1213.4497.

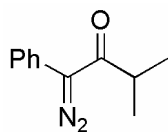
Preparation of [(AuP(C₆F₅)₃O)]BF₄ (1.53d): To a solution of (C₆F₅)₃PAuCl^{28a,c} (330 mg, 0.43 mmol) in acetone (31 mL), freshly prepared silver(I) oxide (360 mg, 1.55 mmol) and NaBF₄ (261 mg, 2.38 mmol) were added. The resulting brown heterogeneous mixture was stirred at room temperature for two hours in the dark. The crude mixture was then concentrated to dryness and the black solid extracted with CH₃Cl (3 x 9 mL). The extracts were filtered to give a colorless liquid. The extracts were filtered to give a colorless liquid. This liquid was then concentrated to dryness to give 255 mg of a brown solid (77%). ³¹P (CD₂Cl₂, 162 MHz): -12.13. Anal. Calcd for C₅₄Au₃BF₄₉OP₃: C, 28.32. Found: C, 28.67. Spectral data was consistent with the values previously reported.⁶⁶

Preparation of [(AuP(*p*-OMe)C₆H₄)₃O)]BF₄ (1.53a): To a solution of ((*p*-OMe)C₆H₄)₃PAuCl^{28d} (330 mg, 0.43 mmol) in acetone (31 mL), freshly prepared silver(I) oxide (360 mg, 1.55 mmol) and NaBF₄ (261 mg, 2.38 mmol) were added. The resulting brown heterogeneous mixture was stirred at room temperature for two hours in the dark. The crude mixture was then concentrated to dryness and the black solid extracted with CH₃Cl (3 x 9 mL). The extracts were filtered to give a colorless liquid. The extracts were filtered to give a colorless liquid. This liquid was then concentrated to dryness to give a light brown solid. This solid was dissolved in benzene (~10 mL) and ether was added. The ether layer was removed and concentrated to give 43 mg of light brown solid (8.4%). ¹H NMR (CD₂Cl₂, 400 MHz): δ 3.78 (s, 27H), 6.80 (d, 18H, J = 11.6 Hz), 7.40 (m, 18H). ¹³C NMR (CD₂Cl₂, 100 MHz): δ 55.5, 114.7, 119.2, 120.0, 135.3, 162.2. ³¹P (CD₂Cl₂, 162 MHz): 18.16. LRMS (FAB): *m/z* = 1664 ((M⁺+1)-BF₄) (MW too large for HRMS); Anal. Calcd for C₆₃H₆₃Au₃BF₄O₁₀P₃: C, 43.22; H, 3.63. Found: C, 43.03; H, 3.47. Spectral data was consistent with the values previously reported.⁶⁶

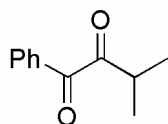
Preparation of (XANTPHOS)AuCl (1.57): The compound was prepared according to the published procedure.²⁴ ¹H NMR (CDCl₃, 400 MHz): δ 1.66 (s, 6 H), 6.55–6.65 (m, 2H), 7.11 (t, 2H, J = 8.0 Hz), 7.22–7.36 (m, 12H), 7.40–7.50 (m, 8H), 7.56 (d, 2H, J = 8.0 Hz). ¹³C NMR (CDCl₃, 100 MHz): δ 28.0 (CH₃), 35.7, 119.3, 124.7, 127.0, 128., 130.3, 131.7, 133.0, 133., 134.1, 155.1. ³¹P NMR (CDCl₃, 162 MHz): δ 28.26. Spectral data was consistent with the values previously reported.²⁴

Preparation of [(AuPPh₃)₃O)]BPh₄ (1.55): To a solution of [(AuPPh₃)₃O)]BF₄ (300 mg, 203 mmol) in acetone (40 mL) was added a solution of NaBF₄ (269 mg, 783 mmol) in methanol (55 mL). The mixture was stirred at room temperature for 20 h. and concentrated to dryness. The solid was extracted with CH₂Cl₂ and the extract was concentrated to a grey solid. This solid was dissolved in an acetone/methanol mixture (0.6 mL/0.4 mL) and rotvapped until white solid precipitated. This white solid was filtered and dried in vacuo to yield 197 mg of product (57%). ¹H NMR (CD₂Cl₂, 500 MHz): δ 7.05 (m, 8H), 7.23 (m, 12H), 7.49-7.56 (m, 27H), 7.61-7.64 (m, 18H). ³¹P NMR (CD₂Cl₂, 162 MHz): δ 42.1. LRMS (FAB): *m/z* = 1409 (M⁺-BF₄+O) (MW too large for HRMS); Anal. Calcd for C₇₈H₆₅Au₃OBP₃: C, 54.69; H, 3.82. Found: C, 54.62; H, 3.72.

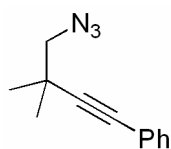
Preparation of In(ONf)₃ (1.51): The compound was prepared according to the published procedure.²¹ ¹⁹F NMR (CD₃CN, 339 MHz): δ -125.9, -121.4, -113.8, -80.9. Spectral data was consistent with the values previously reported.²¹



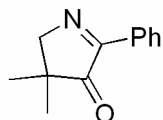
Preparation of 1.82. To a flask containing benzyl isopropyl ketone (811 mg, 5.0 mmol) in acetonitrile (17 mL, 0.3 M) was added *p*-toluenesulfonyl azide (1.18 g, 6.0 mmol). The reaction mixture was cooled to 0 °C and DBU (0.90 mL, 6.0 mmol) was added dropwise and the mixture was warmed to room temperature. The mixture was then stirred at room temperature for 15 h. Then, NaHCO₃ (saturated, 15 mL) was added and the aqueous phase was extracted with Et₂O (3x10 mL). The organic layers were combined and washed with brine (20 mL), dried over MgSO₄, filtered and concentrated to a brown oil. The oil was purified by flash chromatography (7% ethyl acetate/hexanes) to afford the product as an orange oil (682 mg, 3.6 mmol, 72%). ¹H NMR (CDCl₃, 400 MHz) δ 1.23 (s, 3H), 1.25 (s, 3H), 3.03 (quintet, *J* = 6.8 Hz, 1H), 7.28-7.33 (m, 1H), 7.45 (t, *J* = 8.4 Hz, 2H), 7.57 (d, *J* = 7.2 Hz, 2H). ¹³C NMR (CDCl₃, 100 MHz) δ 18.9, 36.5, 125.8, 126.0, 126.9, 129.0, 197.2. HRMS (EI) calc. for C₁₁H₁₂N₂O 188.0945, found 188.0950.



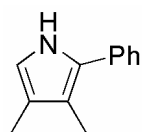
Preparation of 1.83. **1.82** (37.6 mg, 0.2 mmol) was dissolved in CH₂Cl₂ (2 mL, 0.1 M) in a scintillation vial. Diphenyl sulfoxide (162 mg, 0.8 mmol) was added and the reaction mixture was cooled to 0 °C. Then, a premixed solution of Ph₃PAuCl (9.9 mg, 0.02 mmol) and AgSbF₆ (6.9 mg, 0.02 mmol) in CH₂Cl₂ (0.1 mL) was added. Moderate bubbling ensued and when the bubbling had dissipated, the vial was sealed and the reaction mixture was maintained at 0 °C for 3 h. The crude mixture was concentrated and purified by flash chromatography (5% ethyl acetate/hexanes) to yield **1.83** (31.0 mg, 0.18 mmol, 88%). ¹H NMR (CDCl₃, 500 MHz) δ 1.20 (s, 3H), 1.21 (s, 3H), 3.35 (quintet, *J* = 7.0 Hz, 1H), 7.50 (t, *J* = 8.0 Hz, 2H), 7.64 (t, *J* = 6.5 Hz, 1H), 7.92 (d, *J* = 8.5 Hz, 1H). ¹³C NMR (CDCl₃, 125 MHz) δ 16.8, 36.5, 128.8, 129.9, 132.5, 134.5, 194.0, 206.5. This data is consistent with that previously reported.⁶⁷



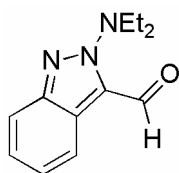
1.93 was prepared by the method of Knouzi *et al.* via tosylation of the corresponding homopropargyl alcohol followed by displacement with sodium azide⁶⁸ and isolated as a clear oil. ¹H NMR (CDCl₃, 500 MHz): δ 1.35 (s, 6H), 3.29 (s, 2H), 7.30 (m, 3H), 7.44 (m, 2H). ¹³C NMR (CDCl₃, 125 MHz): δ 26.6, 33.7, 61.7, 81.8, 93.9, 123.2, 127.9, 128.2, 131.6. HRMS (EI) calc. for C₁₂H₁₃N₃ 199.1108, found 199.1109.



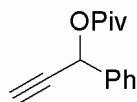
Preparation of 1.94: Compound **1.93** (80.0 mg, 0.4 mmol) was dissolved in CH₂Cl₂ (4.0 mL, 0.1 M) in a scintillation vial. Diphenyl sulfoxide (324 mg, 1.6 mmol) was added followed by premixed IPrAuCl (25 mg, 10 mol%) and AgSbF₆ (14 mg, 10 mol%) in CH₂Cl₂ (0.2 mL). The vial was sealed and the reaction mixture was maintained room temperature for 18 h. The crude reaction mixture was purified by flash chromatography (5% ethyl acetate/hexanes on activated, neutral alumina) to afford **1.94** (53.5 mg, 0.29 mmol, 73%). ¹H NMR (CDCl₃, 400 MHz): δ 1.23 (s, 6H), 4.22 (s, 2H), 7.48-7.56 (m, 3H), 8.28 (d, *J* = 6.8 Hz, 2H). ¹³C NMR (CDCl₃, 125 MHz): δ 23.6, 43.2, 69.5, 128.0, 128.5, 130.9, 131.3, 166.4, 207.3. HRMS (EI) calcd for C₁₂H₁₃NO 187.0997, found 187.0997.



1.95. (4.3 mg, 0.025 mmol, 6%) ¹H NMR (C₆D₆, 400 MHz): δ 2.08 (s, 3H), 2.16 (s, 3H), 6.60 (s, 1H), 7.20-7.39 (m, 5H). This data is consistent with that previously reported.⁶⁹



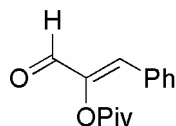
Preparation of 1.109: Triazene **1.107**³⁹ (27.5 mg, 0.14 mmol) was dissolved in CH₂Cl₂ (1.4 mL, 0.1 M) in a scintillation vial. Diphenyl sulfoxide (113 mg, 0.56 mmol) was added followed by premixed IPrAuCl (6.9 mg, 10 mol%) and AgSbF₆ (4.8 mg, 10 mol%) in CH₂Cl₂ (0.1 mL). The vial was sealed and the reaction mixture was maintained room temperature for 2 h. The crude reaction mixture was purified by flash chromatography (5% ethyl acetate/hexanes). ¹H NMR (CD₂Cl₂, 400 MHz): δ 0.88 (t, *J* = 7.2 Hz, 6H), 3.37 (br s, 4H), 7.36-7.57 (m, 2H), 7.79 (d, *J* = 8.4 Hz, 1H), 8.18 (d, *J* = 8.0 Hz, 1H), 10.4 (s, 1H). This data is consistent with that previously reported.³⁹



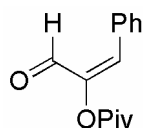
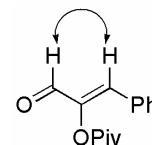
1.105. Prepared via the method of Gulhane *et al.*⁵⁹ as a pale yellow oil (96%). ¹H NMR (CDCl₃, 400 MHz) δ 1.23 (s, 9H), 2.63 (d, *J* = 2.4 Hz, 1H), 6.43 (d, *J* = 2.4 Hz, 1H), 7.35-7.42 (m, 3H), 7.52 (dd, *J* = 1.8 and 7.8 Hz, 2H). ¹³C NMR (CDCl₃, 75 MHz) δ 27.2, 39.0, 65.3, 75.4, 80.7, 127.6, 128.9, 129.1, 137.1, 177.4. HRMS (EI) calc. for C₁₄H₁₆O₂ 216.1153, found 216.1150.

General Procedure for Oxidative Rearrangement of Propargyl Pivaloates: A scintillation vial was charged with propargyl pivaloate, diphenyl sulfoxide (2 equiv), 5Å sieves (20 mg) and the indicated solvent (0.1 M). After stirring for 5 minutes, the catalyst (5 mol%) was added and

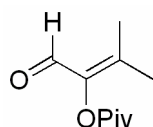
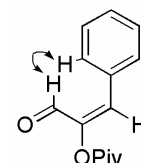
the mixture was stirred for the specified time at the indicated temperature. The crude reaction mixture was purified by flash chromatography (5% ethyl acetate/hexanes).



1.106-(Z). Colorless oil. ^1H NMR (CDCl_3 , 500 MHz) δ 1.41 (s, 9H), 7.01 (s, 1H), 7.42-7.44 (m, 3H), 7.65-7.67 (m, 2H), 9.40 (s, 1H). ^{13}C NMR (CDCl_3 , 125 MHz) δ 27.6, 39.6, 129.3, 130.8, 131.2, 132.2, 136.9, 146.9, 175.7, 185.9. HRMS (EI) calc. for $\text{C}_{14}\text{H}_{16}\text{O}_3$ 232.1102, found 232.1099. See below for important nOe correlations:

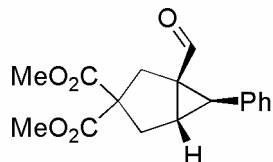


1.106-(E). Colorless oil. ^1H NMR (CDCl_3 , 500 MHz) δ 1.38 (s, 9H), 7.38-7.47 (m, 6H), 9.53 (s, 1H). ^{13}C NMR (CDCl_3 , 125 MHz) δ 27.6, 39.4, 129.2, 130.2, 130.4, 131.6, 137.0, 147.0, 177.0, 184.4. HRMS (FAB) calc. for $\text{C}_{14}\text{H}_{16}\text{O}_3$ 232.1103, found 232.1099. See below for important nOe correlations:

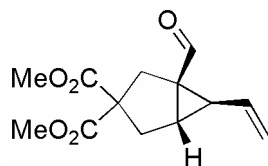


1.104. Colorless oil (70%). ^1H NMR (CDCl_3 , 500 MHz) δ 9.82 (s, 1H), 2.22 (s, 3H), 1.86 (s, 3H), 1.32 (s, 9H). ^{13}C NMR (CDCl_3 , 125 MHz) δ 181.8, 176.4, 145.7, 142.9, 39.1, 27.4, 20.0, 18.1. HRMS (FAB) calc. for $\text{C}_{10}\text{H}_{15}\text{O}_3$ 183.1021, found 183.1021.

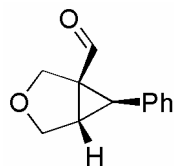
General Procedure for 1,6-enyne Oxidative Rearrangement Catalyzed by $\text{IPrAuCl}/\text{AgSbF}_6$: A 0.10 mmol sample of starting material was dissolved in 1.0 mL of CH_2Cl_2 (0.1 M) in a scintillation vial. Two equivalents of diphenyl sulfoxide were added followed by 2.5 mol% (5 mol% for substrate **1.123**) of premixed catalyst in 0.1 mL CH_2Cl_2 was added. The vial was sealed and the reaction mixture was maintained at room temperature for the specified time. Crude reaction mixtures were purified by flash chromatography (5% ethyl acetate/hexanes).



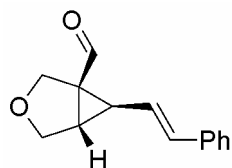
1.117. White solid (90%). ^1H NMR (CDCl_3 , 500 MHz): δ 2.70 (d, 2H, $J = 14.5$ Hz), 2.78 (d, $J = 5.5$ Hz, 1H), 2.83-2.92 (m, 2H), 3.11 (d, $J = 14.5$ Hz, 1H), 3.74 (s, 3H), 3.77 (s, 3H), 7.26-7.40 (m, 5H), 8.73 (s, 1H). ^{13}C NMR (CDCl_3 , 100 MHz): δ 32.7, 34.6, 35.7, 38.9, 47.9, 53.2, 53.3, 61.3, 127.4, 128.7, 129.0, 134.5, 171.5, 172.6, 198.9. HRMS (EI) calc. for $\text{C}_{17}\text{H}_{18}\text{O}_5$ 302.1158, found 302.1154. (X-ray data for this compound can be found in Chapter 1 Appendix 2.)



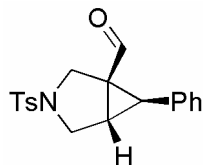
1.124. Colorless oil (68%). ^1H NMR (CDCl_3 , 400 MHz): δ 2.05 (m, 1H), 2.42 (t, $J = 5.6$ Hz, 1H), 2.53 (d, $J = 14.4$ Hz, 1H), 2.56 (d, $J = 14.4$ Hz, 1H), 2.72 (dd, $J = 5.6$ and 14.4 Hz, 1H), 2.99 (d, $J = 14.4$ Hz, 1H), 3.70 (s, 3H), 3.74 (s, 3H), 5.14 (d, $J = 10.4$ Hz, 1H), 5.25 (ddd, $J = 8.0, 10.4$ and 17.6 Hz, 1H), 5.80 (d, $J = 10.4$ Hz, 1H), 9.21 (s, 1H). ^{13}C NMR (CDCl_3 , 100 MHz): δ 34.6, 35.0, 35.4, 38.6, 47.9, 53.1, 53.2, 60.7, 117.8, 132.5, 171.3, 172.5, 198.6. HRMS (EI) calc. for $\text{C}_{13}\text{H}_{16}\text{O}_5$ 252.0998, found 252.0996.



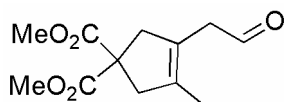
1.125. Colorless oil (94%). ^1H NMR (CDCl_3 , 400 MHz): δ 2.93 (d, $J = 5.6$ Hz, 1H), 3.00 (dd, $J = 3.2$ and 5.6 Hz, 1H), 3.90 (dd, $J = 3.2$ and 8.8 Hz, 1H), 4.03 (d, $J = 9.2$ Hz, 1H), 4.08 (d, $J = 8.8$ Hz, 1H), 4.21 (d, $J = 9.2$ Hz, 1H), 7.21-7.42 (m, 5H), 8.96 (s, 1H). ^{13}C NMR (CDCl_3 , 100 MHz): 31.9, 33.4, 46.8, 68.0, 68.8, 127.4, 128.8, 128.9, 133.9, 198.3. HRMS (EI) calc. for $\text{C}_{12}\text{H}_{12}\text{O}_2$ 188.0837, found 188.0840.



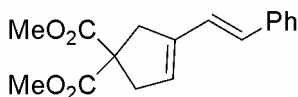
1.126. Colorless oil (83%). Compound generated, isolated and characterized by Dr. Pablo Mauleón.



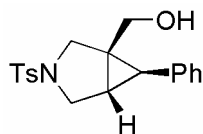
1.127. White solid (91%). ^1H NMR (CDCl_3 , 400 MHz): δ 2.48 (s, 3H), 2.87 (t, $J = 5.2$ Hz, 1H), 3.15 (d, $J = 5.2$ Hz, 1H), 3.22 (dd, $J = 4.0$ and 9.6 Hz, 1H), 3.51 (d, $J = 10.0$ Hz, 1H), 3.77 (d, $J = 10.0$ Hz, 1H), 3.88 (d, $J = 10.0$ Hz, 1H), 7.17-7.47 (m, 8H), 7.67-7.76 (m, 2H), 8.75 (s, 1H). ^{13}C NMR (CDCl_3 , 100 MHz): δ 21.5, 29.7, 34.1, 44.8, 48.0, 49.1, 127.7, 128.8, 128.9, 129.9, 132.5, 133.2, 144.0, 197.3. HRMS (EI) calc. for $\text{C}_{19}\text{H}_{19}\text{NO}_3\text{S}$ 341.1079, found 341.1086.



1.129. Yellow oil (85%). ^1H NMR (CDCl_3 , 400 MHz): δ 1.70 (s, 3H), 3.07 (s, 4H), 3.18 (s, 2H), 3.78 (s, 6H). ^{13}C NMR (CDCl_3 , 125 MHz): δ 13.6, 43.3, 44.2, 45.7, 52.8, 57.3, 123.0, 134.3, 172.4, 198.5. HRMS (EI) calc. for $\text{C}_{12}\text{H}_{16}\text{O}_5$ 240.1000, found 240.0998.



1.131. Pale yellow solid. ^1H NMR (CDCl_3 , 400 MHz): δ 3.21 (br s, 2H), 3.31 (br s, 2H), 3.81 (s, 6H), 5.75 (br s, 1H), 6.52 (d, $J = 16$ Hz, 1H), 6.94 (d, $J = 16$ Hz, 1H), 7.27 (t, $J = 7.2$ Hz, 1H), 7.26 (t, $J = 7.2$ Hz, 2H), 7.44 (d, $J = 7.6$ Hz, 2H). Spectral data was consistent with the values previously reported.^{40a}



Preparation of 1.134. NaBH_4 (11 mg, 0.281 mmol) was added in one portion to a suspension of **1.127** (80 mg, 0.234 mmol) in MeOH (2.3 mL) at 0 °C. After 5 minutes, water was added (5 drops) and the resulting colourless solution was filtered through a short pad of silica to afford **1.134** quantitatively. White solid (>99%). ^1H NMR (CDCl_3 , 400 MHz): δ 1.96 (t, $J = 4.0$ Hz, 1H), 2.35 (d, $J = 4.0$ Hz, 1H), 2.47 (s, 3H), 3.26 (m, 2H), 3.48 (m, 2H), 3.73 (d, $J = 9.6$ Hz, 1H), 3.86 (d, $J = 9.2$ Hz, 1H), 7.14 (d, $J = 7.2$ Hz, 2H), 7.23 (t, $J = 7.2$ Hz, 1H), 7.30 (t, $J = 7.2$ Hz, 2H), 7.37 (d, $J = 8.0$ Hz, 2H), 7.74 (d, $J = 8.0$ Hz, 2H). ^{13}C NMR (CDCl_3 , 100 MHz): δ 21.5, 24.5, 29.0, 36.8, 50.3, 53.0, 61.0, 126.6, 127.5, 128.3, 128.5, 129.7, 133.4, 136.1, 143.6. HRMS (EI) calc. for $\text{C}_{19}\text{H}_{21}\text{NO}_3\text{S}$ 343.1235, found 343.1242.

Procedure for Determination of Enantioselective Excess (ee). Reaction was prepared and executed in the same manner as described above, with the use of chiral catalysts. The isolated product was injected onto an AS column with the following conditions: 10 μL injection volume, 60 min run, 1.2 mL/min, detector at 230 nm, eluent: 99% Hexanes, 1% isopropanol.

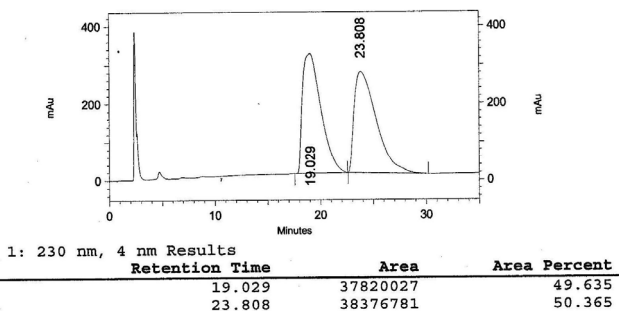


Figure A1.1.1. Racemic trace.

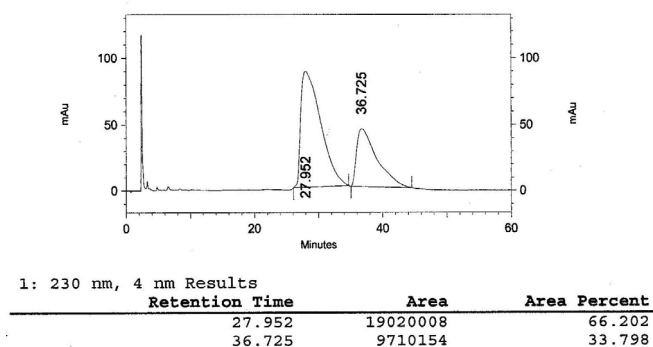
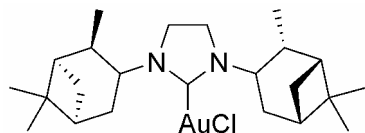
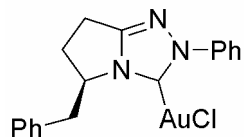


Figure A1.1.2. Trace with 32% ee utilizing xylylBINAP(AuCl)₂.



1.136. Grey solid (material turns purple over time, indicating decomposition of the catalyst and formation of Au nanoparticles). LRMS (FAB): $m/z = 539$ ($M^+ - Cl$). Limited solubility rendered ¹³C NMR difficult, and the complicated nature of ¹H NMR spectra resulted in the requirement that the catalyst be primarily characterized by LRMS. However, ¹H NMR spectra can be found in the appendix. Precursor ligand prepared by the method of Hartwig *et al.*⁴⁴



1.137. White solid (material turns purple over time, indicating decomposition of the catalyst and formation of Au nanoparticles). LRMS (FAB): $m/z = 472$ ($M^+ - Cl$). Limited solubility rendered ¹³C NMR difficult, and the complicated nature of ¹H NMR spectra resulted in the requirement that the catalyst be primarily characterized by LRMS. However, ¹H NMR spectra can be found in the appendix. Precursor ligand prepared by the method of Rovis *et al.*⁴⁵

References

- (1) For reviews of homogeneous gold-catalyzed reactions see: (a) Hashmi, A. S. K. *Gold Bull.* **2004**, *37*, 51. (b) Arcadi, A.; Di Giuseppe, S. *Curr. Org. Chem.* **2004**, *8*, 795. (c) Hashmi, A. S. K.; Hutchings, G. J. *Angew. Chem. Int. Ed.* **2006**, *45*, 7896. (d) Hashmi, A. S. K. *Chem. Rev.* **2007**, *107*, 3180. For short highlights of broad advances in Au catalysis see: (e) Hoffman-Röder, A.; Krause, N. *Org. Biomol. Chem.* **2005**, *3*, 387. (f) Hashmi, A. S. K. *Angew. Chem. Int. Ed.* **2005**, *44*, 6990. (g) Dyker, G. *Angew. Chem. Int. Ed.* **2000**, *39*, 4237.
- (2) (a) Teles, J. H.; Brode, S.; Chabanas, M. *Angew. Chem., Int. Ed.* **1998**, *37*, 1415. (b) Mizushima, E.; Hayashi, T.; Tanaka, M. *Org. Lett.* **2003**, *5*, 3349. (c) Mizushima, E.; Sato, K.; Hayashi, T.; Tanaka, M. *Angew. Chem., Int. Ed.* **2002**, *41*, 4563. (d) Kennedy-Smith, J. J.; Staben, S. T.; Toste, F. D. *J. Am. Chem. Soc.* **2004**, *126*, 4526. (e) Nieto-Oberhuber, C.; Muñoz, M. P.; Buñuel, E.; Nevado, C.; Cárdenas, D. J.; Echavarren, A. M. *Angew. Chem., Int. Ed.* **2004**, *43*, 2402. (f) Mamane, V.; Gress, T.; Krause, H.; Fürstner, A. *J. Am. Chem. Soc.* **2004**, *126*, 8654. (g) Luzung, M. R.; Markham, J. P.; Toste, F. D. *J. Am. Chem. Soc.* **2004**, *126*, 10858. (h) Zhang, L.; Kozmin, S. A. *J. Am. Chem. Soc.* **2004**, *126*, 11806. (i) Nieto-Oberhuber, C.; López, S.; Echavarren, A. M. *J. Am. Chem. Soc.* **2005**, *127*, 6178. (j) Nevado, C.; Echavarren, A. M. *Chem. Eur. J.* **2005**, *11*, 3155.
- (3) Staben, S. T.; Kennedy-Smith, J. J.; Toste, F. D. *Angew. Chem. Int. Ed.* **2004**, *43*, 5350.
- (4) (a) Johansson, M. J.; Gorin, D. J.; Staben, S. T.; Toste, F. D. *J. Am. Chem. Soc.* **2005**, *127*, 18002. (b) Miki, K.; Ohe, K.; Uemura, S. *J. Org. Chem.* **2003**, *68*, 8505. (c) Miki, K.; Uemura, S.; Ohe, K. *Chem. Lett.* **2005**, *34*, 1968. (d) Pujanauski, B. G.; Bhanu Prasad, B. A.; Sarpong, R. *J. Am. Chem. Soc.* **2006**, *128*, 6786. (e) Yeom, H.-S.; Lee, E.-S.; Shin, S. *Synlett* **2007**, *14*, 2292. (f) Peng, Y.; Yu, M.; Zhang, L. *Org. Lett.* **2008**, *10*, 5187. (g) Ye, L.; Cui, L.; Zhang, G.; Zhang, L. *J. Am. Chem. Soc.* **2010**, *132*, 3258.
- (5) Sherry, B. D.; Toste, F. D. *J. Am. Chem. Soc.* **2004**, *126*, 15978.
- (6) (a) Fürstner, A.; Davies, P. W. *Angew. Chem. Int. Ed.* **2007**, *46*, 3410. (b) Jimenez-Nunez, E.; Echavarren, A. M. *Chemical Communications* **2007**, 333. (c) Hashmi, A. S. K. *Gold Bull.* **2003**, *36*, 3.
- (7) Gorin, D. J.; Davis, N. R.; Toste, F. D. *J. Am. Chem. Soc.* **2005**, *127*, 11260.
- (8) Gorin, D. J.; Toste, F. D. *Nature* **2007**, *446*, 395.
- (9) Benitez, D.; Shapiro, N. D.; Tkatchouk, E.; Wang, Y.; Goddard III, W. A.; Toste, F. D. *Nature Chem.* **2009**, *1*, 482.
- (10) (a) Fürstner, A.; Hannen, F. *Chem. Commun.* **2004**, 2546. (b) Zhang, L.; Wang, S. *J. Am. Chem. Soc.* **2006**, *128*, 1442. (c) Horino, Y.; Luzung, M. R.; Toste, F. D. *J. Am. Chem. Soc.* **2006**, *128*, 11364. (d) Lee, J. H.; Toste, F. D. *Angew. Chem. Int. Ed.* **2007**, *46*, 912. (e) Mauleón, P.; Zeldin, R. M.; González, A. Z.; Toste, F. D. *J. Am. Chem. Soc.* **2009**, *131*, 6348. (f) Benitez, D.; Tkatchouk, E.; González, A. Z.; Goddard III, W. A.; Toste, F. D. *Org. Lett.* **2009**, *21*, 4798.
- (11) Fürstner, A. *Chem. Soc. Rev.* **2009**, *38*, 3208.
- (12) (a) Gorin, D. J.; Dube, P.; Toste, F. D. *J. Am. Chem. Soc.* **2006**, *128*, 14480. (b) López, S.; Herrero-Gómez, E.; Pérez-Galán, P.; Nieto-Oberhuber, C.; Echavarren, A. M. *Angew. Chem. Int. Ed.* **2006**, *45*, 6029.
- (13) Davies, H. M. L.; Beckwith, R. E. J. *Chem. Rev.* **2003**, *103*, 2861.

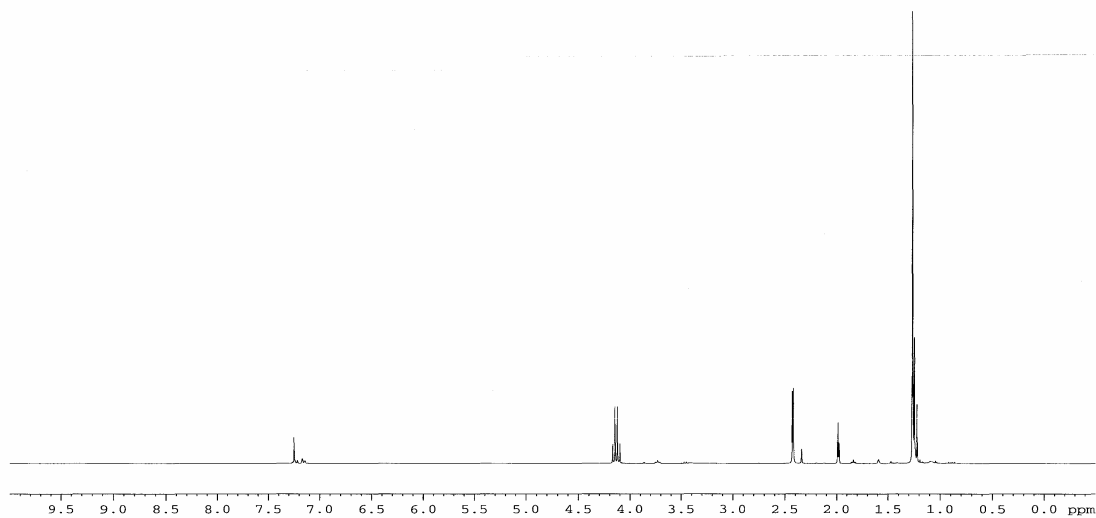
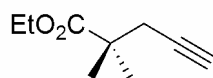
- (14) (a) Padwa, A. *J. Organomet. Chem.* **2000**, *610*, 88. (b) Padwa, A.; Krumpke, K. E.; Kassir, J. *A. J. Org. Chem.* **1992**, *57*, 4940.
- (15) Anslyn, E. V.; Dougherty, D. A. *Modern Physical Organic Chemistry*; University Science Books: Sausalito, 2006.
- (16) (a) Cross, R. J.; Davidson, M. F. *J. Chem. Soc., Dalton Trans.* **1986**, 411. (b) Yang, Y.; Ramamoorthy, V.; Sharp, P. R. *Inorg. Chem.* **1993**, *32*, 1946.
- (17) (a) Sakai, A.; Aoyama, T.; Shiori, T. *Tetrahedron Lett.* **2000**, *41*, 6859. (b) Usami, Y.; Ikura, T.; Amagata, T.; Numata, A. *Tetrahedron: Asymm.* **2000**, *11*, 3711.
- (18) This particular alcohol was synthesized because it was known in the literature.
- (19) Gahman, T. C.; Overman, L. E. *Tetrahedron* **2002**, *58*, 6473.
- (20) Smith III, A. B.; Toder, B. H.; Branca, S. J.; Dieter, R. K. *J. Am. Chem. Soc.* **1981**, *103*, 1996.
- (21) Tsuchimoto, T.; Matsubayashi, H.; Kaneko, M.; Shirakawa, E.; Kawakami, Y. *Ang. Chem. Int. Ed.* **2005**, *44*, 1336.
- (22) Yakelis, N. A.; Bergman, R. G. *Organometallics* **2005**, *24*, 3579.
- (23) Shan, H.; James, A.; Sharp, P. R. *Inorg. Chem.* **1998**, *37*, 5727.
- (24) (a) Kranenburg, M.; van der Burgt, Y. E. M.; Kamer, P. C. J.; van Leeuwen, P. W. N. M.; Goubitz, K.; Fraanje, J. *Organometallics*. **1995**, *14*, 3081. (b) Ito, H.; Takagi, K.; Miyahara, T.; Sawamura, M. *Org. Lett.* **2005**, *7*, 3001.
- (25) Cinellu, M. A.; Minghetti, G.; Pinna, M. V.; Stoccoro, S.; Zucca, A.; Manassero, M. *J. Chem. Soc., Dalton Trans.* **2000**, 1261.
- (26) Pitteri, B.; Marangoni, G.; Visentin, F.; Bobbo, J.; Bertolasi, V.; Gilli, P. *J. Chem. Soc., Dalton Trans.* **1999**, 677.
- (27) (a) Fructos, M. R.; Belderrain, T. R.; de Frémont, P.; Scott, N. M.; Nolan, S. P.; Diaz-Requejo, M. M.; Perez, P. J. *Ang. Chem. Int. Ed.* **2005**, *44*, 2. (b) De Fremont, P.; Scott, N. M.; Stevens, E. D.; Nolan, S. P. *Organometallics* **2005**, *24*, 2411.
- (28) (a) Chen, H. W.; Tiekink, E. R. T. *Acta Cryst.* **2003**, *E59*, m50. (b) Jacob, K.; Voigt, F.; Merzweiler, K.; Pietzsch, C. *J. Organomet. Chem.* **1997**, 421. (c) Nunokawa, K.; Onaka, S.; Tatematsu, T.; Ito, M.; Sakai, J. *Inorg. Chim. Acta* **2001**, *322*, 56. (d) Cross, R. J.; Davidson, M. F. *J. Chem. Soc., Dalton Trans.* **1986**, 411. (e) Schmidbaur, H.; Brachthaeuser, B.; Steigelmann, O.; Beruda, H. *Chem. Ber.* **1992**, *125*, 2705.
- (29) Al-Sa'ady, A. K.; McAuliffe, C. A.; Parish, R. V.; Sandeank, J. A. *Inorg. Syn.* **1985**, 191.
- (30) (a) Kranenburg, M.; van der Burgt, Y. E. M.; Kamer, P. C. J.; van Leeuwen, P. W. N. M.; Goubitz, K.; Fraanje, J. *Organometallics* **1995**, *14*, 3081. (b) Ito, H.; Takagi, K.; Miyahara, T.; Sawamura, M. *Org. Lett.* **2005**, *7*, 3001.
- (31) For oxidation of ruthenium-carbenoid intermediates with *N*-hydroxyimides in ruthenium-catalyzed cycloisomerizations see: (a) Trost, B. M.; Rhee, Y.-H.; *J. Am. Chem. Soc.* **1999**, *121*, 11680. (b) Trost, B. M.; Rhee, Y.-H. *J. Am. Chem. Soc.* **2002**, *124*, 2528.
- (32) Oda, R.; Mieno, M.; Hayashi, Y. *Tetrahedron Lett.* **1967**, 2363.
- (33) Dost, F.; Gosselck, J. *Tetrahedron Lett.* **1970**, 5091. (b) Takebayashi, M.; Kashiwada, T.; Hamaguchi, M.; Ibata, T. *Chem. Lett.* **1973**, 809. (c) Moody, C. J.; Slawin, A. M. Z.; Taylor, R. J.; Williams, D. J. *Tetrahedron Lett.* **1988**, *29*, 6009.
- (34) Small amounts (10%) of related oxidation products have been observed in a rhodium-catalyzed cyclization of diazoacetylenes. See: Padwa, A.; Chiacchio, U.; Fairfax, D. J.; Kassir, J. M.; Litrico, A.; Semones, M. A.; Xu, S. L. *J. Org. Chem.* **1998**, *58*, 6429.

- (35) For examples of gold(I)-catalyzed reactions of α -diazoesters see: (a) Fructos, M. R.; Belderrain, T. R.; de Frémont, P.; Scott, N. M.; Díaz-Requejo, N. M.; Pérez, P. J. *Angew. Chem. Int. Ed.* **2005**, *44*, 5284. (b) Fructos, M. R.; de Frémont, P.; Díaz-Requejo, N. M.; Pérez, P. J. *Organometallics* **2006**, *25*, 2237.
- (36) Gorin, D. 2008. *Stabilized Cationic Reaction Intermediates in Homogeneous Gold Catalysis*. Dissertation, University of California, Berkeley.
- (37) Lataoka, H.; Watanabe, K.; Goto, K. *Tetrahedron Lett.* **1990**, *31*, 4181.
- (38) For examples of reaction showing different reactivity when gold(I) and gold(III) complexes are employed as catalysts see: (a) Sromek, A. W.; Rubina, M.; Gevorgyan, V. *J. Am. Chem. Soc.* **2005**, *127*, 10500. (b) Lemiére, G.; Gandom, V.; Agenet, N.; Goddard, J.-P.; de Kozak, A.; Aubert, C.; Fensterback, L.; Malacria, M. *Angew. Chem. Int. Ed.* **2006**, *45*, 7596. (c) Hashmi, A. S. K.; Salathé, R.; Frey, W. *Chem. – Eur. J.* **2006**, *12*, 6991.
- (39) (a) Kimball, D. B.; Herges, R.; Haley, M. M. *J. Am. Chem. Soc.* **2002**, *124*, 1572. (b) Kimball, D. B.; Hayes, A. G.; Haley, M. M. *Org. Lett.* **2000**, *2*, 3825.
- (40) (a) Nieto-Oberhuber, C.; Muñoz, M. P.; López, S.; Jiménez-Núñez, E.; Nevado, C.; Herrero-Gómez, E.; Raducan, M.; Echavarren, A. M. *Chem. Eur. J.* **2006**, *12*, 1677. (b) Amijs, C. H. M.; Ferrer, C.; Echavarren, A. M. *Chem. Comm.* **2007**, 698. (c) Jiménez-Núñez, E.; Claverie, C. K.; Nieto-Oberhuber, C.; Echavarren, A. M. *Angew. Chem. Int. Ed.* **2006**, *45*, 5452. (d) Nieto-Oberhuber, C.; López, S.; Muñoz, M. P.; Jiménez-Núñez, E.; Buñuel, E.; Cárdenas, D. J.; Echavarren, A. M. *Chem. Eur. J.* **2006**, *12*, 1694. (e) Mamane, V.; Gress, T.; Krause, H.; Fürstner, A. *J. Am. Chem. Soc.* **2004**, *126*, 8654.
- (41) (a) Nieto-Oberhuber, C.; López, S.; Jiménez-Núñez, E.; Echavarren, A. M. *Chem. Eur. J.* **2006**, *12*, 5916. (b) Cabello, N.; Jiménez-Núñez, E.; Buñuel, E.; Cárdenas, D. J.; Echavarren, A. M. *Eur. J. Org. Chem.* **2007**, 4217.
- (42) Ravikumar, K. S.; Zhang, Y. M.; Bégué, J.-P.; Bonnet-Delpon, D. *Eur. J. Org. Chem.* **1998**, *12*, 2937.
- (43) For an excellent review see: Gorin, D. J.; Sherry, B. D.; Toste, F. D. *Chem. Rev.* **2008**, *108*, 3351.
- (44) (a) Lee, S.; Hartwig, J. F. *J. Org. Chem.* **2001**, *66*, 3402. (b) Herrmann, W. A.; Goossen, L. J.; Artus, G. R. J.; Köcher, C. *Organometallics* **1997**, *16*, 2472. (c) Kano, T.; Sasaki, K.; Maruoka, K. *Org. Lett.* **2005**, *7*, 1347. (d) Suzuki, Y.; Muramatsu, K.; Yamauchi, K.; Morie, Y.; Sato, M. *Tetrahedron* **2006**, *62*, 302.
- (45) Kerr, M. S.; de Alaniz, J. R.; Rovis, T. *J. Org. Chem.* **2005**, *70*, 5725.
- (46) (a) Chianese, A. R.; Crabtree, R. H. *Organometallics* **2005**, *24*, 4432. (b) Duan, W.-L.; Shi, M.; Rong, G.-B. *Chem. Comm.* **2003**, 2916. (c) Xu, Q.; Gu, X.; Liu, S.; Dou, Q.; Shi, M. *J. Org. Chem.* **2007**, *72*, 2240.
- (47) LaLonde, R. L.; Sherry, B. D.; Kang, E. J.; Toste, F. D. *J. Am. Chem. Soc.* **2007**, *129*, 2452.
- (48) (a) Scarborough, C. C.; Grady, M. J. W.; Guzei, I. A.; Gandhi, B. A.; Bunel, E. E.; Stahl, S. S. *Angew. Chem. Int. Ed.* **2005**, *44*, 5269. (b) Tonzetich, Z. J.; Lu, C. C.; Schrock, R. R.; Hock, A. S.; Bonitatebus Jr.; P. J. *Organometallics* **2004**, *23*, 4362.
- (49) Bruce, M. I.; Nicholson, B. K.; Binshawkataly, O.; Shapley Jr., H. T. *Inorg. Syn.* **1989**, *26*, 324.
- (50) Nishina, N.; Yamamoto, Y. *Synlett* **2007**, *11*, 1767.
- (51) Brandys, M.-C.; Jennings, M. C.; Puddephatt, R. J. *Dalton* **2000**, *24*, 4601.
- (52) Westland, A. D. *Can. J. Chem.* **1969**, *47*, 4135.
- (53) Mook Jr., R.; Sher, P. M. *Org. Syn.* **1988**, *66*, 75.

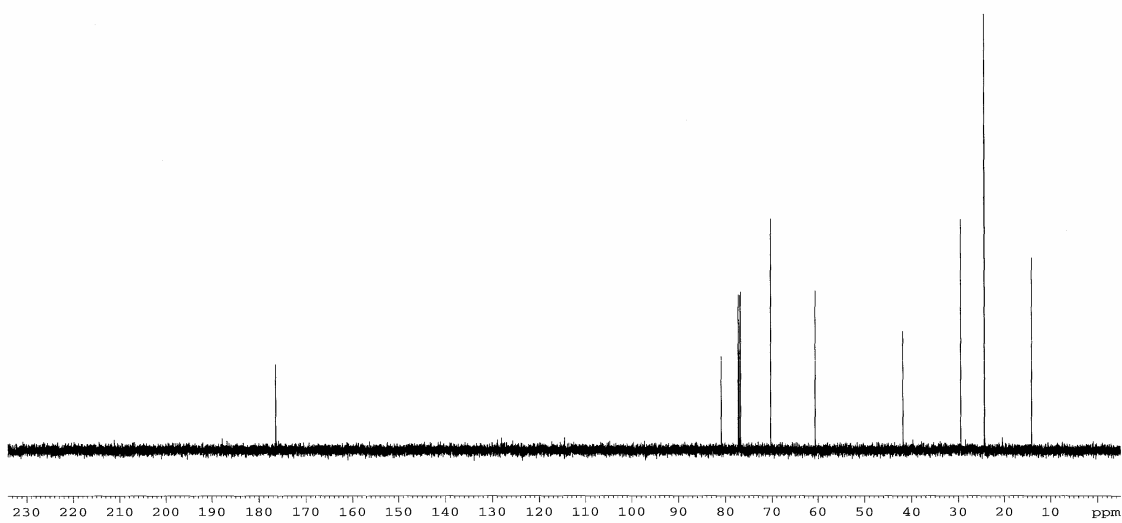
- (54) Chatani, N.; Morimoto, T.; Muto, S.; Murai, J. *J. Am. Chem. Soc.* **1994**, *116*, 6049.
- (55) Lian, J.-J.; Chen, P.-C.; Lin, Y.-P.; Ting, H.-C.; Liu, R.-S. *J. Am. Chem. Soc.* **2006**, *128*, 11372.
- (56) Harvey, D. F.; Lund, K. P. *J. Am. Chem. Soc.* **1991**, *113*, 5066.
- (57) Miura, K.; Saito, H.; Fujisawa, N.; Hosomi, A. *J. Org. Chem.* **2000**, *65*, 8119.
- (58) Nevado, C.; Charruault, L.; Michelet, V.; Nieto-Oberhuber, C.; Muñoz, M. P.; Méndez, M.; Rager, M-N.; Gênét, J-P.; Echavarren, A. M. *Eur. J. Org. Chem.* **2003**, *4*, 706.
- (59) Chakraborti, A. K.; Sharma, L.; Gulhane, R. *Tetrahedron* **2003**, *59*, 7661.
- (60) Lee, S. I.; Park, S. Y.; Park, J. H.; Jung, I. G.; Choi, S. Y.; Chung, Y. K. *J. Org. Chem.* **2006**, *71*, 91.
- (61) For characterization data see: Ming-Yuan, L.; Madhushaw, R. J.; Liu, R.-S. *J. Org. Chem.* **2004**, *69*, 7700.
- (62) Prepared by portionwise adding of 12.0 g (116 mmol) of *N*-methyl-*N*-nitrosourea to a mixture of KOH (40% w/v, 42 mL) and ether (120 mL).
- (63) Schelper, M.; De Meijere, A. *Eur. J. Org. Chem.* **2005**, *3*, 582.
- (64) Prepared according to appropriate modification of the method in reference MMM.
- (65) Nishimura, T.; Washitake, Y.; Nishiguchi, Y.; Maeda, Y.; Uemura, S. *Chem. Comm.* **2004**, *11*, 1312.
- (66) (a) Nesmeyanov, A. N.; Perevalova, E. G.; Struchkov, Yu.T.; Antipin, M. Yu.; Grandberg, K. I.; Dyadchenko, V. P. *J. Organomet. Chem.* **1980**, *201*, 343. (b) Kolb, A.; Bissinger, P.; Schmidbaur, H. *Z. Anorg. Allg. Chem.* **1993**, *619*, 1580.
- (67) Chang, C-L.; Kumar, M. P.; Liu, R-S. *J. Org. Chem.* **2001**, *69*, 2793.
- (68) Knouzi, N.; Vaultier, M.; Carrie, R. *Bull. Chim. Soc. Fr.* **1985**, 815. Alcohol tosylation was accomplished by the method of Kabalka: Kabalka, G. W.; Varma, M.; Varma, R. S.; Srivastava, P. C.; Knapp Jr., F. F. *J. Org. Chem.* **1986**, *51*, 2386. Alcohol was generated by LiAlH₄ reduction of the ethyl ester produced by the method of Kende, A. S.; Fludzinski, P.; Hill, J. H. *J. Am. Chem. Soc.* **1984**, *106*, 3551.
- (69) Enders, D.; Maaßen, R.; Han, S-H. *Liebigs Ann.* **1996**, 1565.

Chapter 1 Appendix 1. Selected Spectral Data.

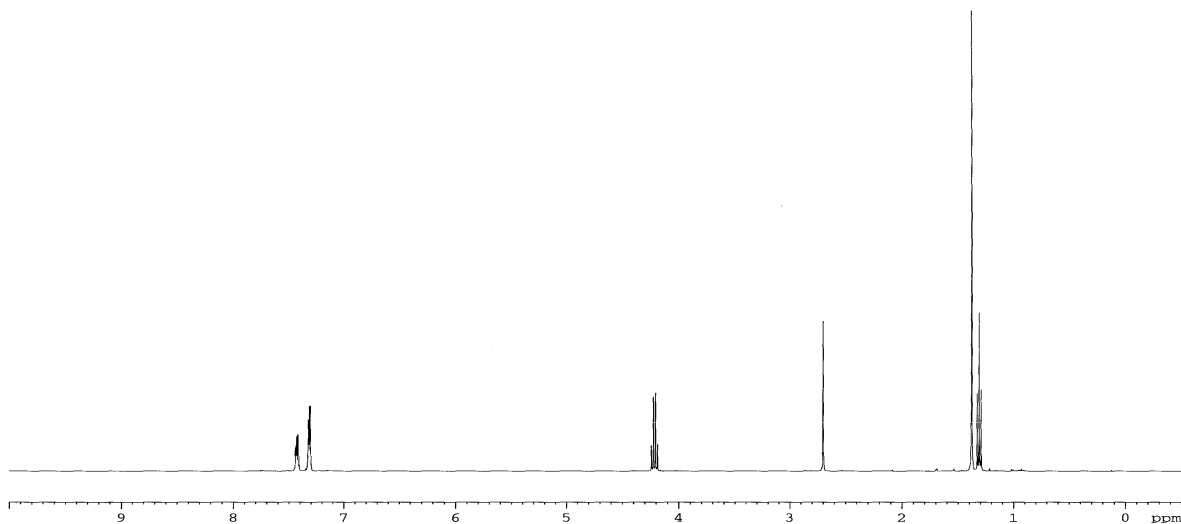
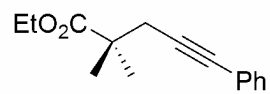
^1H NMR (CDCl_3 , 300 MHz) for **1.67**



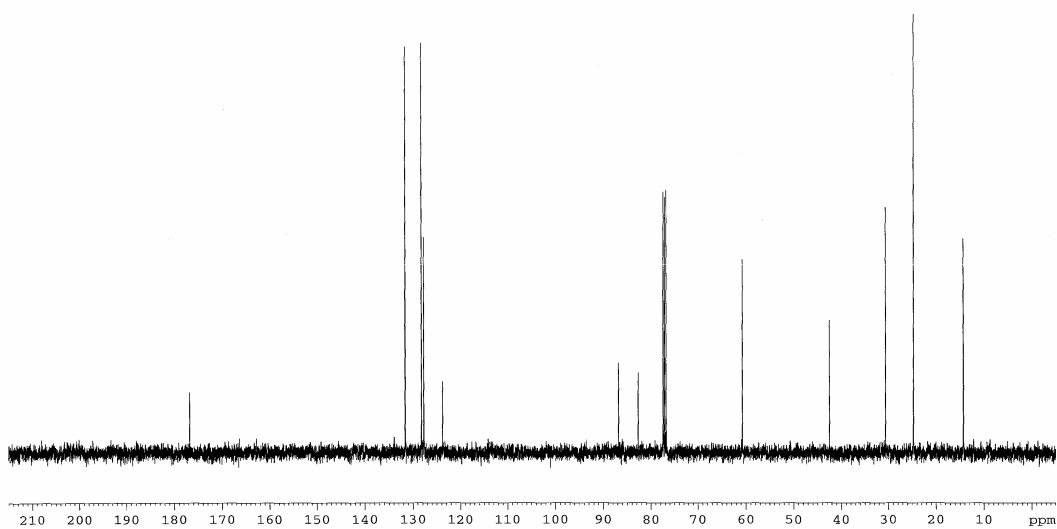
^{13}C NMR (CDCl_3 , 100 MHz) for **1.67**



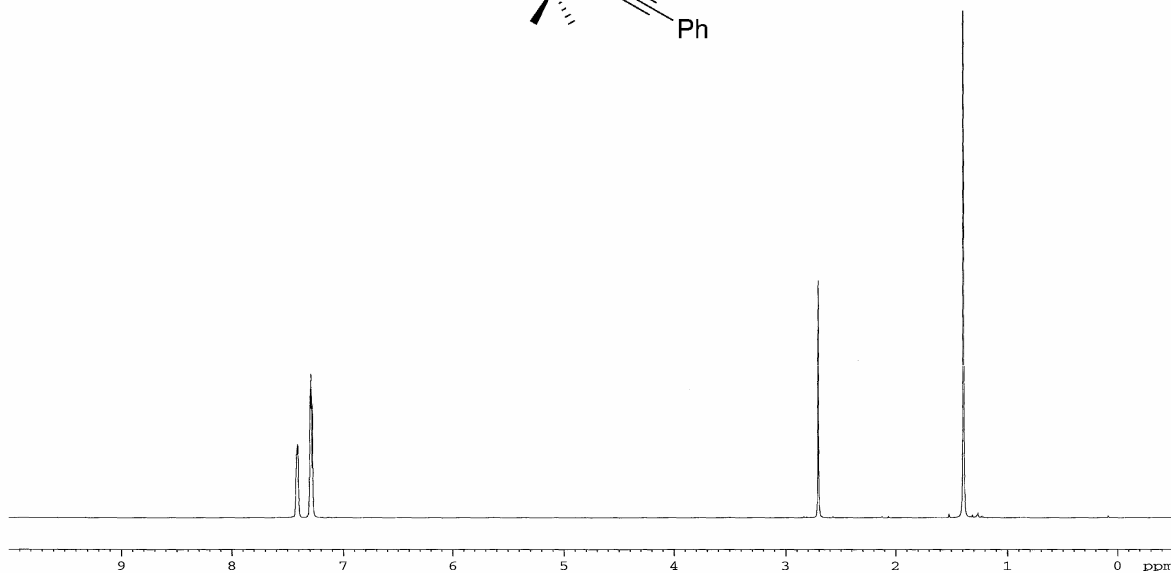
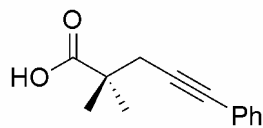
^1H NMR (CDCl_3 , 400 MHz) for **2,2-dimethyl-5-phenyl ethyl pentynoate**



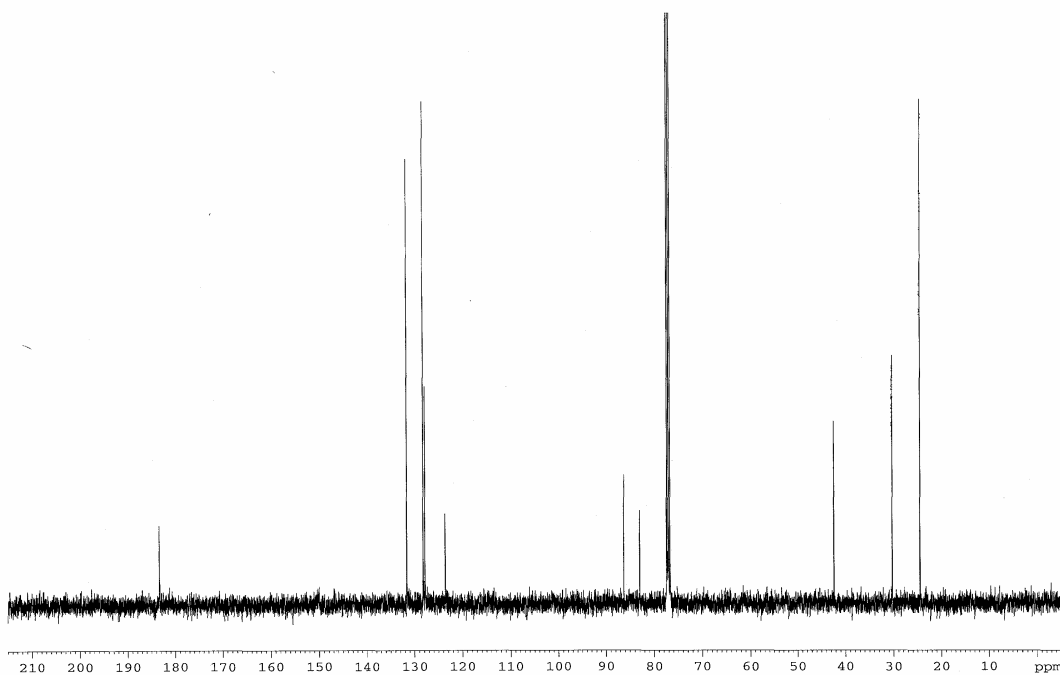
^{13}C NMR (CDCl_3 , 100 MHz) for **2,2-dimethyl-5-phenyl ethyl pentynoate**



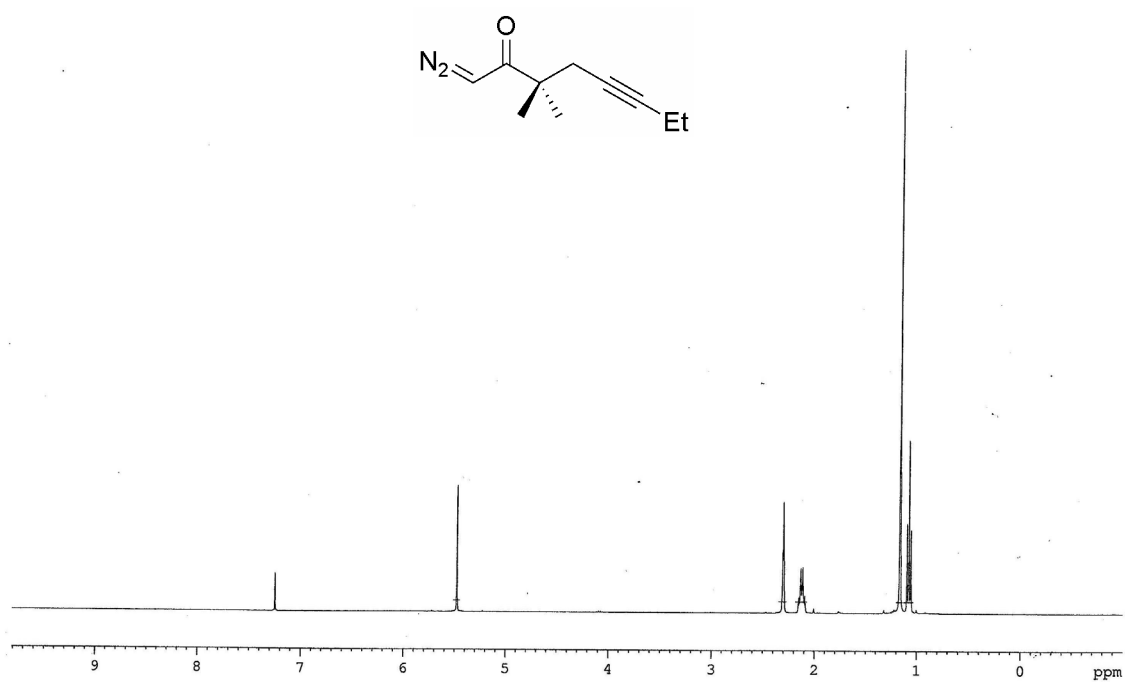
^1H NMR (CDCl_3 , 400 MHz) for **2,2-dimethyl-5-phenyl-4-pentynoic acid**



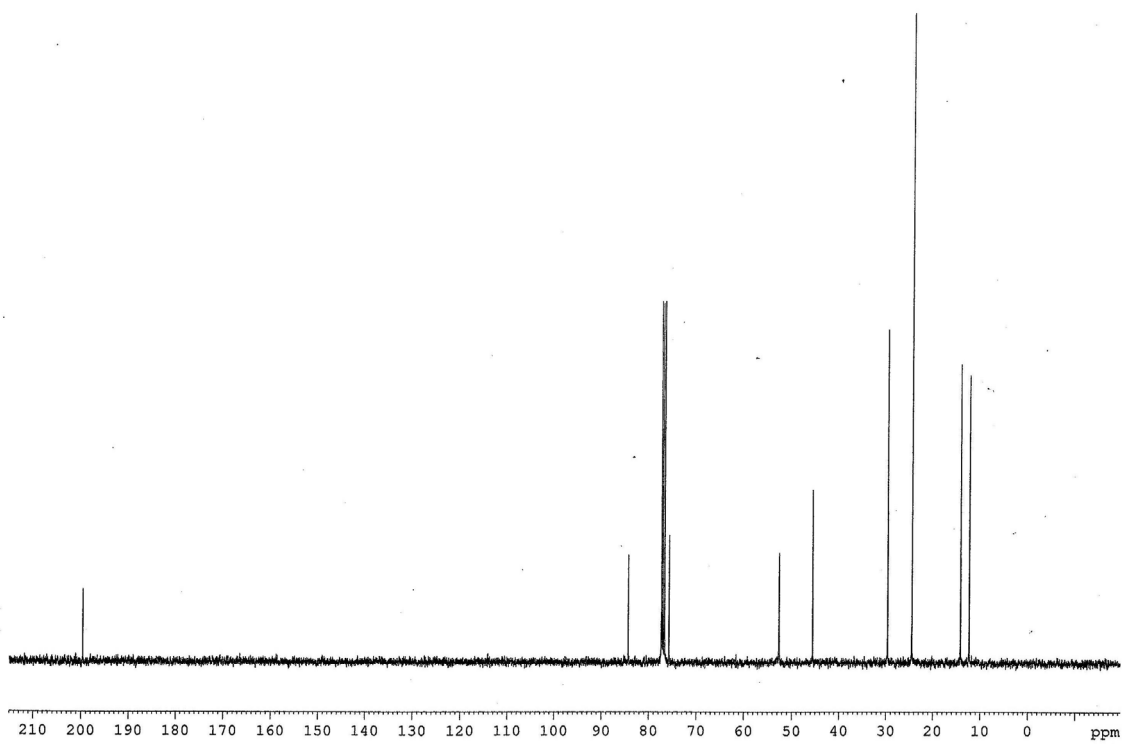
^{13}C NMR (CDCl_3 , 100 MHz) for **2,2-dimethyl-5-phenyl-4-pentynoic acid**



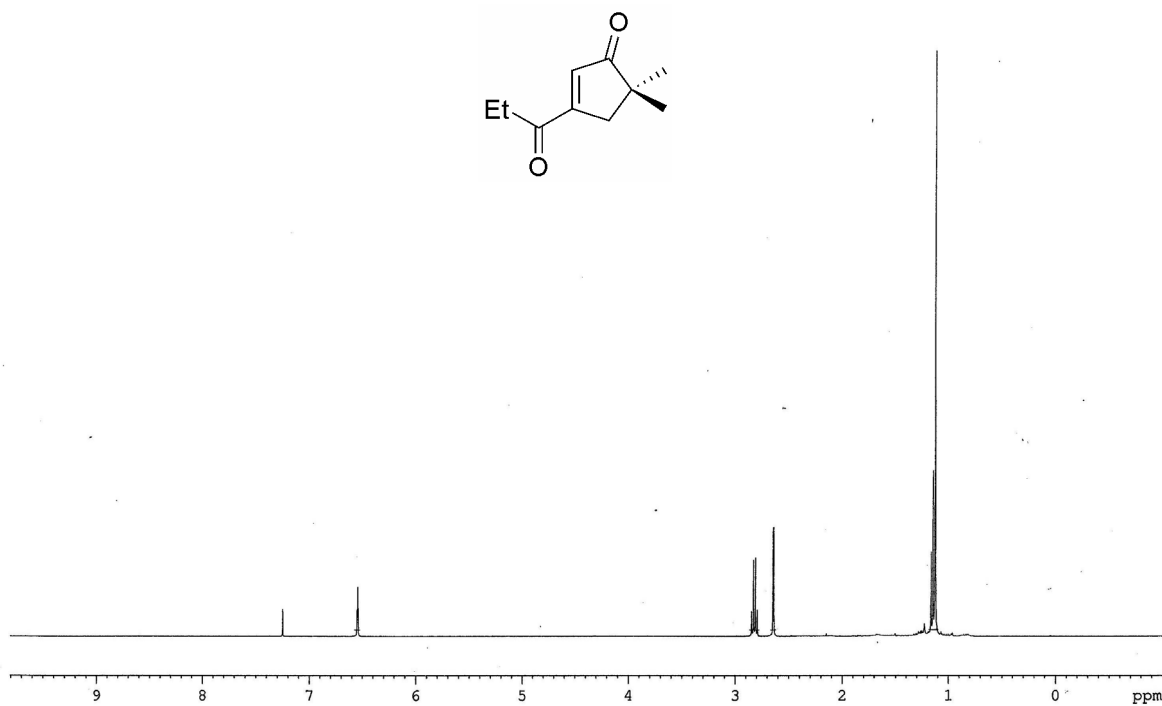
^1H NMR (CDCl_3 , 400 MHz) for **1.32**



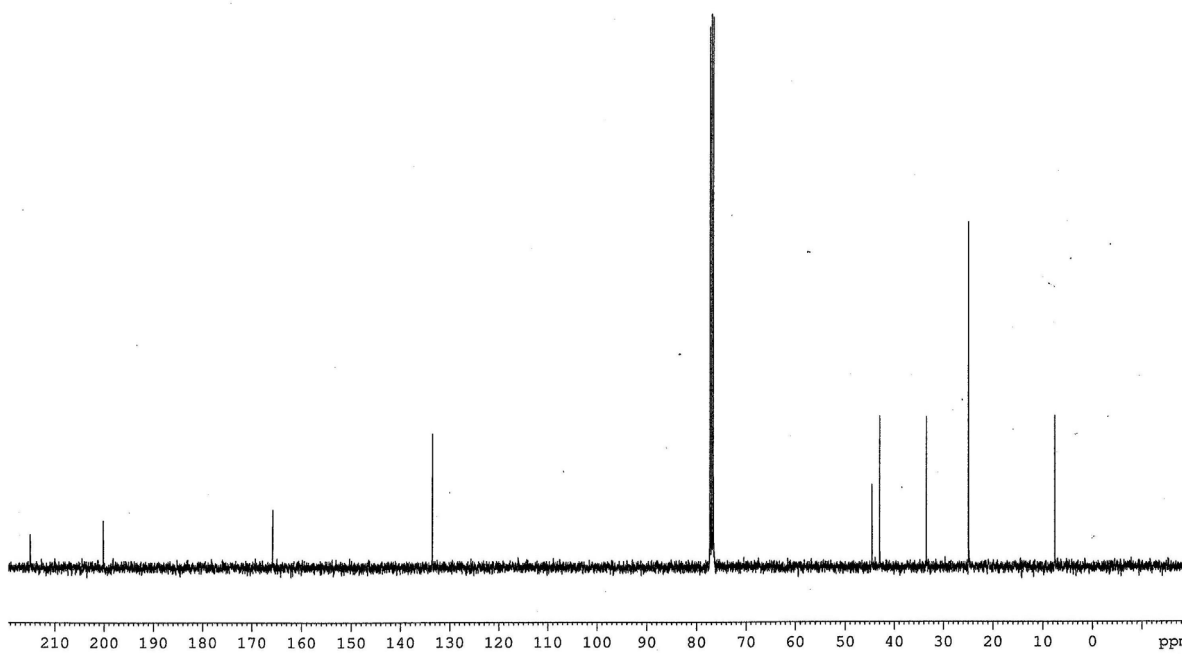
^{13}C NMR (CDCl_3 , 100 MHz) for **1.32**



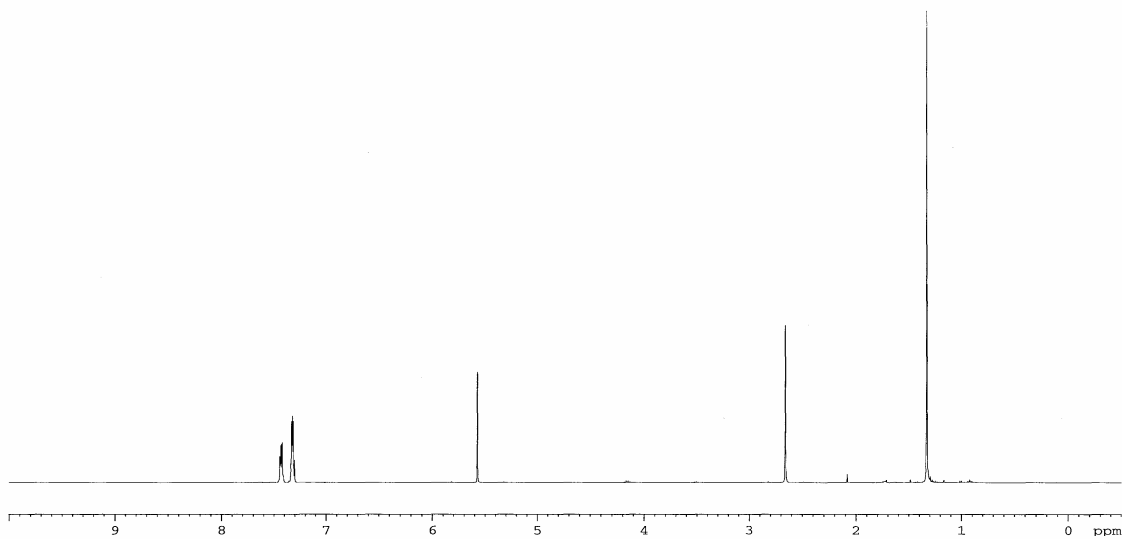
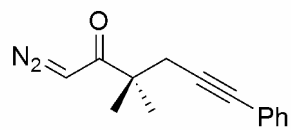
^1H NMR (CDCl_3 , 400 MHz) for **1.35**



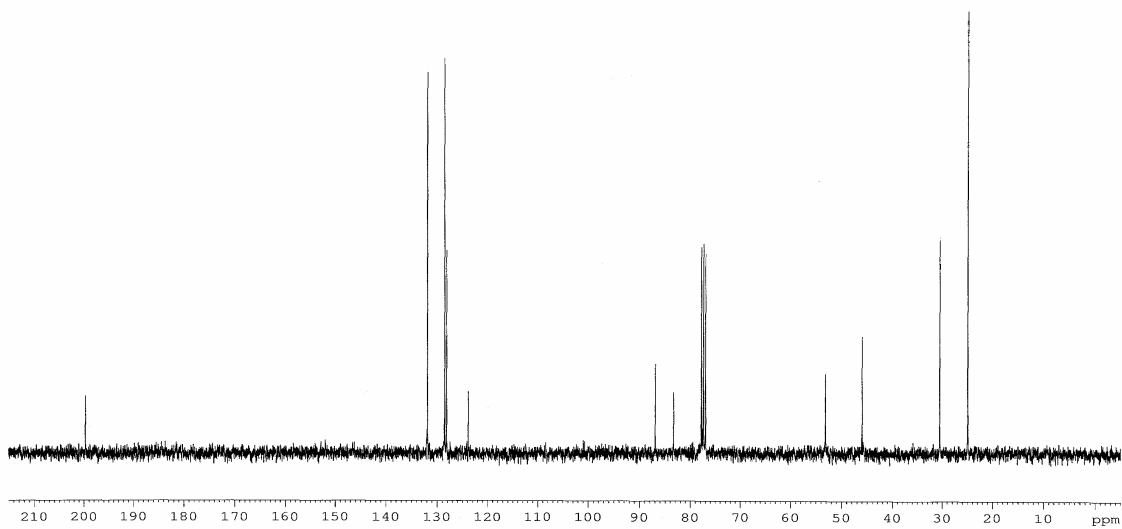
^{13}C NMR (CDCl_3 , 100 MHz) for **1.35**



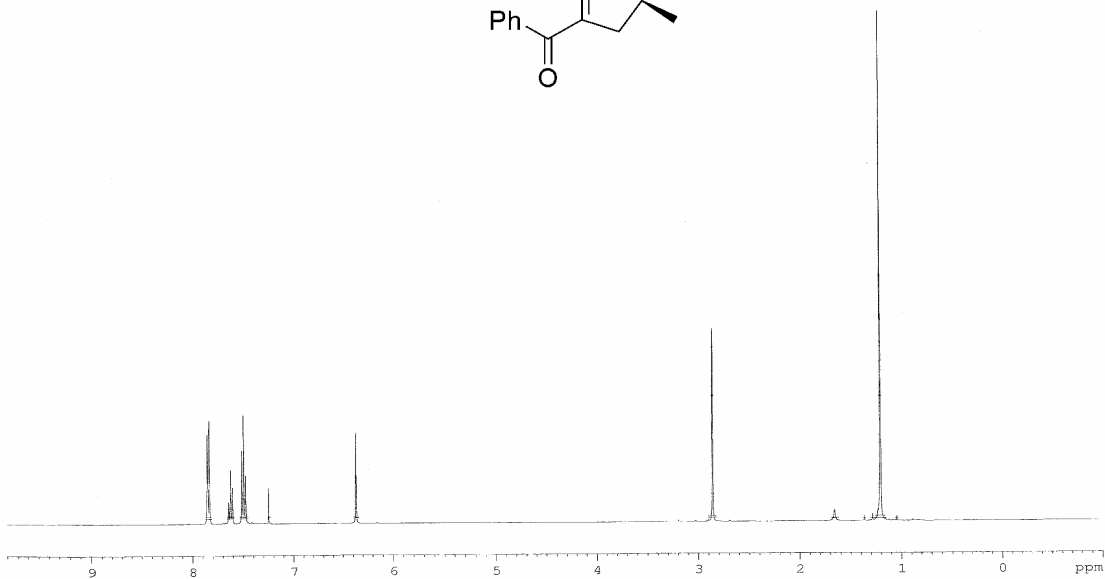
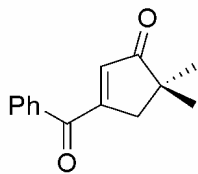
^1H NMR (CDCl_3 , 400 MHz) for **1.36**



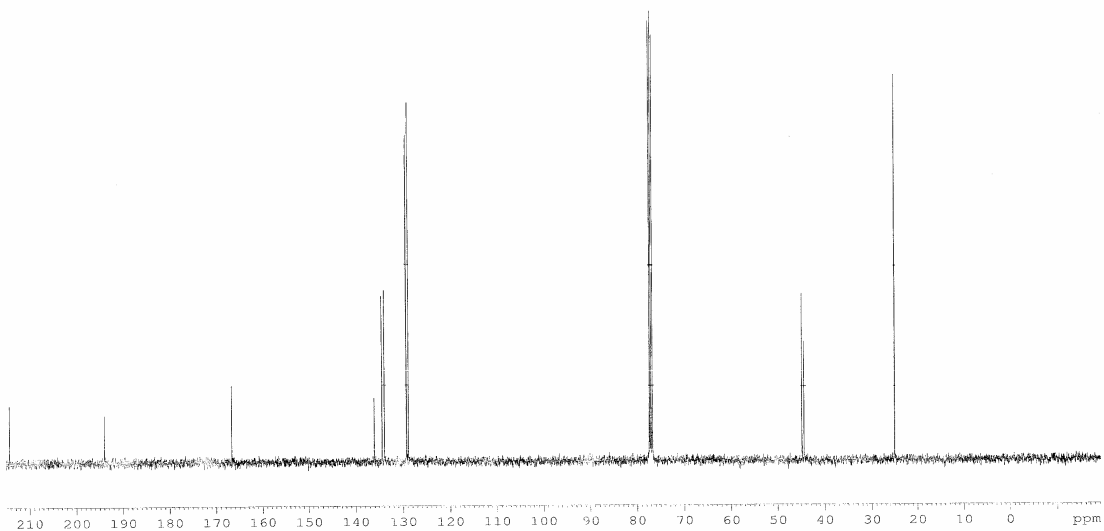
^{13}C NMR (CDCl_3 , 100 MHz) for **1.36**



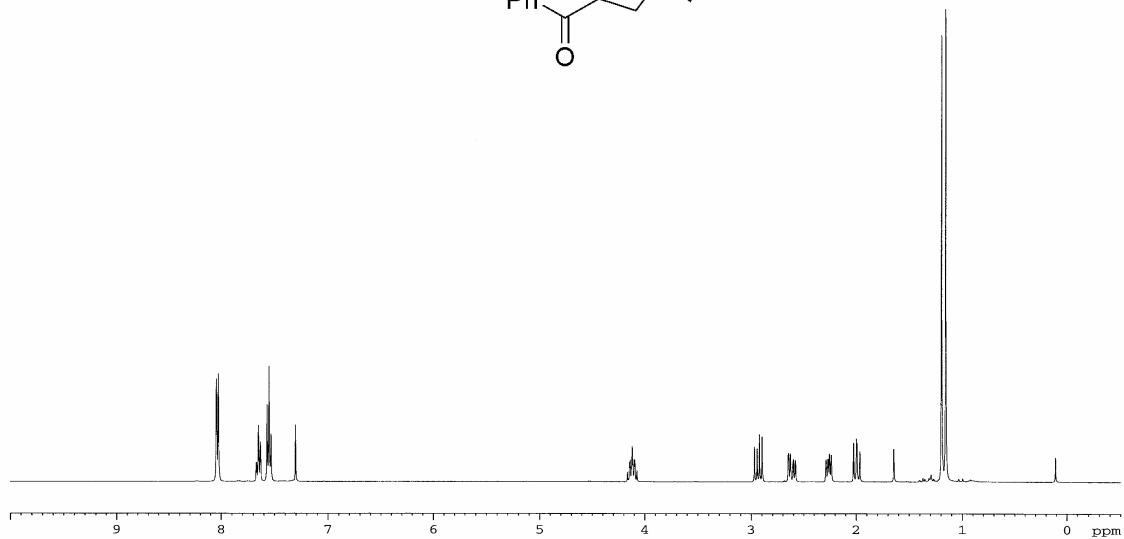
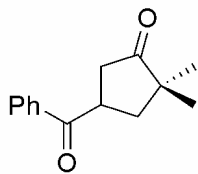
^1H NMR (CDCl_3 , 400 MHz) for **1.37**



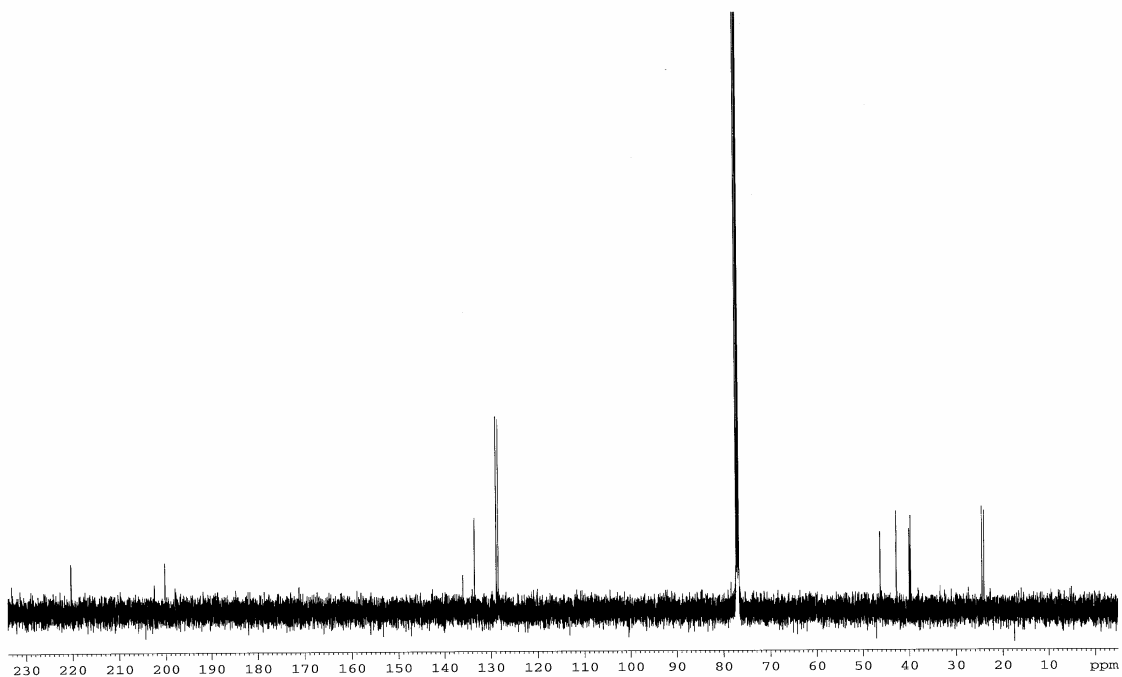
^{13}C NMR (CDCl_3 , 100 MHz) for **1.37**



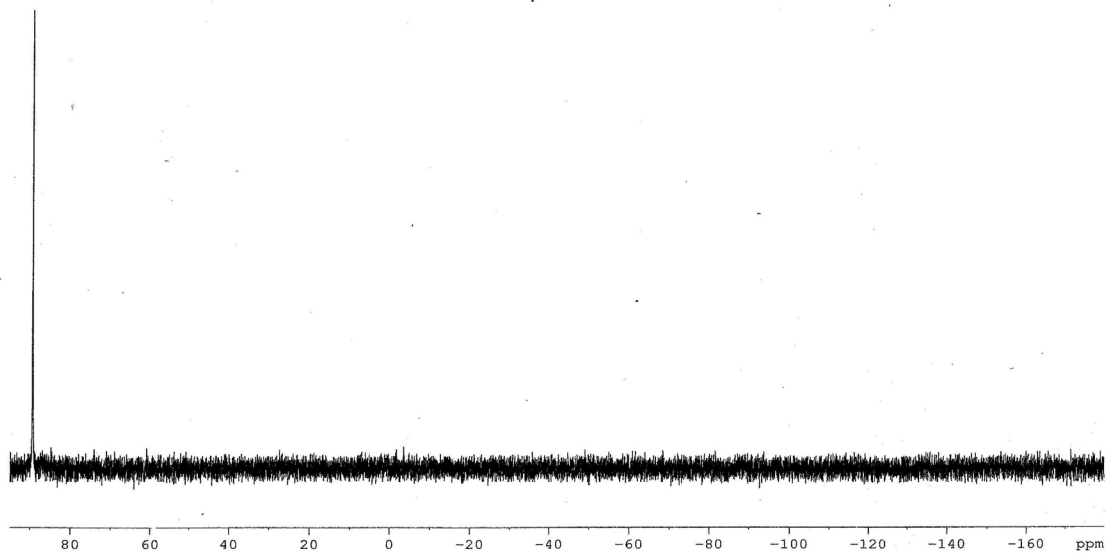
^1H NMR (CDCl_3 , 400 MHz) for **1.49**



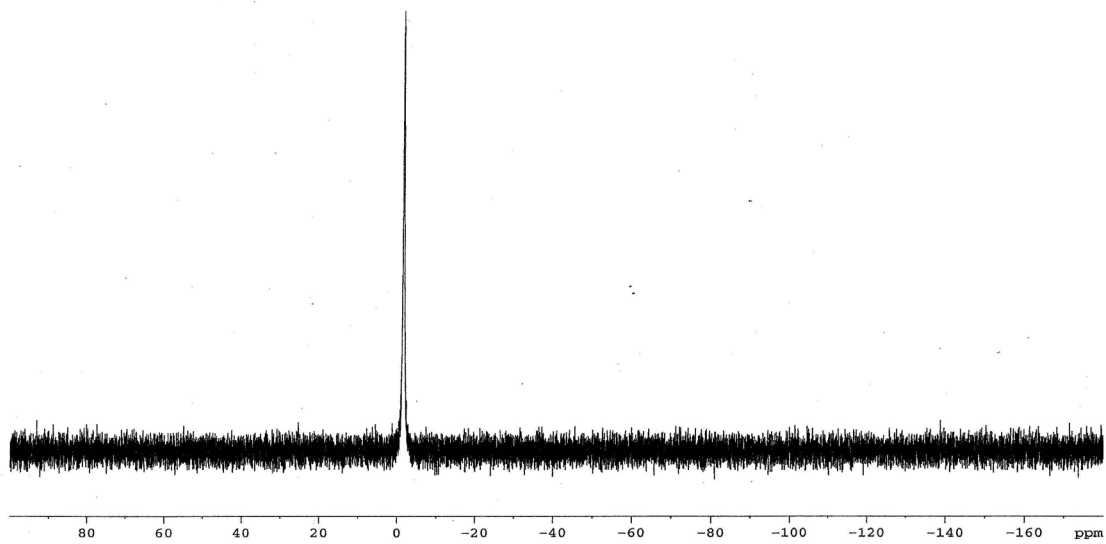
^{13}C NMR (CDCl_3 , 125 MHz) for **1.49**



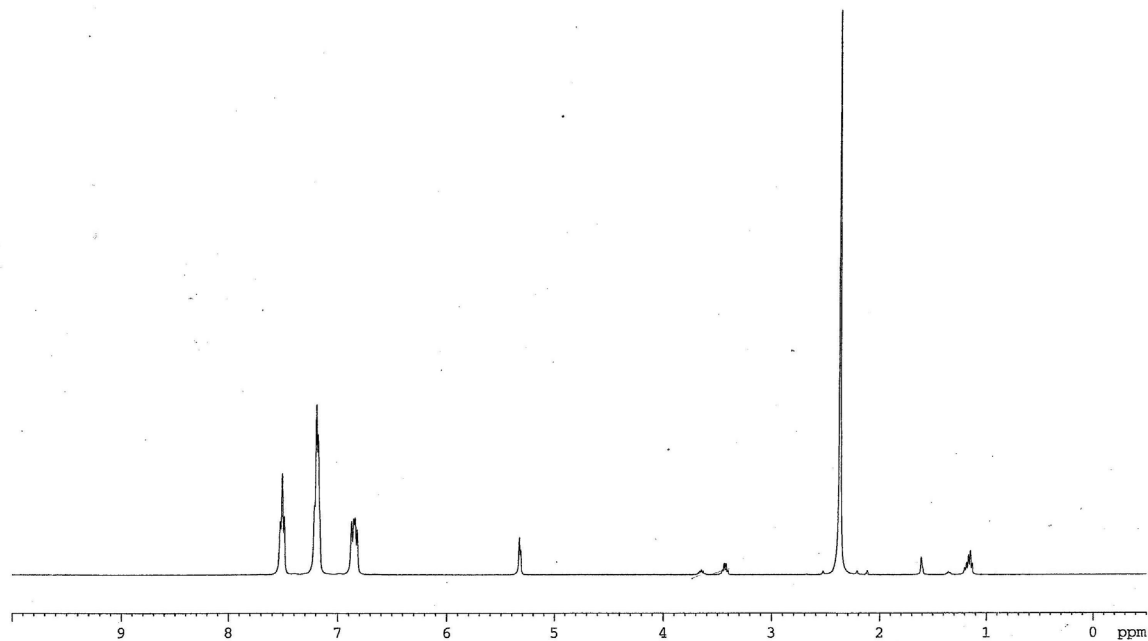
^{31}P NMR (CDCl_3 , 162 MHz) for **1.53e**



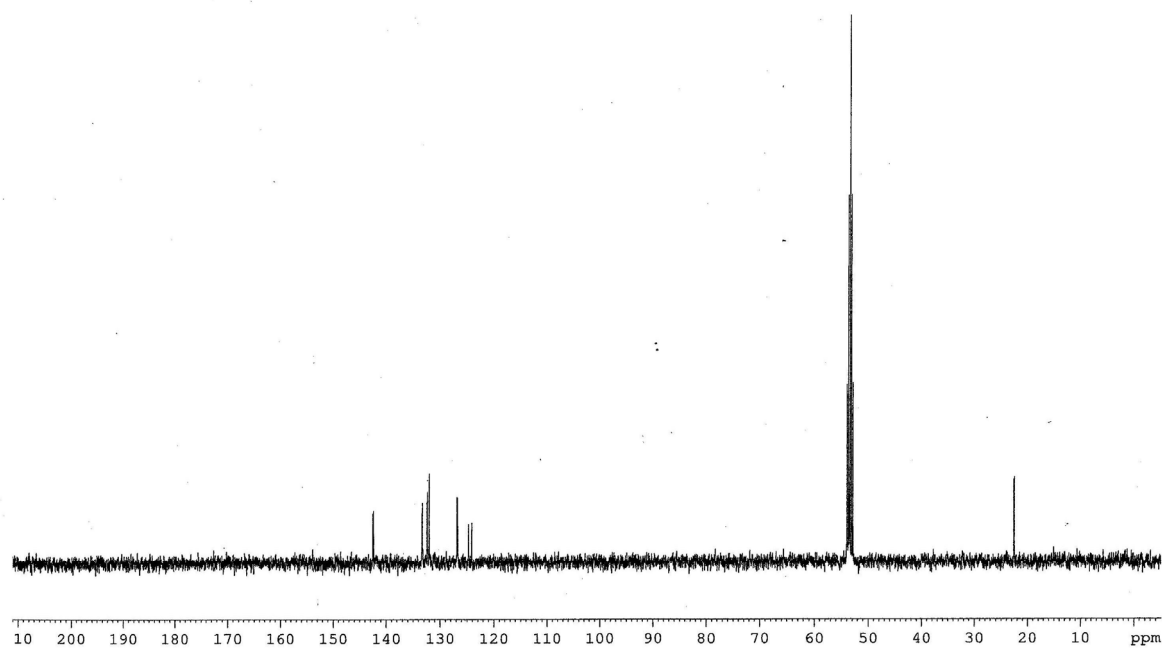
^{31}P NMR (CDCl_3 , 162 MHz) for **1.54**



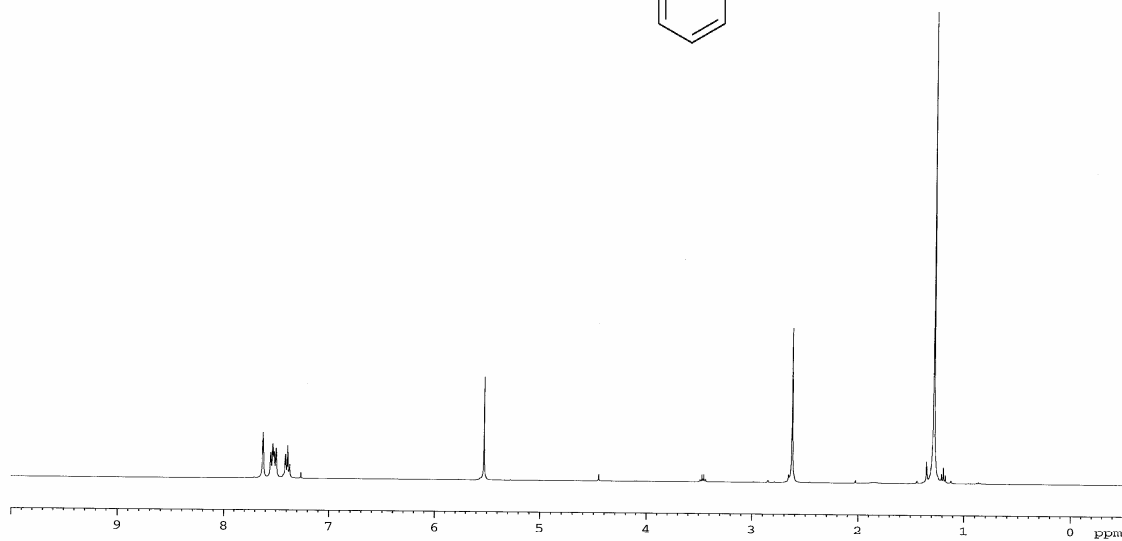
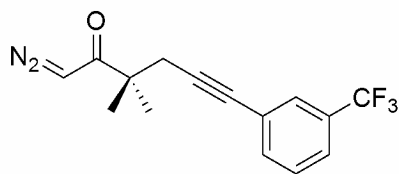
^1H NMR (CDCl_3 , 400 MHz) for **1.54**



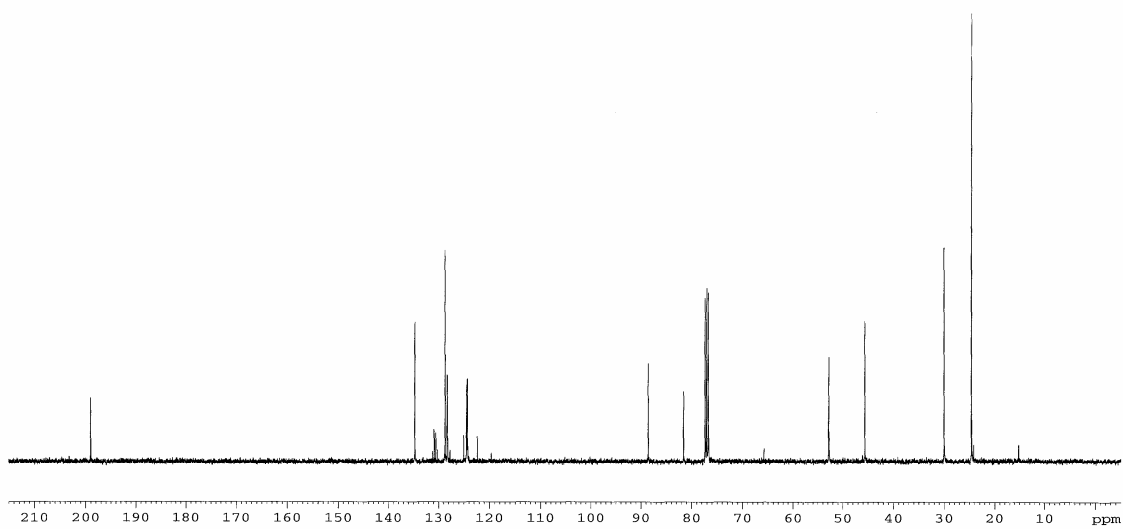
^{13}C NMR (CDCl_3 , 100 MHz) for **1.54**



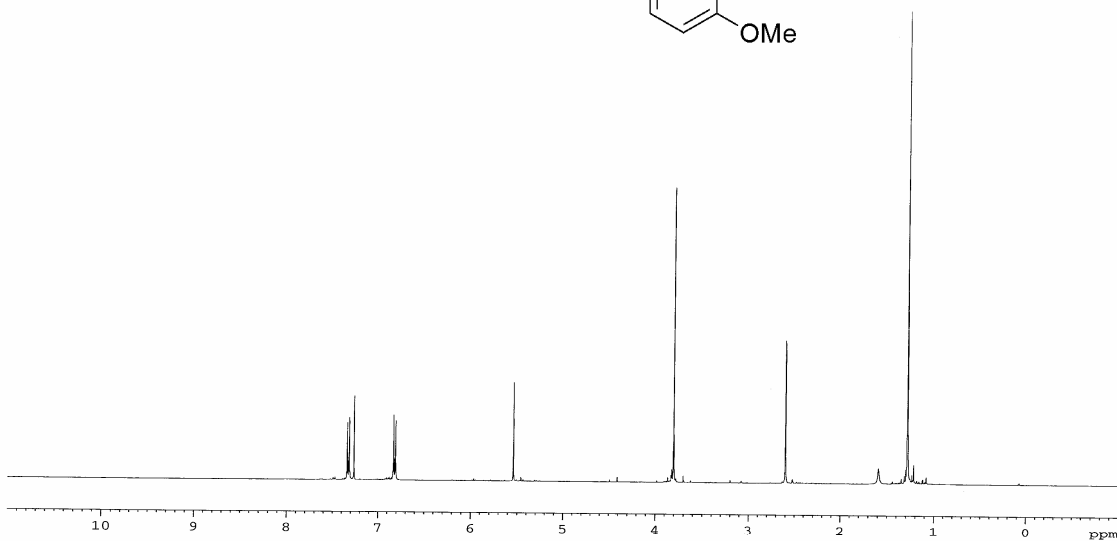
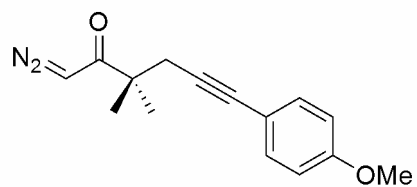
^1H NMR (CDCl_3 , 400 MHz) for **1.70**



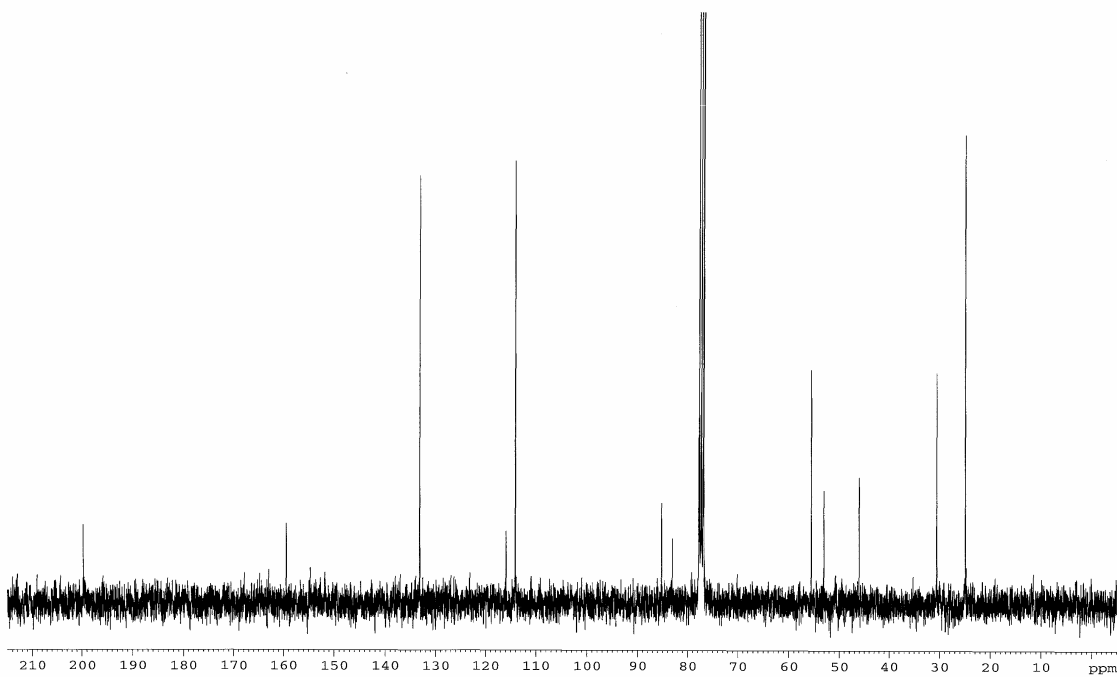
^{13}C NMR (CDCl_3 , 100 MHz) for **1.70**



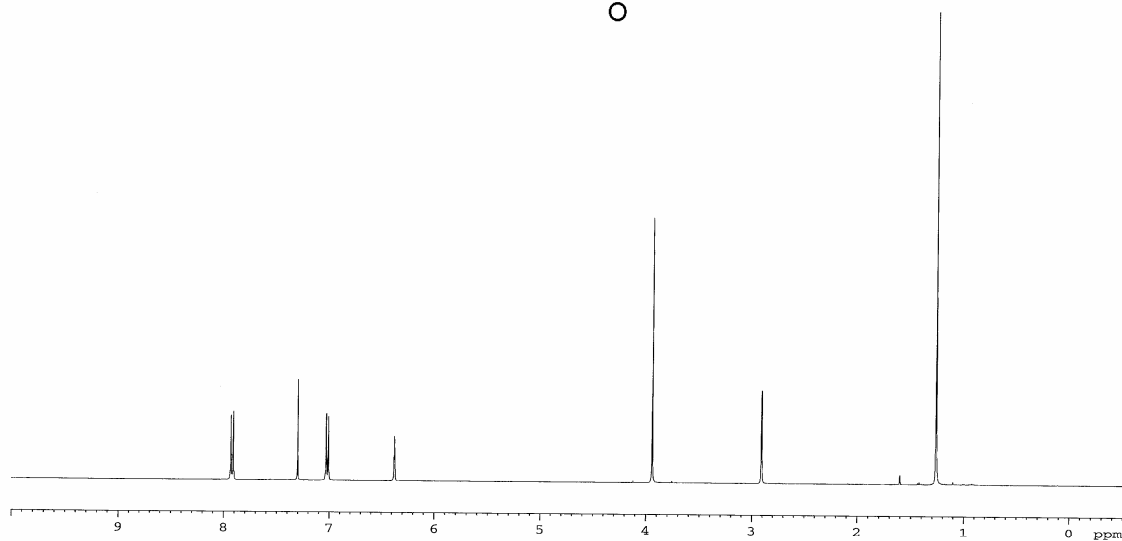
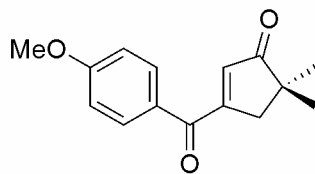
^1H NMR (CDCl_3 , 400 MHz) for **1.71**



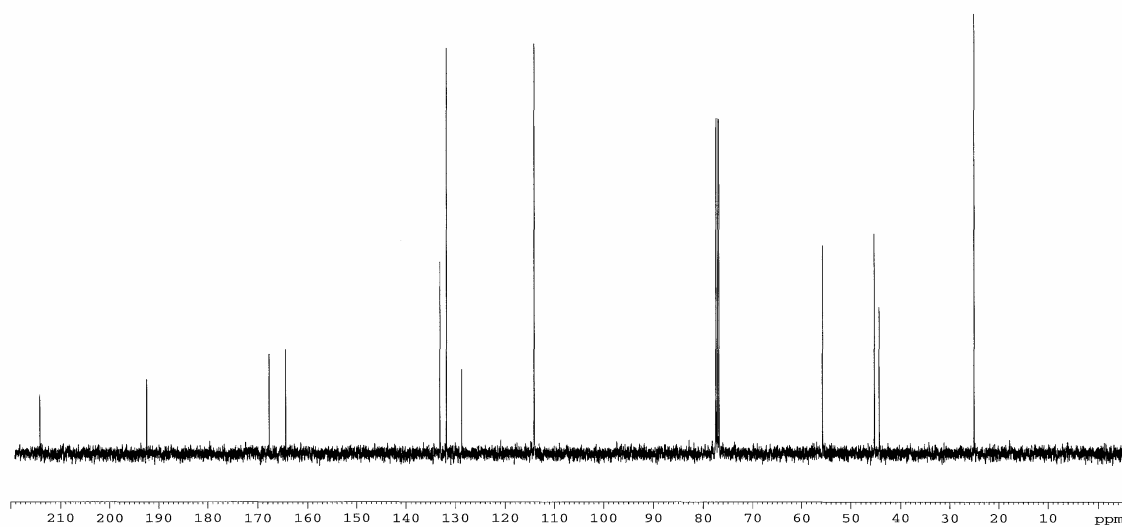
^{13}C NMR (CDCl_3 , 100 MHz) for **1.71**



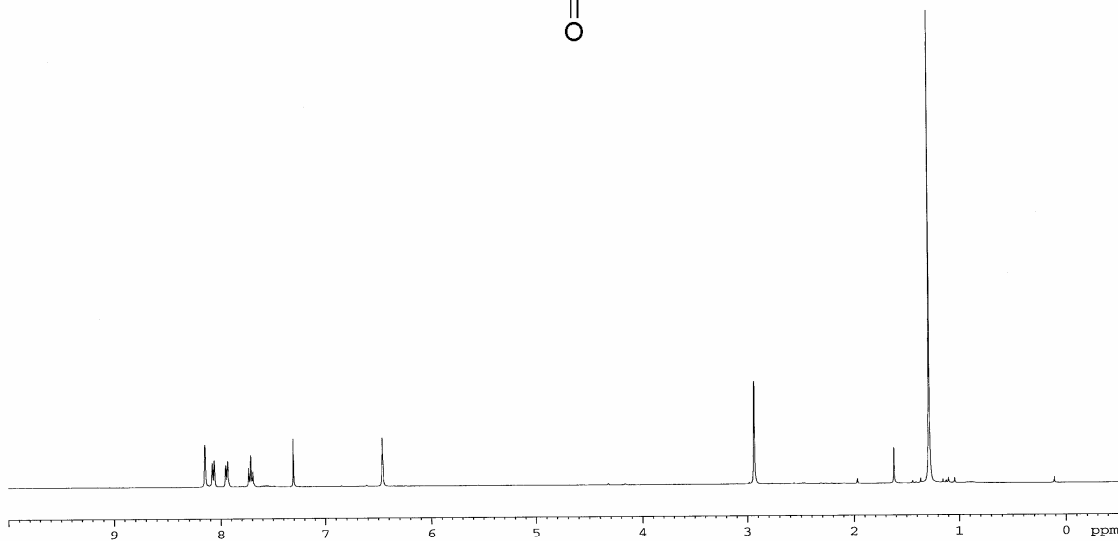
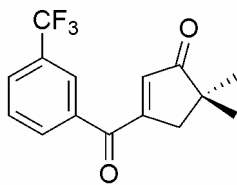
^1H NMR (CDCl_3 , 400 MHz) for **1.73**



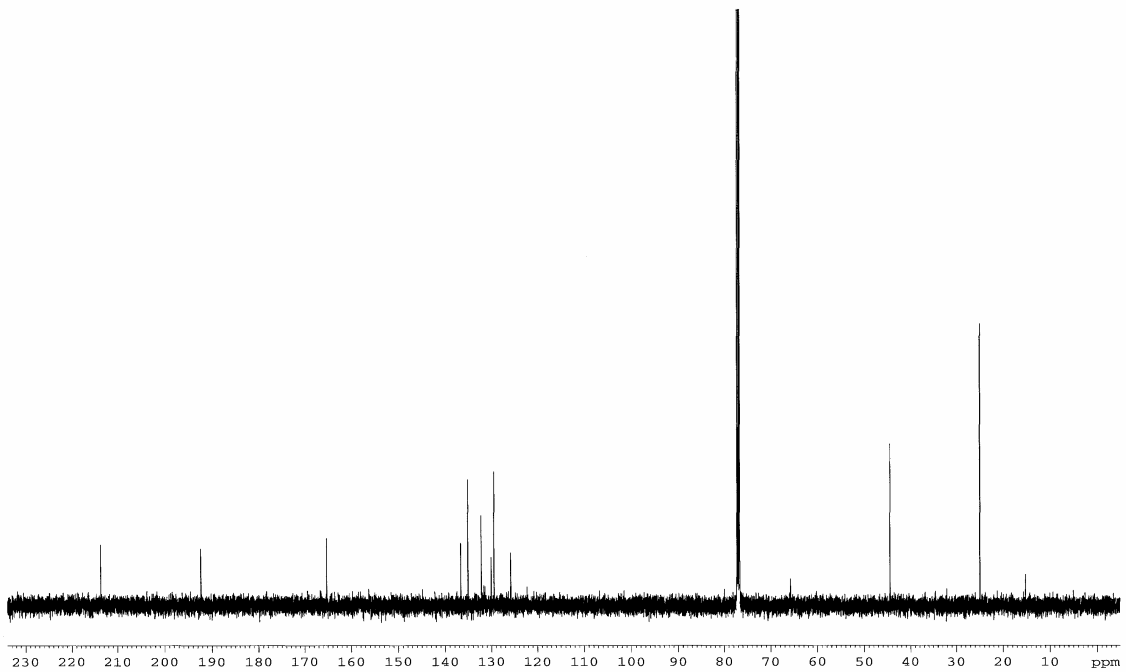
^{13}C NMR (CDCl_3 , 125 MHz) for **1.73**



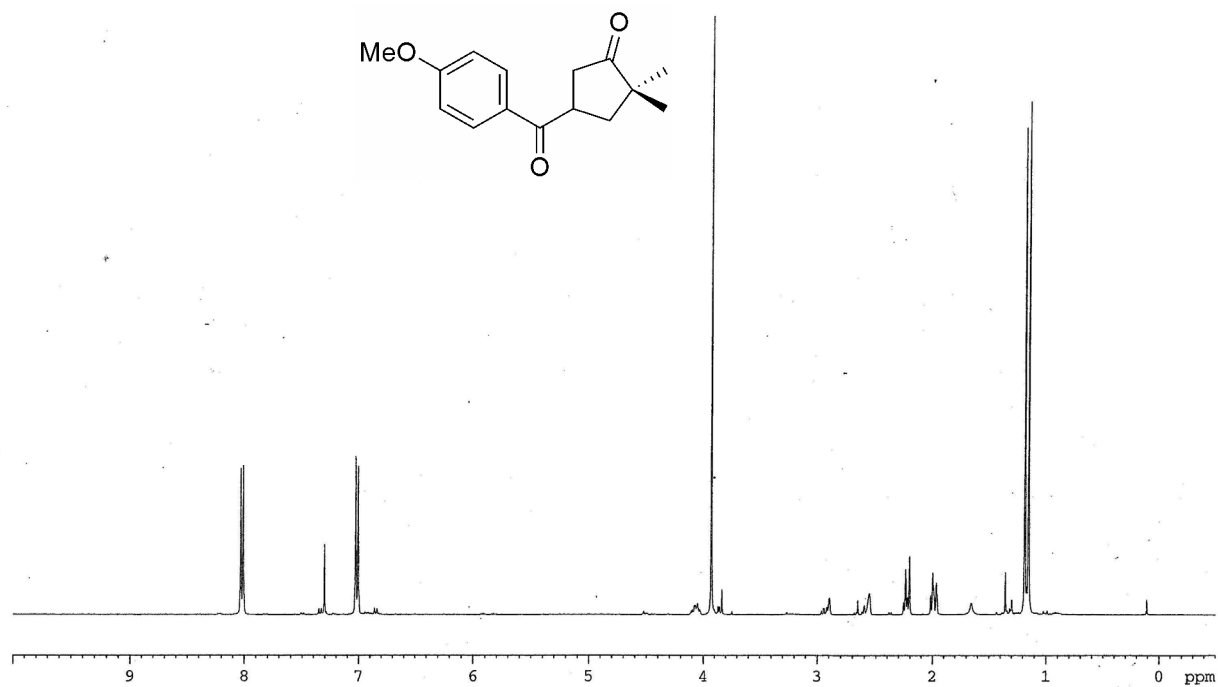
^1H NMR (CDCl_3 , 400 MHz) for **1.74**



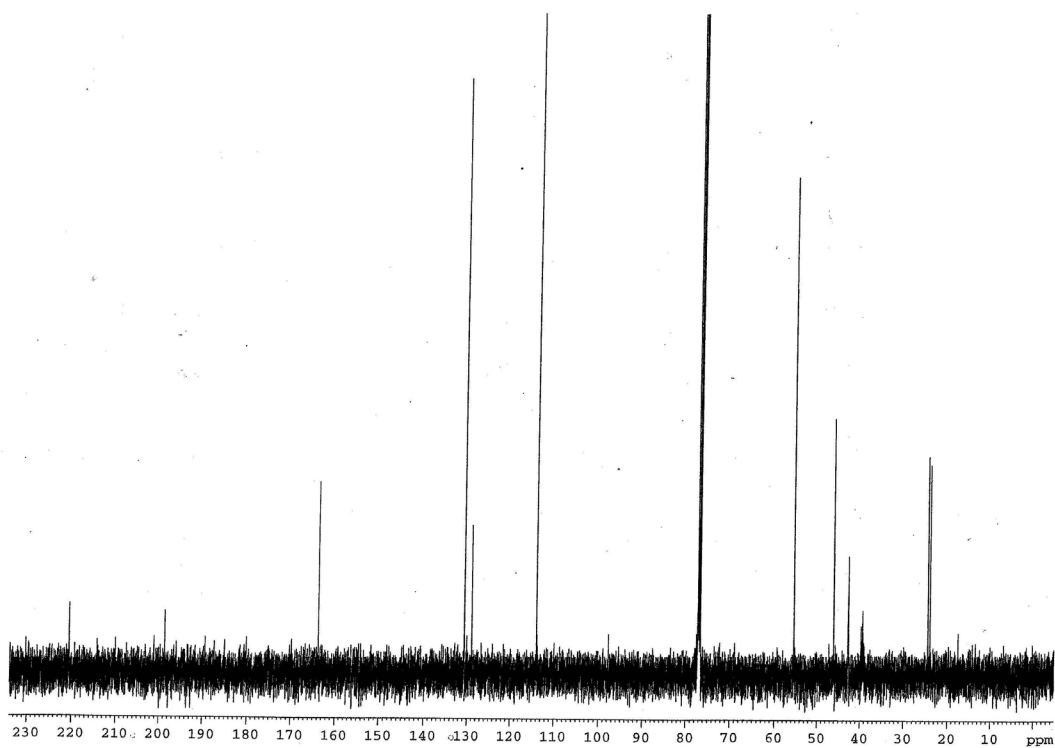
^{13}C NMR (CDCl_3 , 100 MHz) for **1.74**



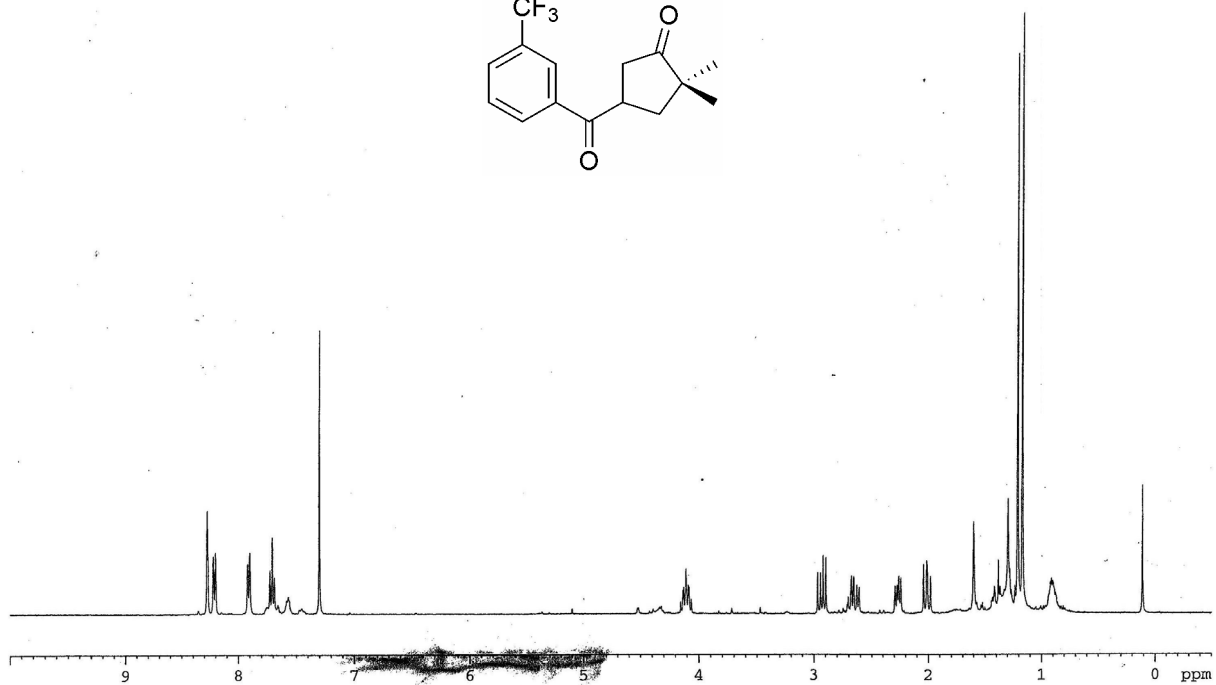
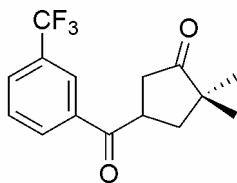
^1H NMR (CDCl_3 , 400 MHz) for **1.75**



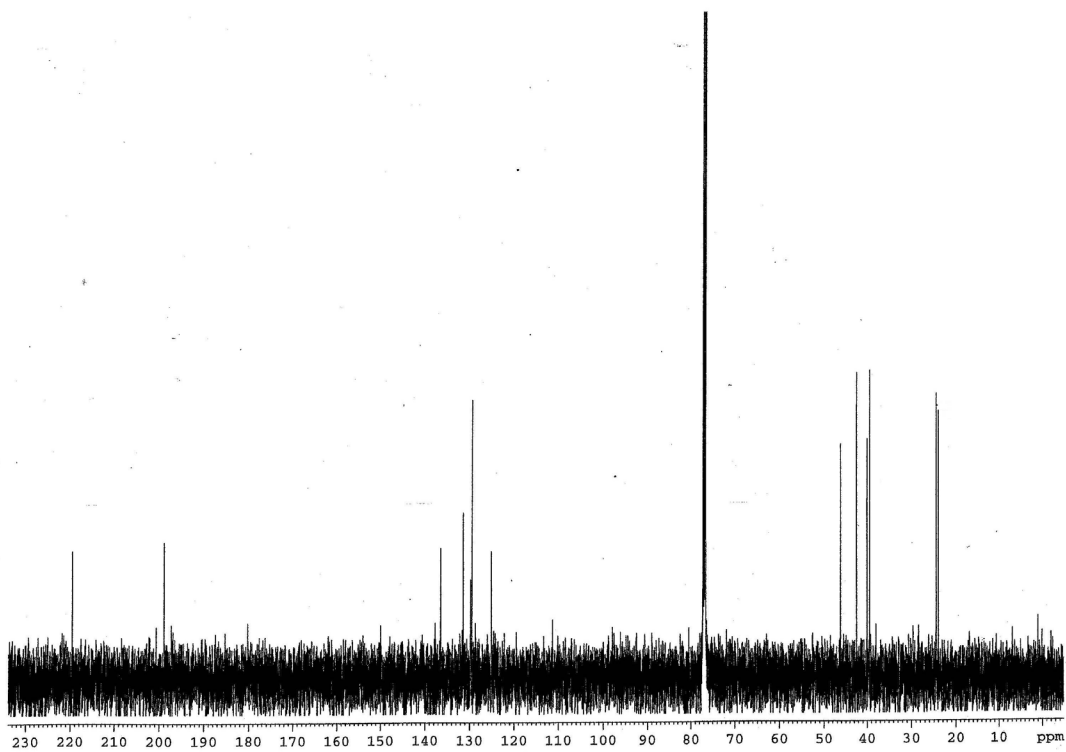
^{13}C NMR (CDCl_3 , 125 MHz) for **1.75**



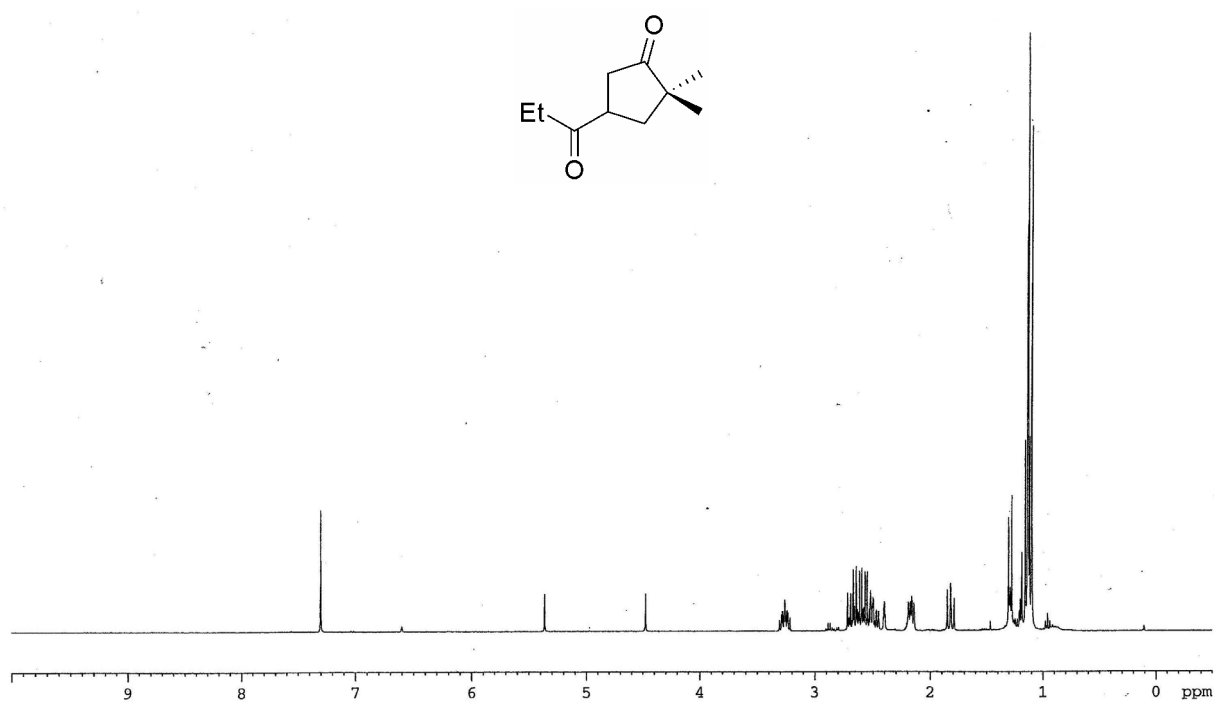
^1H NMR (CDCl_3 , 400 MHz) for **1.76**



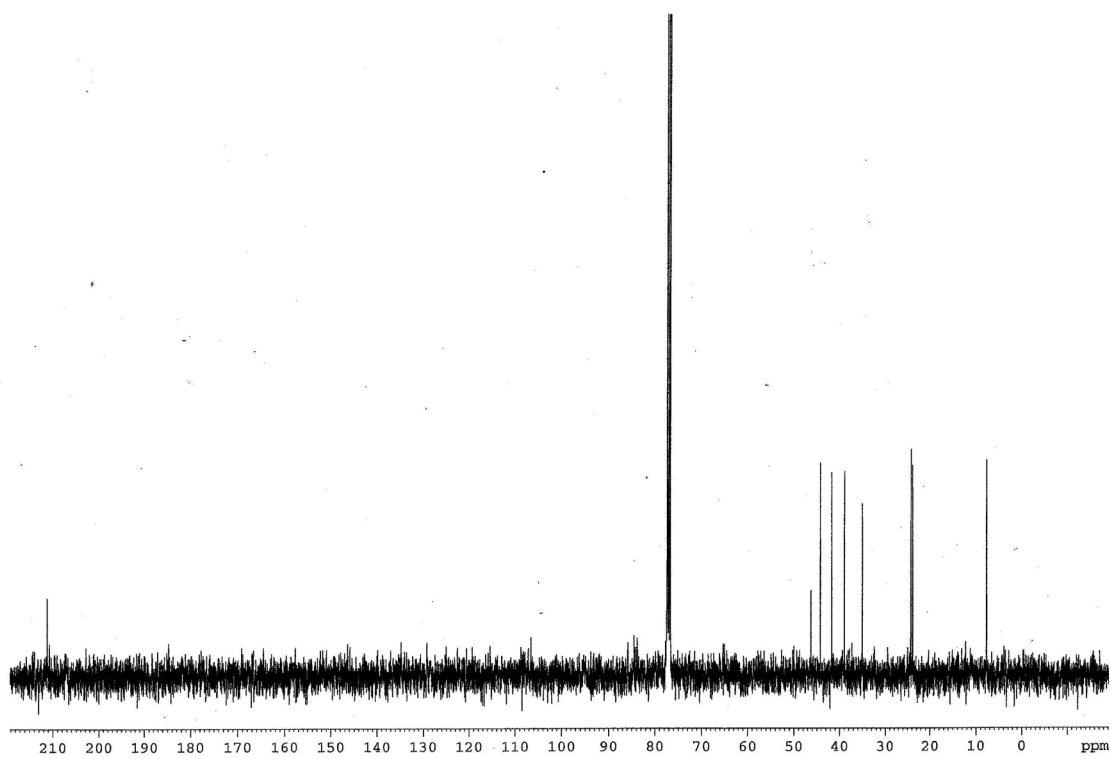
^{13}C NMR (CDCl_3 , 125 MHz) for **1.76**



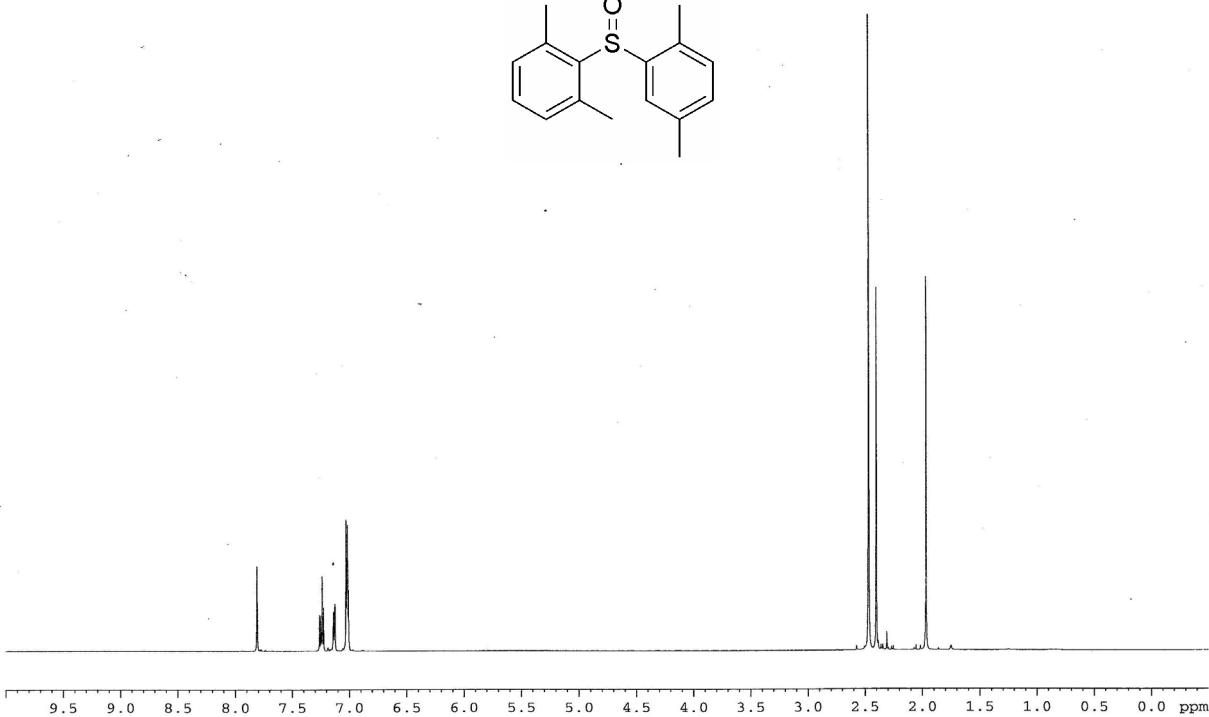
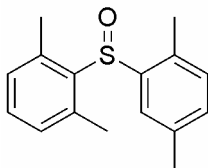
^1H NMR (CDCl_3 , 400 MHz) for **1.77**



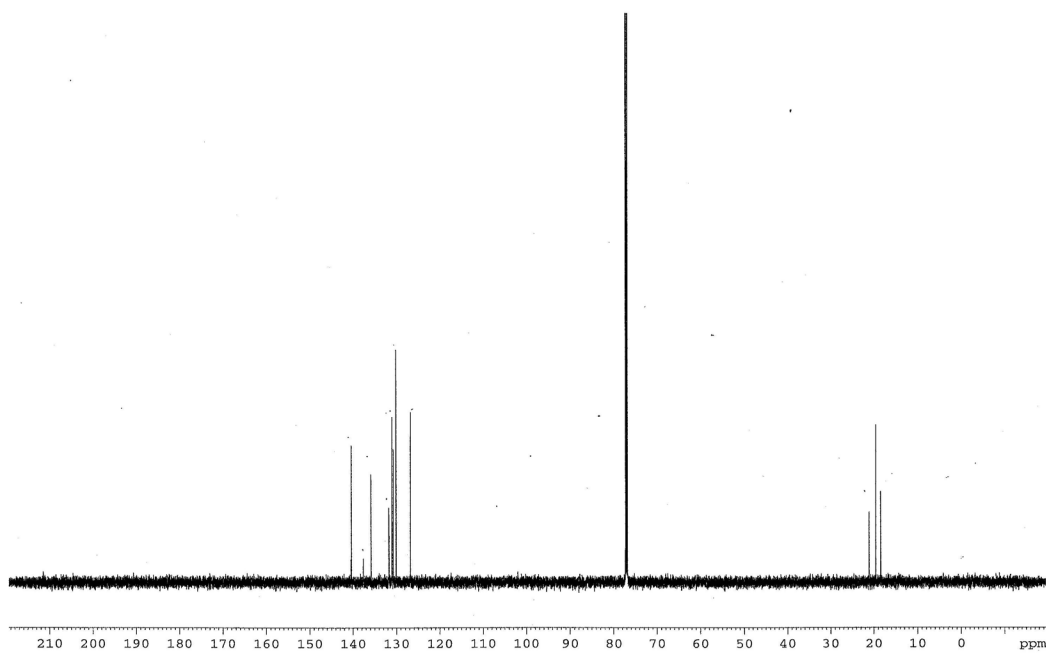
^{13}C NMR (CDCl_3 , 100 MHz) for **1.77**



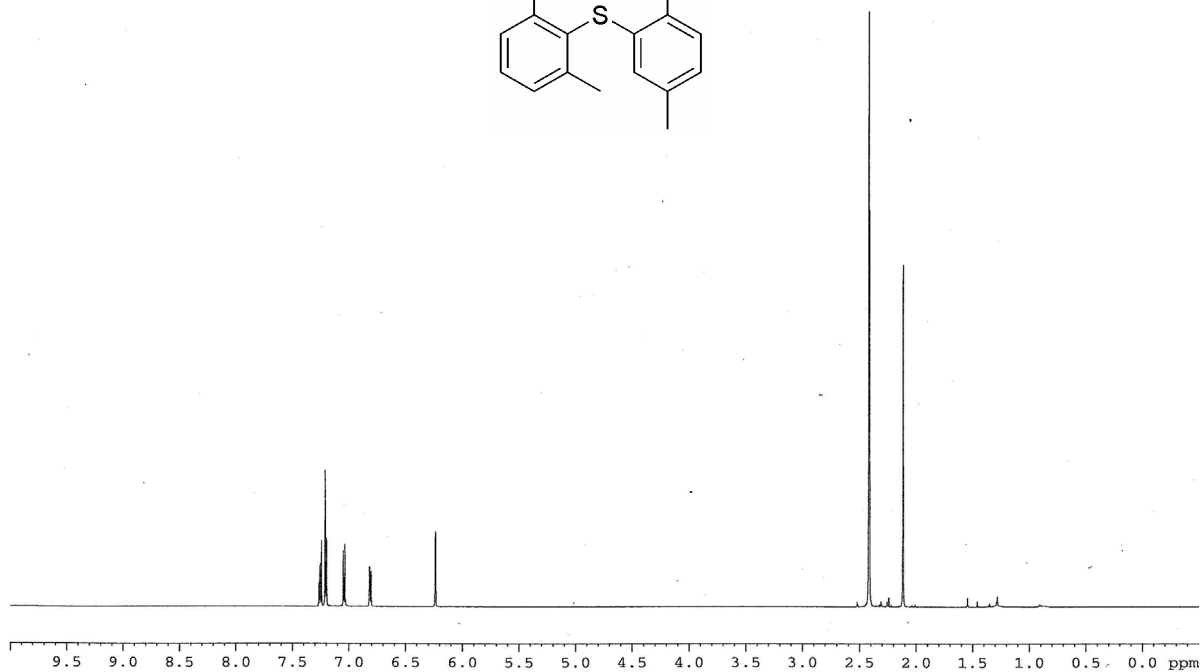
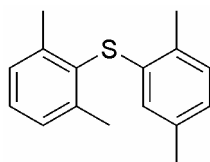
^1H NMR (CDCl_3 , 600 MHz) for **1.80**



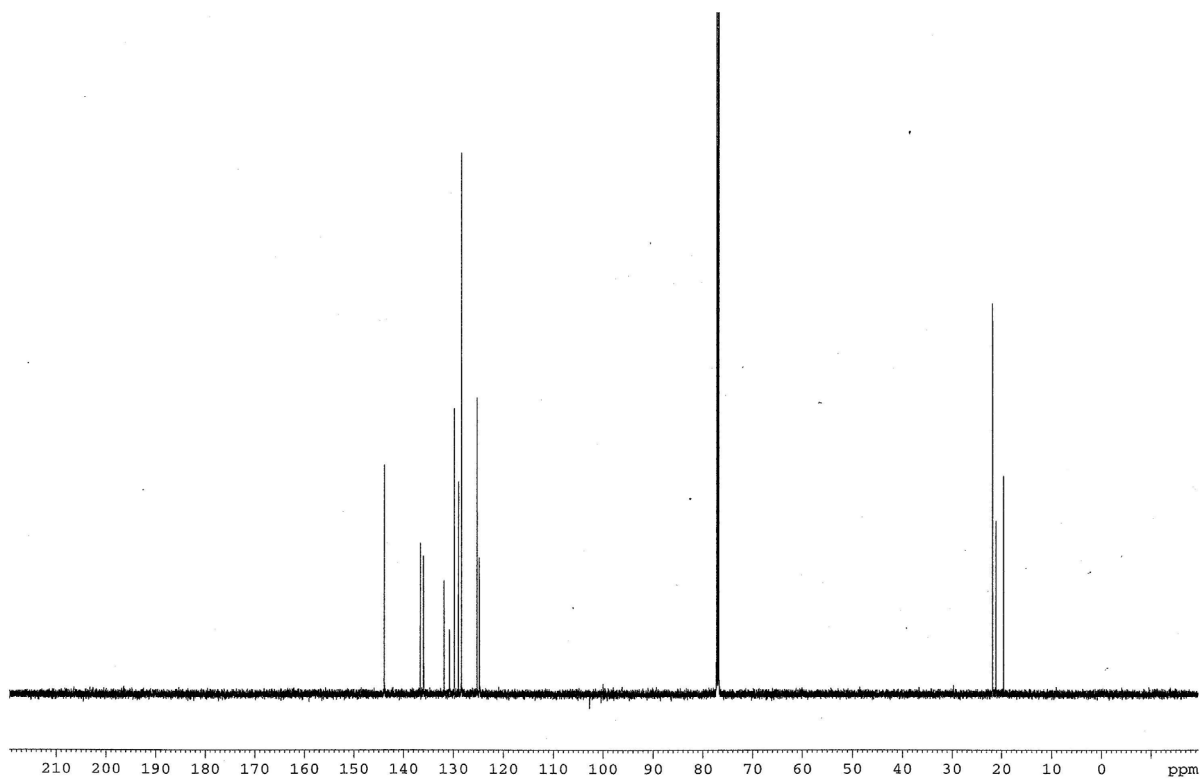
^{13}C NMR (CDCl_3 , 150 MHz) for **1.80**



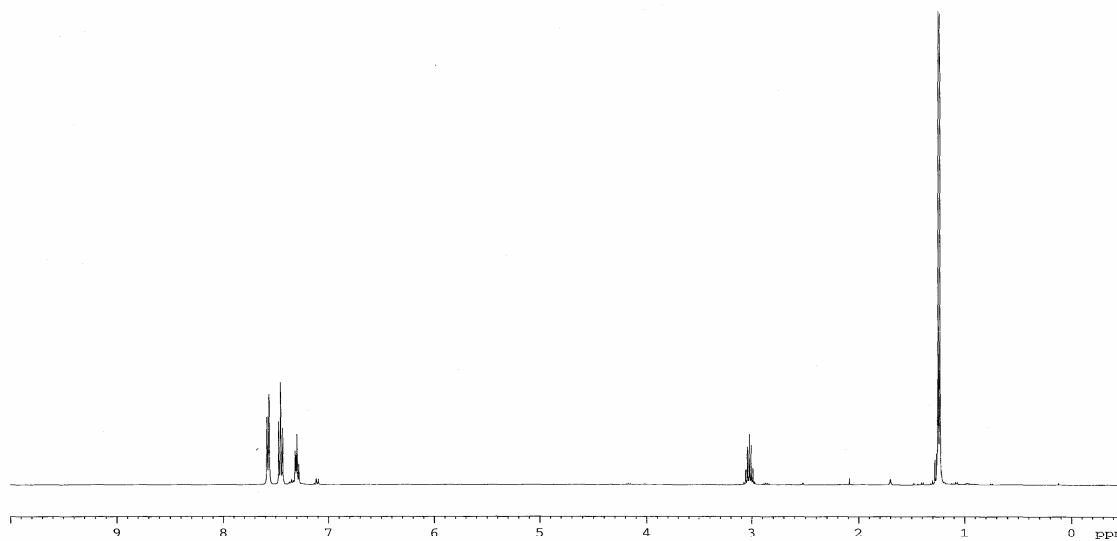
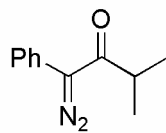
^1H NMR (CDCl_3 , 600 MHz) for **1.81**



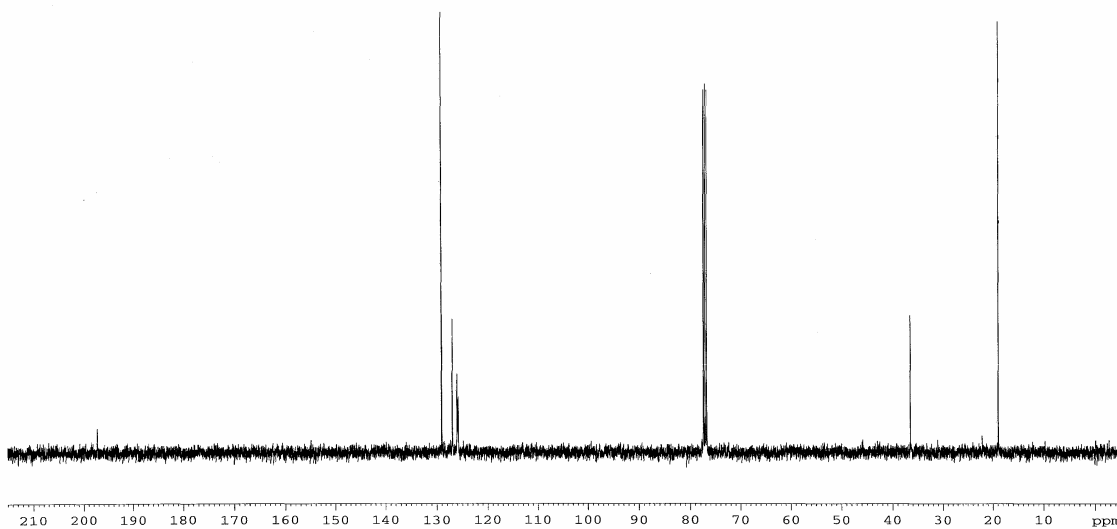
^{13}C NMR (CDCl_3 , 150 MHz) for **1.81**



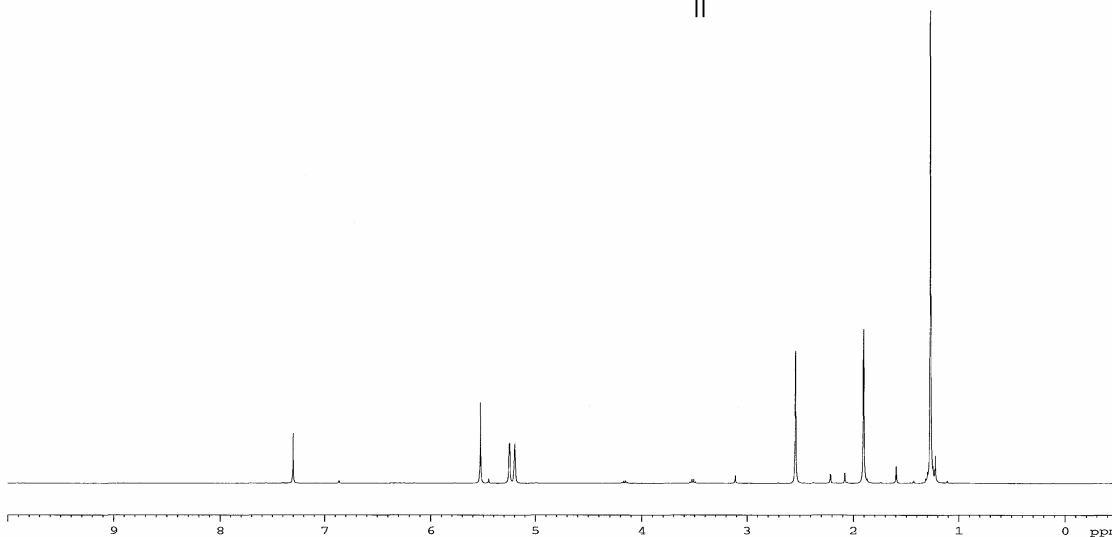
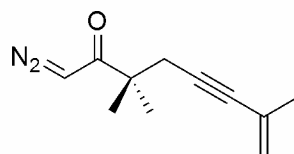
^1H NMR (CDCl_3 , 500 MHz) for **1.82**



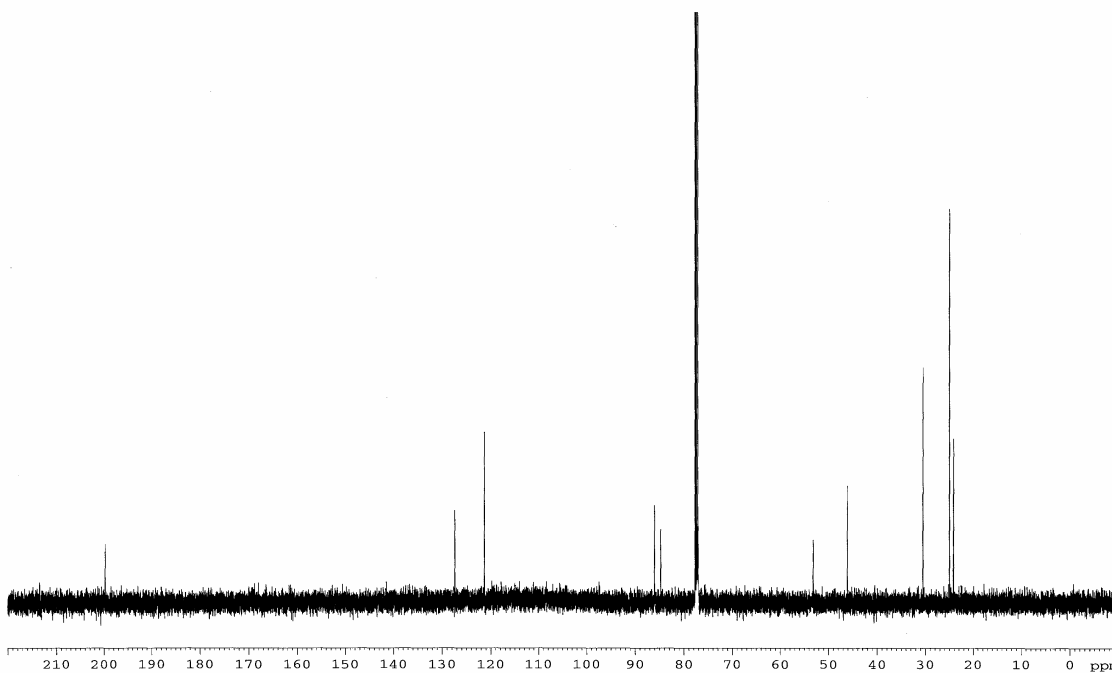
^{13}C NMR (CDCl_3 , 125 MHz) for **1.82**



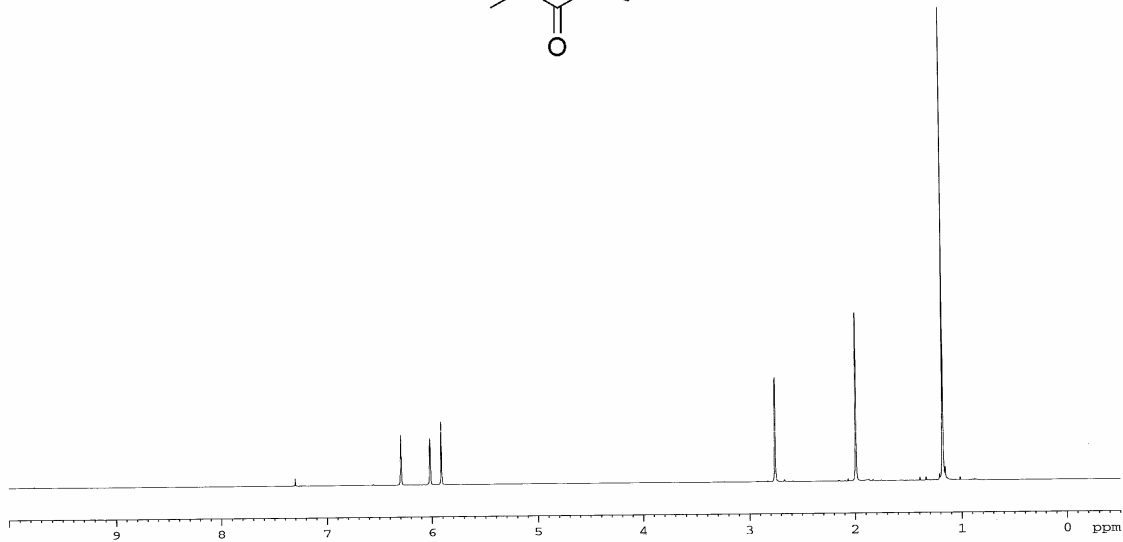
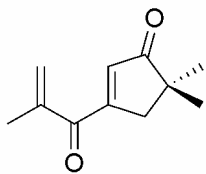
^1H NMR (CDCl_3 , 400 MHz) for **1.84**



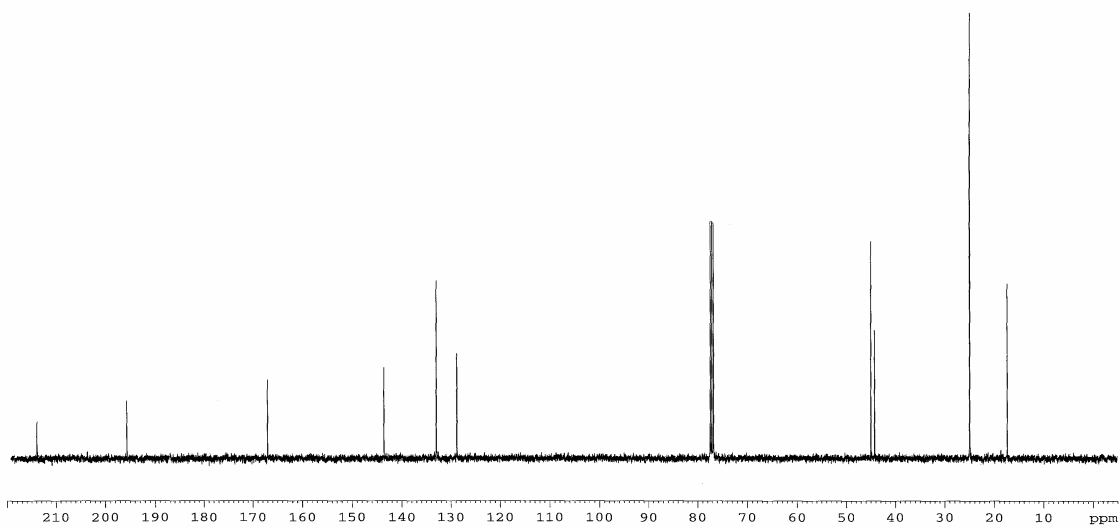
^{13}C NMR (CDCl_3 , 125 MHz) for **1.84**



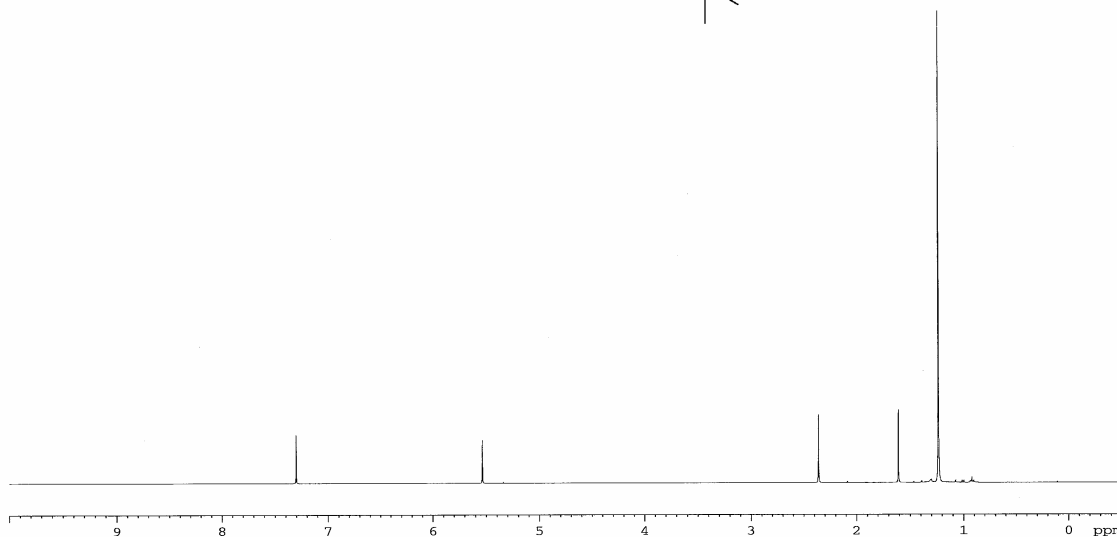
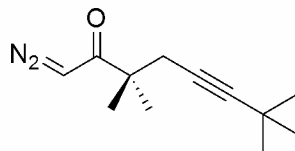
^1H NMR (CDCl_3 , 500 MHz) for **1.86**



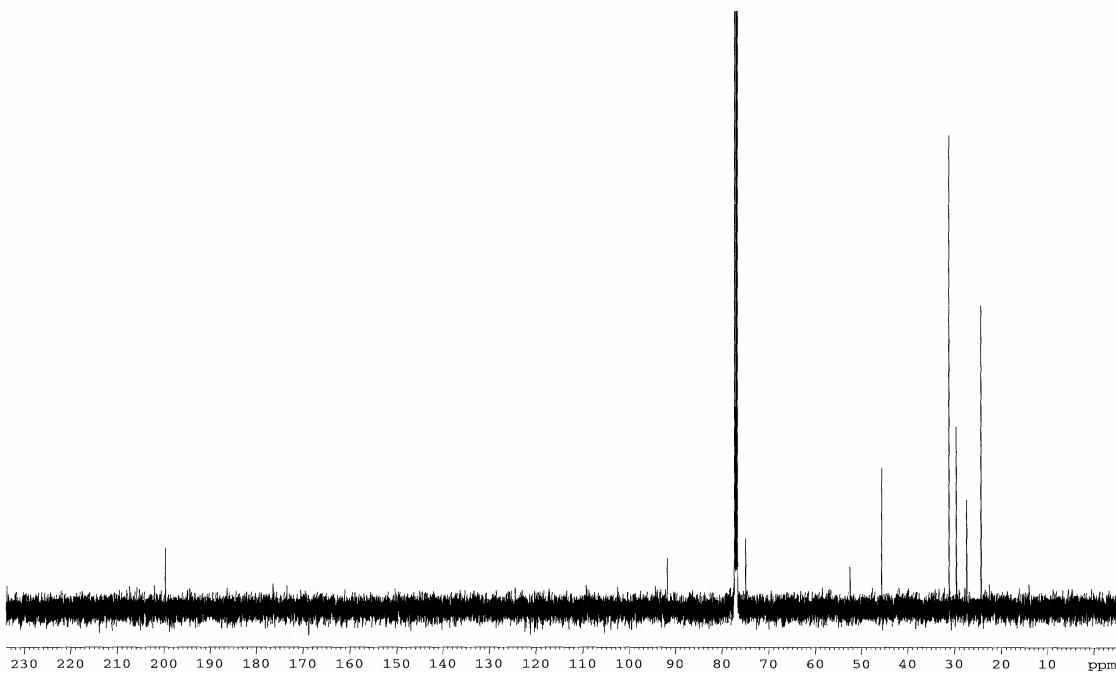
^{13}C NMR (CDCl_3 , 125 MHz) for **1.86**



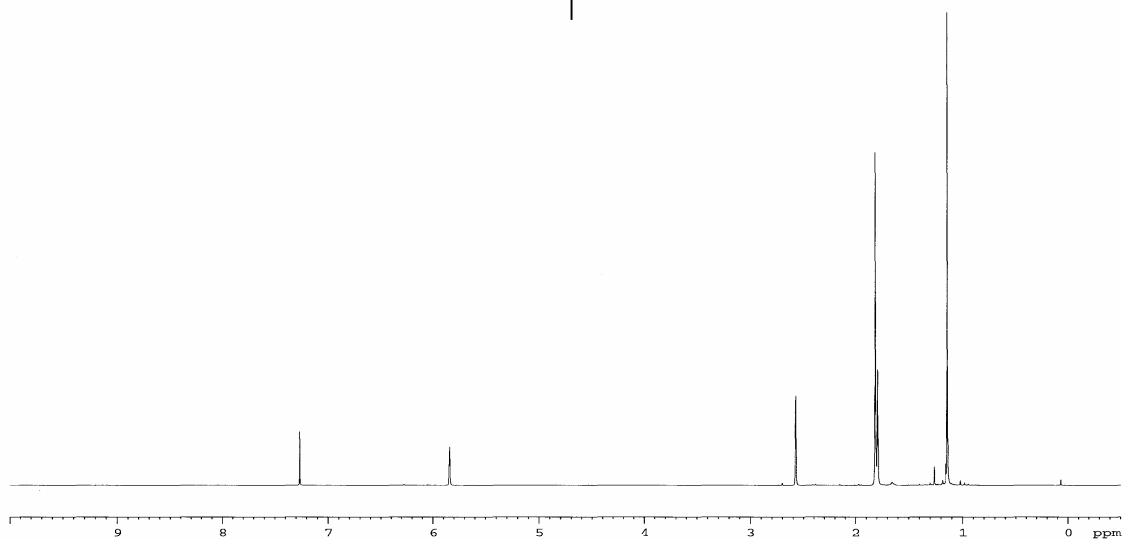
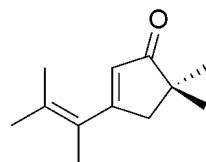
^1H NMR (CDCl_3 , 400 MHz) for **1.89**



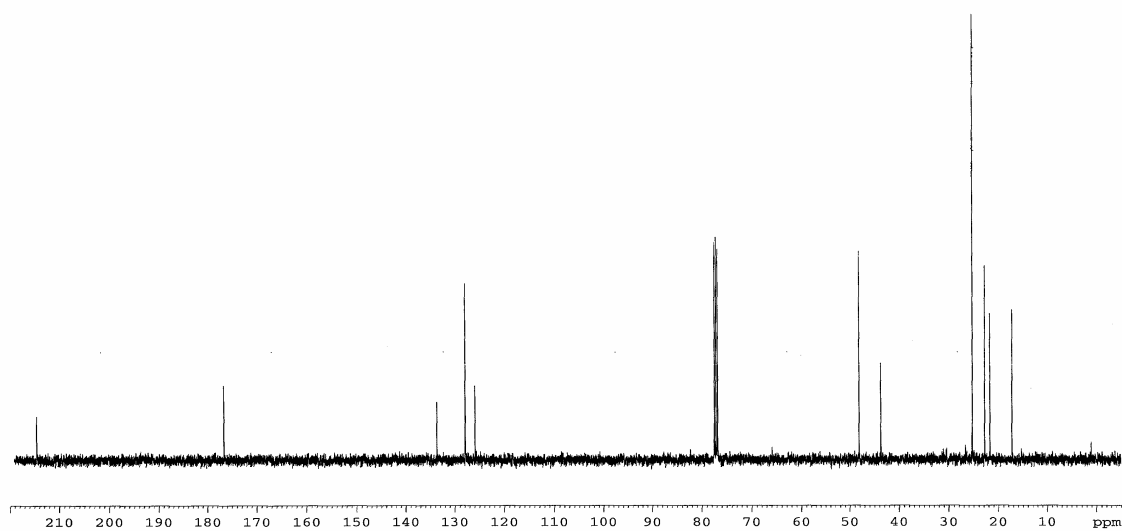
^{13}C NMR (CDCl_3 , 125 MHz) for **1.89**



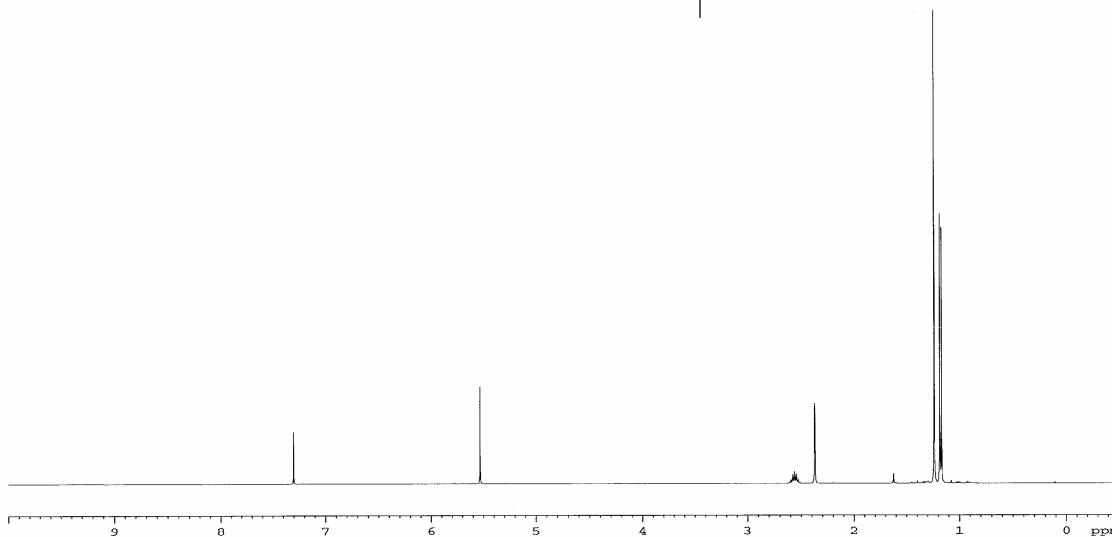
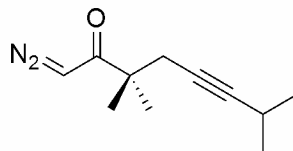
^1H NMR (CDCl_3 , 400 MHz) for **1.90**



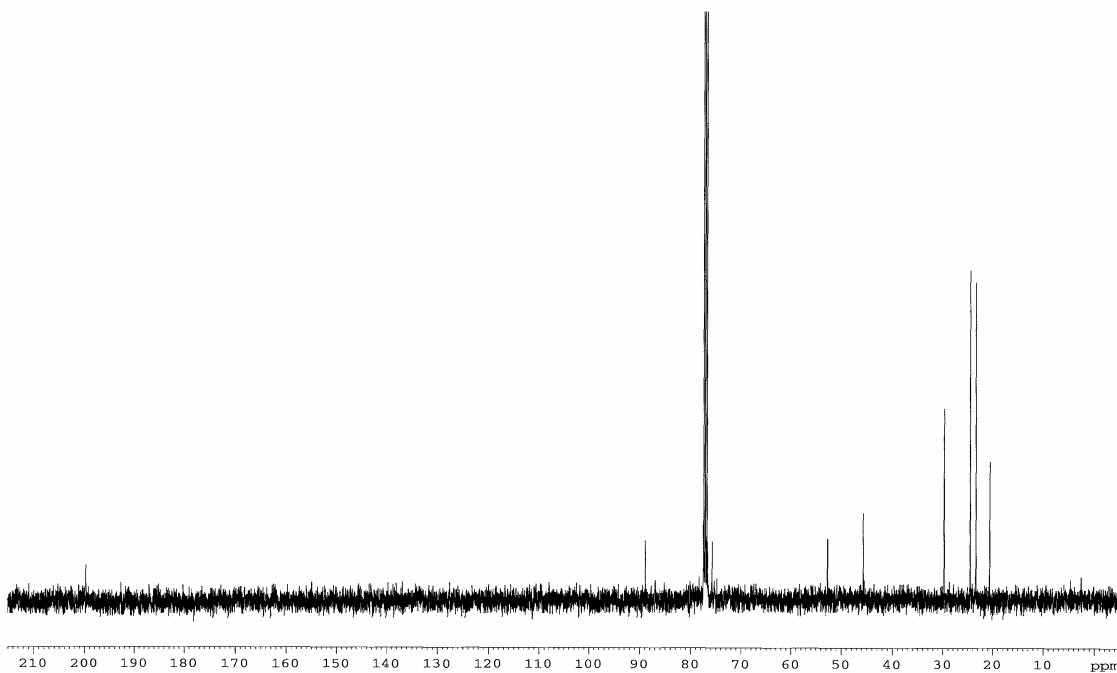
^{13}C NMR (CDCl_3 , 100 MHz) for **1.90**



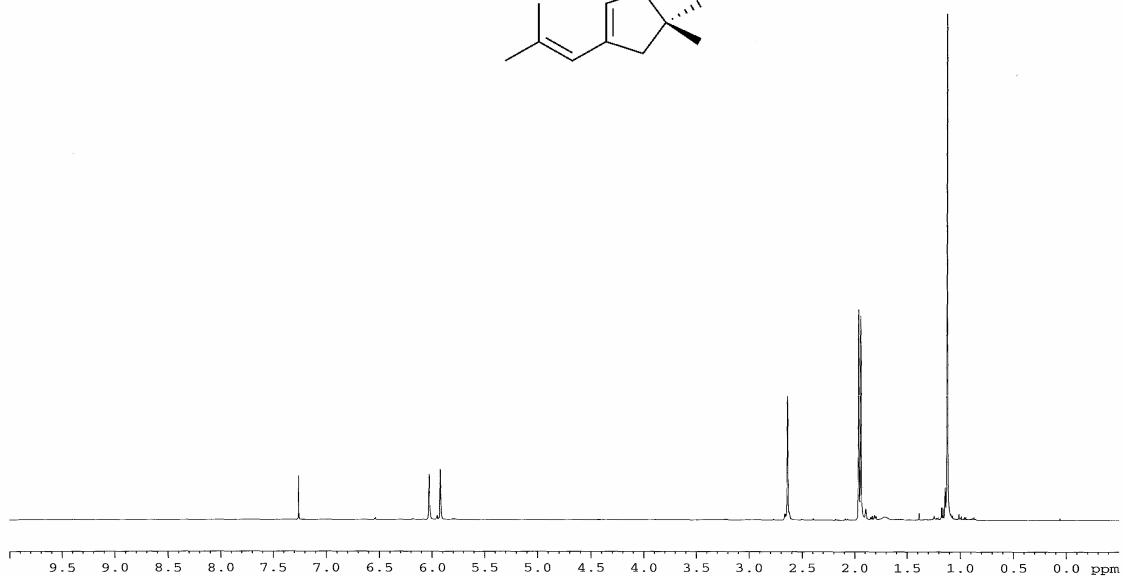
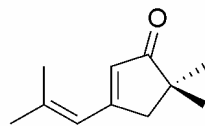
^1H NMR (CDCl_3 , 400 MHz) for **1.91**



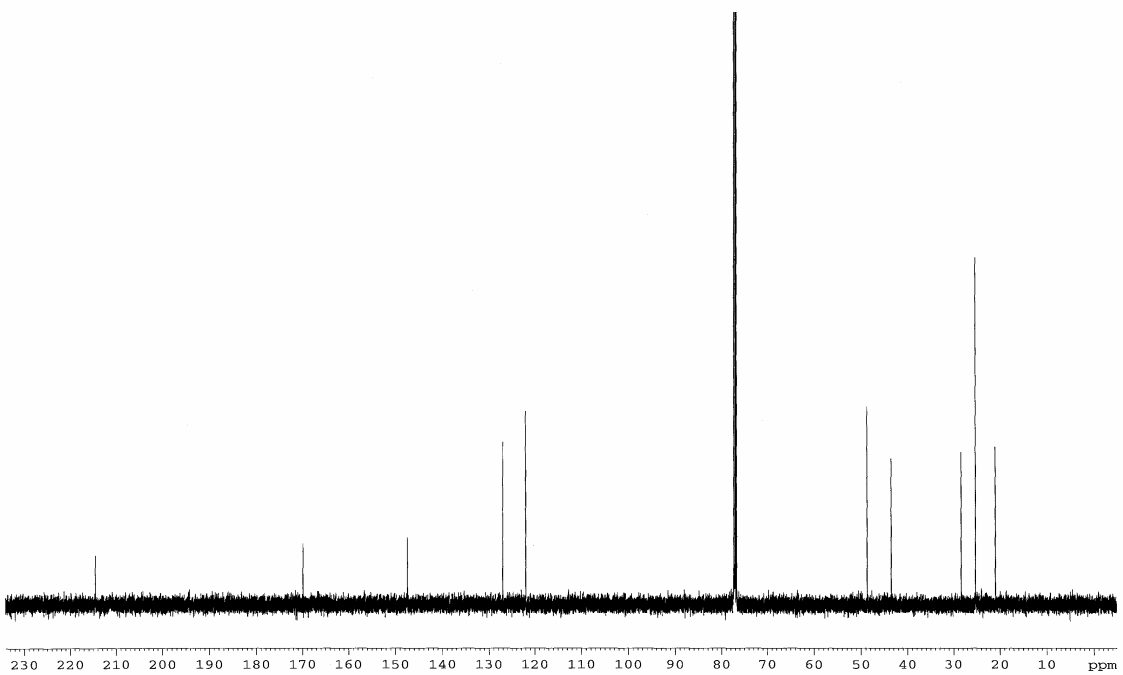
^{13}C NMR (CDCl_3 , 100 MHz) for **1.91**



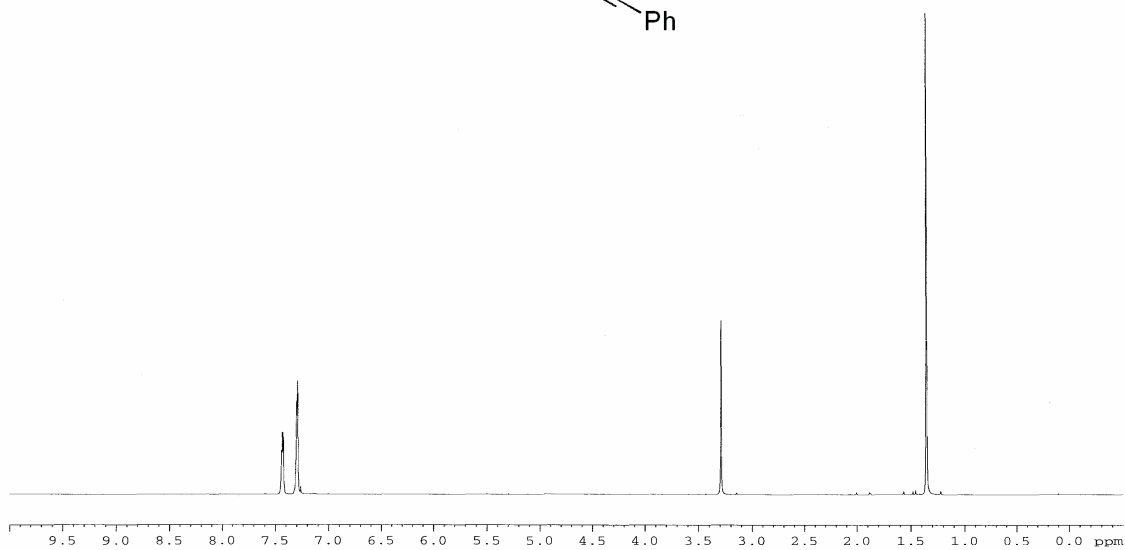
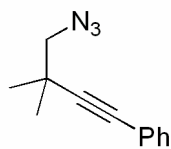
^1H NMR (CDCl_3 , 500 MHz) for **1.92**



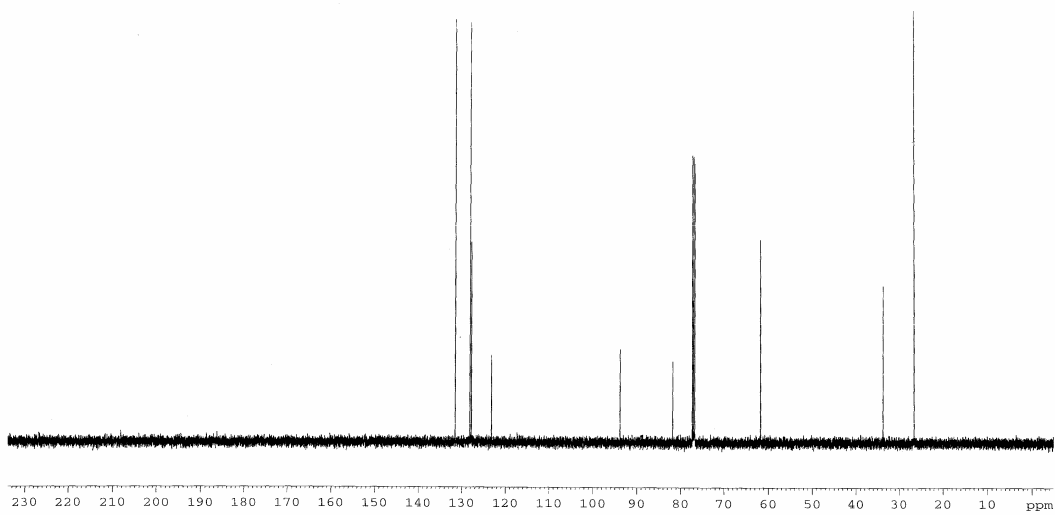
^{13}C NMR (CDCl_3 , 125 MHz) for **1.92**



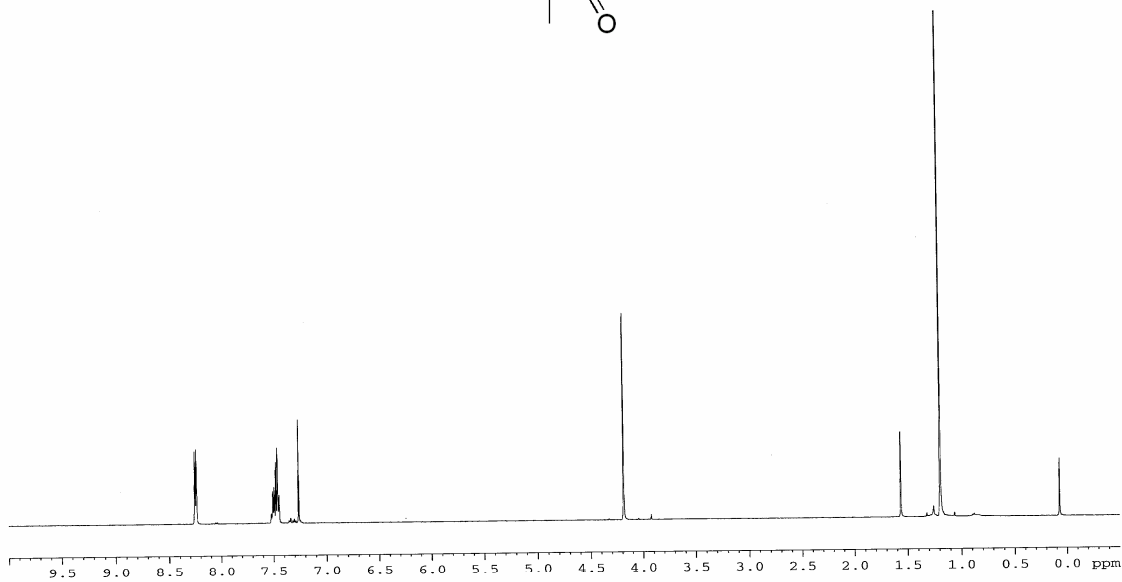
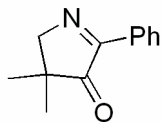
^1H NMR (CDCl_3 , 500 MHz) for **1.93**



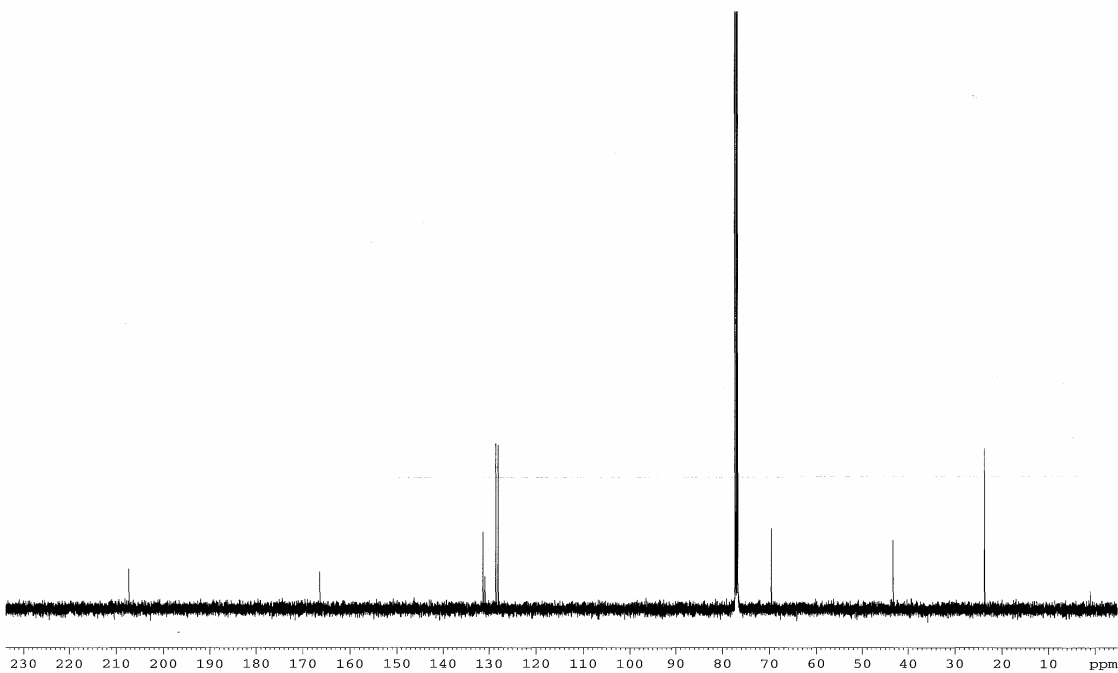
^{13}C NMR (CDCl_3 , 100 MHz) for **1.93**



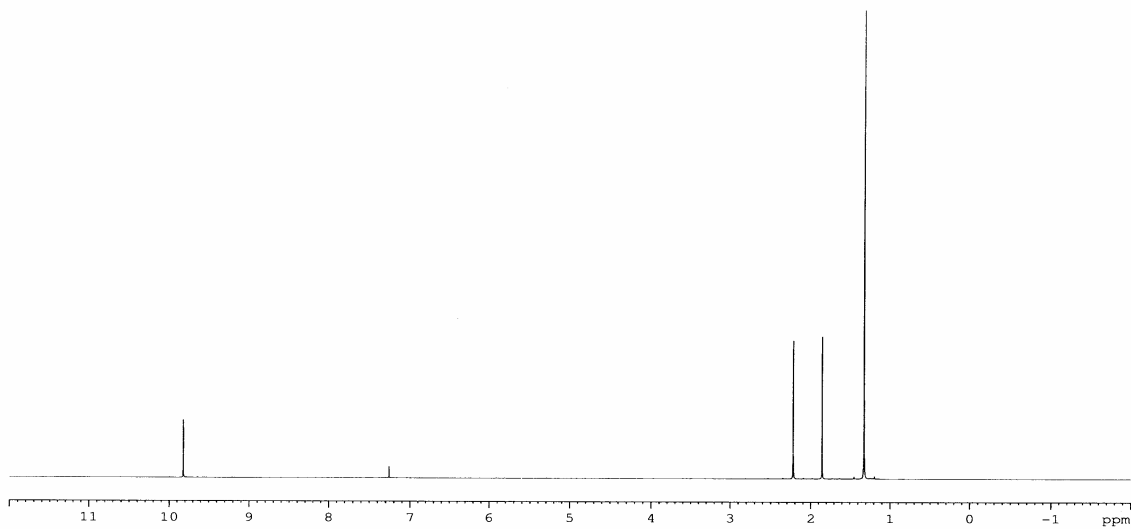
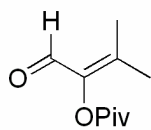
¹H NMR (CDCl₃, 400 MHz) for **1.94**



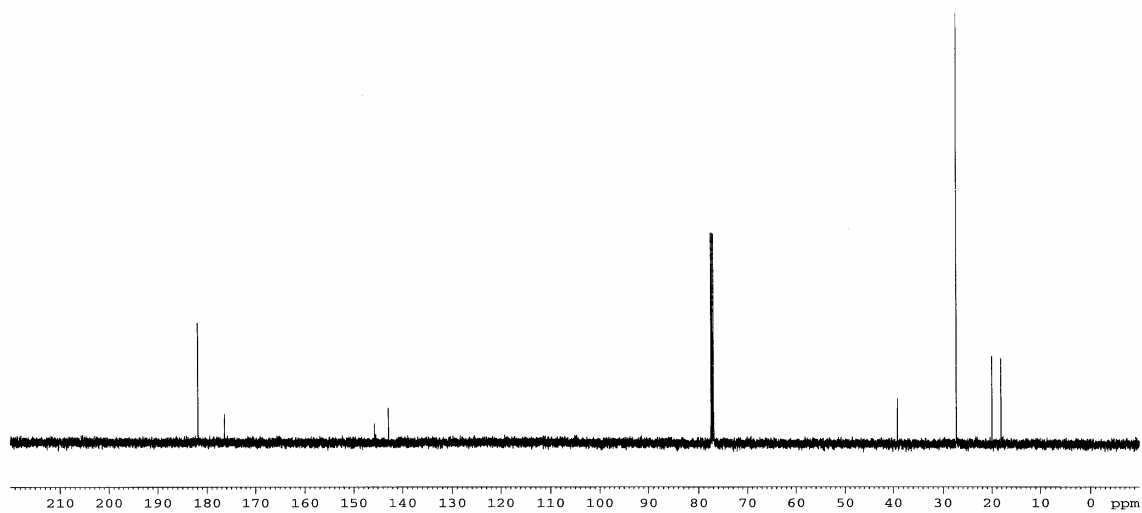
¹³C NMR (CDCl₃, 125 MHz) for **1.94**



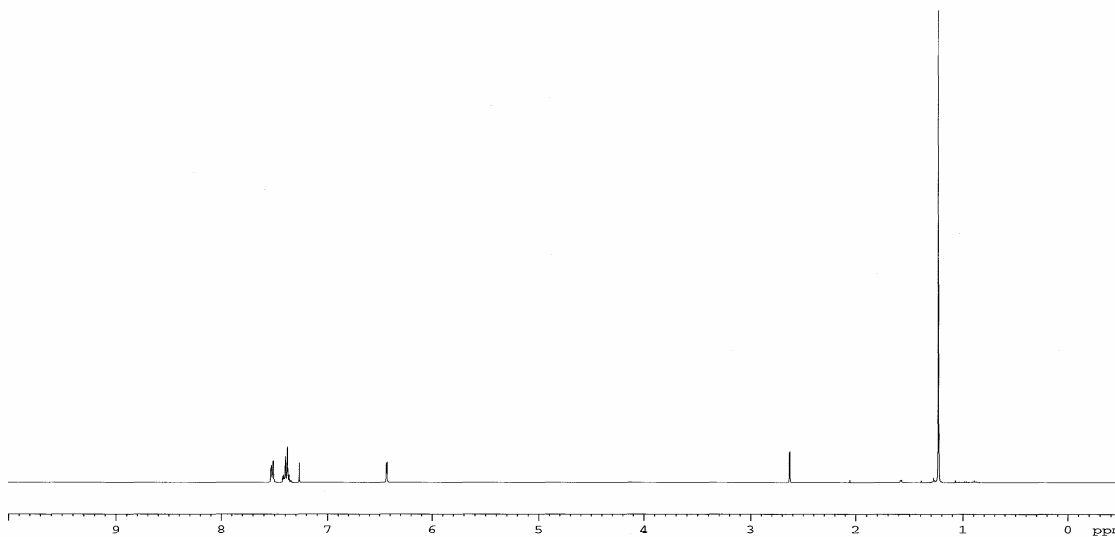
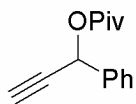
^1H NMR (CDCl_3 , 500 MHz) for **1.104**



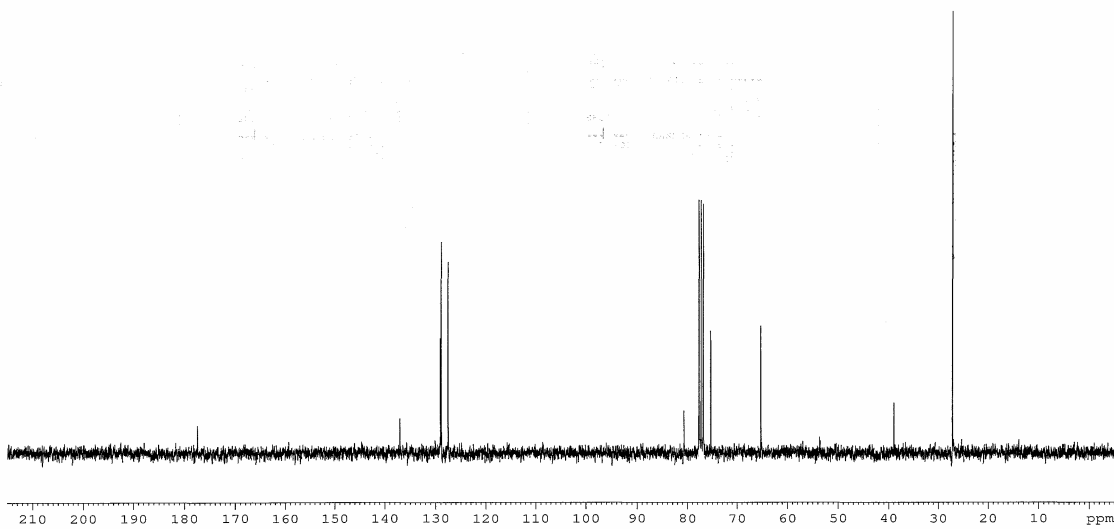
^{13}C NMR (CDCl_3 , 125 MHz) for **1.104**



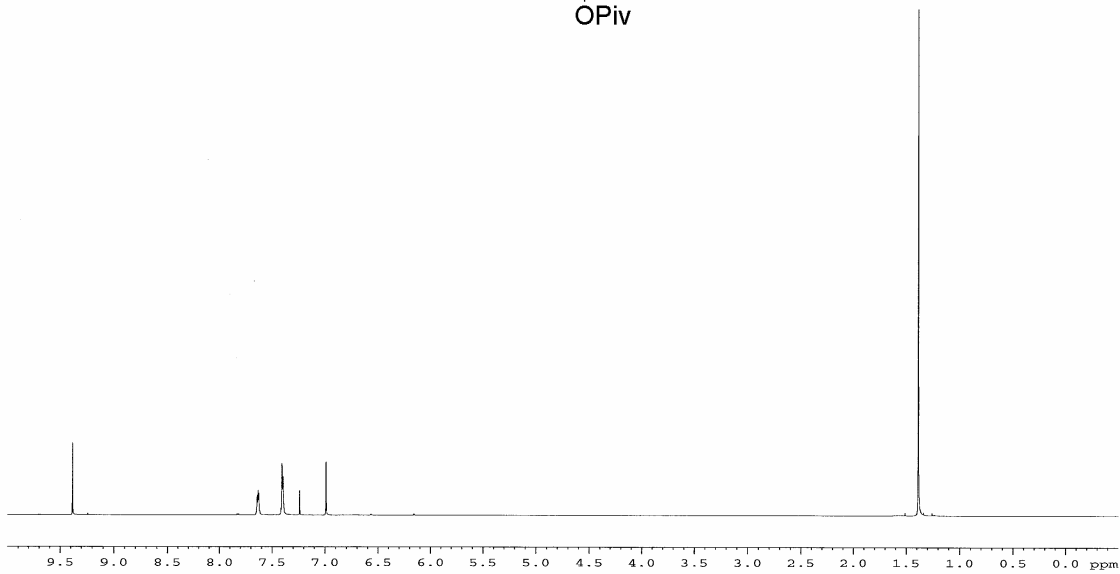
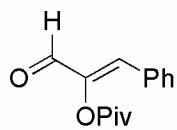
^1H NMR (CDCl_3 , 400 MHz) for **1.105**



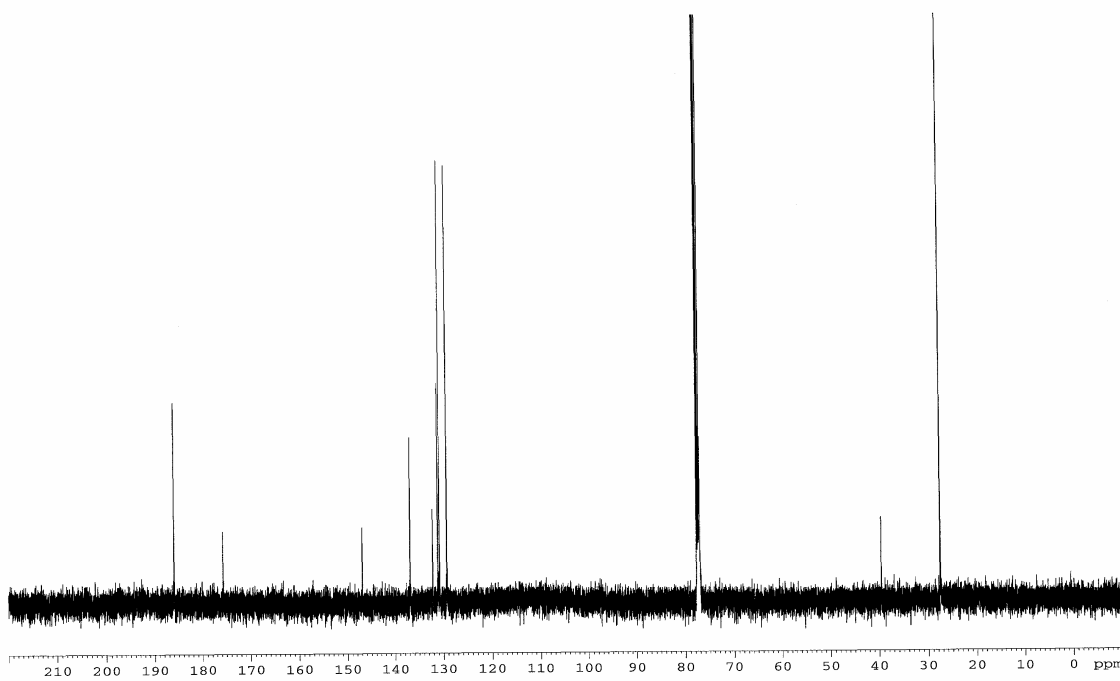
^{13}C NMR (CDCl_3 , 75 MHz) for **1.105**



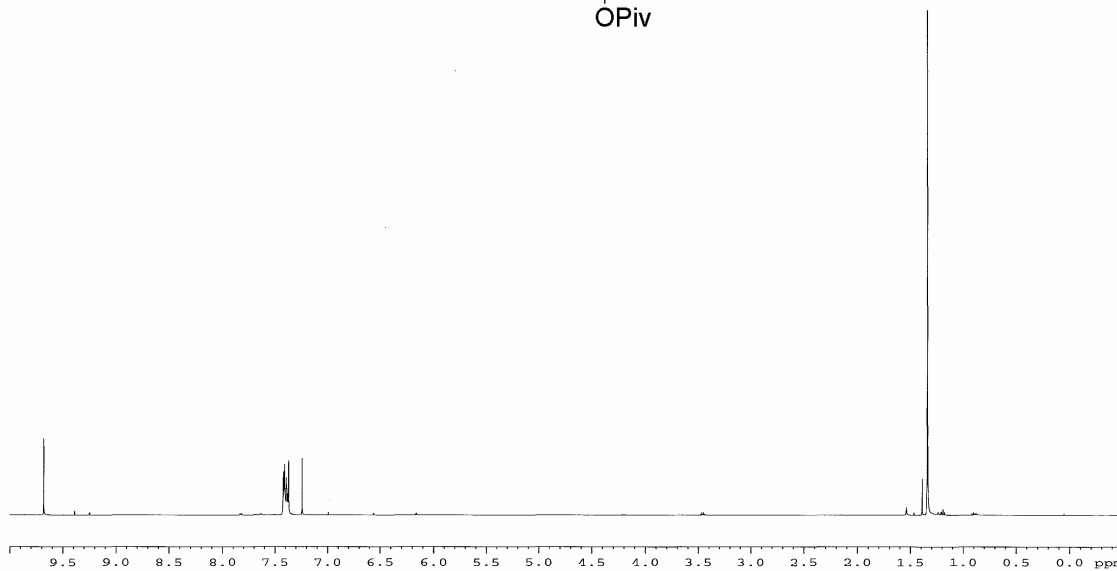
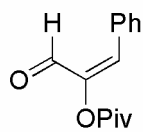
^1H NMR (CDCl_3 , 500 MHz) for **1.106-(Z)**



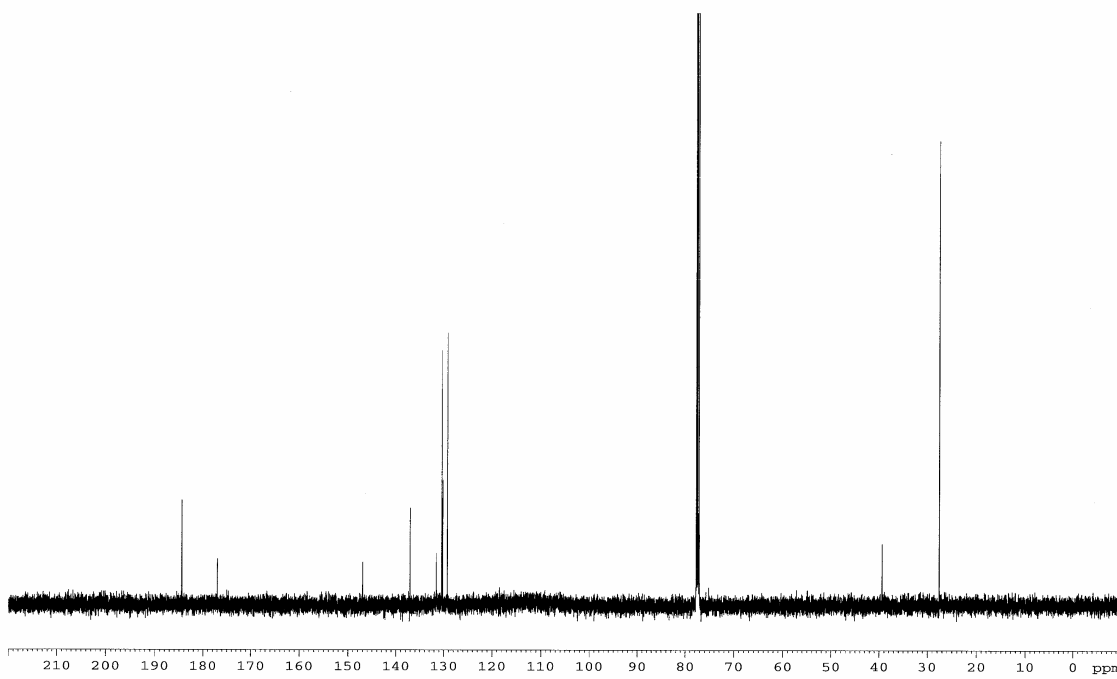
^{13}C NMR (CDCl_3 , 125 MHz) for **1.106-(Z)**



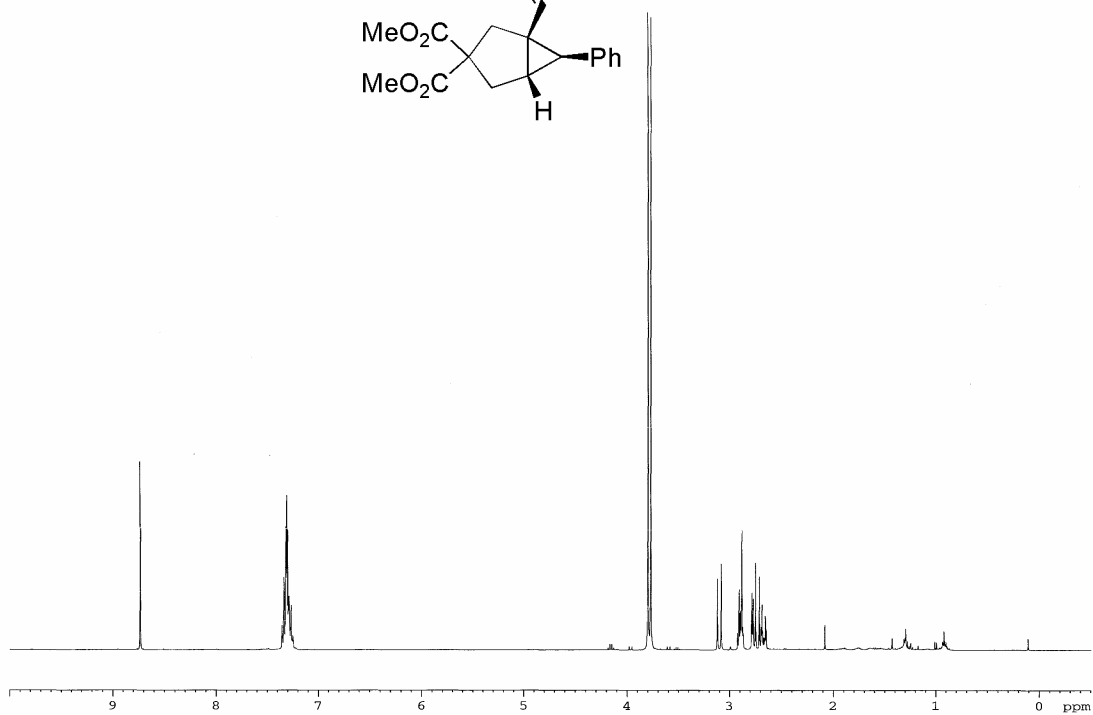
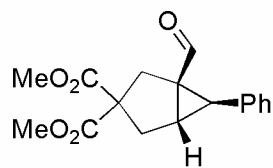
^1H NMR (CDCl_3 , 500 MHz) for **1.106-(E)**



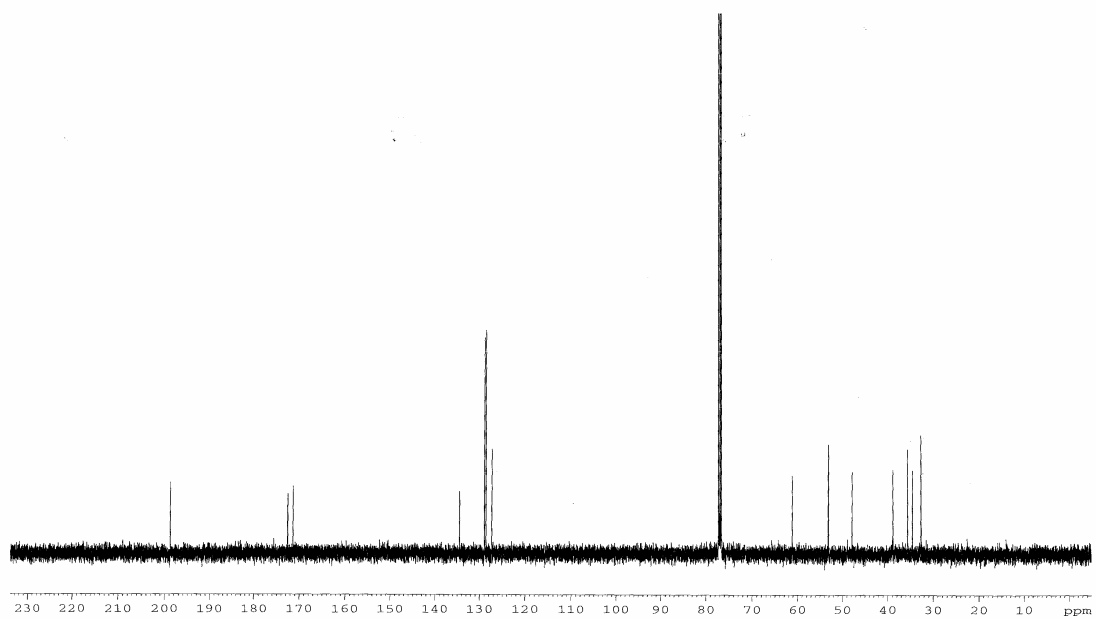
^{13}C NMR (CDCl_3 , 125 MHz) for **1.106-(E)**



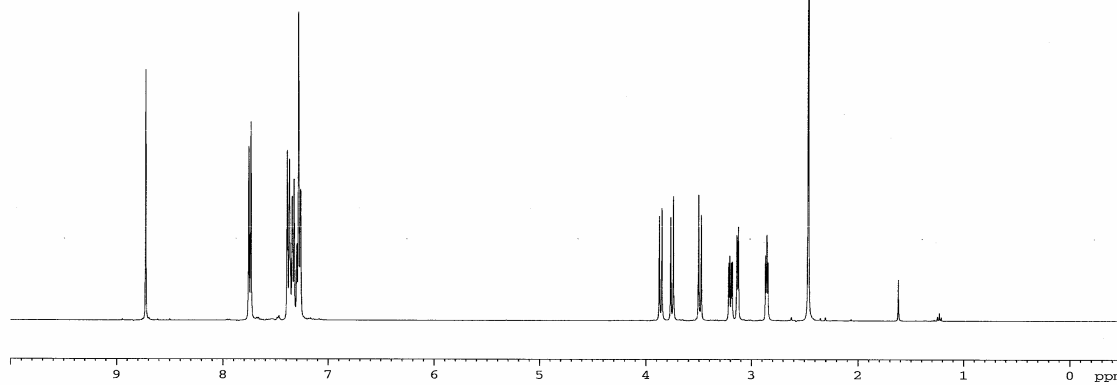
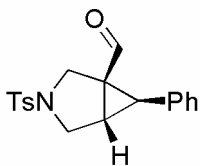
^1H NMR (CDCl_3 , 500 MHz) for **1.117**



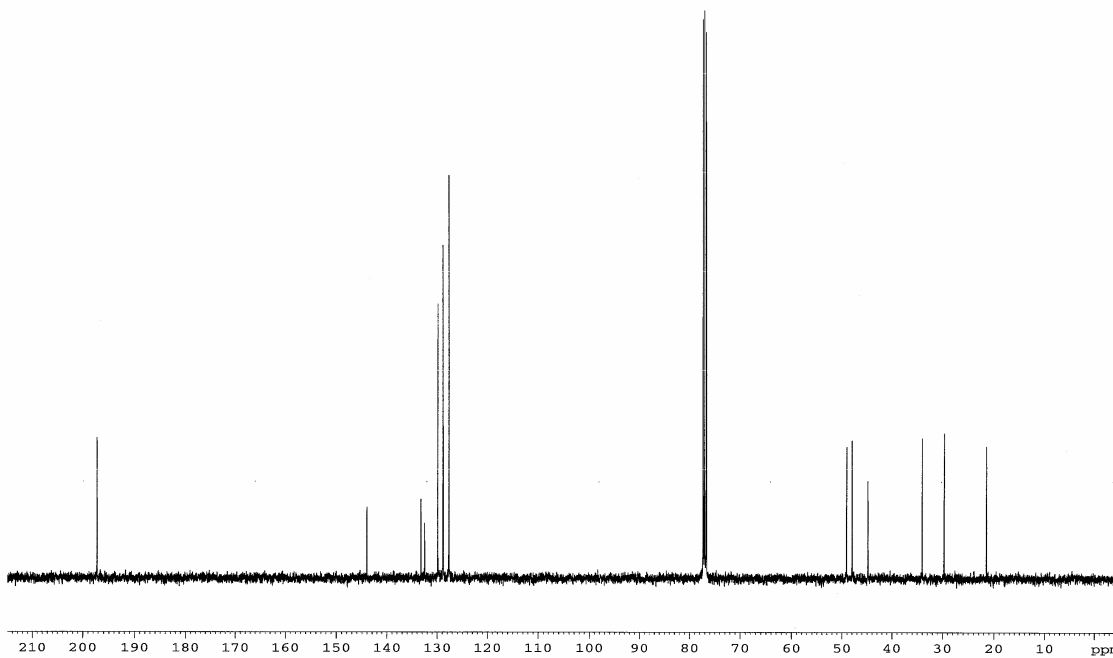
^{13}C NMR (CDCl_3 , 100 MHz) for **1.117**



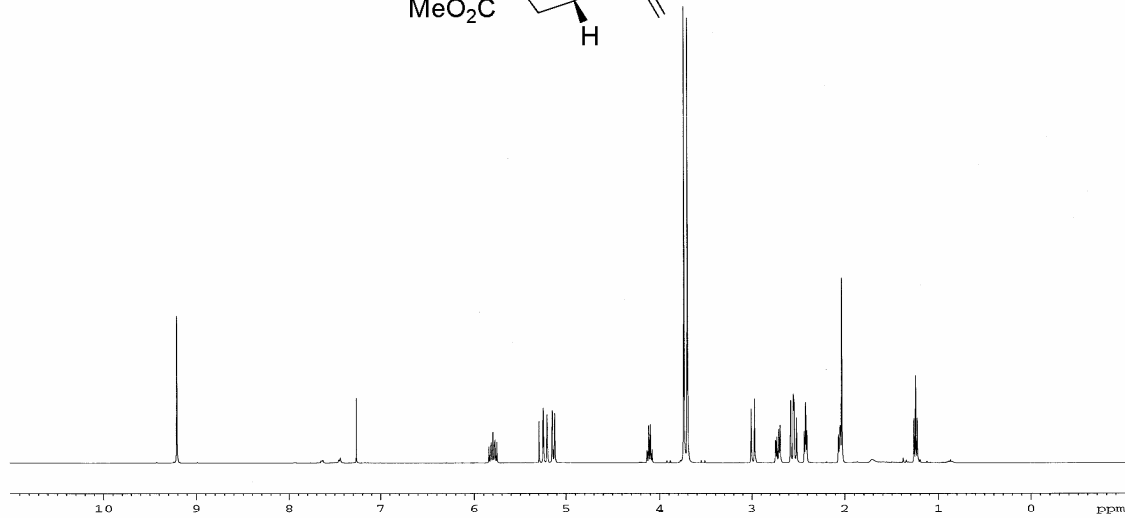
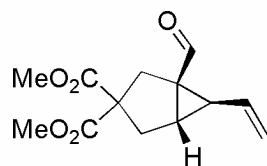
^1H NMR (CDCl_3 , 400 MHz) for **1.127**



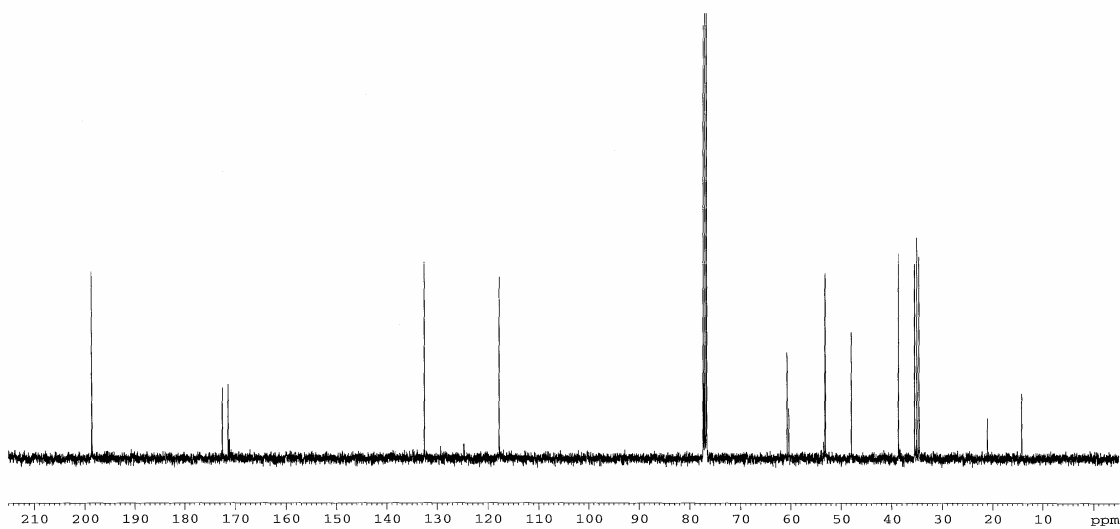
^{13}C NMR (CDCl_3 , 100 MHz) for **1.127**



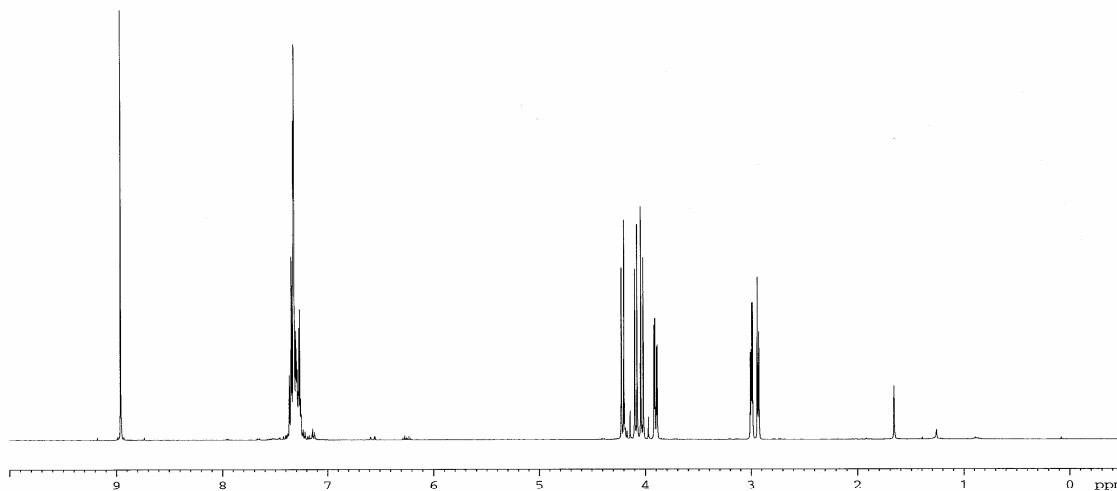
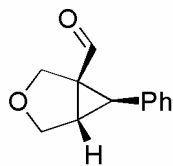
^1H NMR (CDCl_3 , 400 MHz) for **1.124**



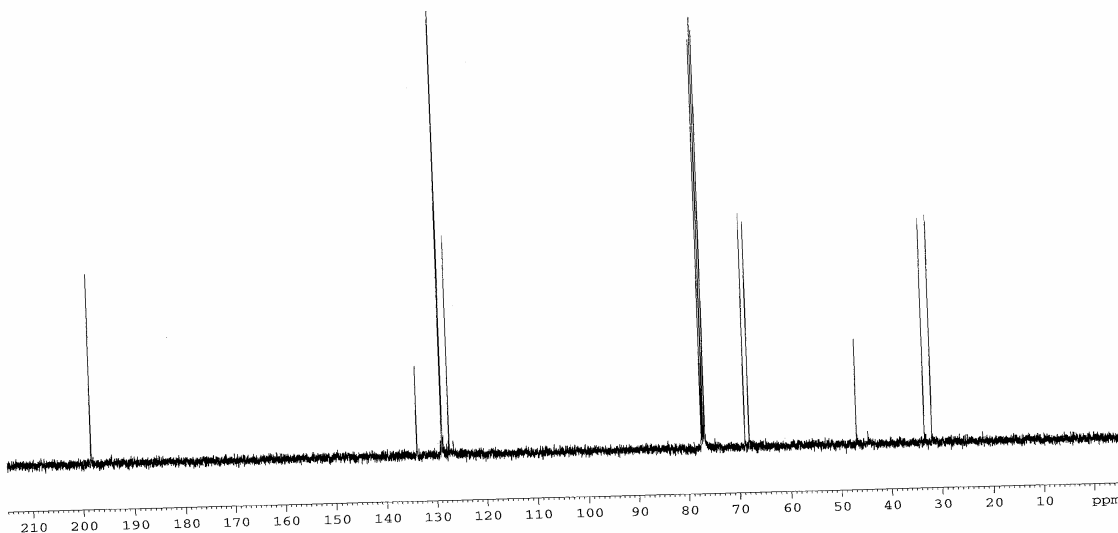
^{13}C NMR (CDCl_3 , 100 MHz) for **1.124**



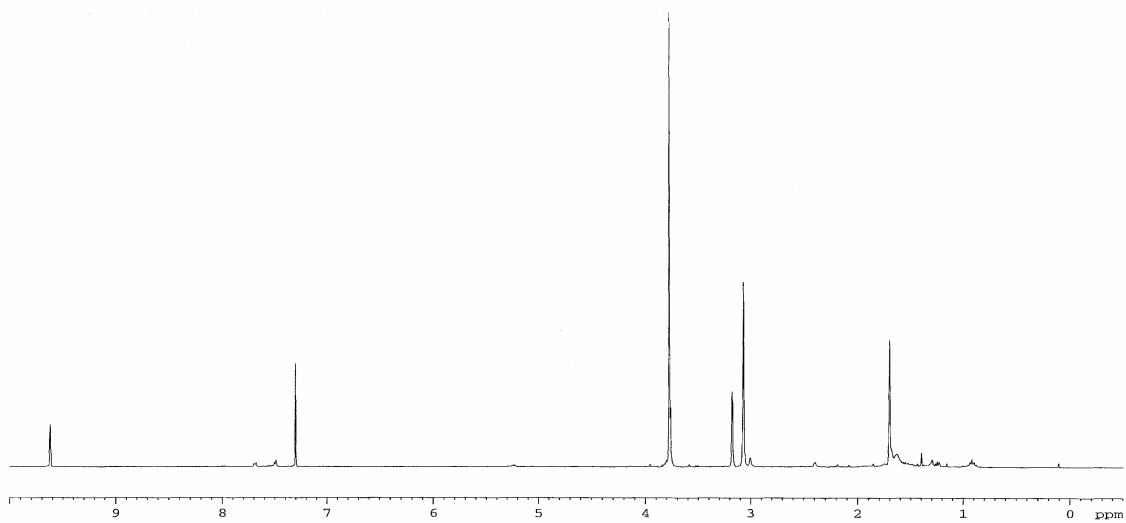
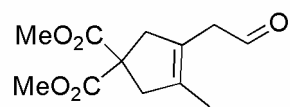
^1H NMR (CDCl_3 , 400 MHz) for **1.125**



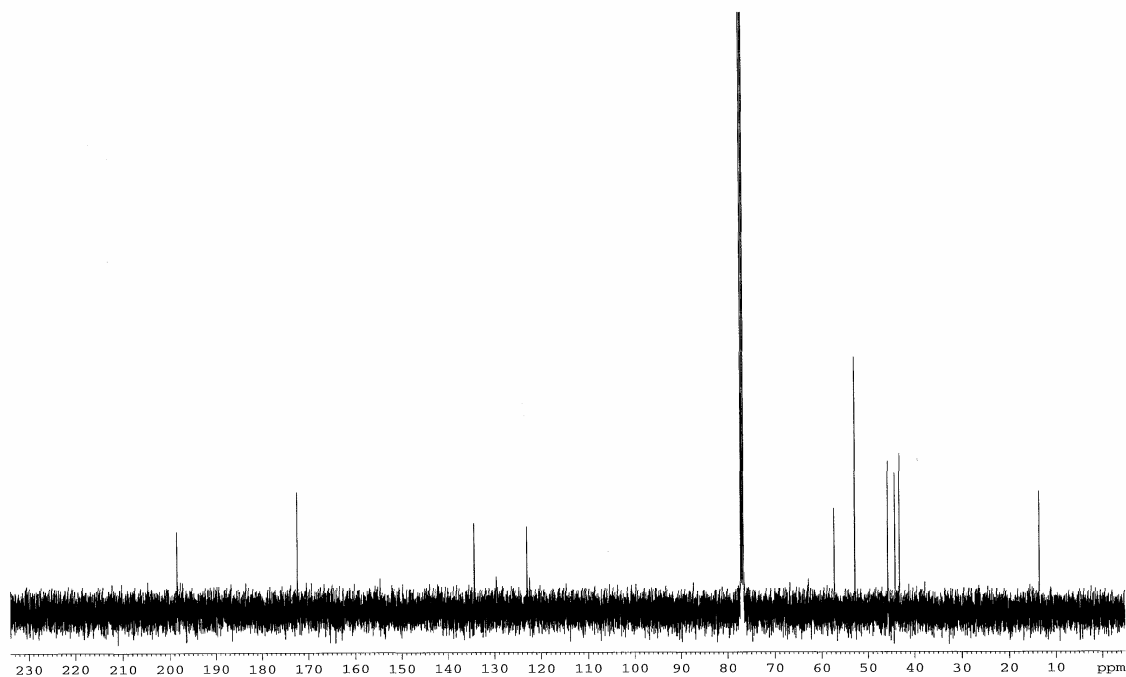
^{13}C NMR (CDCl_3 , 100 MHz) for **1.125**



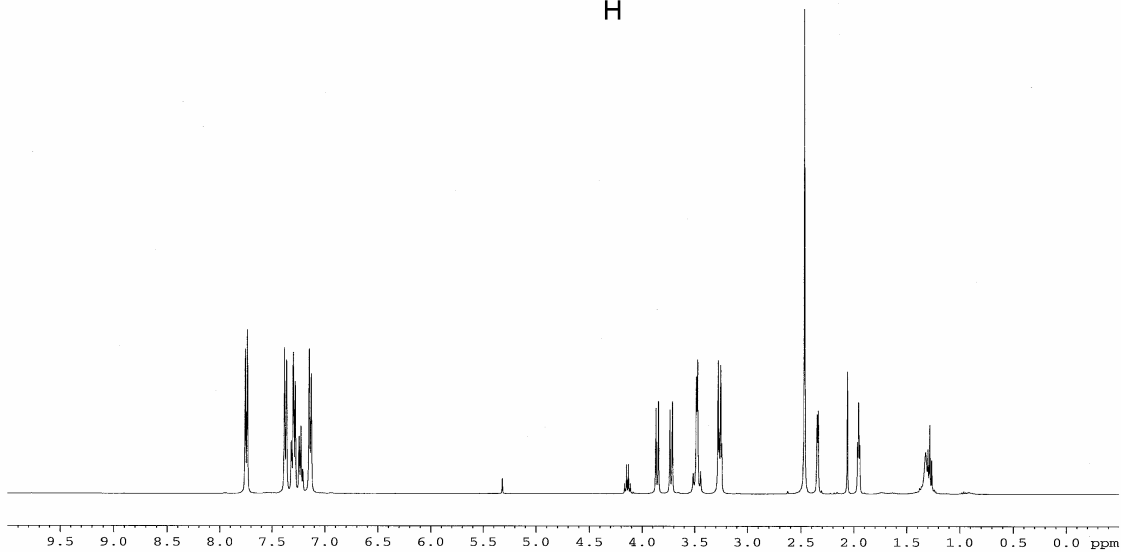
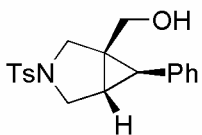
^1H NMR (CDCl_3 , 400 MHz) for **1.129**



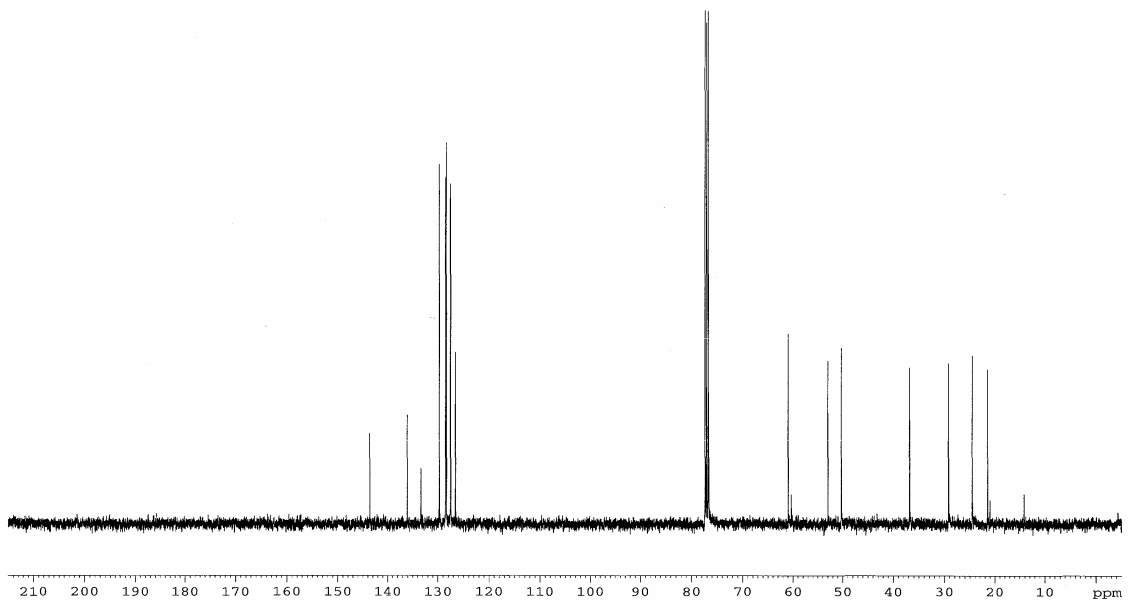
^{13}C NMR (CDCl_3 , 125 MHz) for **1.129**



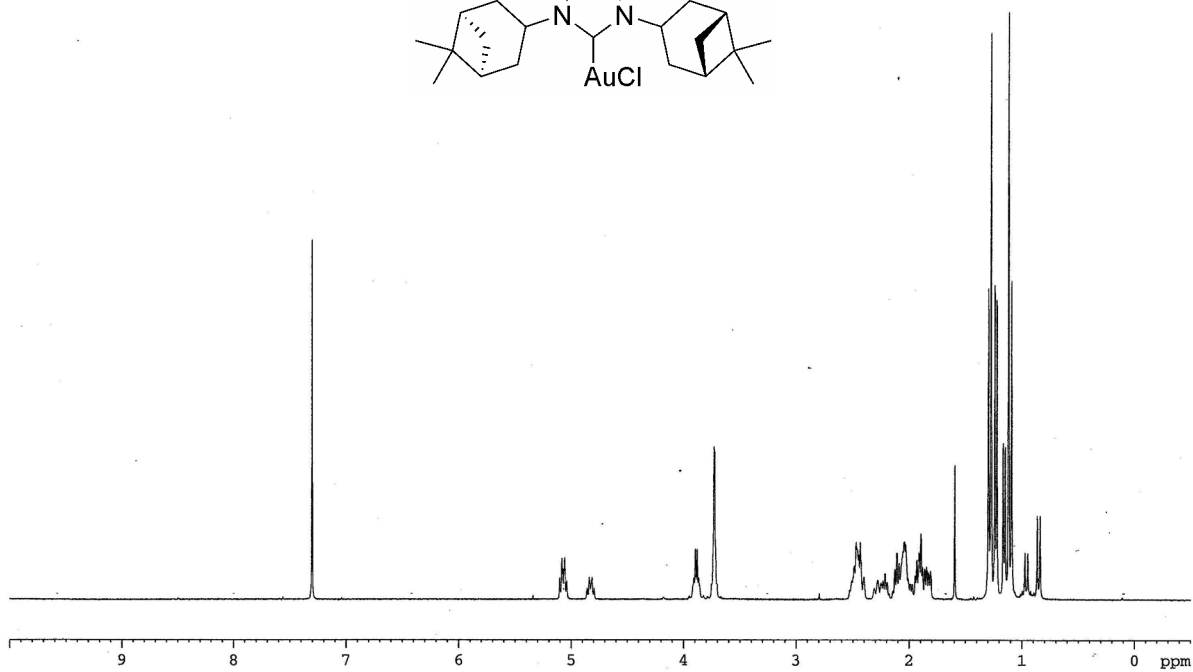
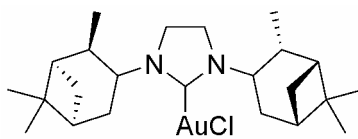
^1H NMR (CDCl_3 , 400 MHz) for **1.134**



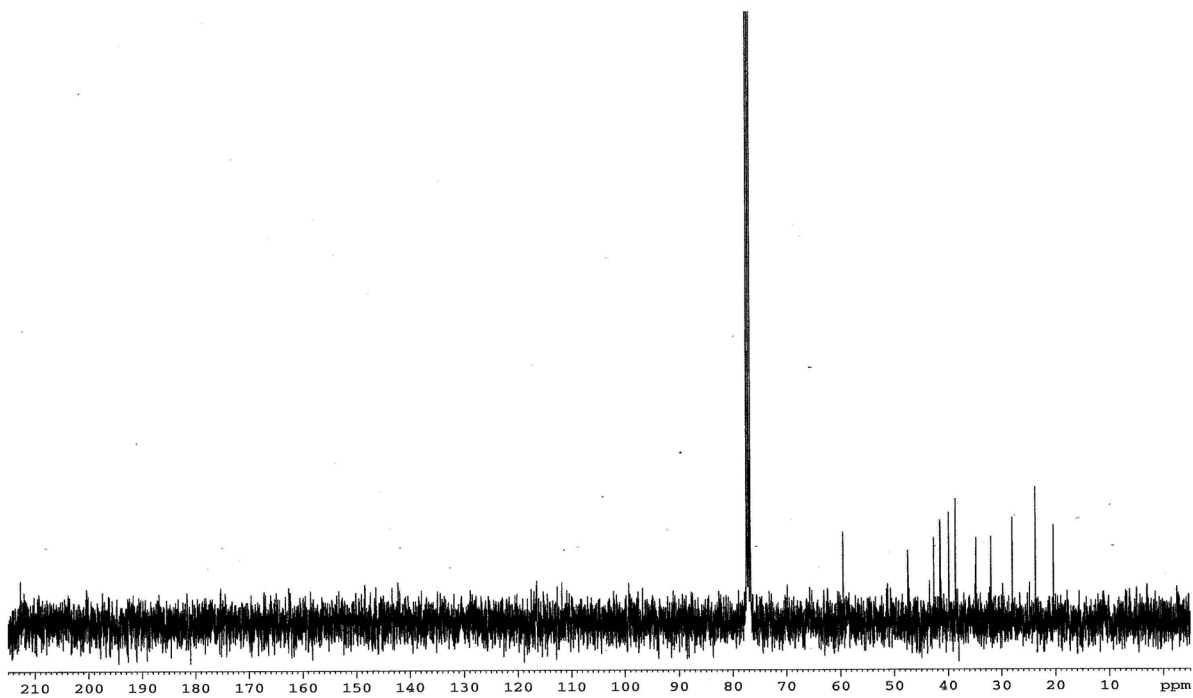
^{13}C NMR (CDCl_3 , 100 MHz) for **1.134**



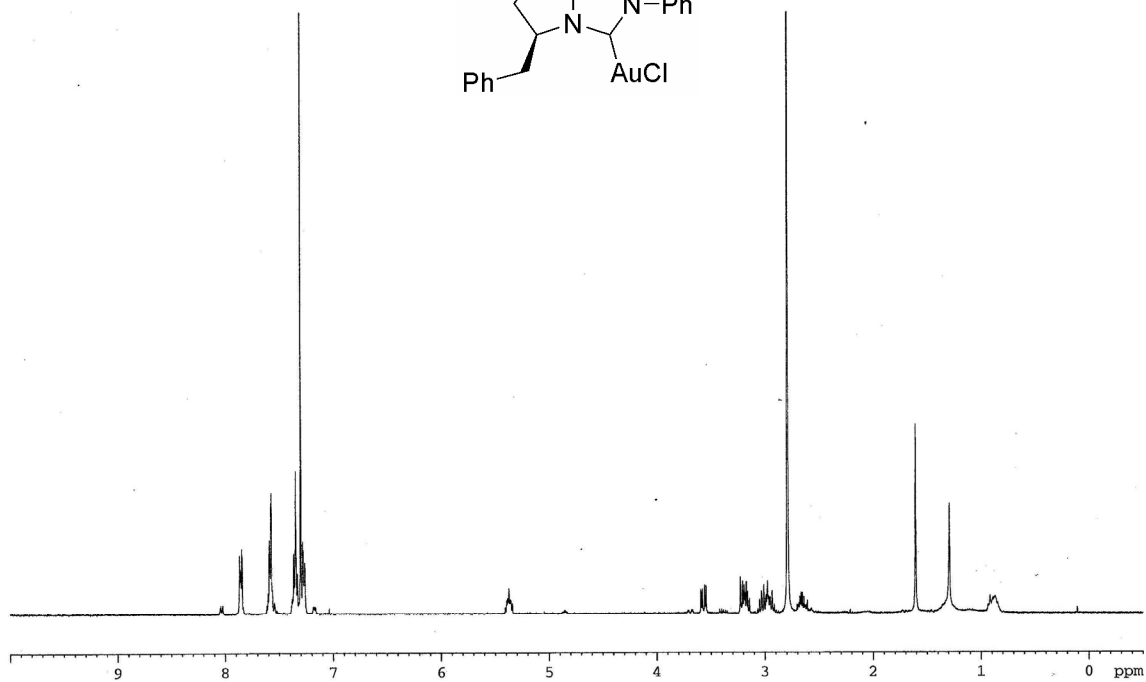
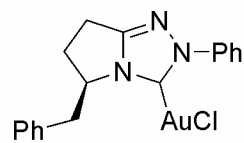
^1H NMR (CDCl_3 , 400 MHz) for **1.136**



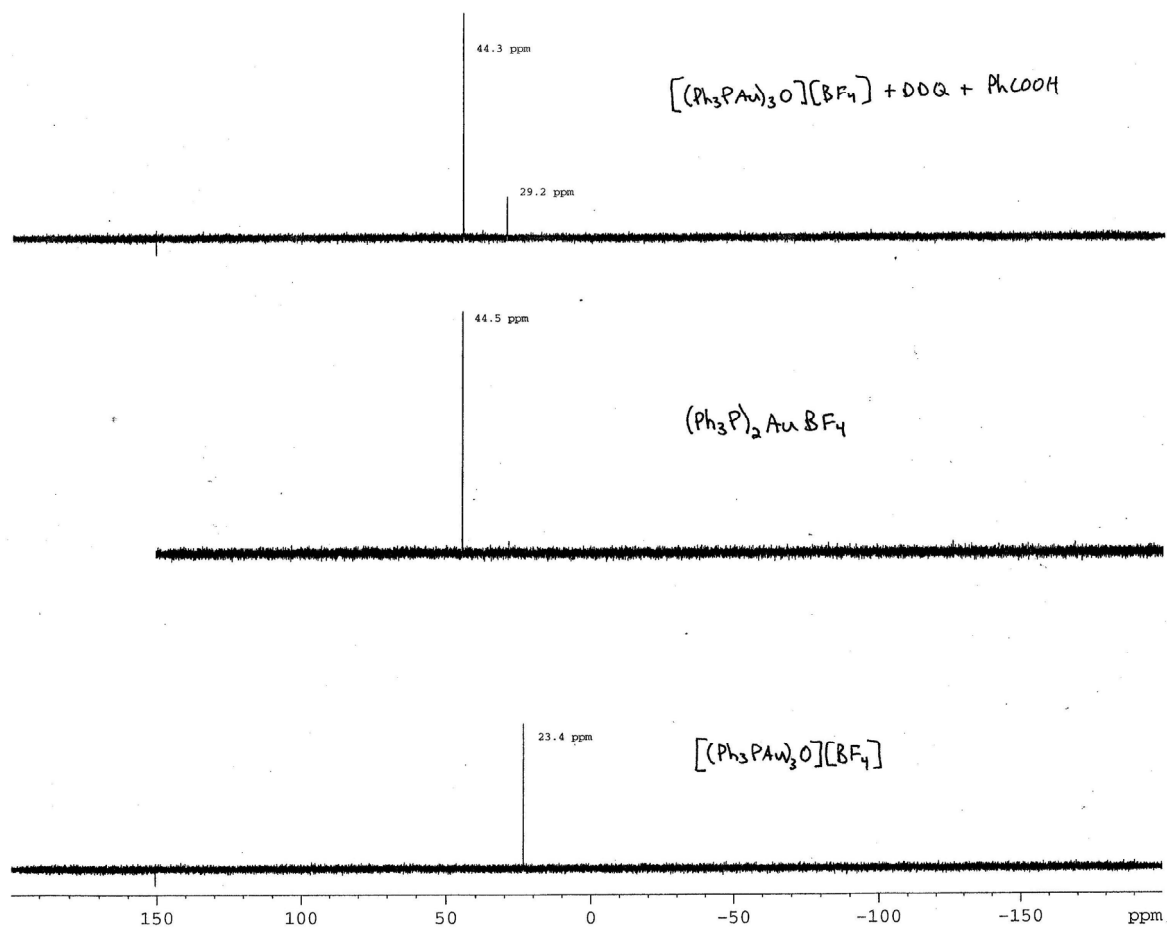
^{13}C NMR (CDCl_3 , 100 MHz) for **1.136**



^1H NMR (CDCl_3 , 400 MHz) for **1.137**



^{31}P NMR (CDCl_3 , 162 MHz) for Gold Trimer Catalysts



Chapter 1 Appendix 2.

Data Acquisition Details for X-Ray Crystal Structure of Complex **1.117**.

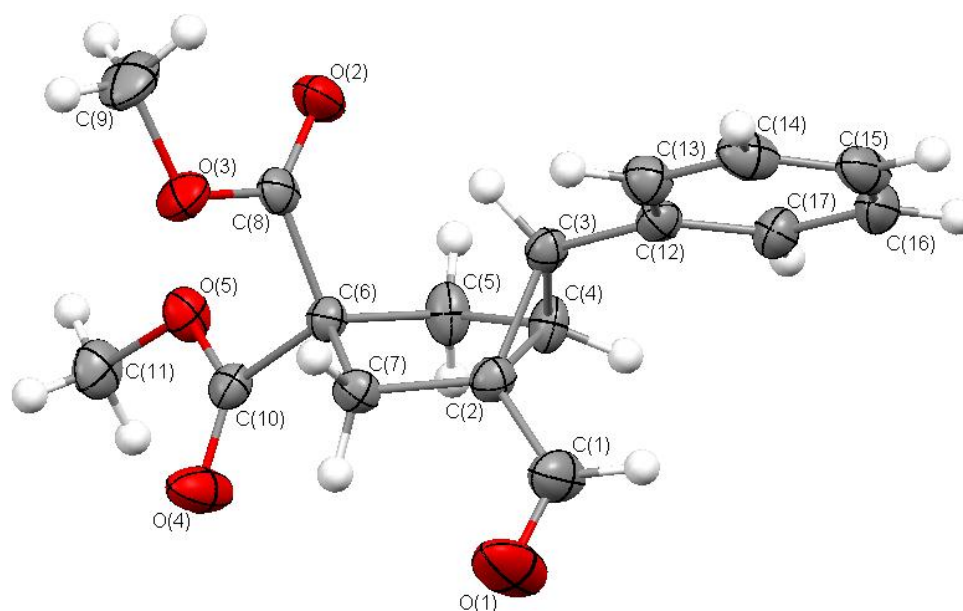


Figure A1.2.1. ORTEP representation of the solid state structure of **1.117** at 50% probability.

EXPERIMENTAL DETAILS

A. Crystal Data

Empirical Formula	C ₁₇ O ₅ H ₁₈
Formula Weight	302.33
Crystal Color, Habit	colorless, polyhedral
Crystal Dimensions	0.09 X 0.33 X 0.39 mm
Crystal System	monoclinic
Lattice Type	Primitive
Lattice Parameters	a = 9.747(2) Å b = 7.882(1) Å c = 20.522(4) Å β = 102.460(2)° V = 1539.4(5) Å ³
Space Group	P2 ₁ /n (#14)
Z value	4
D _{calc}	1.304 g/cm ³
F ₀₀₀	640.00
μ(MoKα)	0.96 cm ⁻¹

B. Intensity Measurements

Diffractometer	Bruker SMART CCD
Radiation	MoKα (λ = 0.71069 Å) graphite monochromated
Detector Position	60.00 mm
Exposure Time	10.0 seconds per frame.
Scan Type	ω (0.3 degrees per frame)
2θ _{max}	52.8°
No. of Reflections Measured	Total: 12035 Unique: 2169 (R _{int} = 0.018)
Corrections	Lorentz-polarization Absorption (T _{max} = 1.00, T _{min} = 0.89)

C. Structure Solution and Refinement

Structure Solution	Direct Methods (SIR97)
Refinement	Full-matrix least-squares
Function Minimized	Σ w (F _o - F _c) ²
Least Squares Weights	1/σ ² (F _o) = 4F _o ² /σ ² (F _o ²)
p-factor	0.0300

Anomalous Dispersion	All non-hydrogen atoms
No. Observations ($I > 3.00\sigma(I)$)	2267
No. Variables	199
Reflection/Parameter Ratio	11.39
Residuals: R; Rw; Rall	0.039 ; 0.049; 0.055
Goodness of Fit Indicator	2.21
Max Shift/Error in Final Cycle	0.00
Maximum peak in Final Diff. Map	0.20 e ⁻ /Å ³
Minimum peak in Final Diff. Map	-0.21 e ⁻ /Å ³

Table A1.2.1. Atomic coordinates and $B_{\text{iso}}/B_{\text{eq}}$

atom	x	y	z	B_{eq}
O(1)	-0.3078(2)	-0.3618(2)	-0.74336(7)	5.54(4)
O(2)	-0.3956(1)	0.2520(2)	-0.56675(6)	3.50(3)
O(3)	-0.1753(1)	0.2125(1)	-0.57872(6)	2.83(3)
O(4)	-0.1360(1)	-0.2214(2)	-0.51263(6)	3.97(3)
O(5)	-0.2308(1)	-0.0178(1)	-0.46097(5)	2.44(3)
C(1)	-0.4063(2)	-0.2725(2)	-0.73989(8)	3.40(4)
C(2)	-0.4035(2)	-0.1389(2)	-0.69074(7)	2.09(3)
C(3)	-0.5100(2)	0.0068(2)	-0.70535(7)	1.95(3)
C(4)	-0.5253(2)	-0.1234(2)	-0.65515(8)	2.29(3)
C(5)	-0.4624(2)	-0.0955(2)	-0.58182(8)	2.54(4)
C(6)	-0.3102(2)	-0.0334(2)	-0.57765(7)	1.82(3)
C(7)	-0.2681(2)	-0.1053(2)	-0.64062(7)	2.06(3)
C(8)	-0.3019(2)	0.1594(2)	-0.57385(7)	2.11(3)
C(9)	-0.1533(2)	0.3943(2)	-0.5773(1)	4.02(5)
C(10)	-0.2137(2)	-0.1036(2)	-0.51467(7)	2.05(3)
C(11)	-0.1487(2)	-0.0762(2)	-0.39775(8)	2.84(4)
C(12)	-0.6090(2)	0.0200(2)	-0.77191(7)	2.13(3)
C(13)	-0.5677(2)	0.1118(2)	-0.82222(8)	2.58(4)
C(14)	-0.6533(2)	0.1241(2)	-0.88534(8)	3.11(4)
C(15)	-0.7824(2)	0.0451(2)	-0.89936(8)	3.23(4)
C(16)	-0.8268(2)	-0.0438(2)	-0.84965(9)	3.11(4)
C(17)	-0.7412(2)	-0.0562(2)	-0.78621(8)	2.60(4)
H(1)	-0.4918	-0.2907	-0.7715	4.0930
H(2)	-0.4750	0.1127	-0.6868	2.3426
H(3)	-0.6004	-0.2021	-0.6666	2.7474
H(4)	-0.5145	-0.0124	-0.5640	3.0547
H(5)	-0.4620	-0.1987	-0.5578	3.0547
H(6)	-0.2166	-0.2078	-0.6302	2.4656
H(7)	-0.2124	-0.0253	-0.6580	2.4656
H(8)	-0.2084	0.4435	-0.6166	4.8346
H(9)	-0.1802	0.4409	-0.5393	4.8346
H(10)	-0.0568	0.4176	-0.5752	4.8346
H(11)	-0.1736	-0.0133	-0.3626	3.4014
H(12)	-0.1667	-0.1932	-0.3924	3.4014
H(13)	-0.0516	-0.0604	-0.3968	3.4014
H(14)	-0.4790	0.1672	-0.8131	3.1031
H(15)	-0.6228	0.1871	-0.9191	3.7304
H(16)	-0.8405	0.0518	-0.9429	3.8851
H(17)	-0.9164	-0.0969	-0.8589	3.7258

Table A1.2.2. Atomic coordinates and $B_{\text{iso}}/B_{\text{eq}}$ (continued)

atom	x	y	z	B_{eq}
H(18)	-0.7730	-0.1171	-0.7523	3.1231

$$B_{\text{eq}} = 8/3 \pi^2 (U_{11}(aa^*)^2 + U_{22}(bb^*)^2 + U_{33}(cc^*)^2 + 2U_{12}(aa^*bb^*)\cos \gamma + 2U_{13}(aa^*cc^*)\cos \beta + 2U_{23}(bb^*cc^*)\cos \alpha)$$

Table A1.2.3. Anisotropic Displacement Parameters

atom	U_{11}	U_{22}	U_{33}	U_{12}	U_{13}	U_{23}
O(1)	0.078(1)	0.074(1)	0.0494(9)	0.0392(9)	-0.0056(8)	-0.0300(8)
O(2)	0.0375(7)	0.0422(8)	0.0472(8)	0.0159(6)	-0.0044(6)	-0.0126(6)
O(3)	0.0391(7)	0.0257(7)	0.0425(7)	-0.0073(5)	0.0085(5)	0.0007(5)
O(4)	0.0718(10)	0.0393(8)	0.0310(7)	0.0244(7)	-0.0082(6)	-0.0057(6)
O(5)	0.0324(7)	0.0408(7)	0.0189(6)	0.0039(5)	0.0038(4)	-0.0001(5)
C(1)	0.054(1)	0.041(1)	0.0286(9)	0.0111(10)	-0.0036(8)	-0.0078(8)
C(2)	0.0313(9)	0.0257(9)	0.0218(8)	-0.0002(7)	0.0047(7)	-0.0020(6)
C(3)	0.0250(8)	0.0265(9)	0.0226(8)	-0.0012(7)	0.0052(6)	-0.0049(6)
C(4)	0.0261(8)	0.0350(10)	0.0251(8)	-0.0105(7)	0.0040(6)	-0.0013(7)
C(5)	0.0272(8)	0.047(1)	0.0226(8)	-0.0075(8)	0.0057(6)	0.0016(7)
C(6)	0.0234(8)	0.0251(9)	0.0200(8)	-0.0011(7)	0.0035(6)	-0.0008(6)
C(7)	0.0276(8)	0.0284(9)	0.0227(8)	0.0035(7)	0.0067(6)	-0.0009(7)
C(8)	0.0277(9)	0.0309(9)	0.0186(8)	0.0042(8)	-0.0015(6)	-0.0014(7)
C(9)	0.069(1)	0.027(1)	0.051(1)	-0.0134(10)	-0.0003(10)	0.0071(9)
C(10)	0.0288(9)	0.0248(9)	0.0235(8)	-0.0048(7)	0.0036(6)	-0.0017(7)
C(11)	0.044(1)	0.041(1)	0.0198(8)	-0.0016(9)	-0.0002(7)	0.0015(7)
C(12)	0.0301(9)	0.0260(9)	0.0240(8)	0.0035(7)	0.0039(7)	-0.0060(7)
C(13)	0.0343(9)	0.034(1)	0.0293(9)	0.0034(8)	0.0056(7)	0.0003(7)
C(14)	0.052(1)	0.038(1)	0.0268(9)	0.0130(9)	0.0071(8)	0.0033(8)
C(15)	0.048(1)	0.040(1)	0.0270(9)	0.0174(9)	-0.0086(8)	-0.0082(8)
C(16)	0.035(1)	0.037(1)	0.039(1)	0.0028(8)	-0.0062(8)	-0.0094(8)
C(17)	0.0332(9)	0.0323(10)	0.0315(9)	-0.0017(8)	0.0026(7)	-0.0049(8)

The general temperature factor expression:

$$\exp(-2\pi^2(a^{*2}U_{11}h^2 + b^{*2}U_{22}k^2 + c^{*2}U_{33}l^2 + 2a^*b^*U_{12}hk + 2a^*c^*U_{13}hl + 2b^*c^*U_{23}kl))$$

Table A1.2.4. Bond Lengths(Å)

atom	atom	distance	atom	atom	distance
O1	C1	1.204(2)	O2	C8	1.202(2)
O3	C8	1.328(2)	O3	C9	1.448(2)
O4	C10	1.193(2)	O5	C10	1.334(2)
O5	C11	1.445(2)	C1	C2	1.455(2)
C2	C3	1.533(2)	C2	C4	1.527(2)
C2	C7	1.511(2)	C3	C4	1.484(2)
C3	C12	1.496(2)	C4	C5	1.513(2)
C5	C6	1.547(2)	C6	C7	1.546(2)
C6	C8	1.523(2)	C6	C10	1.529(2)
C12	C13	1.390(2)	C12	C17	1.394(2)
C13	C14	1.385(2)	C14	C15	1.377(3)
C15	C16	1.382(3)	C16	C17	1.390(2)

Table A1.2.5. Bond Lengths(Å)

atom	atom	distance	atom	atom	distance
C1	H1	0.95	C3	H2	0.95
C4	H3	0.95	C5	H4	0.95
C5	H5	0.95	C7	H6	0.95
C7	H7	0.95	C9	H8	0.95
C9	H9	0.95	C9	H10	0.95
C11	H11	0.95	C11	H12	0.95
C11	H13	0.95	C13	H14	0.95
C14	H15	0.95	C15	H16	0.95
C16	H17	0.95	C17	H18	0.95

Table A1.2.6. Bond Angles(°)

atom	atom	atom	angle	atom	atom	atom	angle
C8	O3	C9	116.5(1)	C10	O5	C11	115.9(1)
O1	C1	C2	124.6(2)	C1	C2	C3	119.7(1)
C1	C2	C4	119.3(1)	C1	C2	C7	118.8(1)
C3	C2	C4	58.0(1)	C3	C2	C7	117.2(1)
C4	C2	C7	108.4(1)	C2	C3	C4	60.8(1)
C2	C3	C12	120.4(1)	C4	C3	C12	122.7(1)
C2	C4	C3	61.2(1)	C2	C4	C5	107.3(1)
C3	C4	C5	120.7(1)	C4	C5	C6	106.2(1)
C5	C6	C7	105.2(1)	C5	C6	C8	111.0(1)
C5	C6	C10	109.9(1)	C7	C6	C8	112.9(1)
C7	C6	C10	110.4(1)	C8	C6	C10	107.6(1)
C2	C7	C6	106.4(1)	O2	C8	O3	124.1(2)
O2	C8	C6	125.4(2)	O3	C8	C6	110.5(1)
O4	C10	O5	123.9(1)	O4	C10	C6	125.5(1)
O5	C10	C6	110.6(1)	C3	C12	C13	118.8(1)
C3	C12	C17	123.2(1)	C13	C12	C17	118.1(1)
C12	C13	C14	121.3(2)	C13	C14	C15	120.2(2)
C14	C15	C16	119.5(1)	C15	C16	C17	120.4(2)
C12	C17	C16	120.5(2)				

Table A1.2.7. Bond Angles(°)

atom	atom	atom	angle	atom	atom	atom	angle
O1	C1	H1	117.7	C2	C1	H1	117.7
C2	C3	H2	114.2	C4	C3	H2	114.2
C12	C3	H2	114.2	C2	C4	H3	117.8
C3	C4	H3	117.8	C5	C4	H3	117.8
C4	C5	H4	110.3	C4	C5	H5	110.3
C6	C5	H4	110.3	C6	C5	H5	110.3
H4	C5	H5	109.5	C2	C7	H6	110.2
C2	C7	H7	110.2	C6	C7	H6	110.2
C6	C7	H7	110.3	H6	C7	H7	109.4
O3	C9	H8	109.4	O3	C9	H9	109.5
O3	C9	H10	109.4	H8	C9	H9	109.5
H8	C9	H10	109.4	H9	C9	H10	109.5
O5	C11	H11	109.5	O5	C11	H12	109.5
O5	C11	H13	109.5	H11	C11	H12	109.5
H11	C11	H13	109.5	H12	C11	H13	109.4
C12	C13	H14	119.3	C14	C13	H14	119.4
C13	C14	H15	119.9	C15	C14	H15	119.9
C14	C15	H16	120.3	C16	C15	H16	120.2
C15	C16	H17	119.8	C17	C16	H17	119.8
C12	C17	H18	119.8	C16	C17	H18	119.7

Table A1.2.8. Torsion Angles(°)

atom	atom	atom	atom	angle	atom	atom	atom	atom	angle
O1	C1	C2	C3	157.2(2)	O1	C1	C2	C4	-135.1(2)
O1	C1	C2	C7	1.0(3)	O2	C8	O3	C9	-2.0(2)
O2	C8	C6	C5	8.5(2)	O2	C8	C6	C7	126.3(2)
O2	C8	C6	C10	-111.7(2)	O3	C8	C6	C5	-172.2(1)
O3	C8	C6	C7	-54.4(2)	O3	C8	C6	C10	67.6(2)
O4	C10	O5	C11	-0.3(2)	O4	C10	C6	C5	101.4(2)
O4	C10	C6	C7	-14.1(2)	O4	C10	C6	C8	-137.7(2)
O5	C10	C6	C5	-76.7(2)	O5	C10	C6	C7	167.7(1)
O5	C10	C6	C8	44.2(2)	C1	C2	C3	C4	107.9(2)
C1	C2	C3	C12	-5.0(2)	C1	C2	C4	C3	-108.7(2)
C1	C2	C4	C5	135.3(2)	C1	C2	C7	C6	-151.8(2)
C2	C3	C4	C5	93.9(2)	C2	C3	C12	C13	-89.9(2)
C2	C3	C12	C17	89.8(2)	C2	C4	C3	C12	109.3(2)
C2	C4	C5	C6	19.1(2)	C2	C7	C6	C5	22.8(2)
C2	C7	C6	C8	-98.3(1)	C2	C7	C6	C10	141.3(1)
C3	C2	C4	C5	-116.0(1)	C3	C2	C7	C6	51.5(2)
C3	C4	C2	C7	111.1(1)	C3	C4	C5	C6	-47.2(2)
C3	C12	C13	C14	178.1(1)	C3	C12	C17	C16	-178.0(2)
C4	C2	C3	C12	-112.9(2)	C4	C2	C7	C6	-11.3(2)
C4	C3	C2	C7	-95.6(1)	C4	C3	C12	C13	-162.7(2)
C4	C3	C12	C17	17.0(2)	C4	C5	C6	C7	-25.9(2)
C4	C5	C6	C8	96.5(1)	C4	C5	C6	C10	-144.7(1)
C5	C4	C2	C7	-4.9(2)	C5	C4	C3	C12	-156.8(1)
C6	C8	O3	C9	178.7(1)	C6	C10	O5	C11	177.9(1)
C7	C2	C3	C12	151.5(1)	C12	C13	C14	C15	0.2(3)
C12	C17	C16	C15	-0.4(3)	C13	C12	C17	C16	1.7(2)
C13	C14	C15	C16	1.2(3)	C14	C13	C12	C17	-1.6(2)
C14	C15	C16	C17	-1.1(3)					

Table A1.2.9. Non-bonded Contacts out to 3.80 Å

atom	atom	distance	ADC	atom	atom	distance	ADC
O1	C7	3.265(2)	44302	O1	C2	3.470(2)	44302
O1	C13	3.623(2)	44302	O1	C3	3.631(2)	44302
O1	O3	3.666(2)	44302	O2	C16	3.294(2)	35302
O2	C15	3.733(2)	4	O3	O4	3.204(2)	55403
O3	C11	3.466(2)	55403	O4	C9	3.297(2)	54501
O4	C9	3.312(2)	55403	O5	C5	3.412(2)	45403
O5	C14	3.479(2)	4	C1	C11	3.768(2)	44404
C4	C15	3.535(2)	34302	C4	C16	3.624(2)	34302
C5	C15	3.734(2)	34302	C9	C13	3.707(3)	45302
C9	C14	3.713(3)	45302	C11	C14	3.573(3)	4
C11	C16	3.701(3)	54504				

The ADC (atom designator code) specifies the position of an atom in a crystal. The 5-digit number shown in the table is a composite of three one-digit numbers and one two-digit number: TA (first digit) + TB (second digit) + TC (third digit) + SN (last two digits). TA, TB and TC are the crystal lattice translation digits along cell edges a, b and c. A translation digit of 5 indicates the origin unit cell. If TA = 4, this indicates a translation of one unit cell length along the a-axis in the negative direction. Each translation digit can range in value from 1 to 9 and thus $\square 4$ lattice translations from the origin (TA=5, TB=5, TC=5) can be represented.

The SN, or symmetry operator number, refers to the number of the symmetry operator used to generate the coordinates of the target atom. A list of symmetry operators relevant to this structure are given below.

For a given intermolecular contact, the first atom (origin atom) is located in the origin unit cell and its position can be generated using the identity operator (SN=1). Thus, the ADC for an origin atom is always 55501. The position of the second atom (target atom) can be generated using the ADC and the coordinates of the atom in the parameter table. For example, an ADC of 47502 refers to the target atom moved through symmetry operator two, then translated -1 cell translations along the a axis, +2 cell translations along the b axis, and 0 cell translations along the c axis.

An ADC of 1 indicates an intermolecular contact between two fragments (eg. cation and anion) that reside in the same asymmetric unit.

				Symmetry Operators:		
(1)	X,	Y,	Z	(2)	1/2-X,	1/2+Y, 1/2-Z
(3)	-X,	-Y,	-Z	(4)	1/2+X,	1/2-Y, 1/2+Z

Table A1.2.10. Least Squares Planes

Plane number 1

Atoms defining plane	Distance
C2	0.026(2)
C4	-0.029(2)
C5	0.019(2)
C7	-0.015(2)
Additional Atoms	Distance
C6	-0.386
C1	0.903
C3	-1.196

Plane number 2

Atoms defining plane	Distance
C2	0.0
C3	0.0
C4	0.0

Plane number 3

Atoms defining plane	Distance
C12	0.010(2)
C13	-0.007(2)
C14	-0.005(2)
C15	0.009(2)
C16	-0.003(2)
C17	-0.007(2)
Additional Atoms	Distance
C3	0.050

Summary

plane	mean deviation	χ^2
1	0.0223	847.0
2	0.0000	0.0
3	0.0068	112.4

Dihedral angles between planes (°)

plane	1	2
2	66.56	
3	37.89	63.59

Chapter 2

Late Metal Nanoparticles in Solution-Phase Heterogeneous Catalysis.

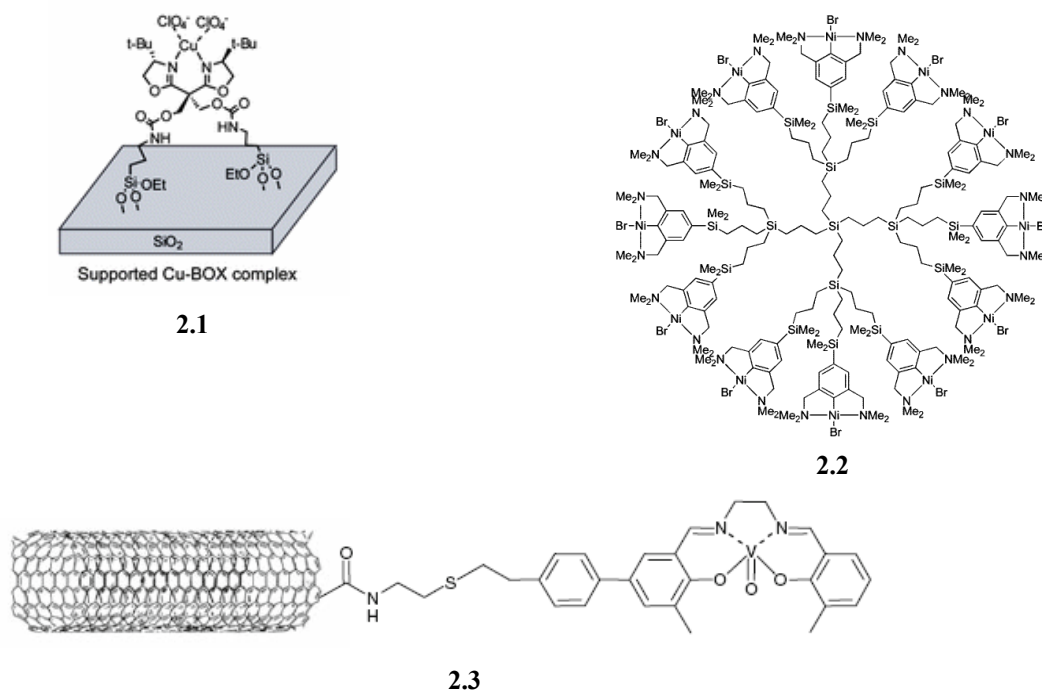
*Portions of the work in this chapter have been published:
Witham, C. A.; Huang, W.; Tsung, C.-K.; Kuhn, J. N.; Somorjai, G. A.; Toste, F. D.
Nature Chemistry* **2009**, 2, 36.

Introduction

A current and major goal in the field of catalysis is the transformation of processes from homogeneous to heterogeneous. Homogeneous catalysis is characterized by a broad range of well-understood inorganic, organometallic and organic molecules that exist in the same phase as the reactants for a given reaction and are easily tuned and highly selective with excellent activity for a plethora of transformations. Heterogeneous catalysts, while in many ways similar to homogeneous analogues, also offer distinct advantages including recyclability, ease of separation from the reaction mixture, and use in continuous flow systems as they exist in a different phase from the reactants. In addition, where chemistry at a surface is desired, heterogeneous catalysts are uniquely capable of facilitating this type of reactivity as they provide a medium on which a reaction can take place. Thus, the development of systems that blend the advantages of heterogeneous catalysis with the versatility of homogeneous catalysts is very desirable and would result in a new and powerful class of catalysts.¹⁻³

To date, most efforts to address this synergy approach from the homogeneous side, and are mainly comprised of immobilized homogeneous catalyst species that can promote reactions already accessible by homogeneous solution-state conditions.^{1,4,5} Common methods involve using dendrimers as ligands for metal complexes and covalently binding metals to polymers and solids like silica and carbon nanotubes.^{1,6,7} Figure 2.1 illustrates representative examples: **2.1** shows a SiO₂ supported Cu-BOX complex,^{1b} **2.2** is a carbosilane dendrimer-ligated Ni complex,⁴ and **2.3** depicts a vanadyl salen complex covalently anchored to a single walled carbon nanotube.^{1a}

Figure 2.1. Selected Examples of Supported Homogeneous Catalysts.

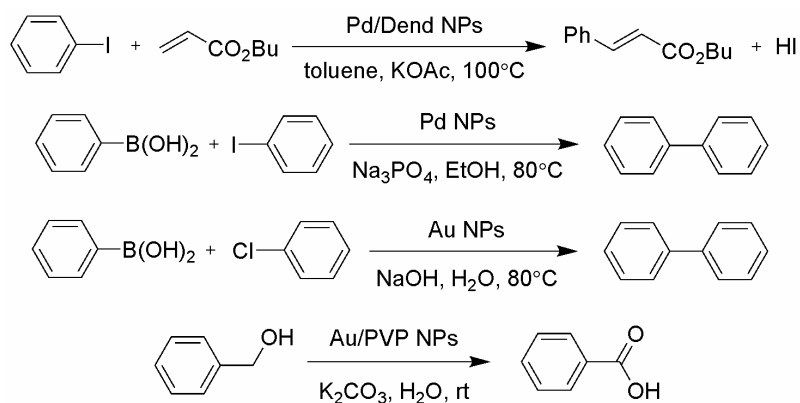


Thus, by these immobilization methods, metal catalysts are rendered heterogeneous, and most of the advantages of such catalysts, like recyclability and easy isolation, are accessible.

Furthermore, the ligand based nature of the catalyst is retained, allowing for quick and easy tuning to maintain the reactivity and selectivity typically associated with homogeneous catalysts.

While this method is powerful and effective, we sought to utilize an alternative approach wherein heterogeneous catalysts are extended to reactions previously only catalyzed by homogeneous species. To this end, nanoparticles represent a new frontier in heterogeneous catalysis, where our goal of converting homogeneous to heterogeneous is supplemented by the ability to obtain new or divergent reactivity and selectivity. More specifically, metal nanoparticles (NPs) can serve as heterogeneous catalysts where the particle size and oxidation state can be characterized. Due to the fact that monodisperse metal NPs are a well-defined system, unlike standard, amorphous heterogeneous catalysts, it is possible to obtain detailed and meaningful information regarding the synthesized NP catalyst. For example, X-ray absorption spectroscopy (XAS) and X-ray photoelectron spectroscopy (XPS) can provide information on the oxidation state and coordinating environment of metal atoms in the nanoclusters and transmission electron microscopy (TEM) allows for visual determination of the NP size and shape. Additionally, it is known that the reactivity and selectivity of monodisperse metal NPs can be altered by changing their size and shape.⁸ Palladium and gold NPs have been demonstrated to catalyze a range of cross-coupling and oxidation/reduction reactions in solution, previously believed to be the exclusive purview of homogeneous catalysis (Scheme 2.1).^{14,9-13} Rhodium and ruthenium are known to catalyze various selective hydrogenations, hydroformylations and couplings.^{14,15}

Scheme 2.1. Selected Reactions Catalyzed by Nanoparticles.¹⁶⁻¹⁹



All of these examples utilize polymers or dendrimers for encapsulation and are thus most relevant to our work present herein. It should be noted, however, that there exist several other methods of protection and stabilization of NPs including, but not limited to, aerogels, organic ligands, ionic liquids, metal oxides, carbon and micelles.

Despite these and many other significant efforts in the area, focusing both on catalytic applications as well as new NP design and synthesis, studies have not yet yielded the control necessary to develop new NP catalysts applicable to a wider variety of reactions. Thus, our goal was both to create a catalyst system capable of new reactivity and to perform the necessary experiments to understand the nature of the observed activity and the structure of the active NP catalyst.

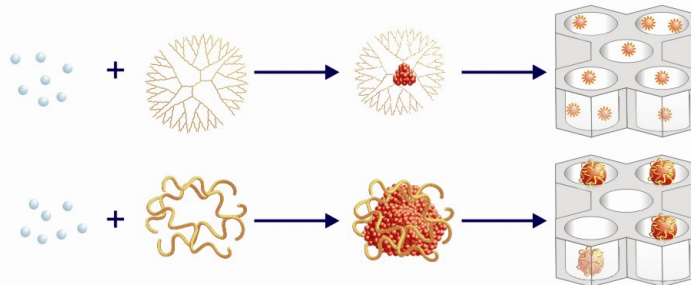
As stated above, carbon-carbon bond forming reactions with metal NPs are known, but are limited in scope. In fact, at the time our investigations began, there were no published

examples of metal NPs activating π -bond towards nucleophilic attack to form C-C bonds.²¹ To accomplish this, the NP catalysts would require significant electrophilic character likely imparted by an increase in metal oxidation state similar to that found in electron-deficient, late-metal homogeneous catalysts. Consequently, if this type of activity were obtained with heterogeneous NPs, we would obtain new activity from heterogeneous metal NP catalysts resulting in selective, solution-phase carbon-carbon and carbon-heteroatom bond forming reactivity previously only obtained with homogeneous catalysts. And perhaps, due to the unique properties of NPs, new or different reactivity and selectivity could be discovered.

Design, Synthesis and Development of Platinum Nanoparticle Catalysts

Given that the aforementioned set of desired transformations are currently known to be catalyzed by homogeneous Pt halides, we focused our initial studies on Pt NPs. Two general types of NPs were prepared in a range of sizes that allow for thorough investigation of the effects of various parameters on reactivity. These Pt NPs were synthesized utilizing two techniques: polymer or dendrimer encapsulation (Figure 2.2).

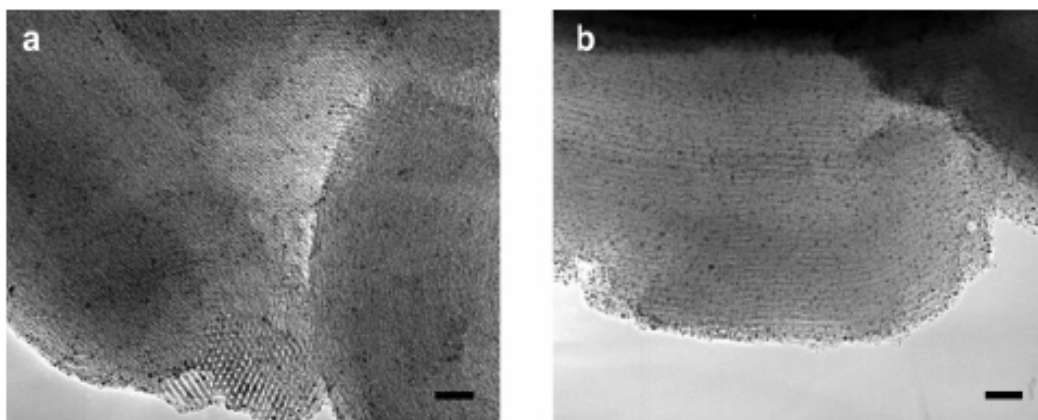
Figure 2.2. Depiction of the Nanoparticle Synthesis for the Two Capping Agents. Top: Pt ions are loaded onto a PAMAM dendrimer and reduced to form a dendrimer encapsulated NP. Bottom: polyvinylpyrrolidone encapsulates the NP. Deposition on SBA-15 follows to produce the catalyst.



Polyvinylpyrrolidone (PVP) was used to generate 1.5, 2.9 and 5.0 nm sized NPs by existing procedures (bottom scheme, Figure 2.2).²² Alternatively, fourth generation hydroxyl terminated polyamidoamine (PAMAM) dendrimers (G4OH) were used as the templating agent for smaller sized 1.0 nm NPs (top scheme, Figure 2.2). These G4OH NPs have been described previously and are known to contain an average of 40 metal atoms per NP and are denoted Pt₄₀.^{8j,23} Larger sized NPs with 100 and 200 average metal atoms per NP were synthesized on sixth generation hydroxyl terminated PAMAM dendrimers. These NPs have been determined to be 1.2 and 1.5 nm in size, respectively.²⁴ Sixth generation dendrimers were required for these larger sizes to provide the required amount of available tertiary amine groups necessary for synthesis of the NPs. The Pt NPs were deposited onto SBA-15 or MCF-17 silica at loadings of less than 1 wt%, with the larger pore size of MCF-17 needed to successfully incorporate the larger sized NPs. These supported NPs have previously been reported and characterized.^{8j,23} Notably, while the PVP NPs are calcined to remove the capping agent, we found during the course of this research that the PAMAM dendrimers are stable to the reaction conditions when supported on SBA-15

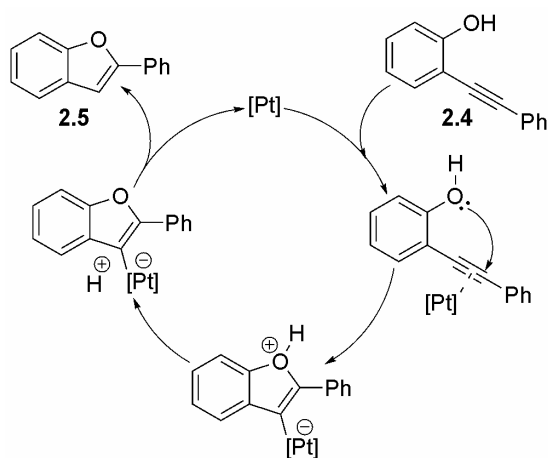
silica, consistent with results published earlier for gas-phase reactivity.²⁵ In fact, it has been shown that loading the PAMAM dendrimer NPs on SBA-15 imparted additional thermal stability against aggregation under the reaction conditions.^{4,23} Furthermore, supporting the NPs on SBA-15 allowed for significantly easier filtration, recovery and recycling of the catalysts. Representative TEM images of Pt NPs on SBA-15 support can be seen below in Figure 2.3.

Figure 2.3. Transmission Electron Micrographs of Pt NPs on SBA-15.
Scale bars = 20 nm.

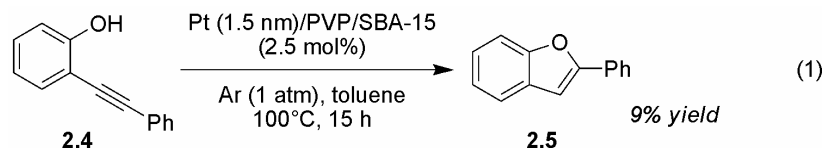


Our initial studies focused on a hydroalkylation reaction in which an electrophilic Pt catalyst activates an alkyne towards nucleophilic attack by an oxygen functionality (Scheme 2.2).²⁶

Scheme 2.2. Catalytic Cycle for Pt Catalyzed Hydroalkoxylation.

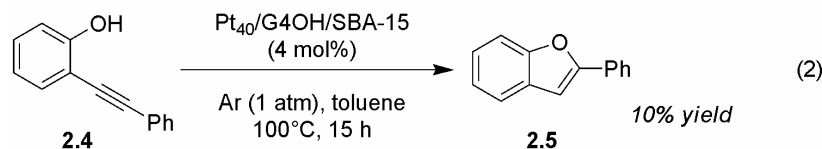
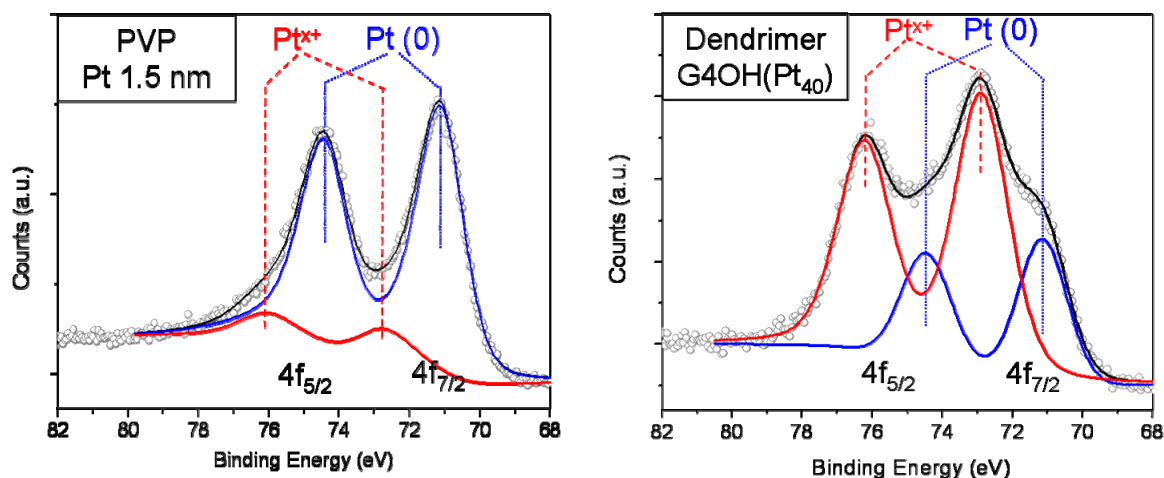


When 1.5 nm Pt/PVP/SBA-15 NPs were used, no appreciable reaction was observed (eq. 1). Given that the homogeneous Pt catalysts for this type of reaction exist in the (+2) or (+4) oxidation state, we hypothesized that the failure of the NPs was due to an overabundance of Pt in the (0) oxidation state, as expected for a metal NP.



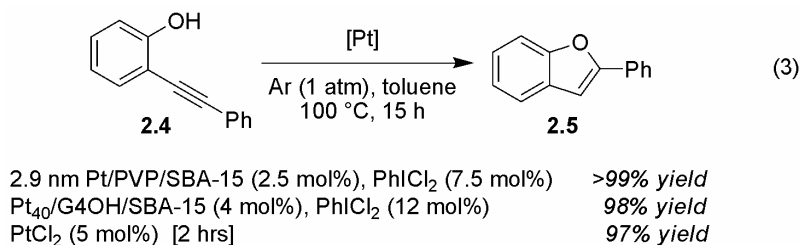
In fact, X-ray photoelectron spectroscopy (XPS) studies on these Pt/PVP NPs have confirmed that >90% of the metal exists in a metallic Pt(0) oxidation state (Figure 2.4). Thus, we turned to the Pt₄₀/G4OH NPs, which are >70% oxidized as determined by XPS (Figure 2.4).²⁷ However, exposure of alkyne **2.4** to 1.0 nm Pt₄₀/G4OH NPs generated only a 10% yield of product (eq. 2). This result is likely due to the presence of catalytically inactive Pt oxide species on the Pt₄₀/G4OH NP surface. To address this lack of activity, we postulated that known oxidizing agents for metals might be used to selectively modify the NP surface to produce a catalyst species with the requisite activity.

Figure 2.4. XPS Spectra for PVP and G4OH Capped Pt Nanoparticles. Fitting depicts relative contribution of Pt(0) and Pt(X+) species.

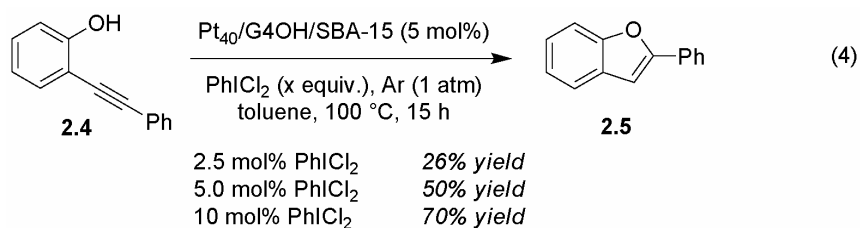


Recent work has shown the formation of oxidized $[\text{PtCl}_4]^{2-}$ layers on Pt surfaces with Cl_2 etching,²⁸ as well as oxidation of Pd catalysts to form Pd—Cl bonds with the hypervalent iodine species iodosobenzene dichloride (PhICl_2).²⁹ These precedents serve to reinforce the ability of PhICl_2 to act as a mild oxidant to transform the Pt NP surface into a catalytically active state. Furthermore, if successful, the oxidative treatment would represent a direct translation of technology developed for homogeneous catalysts to heterogeneous catalysis. More specifically, existing methodology that can be utilized to modify metal atoms in homogeneous compounds can also be used, under the right circumstances, to modify metal atoms on a surface in nanocrystals.

Gratifyingly, we found that PhICl_2 successfully generated the desired electrophilic catalyst species.³⁰ Treatment of either $\text{Pt}_{40}/\text{G4OH}/\text{SBA-15}$ (further reduced under H_2 atmosphere at 100°C for 24 h prior to reaction) or $\text{Pt}/\text{PVP}/\text{SBA-15}$ NPs with three equivalents (relative to catalyst loading, total metal basis) of PhICl_2 resulted in an excellent yield of $>95\%$ for benzofuran **2.5** (eq. 3).

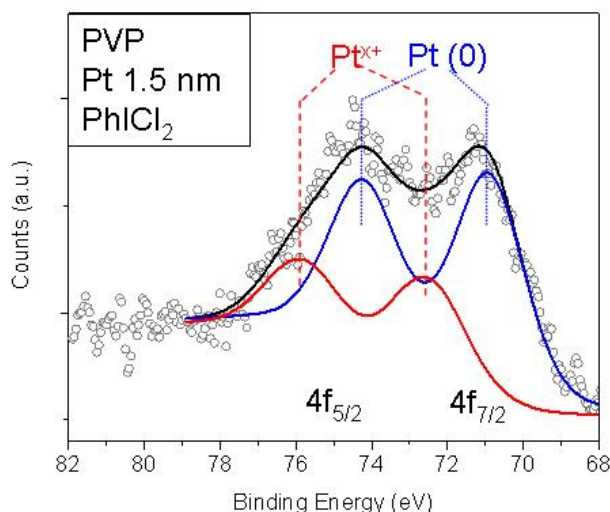


Decreasing the equivalents of oxidant led to a lower yield of reaction (eq. 4). It is important to note that PhICl_2 , SBA-15 and heat either individually, or in any combination did not catalyze the reaction.



Further evidence for the oxidation of the Pt NPs was obtained from an XPS spectrum of 1.5 nm Pt/PVP NPs treated with PhICl_2 showing that $>25\%$ of the Pt was oxidized (Figure 2.6).

Figure 2.6. XPS Spectrum for Oxidized $\text{Pt}_{40}/\text{G4OH}/\text{SBA-15}$ NP Catalyst.



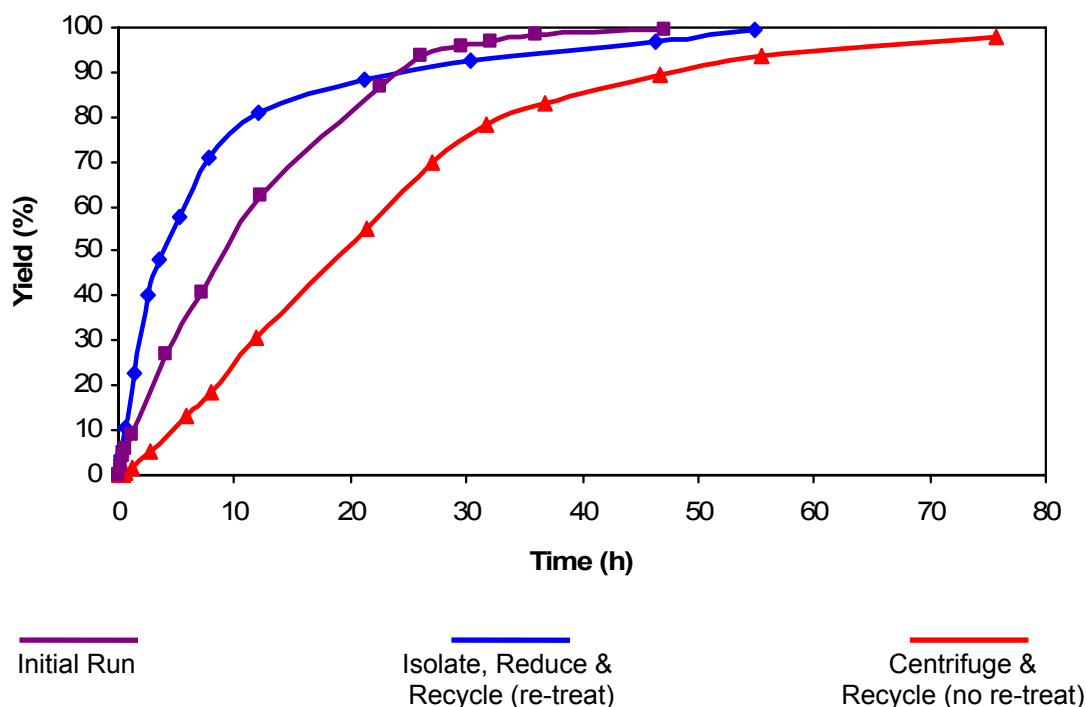
As mentioned above, the inactivity of the ‘as synthesized’ catalyst is likely due to the presence of oxides on the surface of the particles that render the metal centers oxidized but in an inactive form for the electrophilic catalysis desired. Thus, by further reducing the NP under H₂ at elevated temperature, we are able to effectively remove this oxide layer and create a Pt(0) surface on the nanoparticles. Then we can selectively generate the desired metal oxidation state and chemical environment using the PhICl₂ treatment to obtain NP active for the desired electrophilic catalysis. This oxidation/reduction sequence was verified by XPS where the initial oxidation state seen in Figure 2.6 was reduced by H₂ to >90% Pt(0) and then back to oxidized Pt after PhICl₂ treatment. More specific and higher quality data for this phenomenon was also obtained via X-ray absorption spectroscopy (XAS), and will be discussed in a later section.

Upon direct comparison of the NP conditions and Fürsner’s published PtCl₂-catalyzed homogeneous conditions,²⁶ the most apparent difference is the use of argon gas vs carbon monoxide. Carbon monoxide (CO) is known to act as a labile electron withdrawing ligand for the Pt atoms that serves to stabilize it against aggregation. As our catalyst was already a formed NP with stabilization provided by a dendrimer (when present) and SBA-15, we did not expect CO to be necessary or helpful. This proved to be the case as CO and Ar atmosphere gave identical results for the hydroalkoxylation reaction. Inert atmosphere, rather than just air, was preferred due to the exclusion of oxygen and water which could serve to reform the oxide coating on the NP surface and render it inactive or attenuate its activity.

Catalyst Activity Studies

As predicted, the oxidized NP catalysts demonstrated a size and capping agent effect on catalytic activity. Although multiple studies conducted on various reactions in both the gas and solution phase have demonstrated the importance of these NP parameters for reactivity and selectivity, fewer discuss supported NPs in solution.^{8,10i} Under our oxidative modification conditions, additional size and capping agent effects were found for the PVP and dendrimer capped, SBA-15 supported Pt NPs. Results from detailed reaction monitoring indicated that smaller, dendrimer capped NPs are more stable in higher oxidation states than larger NPs and remain in this catalytically active state for prolonged times. Based on previous observations, this trend may be due to the stability imparted by the PAMAM dendrimer NPs to higher oxidation states.^{23,27} It is also possible that, under the reaction conditions, the dendrimer could decompose, questioning the validity of these conclusions. However, any decomposition does not appear to affect the catalytic activity as evidenced by the similar activity of the Pt₄₀/G4OH/SBA-15 NP catalyst after recycling and its consistent difference from the PVP capped NPs. Furthermore, recent reports that suggest harsher conditions are required for complete dendrimer removal.^{27b,31,32} Regardless, Pt₄₀ proved to be the most robust catalyst and, after oxidative modification with PhICl₂, maintained a steady rate of reaction, only to decrease as the reaction neared complete consumption of starting material (Figure 2.7).

Figure 2.7. Monitoring the reaction using Pt₄₀/G4OH/SBA-15 NP catalyst. Graph displays the reaction yield of **2.5** from **2.4** as a function of time. Catalyst treated with PhICl₂ (3 catalytic equivalents).



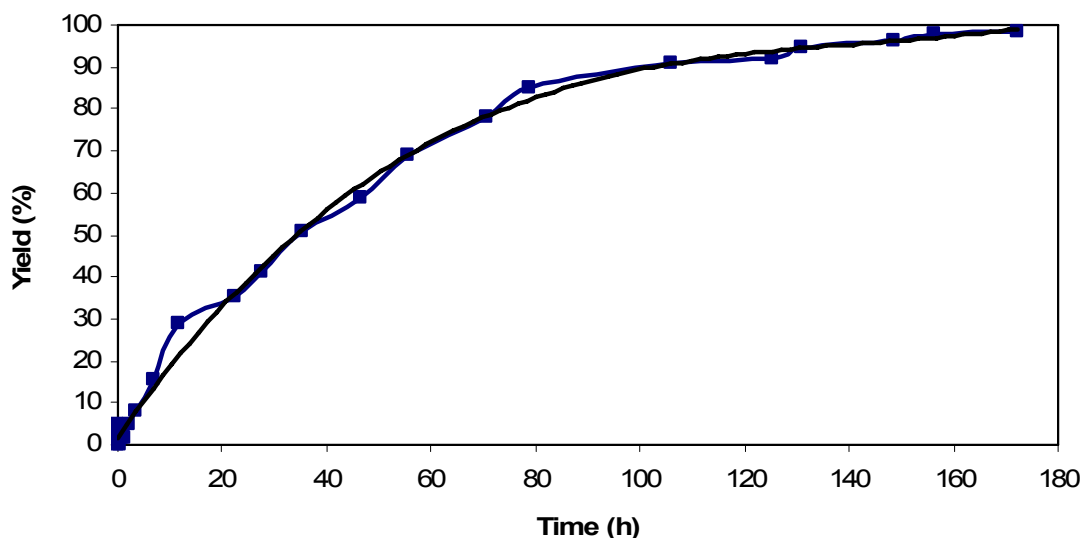
As seen in Figure 2.7, monitoring of the reaction indicated no loss of activity as compared to the initial catalyst use when the catalyst was properly recycled by filtration, isolation, re-reduction (H₂, 100°C, 24h) and resubmission to a new solution of substrate and oxidant (Figure 2.7, blue line). Notably, to separate the metal species from the product solution, simple filtration of the catalyst through a glass microfiber filter was sufficient. In addition, the Pt₄₀/G4OH PAMAM NPs, when supported on SBA-15, showed excellent recyclability over multiple cycles after simple filtration, reduction and retreatment with PhICl₂. A sample of Pt₄₀/G4OH/SBA-15 NPs has been recycled four times with a consistent yield of >90% under the reported reaction conditions. In addition, a single batch of catalyst was active for a month, and a turnover number of 400 (per metal basis) was obtained. Due to the difficulty in knowing the exact number of surface sites on the NPs, a turnover frequency (TOF) cannot be quantified absolutely. However, if the value is based on the overall amount of platinum, rather than the number of active sites, the initial TOF is roughly 3.5 h⁻¹ at a catalyst loading of 3.5 mol%.

When the SBA-15 supported Pt₄₀ catalyst was isolated only by centrifugation and immediately resubmitted to a new solution of substrate without any further PhICl₂, an overall decrease in activity was observed, but the catalyst remained consistently active until all substrate was consumed with no significant further deactivation (Figure 2.7, red line). This is likely due to slow deactivation of the catalyst and potential formation of platinum oxides or other catalytically inactive species on the surface of the NP, especially when handled in air during centrifugation. Despite our best efforts, it is entirely possible that small amounts of air or water could also be present during the reaction to produce this effect. It is also possible that the nature of the NP is

changing during the reaction conditions and slowly being reduced or altered in some other way so as to render the NPs inactive for the desired transformation. As seen from the data, whatever the cause, the deactivation is minimal and does not affect recyclability when properly regenerated. The XAS studies discussed later will revisit this topic in an effort to explain the observed phenomenon.

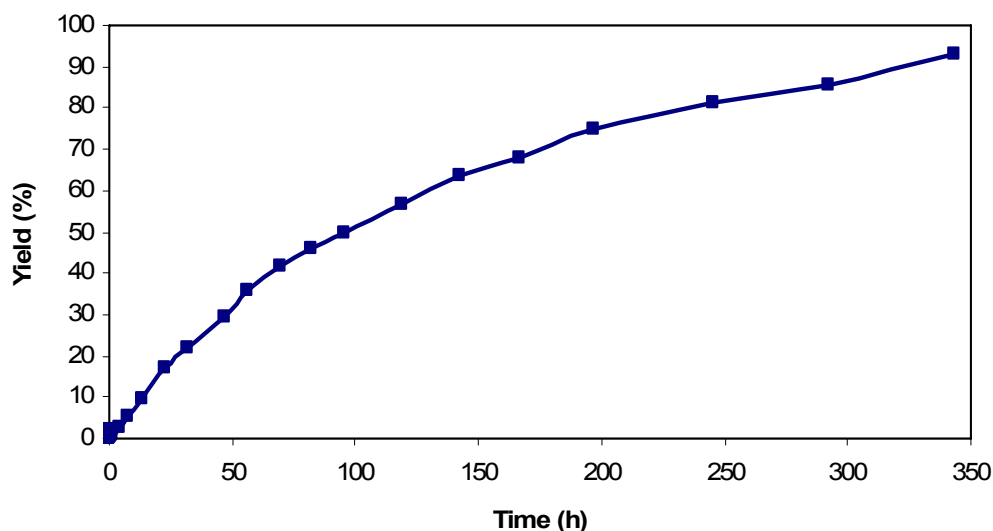
We observed that Pt₂₀₀/G6OH/SBA-15 NPs were less active than their smaller counterpart. This can be attributed to the larger steric bulk of the sixth generation dendrimer which inhibits interactions between substrate and catalyst.^{11,33} PAMAM dendrimers are well known to have an inner pocket, where the NP presumably exists, and a sterically congested but still porous exterior. Depending on the generation of the dendrimer, the size of the pores and thus ease of diffusion into the dendrimer changes. Higher generations result in a more bulky and closed exterior. This explanation is supported by the fact that Pt₂₀₀ in the G6OH dendrimer has an activity vs. time profile very similar to Pt₄₀ in the G4OH dendrimer (Figure 2.8), despite the small size difference of the NPs (Pt₂₀₀ is approximately 1.9 nm in diameter).

Figure 2.8. Monitoring the reaction using Pt₂₀₀/G6OH/SBA-15 NP catalyst. Graph displays the reaction yield of **2.5** from **2.4** as a function of time. Catalyst treated with PhICl₂ (3 catalytic equivalents). Trendline (black) added to improve clarity of results.



In addition, when Pt₄₀ was synthesized in a 6th generation PAMAM dendrimer, a significant rate decrease was observed relative to the 4th generation catalyst (Figure 2.9). It is, therefore, apparent that the steric effect of the dendrimer limits the rate at which substrate molecules can enter the dendrimer and come into contact with the NP catalyst and thus impacts the overall rate of the reaction. The continued reactivity of the catalyst, however, after more than 300 hours of reaction time, is a testament to the stability of the catalyst in its oxidized state.

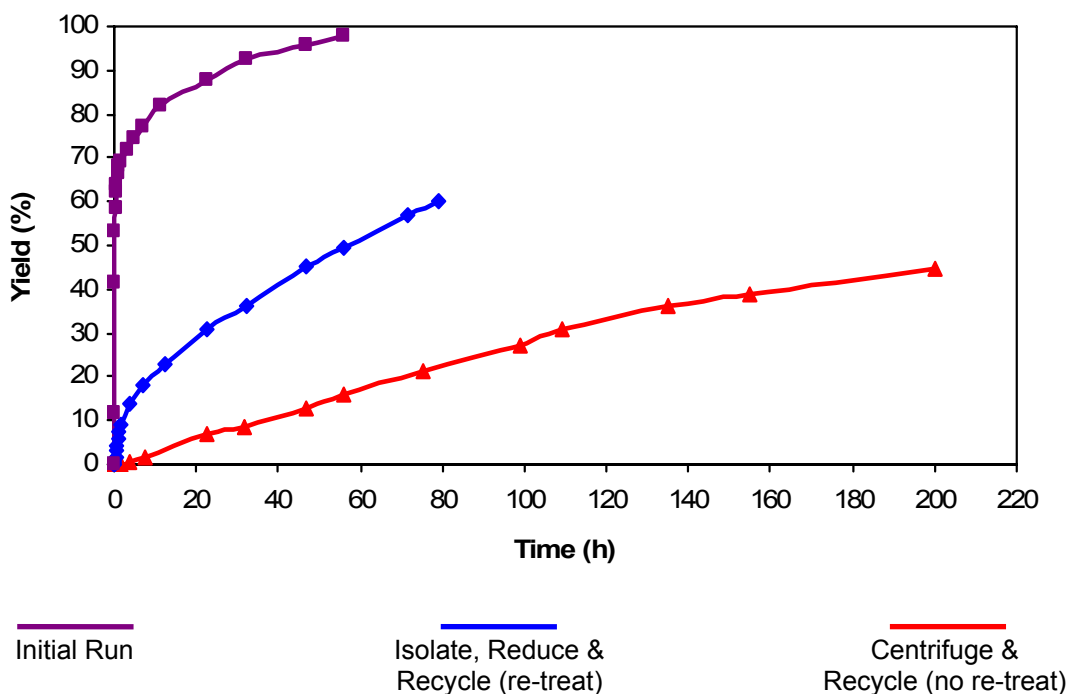
Figure 2.9. Monitoring the reaction using Pt₄₀/G6OH/SBA-15 NP catalyst. Graph displays the reaction yield of **2.5** from **2.4** as a function of time. Catalyst treated with PhICl₂ (3 catalytic equiv.)



Much like their use in the gas-phase, PAMAM dendrimers exhibit significant advantages as NP capping agents in solution. This templating strategy allows for the highly controlled generation of monodisperse NPs as small as 1 nm. It is complemented by the resulting performance enhancements and control, and the potential for further catalyst development in combination with the oxidative modification.

For larger NP sizes, PVP capping was required. However, the 1.5, 2.9 and 5.0 nm Pt/PVP/SBA-15 NPs had distinctly different activity from the smaller, dendrimer capped NPs. In addition to a decrease in activity as NP size increased, these larger NPs demonstrated a marked initial spike in activity, followed by rapid deactivation and prolonged time to reach completion (Figure 2.10). For example, when only 1 mol% of 1.5 nm Pt/PVP/SBA-15 NPs treated with PhICl₂ was used, approximately 70% yield was reached in the first 1.5 hours. Then, nearly 60 hours were required to reach complete conversion to product. Immediate resubmission of the PVP NPs to a new batch of substrate did indeed prove the catalyst was deactivated, as the reaction was extremely slow and never reached completion in significantly more time than required for the first pass.

Figure 2.10. Monitoring the reaction using 1.5 nm Pt/PVP/SBA-15 NP catalyst. Graph displays the reaction yield of **2.5** from **2.4** as a function of time. Catalyst treated with PhICl_2 (3 catalytic equivalents).



Even after reduction and PhICl_2 retreatment of the recycled catalyst, substantial deactivation of the catalyst was observed (Figure 2.10, blue line). A similar effect was observed for 2.9 nm Pt/PVP/SBA-15 NPs treated with PhICl_2 (Figure 2.11), although with improved recycling when re-reduced and retreated.

In comparison, 2 mol% of PhICl_2 oxidized 5.0 nm Pt/PVP/SBA-15 NPs generated only ~14% yield in the initial activity spike, and after 70 hours, only 60% yield was obtained, demonstrating the decrease in activity resulting from larger NP sizes (Figure 2.12). It is important to note that while the PVP capped catalyst did exhibit a more rapid deactivation, a batch of 2.9 nm Pt/PVP/SBA-15 NPs treated with PhICl_2 remained active for one month. A turnover number of 415 (per metal basis) was obtained and an initial TOF based on total metal is 4.3 min^{-1} at a catalyst loading of 1 mol%. This value is not very useful since the rate dramatically decreased within the first hour of reaction to a TOF at a catalyst loading of 1 mol% of roughly 1.2 h^{-1} around the 5-6 hour mark and decaying to 0.6 h^{-1} at the 10-11 hour mark, dropping further as time progresses.

Figure 2.11. Monitoring the reaction using 2.9 nm Pt/PVP/SBA-15 NP catalyst. Graph displays the reaction yield of **2.5** from **2.4** as a function of time. Catalyst treated with PhICl₂ (3 catalytic equivalents).

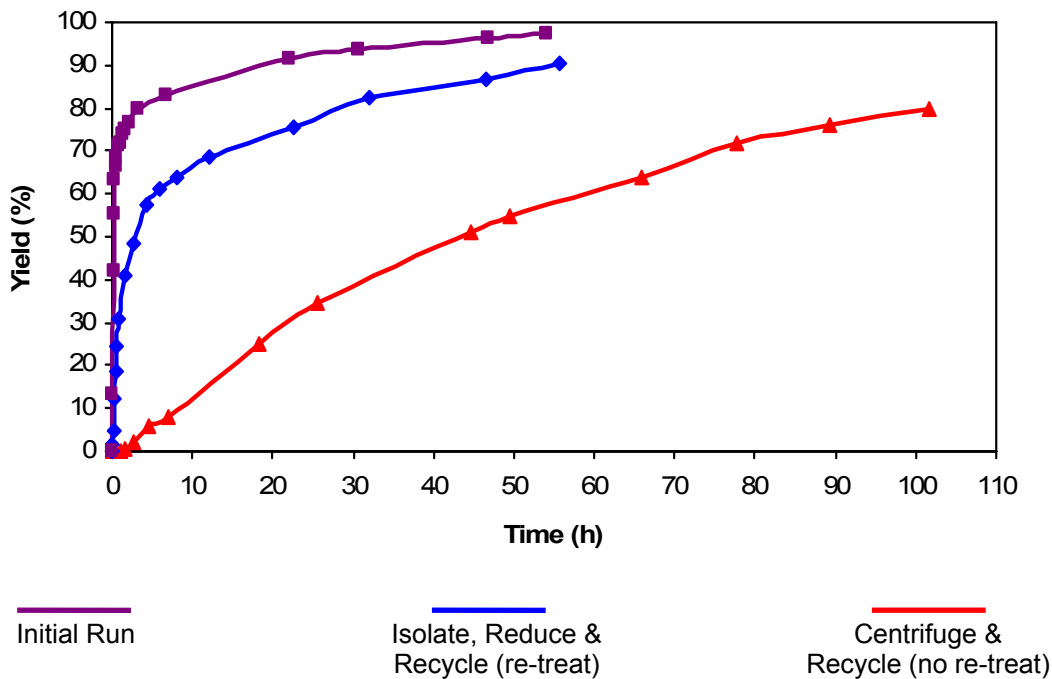
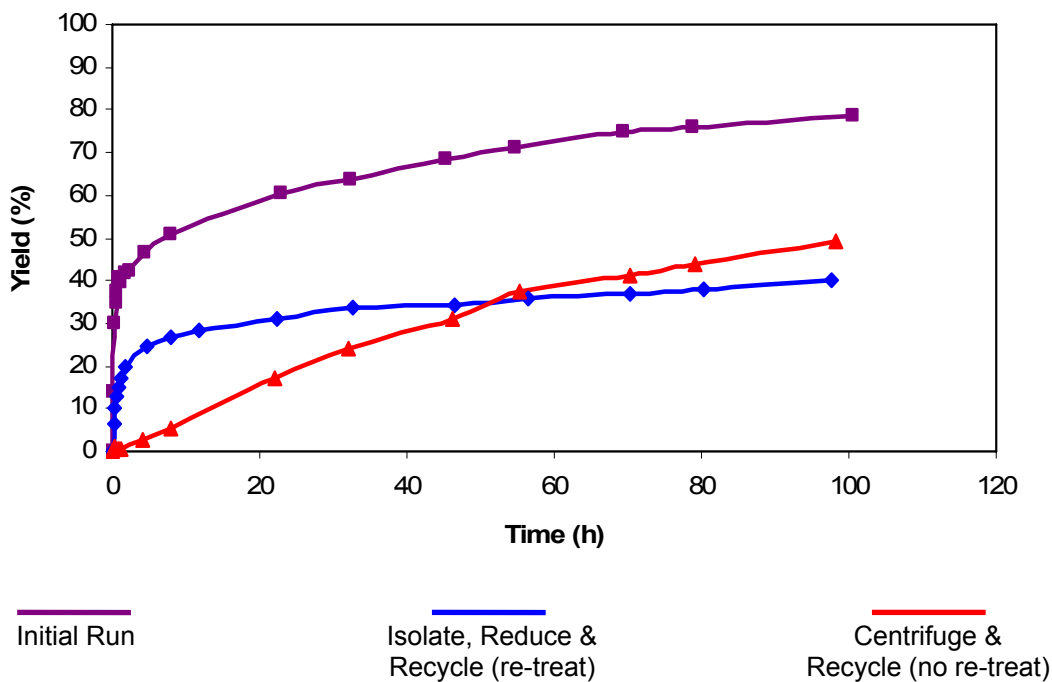


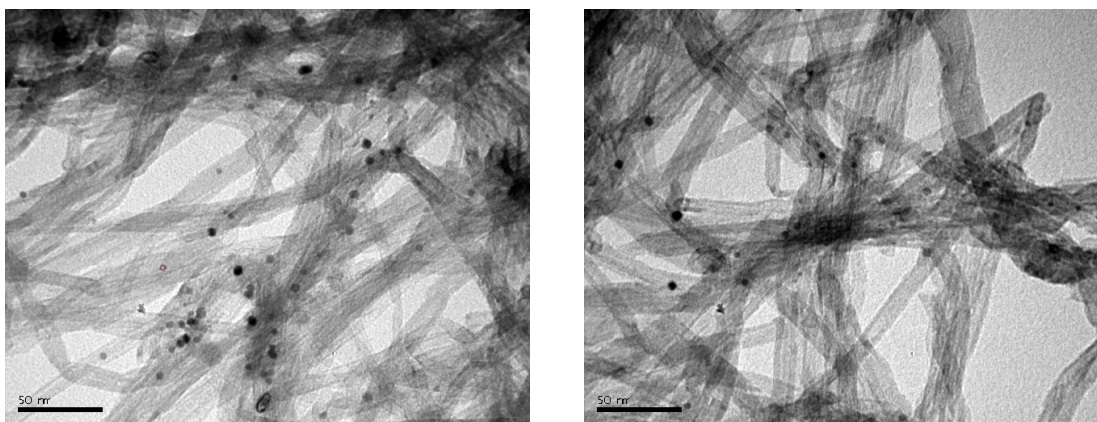
Figure 2.12. Monitoring the reaction using 5.0 nm Pt/PVP/SBA-15 NP catalyst. Graph displays the reaction yield of **2.5** from **2.4** as a function of time. Catalyst treated with PhICl₂ (3 catalytic equivalents).



For these larger NP sizes, we believe that the NP has more metallic character and tends to revert to the Pt(0) oxidation state.³⁴ With smaller sizes, the NP more readily retains its oxidized state as the electronic valency of the surface atoms is less saturated and more atomic character is present. Additionally, decreasing the particle size, especially below 1-2 nm, induces changes in the electronic properties: the particles lose metallic character and become non-metallic or semi-conductive.³⁵ In other words, small nanoparticles are more like the quantum mechanical description of molecules and larger nanoparticles have electronic bands analogous to solids constituted by micrometric particles. This translates to smaller particles behaving more like atomic metal with increased stability in higher oxidation states and larger particles behaving like bulk metal in low oxidation states. Furthermore, in the size range of 2-20 nm, dramatic property changes can be observed for minor variations in size.³⁶ It is also likely that the increased activity of smaller NPs is due to the larger proportion of low coordinated surface edge and corner Pt atoms which become active sites after treatment with PhICl_2 ; the presence of these sites is a key factor for catalytic activity. The size of NPs also affects the relative amounts of various lattice surface structures (eg. Pt(111)) that can affect activity or selectivity.³⁷ In addition to these size considerations, the increased rate of deactivation and limited recyclability for the PVP capping agent renders the oxidatively modified PAMAM dendrimer capped NPs as the optimal catalyst system.³⁸

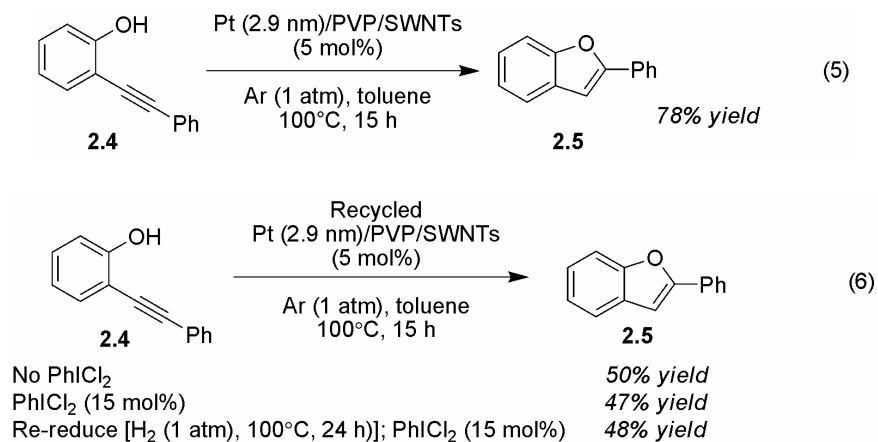
During the course of our investigations, non-silica based solid supports (ie. other than the SBA or MCF classes) were considered. Carbon nanotubes and nanofibers are both extremely well studied, and there exists an abundance of examples detailing their use as solid supports for catalysts.⁶ Based on the previous successes of others, we deposited our 2.9 nm PVP capped Pt NPs onto single walled carbon nanotubes (SWNTs) at a loading of 1.5 wt%. Representative TEM images can be seen in Figure 2.13.

Figure 2.13. Transmission Electron Micrographs of 2.9 nm Pt/PVP Loaded on Single Walled Carbon Nanotubes.



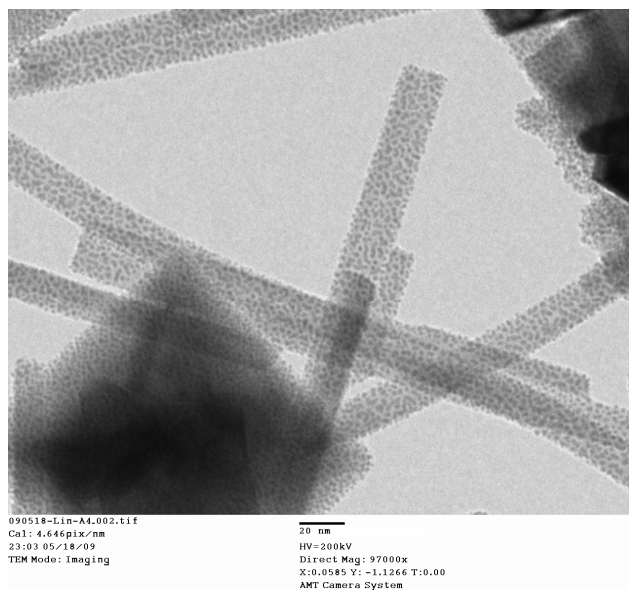
When this catalyst system was used in our electrophilic system with PhICl_2 oxidative modification, the yield obtained was good, but lower than that generated by the SBA-15 supported NPs (eq. 5). The SWNT supported NPs were, however, similar to the PVP capped, SBA-15 supported NPs in that they both displayed substandard recycling, even when re-reduced and retreated with oxidant (eq. 6). Due to the improved performance of the SBA-15 supported NPs, SWNTs were not further pursued, although further investigation into the effects and utility

of this support is warranted. For example, Pt₄₀/G4OH NPs should be loaded onto SWNTs so that a comparison can be made with the currently optimal SBA-15 supported system.

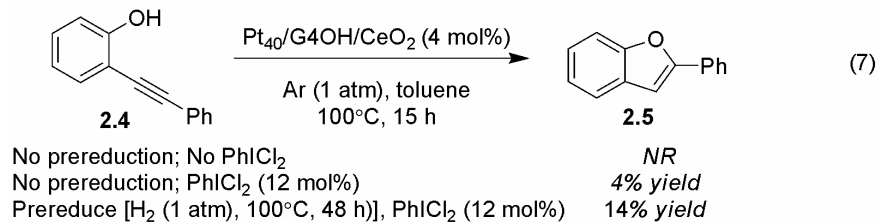


The strong interaction between ceria (CeO₂) and metal atoms or NPs deposited on its surface is well known.³⁷ For instance, ceria can act to stabilize oxides and other higher oxidation states in metals attached to its surface.³⁹ Hoping to capitalize on this effect for our system, we loaded Pt₄₀/G4OH onto CeO₂ nanorods (Figure 2.14).

Figure 2.14. Transmission Electron Micrograph of Pt₄₀/G4OH Loaded on CeO₂ Nanorods.



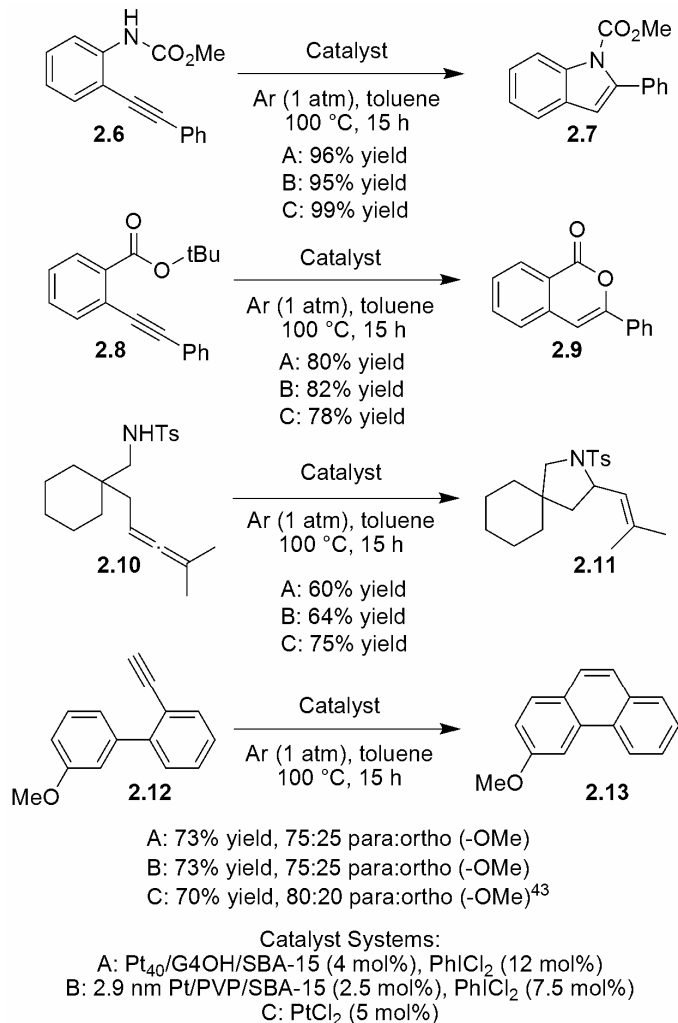
Unfortunately, no combination of reduction and/or treatment produced a catalytically active system to transform **2.4** into benzofuran **2.5** (eq. 7). It is possible that the observed lack of reactivity is due to strong stabilization of oxides by the ceria, rather than the desired Pt-Cl surface species.



Reaction Results and Discussion

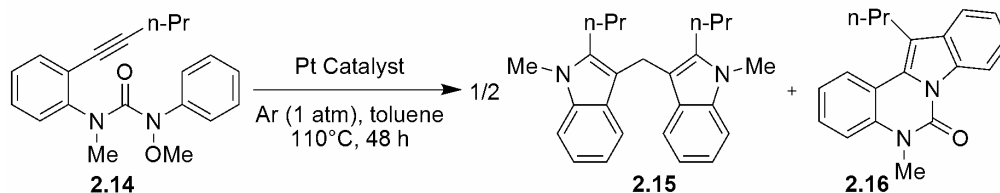
At this point, we have developed two highly active Pt NP catalysts, Pt₄₀/G4OH and 2.9 nm Pt/PVP, supported on SBA-15. Accordingly, we sought to test them for a range of π -bond activation reactions previously known to occur only with electrophilic homogeneous catalysts. Gratifyingly, the NPs were found to catalyze several reactions in the solution-phase under relatively mild conditions with minimal or no side-reactions. Scheme 2.3 shows the results of these reactions with both G4OH PAMAM dendrimer and PVP capping agents and well as homogeneous PtCl₂. Five- and six- membered ring heterocycles were formed by addition of nitrogen and oxygen nucleophiles to alkynes and allenes, activated by the Pt nanoparticle catalysts. In addition to the standard phenol substrate **2.4**,²⁶ the nitrogen of carbamate **2.6** selectively added to the activated alkyne to generate **2.7** in excellent yield with all catalysts. Addition of the carbonyl oxygen of **2.8** and loss of 2-methyl-propene generated **2.9**.⁴⁰ Similarly, the tosyl protected nitrogen of allene **2.10** hydroaminated the attached allene to form **2.11** in good yields relative to the homogeneous catalyst.⁴¹ Carbon-carbon bond formation was accomplished from **2.12** utilizing a hydroarylation reaction to form **2.13**.⁴² It is important to note that all reactions are catalyzed by Pt NPs in yields comparable to, if not slightly better than those obtained with homogeneous PtCl₂. Furthermore, in the case of the cyclization of compound **2.12**, our NP catalysts show selectivity favoring the *para*-isomer **2.13** over the *ortho*-isomer, nearly equivalent to that observed with homogeneous PtCl₂. This highlights the potential of unique heterogeneous catalysts to offer similar selectivities relative to homogeneous species.

Scheme 2.3. Cyclization Reactions of Pt NPs.



We also found that when urea **2.14** was treated with either PtCl₂ or PtCl₄ homogeneous catalyst in toluene at 110°C, both **2.16**⁴³ and a previously unreported product, the bis-indole **2.15**, were observed, although in low yields. However, addition of SBA-15 resulted in a suppression of the formation of **2.16** and a subsequent increase in the yield of bis-indole **2.15** (Scheme 2.4). Interestingly, the use of either Pt/PVP/SBA-15 or Pt₄₀/G4OH/SBA-15 NPs oxidatively modified with PhICl₂ resulted in a much higher 43-48% yield after 48 h for the bis-indole **2.15**. While a small amount of tetracycle **2.16** was still formed by the NP catalysts, the majority of the consumed starting material went towards this alternative catalytic reaction pathway. In this case, the NPs selectively catalyze a reaction cascade different from that obtained with homogeneous catalysts that generates several new carbon-carbon bonds and combines aspects of two starting material molecules to afford **2.15**.

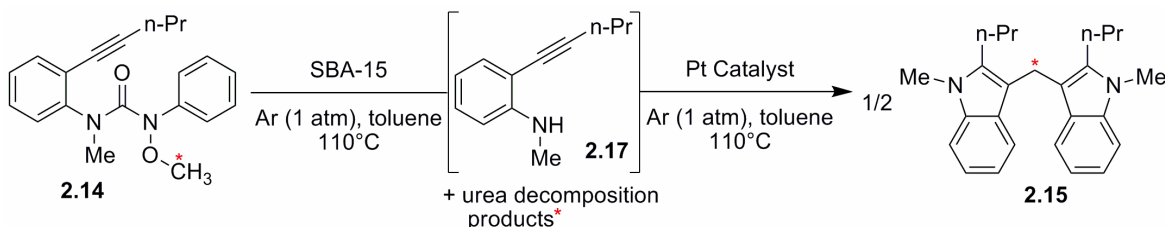
Scheme 2.4. Oxidatively Modified Pt NP Catalyzed Cyclization of Phenylurea **2.14** to Tetracycle **2.16** and Bis-Indole **2.15**.



Catalyst	Yield (2.15 , 2.16)
PtCl ₂ (5 mol%)	8%, 25%
PtCl ₄ (5 mol%)	8%, 13%
PtCl ₂ (5 mol%), SBA-15	16%, 5%
Pt ₄₀ /G4OH/SBA-15 (4 mol%)	43%, 6%
2.9 nm Pt/PVP/SBA-15 (2.5 mol%)	48%, 7%

Based on a ¹³C labeling study, we found that the methyl group of the methoxylamine (indicated by a red asterisk in Scheme 2.5), becomes the bridged methylene carbon in bis-indole **2.15**. We hypothesize that the SBA-15, possibly in cooperation with the Pt NPs, catalyzes a degradation of the urea functionality to unisolable species, based on the observation that SBA-15 alone will convert **2.14** into isolable N-Me intermediate **2.17**. Then, formation of the bis-indole occurs by an as yet unknown mechanism in which the bridging methylene originates from the degraded urea group, as indicated (Scheme 2.5). The potential for homogeneous Pt catalysts to selectively generate **2.15** in the presence of various ligands has not been investigated.

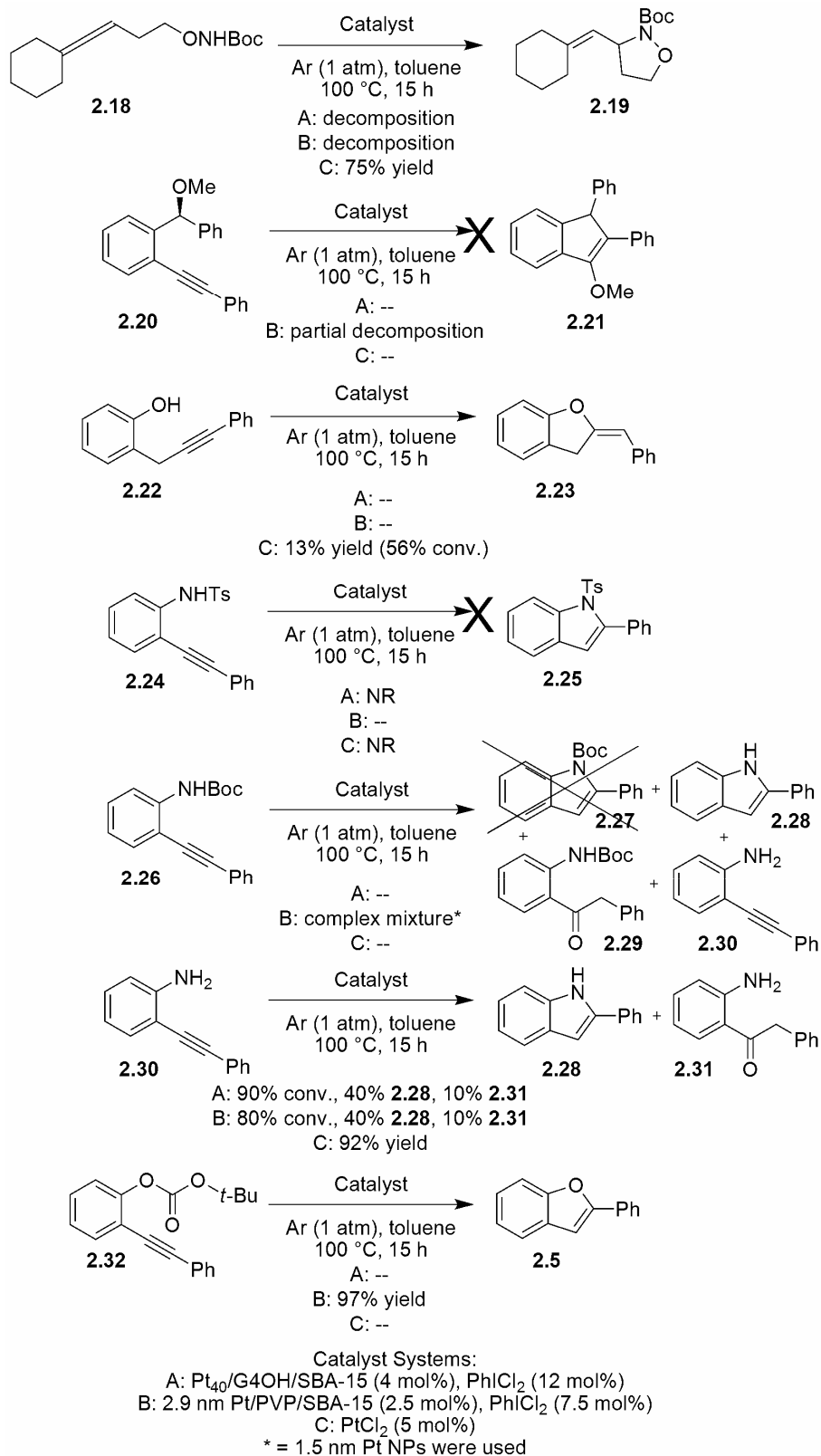
Scheme 2.5. Postulated Mechanism for Formation of Bis-Indole **2.15**.



Regardless of the specific mechanism, by utilizing supported NPs for this process, we have developed a recyclable catalyst system that can access this reactive pathway in yields greater than those obtained by simply mixing homogeneous catalyst with SBA-15. The superior performance of the Pt NP catalysts also suggests that NPs are particularly well suited for the interactions necessary to catalyze the formation of bis-indole **2.15**. Furthermore, we postulate that a cooperative effect exists between the SBA-15 support and the NPs which allows for this new reactive pathway, and, with the necessary future analysis, could be applied to generate new transformations.

While excellent and interesting results were obtained for the above substrates, there were several that failed to transform to product in good yield, decomposed or didn't react at all.⁴⁴ In Scheme 2.6 the substrates that gave no reaction or decomposition are shown. In some cases, homogeneous PtCl₂ was also used to test for theoretical activity towards Pt catalysis, and the resulting yield is shown.

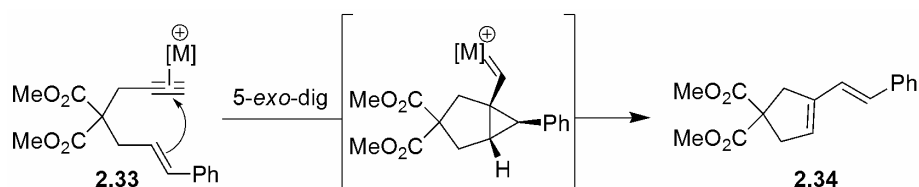
Scheme 2.6. Failed Reactions Under Pt NP Catalysis.



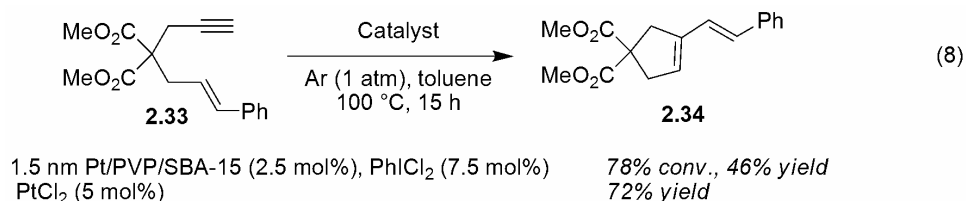
Interestingly, hydroxylamine **2.18**⁴⁵ resulted in decomposition when submitted to the oxidatively modified NP catalyst, but gave 75% yield of product when homogenous PtCl₂ was used. Intramolecular carboalkoxylation of **2.20**⁴⁶ was unsuccessful. In this case, a small amount of decomposition was observed, with most starting material remaining in solution unreacted. Substrate **2.22**⁴⁷ showed reactivity, but the low yield relative to the conversion obtained with homogeneous PtCl₂ precluded its use with the NP catalysts. It appears that out of all the aniline derivatives investigated, only the methyl carbamate **2.6** successfully reacts under our NP catalysis conditions (Scheme 2.5). Tosyl protection (**2.24**)⁴⁸ *t*-butyl ester (**2.26**),⁴⁹ and free amine (**2.30**)⁵⁰ all failed to generate reasonable amounts of desired product (Scheme 2.6). While the tosyl group prevented any reaction from occurring, decomposition, hydration (**2.31**) and the desired indole product **2.28** were all observed for the free amine, and *t*-butyl ester protection gave a complex and intractable mixture that appears to include the deprotection (**2.30**), hydration (**2.29**) and deprotected indole (**2.28**). Finally, the carbonate substrate **2.32** first deprotected under the conditions and then cyclized to form benzofuran **2.5**.

A class of reactions related to the nucleophilic addition to activated alkynes utilizes enyne type substrates where cyclization occurs by nucleophilic addition of electrons from an alkene. This generates a cationic intermediate, and a skeletal rearrangement typically occurs to neutralize the species with protodemetalation or a hydrogen shift to regenerate the catalyst (Scheme 2.7). This chemistry is well preceded both with platinum and gold catalysis.⁵¹⁻⁵³ Thus, we sought to use our Pt NP system for this transformation.

Scheme 2.7. Cyclization of 1,6-Enynes Catalyzed by Platinum or Gold.



However, when the 1,6-enyne **2.33** was submitted, only 46% yield was obtained, while a nearly equivalent amount of starting material decomposed to intractable products under the conditions. This compared poorly to homogeneous PtCl₂ catalysis, where 72% yield of **2.34** was obtained with minimal decomposition or side product formation (eq. 8).



While this result precludes our use of 1,6-enynes with the oxidatively modified NPs, it is not unreasonable. Based on calculations performed by the Echavarren *et al.*, heterogeneous catalysts have higher LUMOs than homogeneous catalysts and thus are less effective at complexing alkenes, a requirement for efficient 1,6-enyne cyclizations.⁵⁴ What is more, different binding modes such as reactant adsorption vs coordination, which are related to the HOMO/LUMO energy levels and the binding energies present, are possible based on whether the

catalyst is heterogeneous or homogeneous.⁵⁴ Echavarren argues that while both can activate alkynes, the different ways they do this and the relative inability of heterogeneous catalysts to activate alkenes renders them less active for reactions involving 1,6-enynes. This effect could be advantageous if reactivity with the alkyne only is desired. The calculations done by Echavarren are for gold rather than platinum, but the conclusions are still valid due to the similar electronic properties of the two metals. Also, while we are further activating the nanoparticles by oxidative treatment with PhICl_2 and an appreciable amount of the desired activity is obtained, it appears that this is insufficient to allow Pt NPs to complex and activate alkenes to the extent of homogeneous Pt. However, our limited empirical observations cannot provide a conclusive resolution to this issue.

As detailed in Chapter 1 of this dissertation, an oxidative rearrangement was developed that utilized sulfoxides to trap late metal carbenoid species formed during a reaction.⁵⁵ It was further shown that this methodology was accessible with Pt catalysts. Thus, we used our $\text{Pt}_{40}/\text{G4OH}$ NP catalyst, supported on SBA-15 to enact the same transformation. As we were using the optimal dendrimer capped NP catalyst, we prereduced the catalyst [H_2 (1 atm), 100°C , 24h] before the reaction. We found that the NPs were capable of catalyzing the rearrangement of **2.35** with a high level of selectivity for the *Z* isomer of **2.36** (Table 2.1, entry 1). However, a low yield of desired product (23%) was obtained (entry 1), especially compared to the homogeneous case where PtCl_2 generated 72% yield with 94:6 *Z:E* at 60°C in the same amount of time and at a lower temperature (entry 2).

Table 2.1. Oxidative Rearrangement of Propargyl Esters.

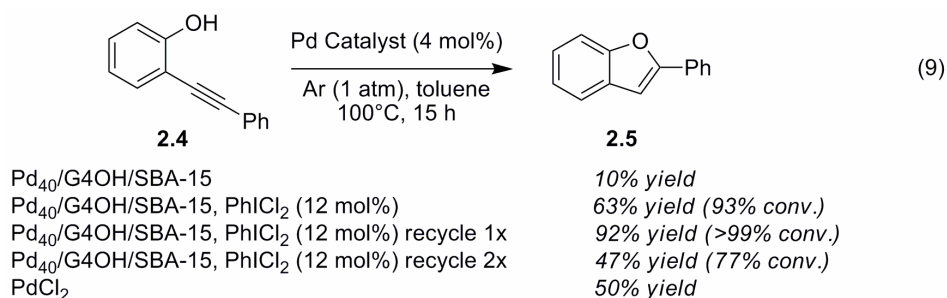
$\text{Catalyst (x mol\%)}$
 $\text{Ph}_2\text{SO (2 equiv.), toluene}$

entry	catalyst	mol% cat.	temp	time	yield ^a	<i>Z/E</i>
1	$\text{Pt}_{40}/\text{G4OH}/\text{SBA-15}$	4	100°C	15 h	23%	98:2
2	PtCl_2	5	60°C	17 h	72%	94:6

^a All yields determined by NMR vs methyl benzoate internal standard.

Extension to Palladium and Gold Nanoparticles

Generality for the oxidative treatment method was demonstrated by using $\text{Pd}_{40}/\text{G4OH}/\text{SBA-15}$ NPs were used for the formation of **2.5** from **2.4** (eq. 9). Just as was found for Pt, the Pd NPs required further reduction [H_2 (1 atm), 100°C , 24h] followed by *in situ* treatment with PhICl_2 to generate electrophilic catalytic activity. The yield obtained with the Pd NPs (63%) was slightly better than that obtained with PdCl_2 homogeneous catalyst (50%).⁵⁶ However, after recycling the catalyst once, the yield, surprisingly, jumped to 92%. Then, when recycled a third time, it dropped to 47% with only 77% conversion (eq. 9). This variability in yield is puzzling and may indicate leaching of the catalyst or some other instability.



Instead of the standard hydroalkoxylation reaction, we investigated the use of Au₅₅/G4OH/SBA-15 NPs for the cyclopropanation of propargyl esters, published previously by Johansson *et al.*⁵⁷ As seen in Table 2.2, Au₅₅ NPs gave excellent results with good selectivity for the *cis* isomer of **2.38** (entry 4) that was equivalent to or better than that obtained with various homogeneous gold catalysts (entries 1-3). As is the case for other metal NPs when encapsulated by PAMAM dendrimer, the catalyst was prereduced [H₂ (1 atm), 100°C, 24h] before reaction. In addition, the solvent used for this reaction was nitromethane, rather than the usual toluene. We found that using toluene resulted in more allene byproduct formed by homogeneous gold catalysts, and lower yields overall. It should be noted that Pt NPs were also used for this reaction, but poor results were obtained from initial experiments and further investigations were deemed unwarranted.

Table 2.2. Gold Catalyzed Cyclopropanation of Propargyl Esters.

entry	catalyst	temp	time	<i>cis</i> -yield ^a	<i>trans</i> -yield ^a
1	AuCl	rt	2.5 h	90%	6%
2	AuCl ₃	rt	2.5 h	91%	8%
3	Ph ₃ PAuCl/AgSbF ₆	rt	2.5 h	74%	9%
4 ^b	Au ₅₅ /G4OH/SBA-15 (with 7.5 mol% PhICl ₂)	50 °C	16 h	85%	6%

^a All yields determined by NMR vs methyl benzoate internal standard. ^b 6% aldehyde product also formed.

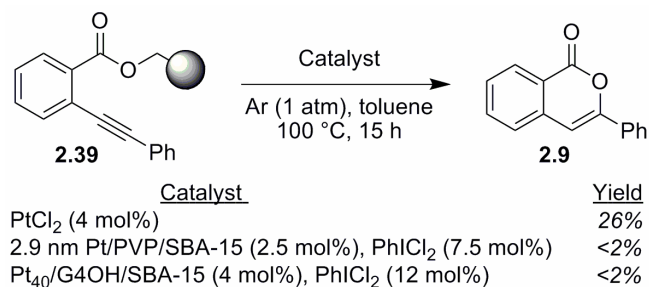
Leaching Tests

In addition to the challenge of understanding the specific nature of the catalyst, the distinction between homogeneous and heterogeneous catalysis is often difficult to determine. This is due to the possibility that metal leaches from a heterogeneous catalyst into solution and acts as the catalytically active species. Thus, it was important for us to consider in our studies the fact that for many of the NPs used in carbon-carbon bond forming reactions, formation of a catalytically active homogeneous species via leaching from the NP precursor cannot be excluded. For example, it is generally accepted that Pd nanoparticles, when used in solution,

degrade into various homogeneous species and provide a strong case for the assumption that a nanoparticle catalyst is leaching in solution until proven heterogeneous.^{1d,2,10a,f,11,20}

While the remarkably consistent recyclability of the PhICl_2 treated $\text{Pt}_{40}/\text{G4OH}/\text{SBA-15}$ NPs is a strong indication of its heterogeneity, we wanted further verification that the NPs were not leaching reversibly to form a homogeneous active catalyst. Two important observations are the striking improvement in long-term activity of the smaller sized PAMAM dendrimer capped NPs over the larger PVP capped NPs and the differing recycling ability based on capping agent. Both results illustrate the effect of size and capping agent, which would not be possible if homogeneous catalysts were generated as the active species even if a 'release and capture' dynamic were present. A 'release and capture' dynamic is one in which a homogeneous catalyst leaches, catalyzes the reaction and reattaches to the solid support during the reaction. In a more rigorous test for the formation of a homogeneous species, a 3-phase test⁵⁸ was employed with Wang resin-bound substrate **2.39** (Scheme 2.8). In this test, one would expect the reaction rate between heterogeneous catalyst and polymer-bound substrate should be negligible.

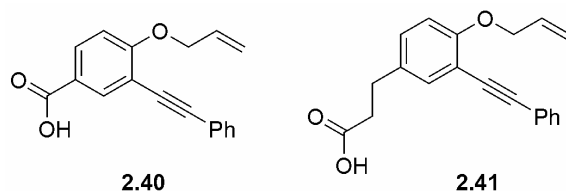
Scheme 2.8. 3-Phase Catalyst Heterogeneity Test.



As expected, in the presence of homogeneous PtCl_2 , 26% conversion of resin bound substrate to product was observed. However, both 2.9 nm $\text{Pt}/\text{PVP}/\text{SBA-15}$ and $\text{Pt}_{40}/\text{G4OH}/\text{SBA-15}$ oxidized with PhICl_2 resulted in <2% conversion.

In the course of designing resin-bound substrate **2.39**, several alternative substrates were proposed. Both **2.40** and **2.41** were synthesized, with the intent to attach them to the resin through the carboxylic (Figure 2.15).⁵⁹ However, before attaching the substrates to the resin, the starting molecule was tested for reactivity with the Pt NP catalysts.

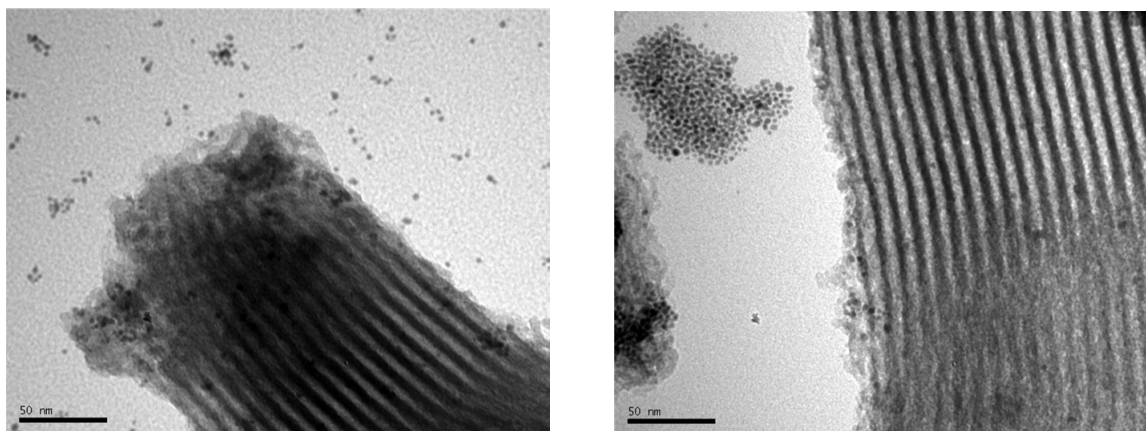
Figure 2.15. Alternative Candidates for Resin-Bound Substrate.



Despite the excellent reactivity shown by Fürstner for a similar molecule (**2.42**, eq. 10),²⁶ both **2.44** and **2.46** cyclized to product in poor yield, leading us to eliminate them as possibilities for resin-bound substrates (eqs. 11 and 12). However, based on the excellent reactivity of **2.8**

this is the most likely location to see any leaching and aggregation; however, only substantial occurrences would be noticeable with this qualitative analytical method.

Figure 2.17. Transmission Electron Micrograph of 4 wt% Loaded Pt NPs After Reaction.



Another common test for catalyst leaching is the mercury test.⁶⁰ Here, elemental mercury is added to a reaction solution, and, if the catalyst is homogeneous, the reaction will proceed as normal. However, if the catalyst is a colloid, then amalgams will form with the mercury and render the catalyst inactive, or at least differently active.⁶⁰ Unfortunately, in our hands, the mercury test gave conflicting and, ultimately, inconclusive results. When 1.5 or 2.9 nm Pt/PVP/SBA-15 NPs were used, no decrease in reaction yield was observed (Table 2.3, entries 1 and 2). However, Pt₄₀/G4OH/SBA-15 with mercury decreased in yield to 17% (entry 3) compared to 98% without mercury, and homogeneous PtCl₂ with mercury gave no reaction at all (entry 4).

Table 2.3. Mercury Test for Catalyst Heterogeneity.

entry	catalyst	mol% cat.	yield ^a
1	2.9 nm Pt/PVP/SBA-15	2.5	98%
2	1.5 nm Pt/PVP/SBA-15	2.5	97%
3	Pt ₄₀ /G4OH/SBA-15	4.0	17%
4	PtCl ₂	3.0	NR

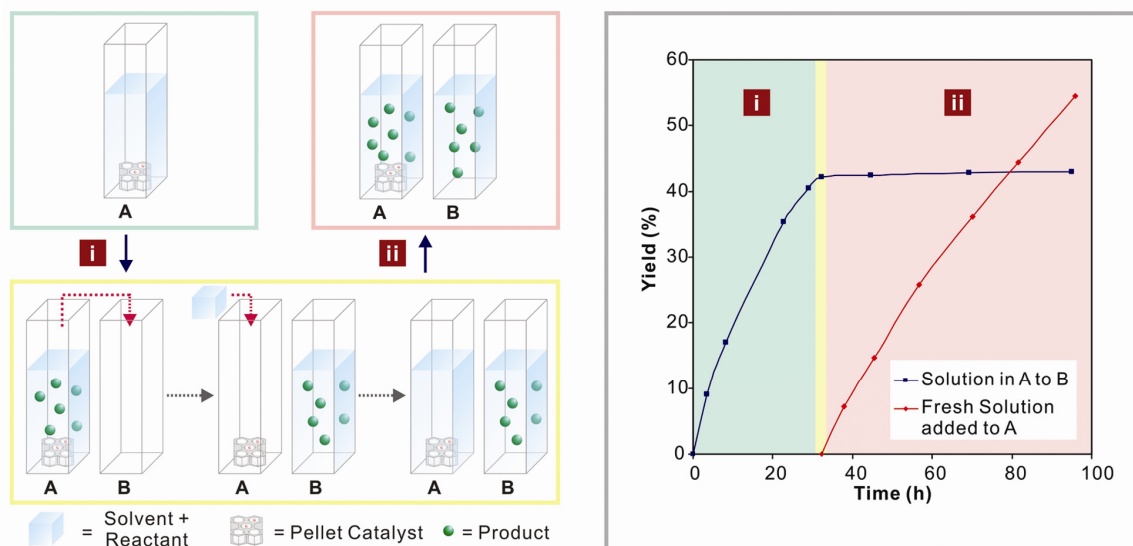
^a All yields determined by NMR vs methyl benzoate internal standard.

The fact that mercury shuts down homogeneous PtCl₂ reactivity is directly contradictory with what should happen based on literature precedent. It suggests that PtCl₂ is not homogeneous but actually a colloid. Furthermore, detailed analysis reveals significant flaws with the mercury test for our catalyst system. By supporting our NP catalysts on SBA-15, we are introducing a previously uninvestigated variable into this test; it is unknown how mercury interacts with SBA-15 and whether it can enter the pores effectively to react with the metal NPs. In addition, the

presence of a dendrimer around the Pt₄₀ NP could inhibit mercury from contacting the NP and might react with it independently. Thus, our system is not amenable to investigation by the mercury test and data collected from this endeavor cannot be used to either prove or disprove the heterogeneity of the catalyst system developed.

Perhaps the best evidence against leaching was obtained from an experiment in which a Pt₄₀/G4OH/mesoporous silica pellet was used to allow for facile removal of the reaction solution from the NP catalyst under the reaction conditions and inert atmosphere. In this case, detailed in Figure 2.18, a solution of starting material, PhICl₂ and solvent are added to the catalyst pellet in a reactor (A) (green section) and begin to generate product (i). After 42% yield is achieved, the reaction solution in A is transferred to a new vessel with no catalyst (B). The oxidized catalyst pellet remains in A. A fresh solution of starting material and solvent is then added into A (yellow section). Both vessel A and B are now stirred and monitored (ii). Now, the solution in A begins to convert to product while the solution in B does not react and remains at 42% yield (red section). This further indicates the active catalyst is heterogeneous. If any homogeneous leached species were present, it would have also been transferred to B and an increase in yield would have been observed for the solution after it was removed from the heterogeneous catalyst pellet in A. Moreover, the new solution added to A begins to react, showing that the active catalyst has, in fact, remained in A.

Figure 2.18. Pellet Transfer Test for Catalyst Heterogeneity. Yield determined by GC vs internal standard. All transfers and reactions conducted under Ar at 100°C. Catalyst pellet pre-reduced under H₂ atmosphere at 100°C for 36 h prior to reaction.



Finally, elemental analysis by inductively coupled plasma of a centrifuged solution (2.4 with Pt₄₀/G4OH/SBA-15 and PhICl₂ in toluene) after reaction was unable to detect any significant amount (<1 ppm) of Pt above the instrument's detection limits. By the same analytical method, no loss of Pt was observed from the Pt₄₀/G4OH/SBA-15 catalyst when it was isolated after the reaction. It is important to realize that, when preparing solutions and samples

for ICP analysis, the reaction is cooled and centrifuged. Thus, it is possible that re-adsorption to the SBA-15 of Pt metal species could occur. For this reason, the results of the 3-phase and pellet test act as the most compelling evidence against leaching as they are *in situ* studies. Accordingly, when the results from this collection of experiments are combined, they strongly indicate that no homogeneous catalytically active species had leached from the treated/oxidized Pt₄₀/G4OH/SBA-15 NPs during the reaction, and that the catalytically active species are, in fact, the heterogeneous NPs.

A pellet test was also performed with 2.9 nm Pt/PVP NPs. However, no reaction was observed. A possible interpretation of this result is as follows. If the NPs were leaching out a homogeneous catalytically active species, then reactivity should have been observed. However, the lack of reactivity when using the NPs loaded onto a silica pellet suggests that the support affected the reactivity, which should theoretically be possible if the catalyst was heterogeneous and inside the pores of the pellet. However, due to the possibility that the pellet simply altered the leaching dynamics, no conclusion can be made. The Pt/PVP/pellet catalyst was unreactive, and thus a complete set of data regarding the leaching from the PVP capped NP was not obtained so we cannot determine to a certainty whether the catalyst leaches. Furthermore, the poor recycling ability of the PVP-capped NPs suggests either leaching is occurring (to either a catalytically active or inactive homogeneous species), or that the oxidative modification affects and alters the surface of the NP differently than the dendrimer capped NP in a destructive and/or irreversible manner. While the experiments that were successfully conducted suggest that leaching does not occur, and that an alternative explanation must be found to explain the empirical activity observations, the possibility for leaching cannot be completely eliminated.

When either Pd or Au NPs were used for the reactions discussed above, a ring of metal would form at the bottom of the reaction vessel. Commonly referred to as ‘plating out,’ this deposition of metal occurs to a larger extent with Au but still significantly so with Pd. The presence of these rings unambiguously indicated that leaching was occurring during the reactions. Either metal NPs were detaching from the SBA-15 support and being deposited on the glass vessel walls, or smaller clusters of metal, perhaps even metal atoms, were leaching off the NP, exiting the SBA-15 pores, and either reaggregating in solution and plating out or directly adsorbing to the glass surface. As we know that Pd NPs will catalyze the standard hydroalkoxylation reaction utilized for the majority of our studies,⁵⁶ it would be logical to apply the series of leaching tests developed to Pd₄₀ NPs. In this way we could use the existing substrates and methodology to verify leaching for a catalyst system for which we could qualitatively show at the outset should test positive for leaching. However, it is also possible the leached metal that results in ‘plating out’ could be non-catalytically active Pd or Au metal, and thus its leaching does not affect the overall catalytic process. Long term degradation of the NP catalyst system could occur over multiple reaction cycles, but the process would still be heterogeneously catalyzed. Unfortunately, the presence of free metal in solution, even if inactive, would nullify some of the advantages of heterogeneous catalysts.

EXAFS/XANES Analysis

In an effort to develop a more complete picture of the structure of the NP catalysts after oxidative treatment, and by doing so gain a better understanding of the observed activity, we completed a series of X-ray absorption spectroscopy (XAS) experiments at the Advanced Light

Source (ALS) at Lawrence Berkeley National Laboratory and Stanford Synchrotron Radiation Lightsource (SSRL) at Stanford University. XAS provides structural information useful for identifying the chemical speciation of an element and can be used to “study differences in the atomic environment of an element within or between individual particles.”⁶¹ XAS can be split into two parts, X-ray absorption near edge structure (XANES) and extended X-ray absorption fine structure (EXAFS). XANES includes the part of the absorption spectrum near an absorption edge for a particular element. The shape of this absorption edge is related to the density of states available for the excitation of the photoelectron. For this reason, the binding geometry and oxidation state of an atom affects the XANES part of the spectrum and can thus be derived from an analysis of this data.⁶² The EXAFS spectrum is “the normalized oscillatory part of the absorption coefficient above the absorption edge to approximately 1000 eV or higher.”⁶² This region can be used to determine the local molecular bonding environments of elements and contains information on the types and number of atoms in coordination with the absorber atoms, that is, the atoms being irradiated and analyzed. In addition, the interatomic distances and degree of local molecular bonding disorder can be obtained.⁶² It should be noted that data collected by XAS represents an average of the absorber atoms irradiated by the X-ray beam.

We sought to use this method of analysis to investigate the oxidation state of the Pt₄₀/G4OH/SBA-15 NPs before and after treatment with PhICl₂ by comparing them with known homogeneous standards. This would allow us to determine what homogeneous species the active sites are analogous to, as well as to provide conclusive evidence for the oxidation of the NPs by PhICl₂. We would also establish the coordination environment of the Pt atoms in the NPs. This can tell us to which elements the Pt atoms are bound and their coordination number, providing insight into the nature of the catalytically active species generated. We compared the treated and untreated NPs to measure the changes in the coordination environment. It was our goal to use the XAS data to describe in detail the effect of the PhICl₂ oxidant and the specific nature of the catalyst generated. Looking forward, by understanding how the modification of the nanoparticle surface occurs and what interactions are generated, we will be able to extend our technology to new treatment methods and nanoparticles.

In these XAS experiments, we focused on the Pt L_{III} edge (11.564 keV) to look for the presence of Pt-Pt, Pt-O and Pt-N (from coordination to amine groups in the dendrimer) for scattering contributions. Furthermore, since we believe PhICl₂ is creating Pt-Cl bonds on the surface of the NP, we expect to detect those interactions for the oxidized NP samples. While XPS analysis indicates the presence of oxidized Pt species, XANES data provides us with a more detailed profile of the NP oxidation state before and after treatments or reactions. The comparison of data obtained from treated NP with that generated from non-oxidized NPs provides an explanation for the specific changes occurring during the treatment that results in the observed electrophilic activity. Specific details regarding sample preparation and analysis can be found in the Experimental section.

Analysis of the data, after background removal and normalization, by the Athena and Artemis suite of programs generated several interesting results and trends. To help understand the results of this analysis, it is important to note that the fitting of the EXAFS data to determine coordination number and actual bond distance is based upon a predicted average bond distance for two particular elements and the expected coordination number, along with several additional variables that depend on the identity of the atoms in question. For the first coordination shell around Pt, these distances are well known. Pt-O and Pt-N are around 2.04 Å, Pt-Pt is 2.74 Å, and Pt-Cl is typically 2.30 Å. However, because XAS determination of coordination

environment does depend on predicted bond/interaction distances we are unable to differentiate between the presence of O or N atoms, as they reside an equivalent distance away from Pt and have very similar properties. This means that while XAS data can generate useful data regarding oxidation state and coordination environment, there do exist specific limitations for our NP system that dictates the level of detail possible. This uncertainty extends to the second shell, where Pt-Cl and Pt-Pt interactions are expected.

In order to generate reasonable guesses for second shell bond/interaction distances, Zeise's dimer [$\{\eta^2\text{-C}_2\text{H}_4\text{PtCl}_2\}_2$] was used. With this Pt(II) species, we are able to reference a known X-ray crystal structure.⁶³ From this structure, we can see Pt-Pt interactions at 3.45 and 4.1 and 4.25 Å, and Pt-Cl interactions at 4.3+ Å. The potential for overlap suggests that, like nitrogen and oxygen, there will be uncertainty as to the identity of the atoms present at these distances. Furthermore, while Zeise's dimer has a defined lattice structure visible by X-ray diffraction, the NP catalyst may not have such order and likely exhibits an alternative lattice structure we cannot reference with known compounds. As such, for Pt₄₀ we are only able to verify the existence of second shell interactions and give their approximate distances and number, and cannot completely isolate the Pt-Cl interactions from the Pt-Pt. It is possible that further calculations and fitting optimization can provide the additional detail and analysis necessary to deconvolute the second shell environment.

Unoptimized, first approximation fitting for standard catalysts and NP samples can be seen in Table 2.4. As a basis for comparison, K₂PtCl₄, PtCl₂, PtCl₄ and Zeise's dimer were analyzed (entries 1-4). For the sake of brevity, second shell will be labeled with a superscript * and first shell will be unlabeled. Interestingly, PtCl₄ showed no Pt-Pt interactions, with five Pt-O/N interactions suggestive of oxides formed from exposure to air and moisture. Pt-Cl interactions were four with significant Pt-Pt/Cl* as expected from a crystalline solid (entry 2). PtCl₂ showed less Pt-O/N and Pt-Cl was also less at the expected two, but Pt-Pt/Cl* remained large (entry 3). Fitting of Zeise's salt matched well with the crystal structure with 2-3 Pt-O/N interactions (that may also include Pt-C) and two Pt-Cl. However, Pt-Pt/Cl* counted for 1-2 at 3.48 Å, when the crystal structure has a count of two Pt at that distance. Four Pt-Pt/Cl* at ~4.2 Å were calculated which may include the one Pt-Pt interaction evident by the crystal structure as well as Pt-Cl interactions (entry 4).

Table 2.4. XAS Analysis and Fitting Results for Pt₄₀/G4OH/SBA-15 NP Catalyst and Standards.

Entry	Catalyst	Conditions ^b	Oxid. State	Pt-Pt (Å)	Pt-O/N (Å)	Pt-Cl (Å)	Pt-Pt/Cl* (Å)	Pt-Pt/Cl* (Å)
1	K ₂ PtCl ₄	---	+2	0	0-1 (2.03)	3 (2.31)	3-4 (3.34)	9-10 (4.18)
2	PtCl ₄	---	+4	0	5 (2.26)	4 (2.30)	3-4 (3.44)	9-10 (4.17)
3	PtCl ₂	---	+2	0	2-3 (2.28)	2-3 (2.32)	3-4 (3.37)	9-10 (4.18)
4	Zeise's Dimer	---	+2	0	2-3 (2.17)	2 (2.30)	1-2 (3.48)	3-4 (4.17)
5	Pt ₄₀ NPs ^a	Reduced	+0	5-6 (2.75)	1-2 (2.03)	0	NC	NC
6	Pt ₄₀ NPs ^a	Reduced then Oxidized	+4	1 (2.76)	4-5 (2.14)	1-2 (2.35)	NC	NC
7	Pt ₄₀ NPs ^a	Reduced, Oxidized, Recycled and Re-reduced	+0	6-7 (2.76)	2-3 (2.10)	0	NC	NC
8	Pt ₄₀ NPs ^a	Reduced, Oxidized, Recycled, Re-reduced, Re-oxidized	+4	0	3-4 (2.12)	2-3 (2.33)	0-1 (3.49)	4-5 (4.21)
9	Pt ₄₀ NPs ^a	Reduced, Reaction	+2 to +4	1 (2.75)	4-5 (2.09)	1-2 (2.35)	NC	NC
10	Pt ₄₀ NPs ^a	Reduced, Reaction, Recycle, Re-reduce	+0	3-4 (2.76)	2 (2.09)	0-1 (2.31)	NC	NC
11	Pt ₄₀ NPs ^a	Reduce, Reaction, Recycle, Re-reduce, Reaction	+2 to +4	1-2 (2.76)	2-3 (2.04)	1-2 (2.32)	NC	NC

^a Pt₄₀ NPs = Pt₄₀/G4OH/SBA-15. ^b Reduced = H₂, 100°C, 24 h; Oxidized = PhICl₂ (3 equiv.-total metal basis), toluene, 100°C, 45 min., Recycled = Catalyst filtered, dried and recovered, Reaction = Catalyst is 4 mol%, **2.4**, PhICl₂ (3 equiv.- total metal basis), toluene, 100°C, 15 h. All manipulations performed under Ar atmosphere.; NC = Not Calculated.

For Pt₄₀/G4OH/SBA-15, a series of samples was prepared that represented each phase of the reaction process including oxidations, reductions and recyclings. After initial reduction of the catalyst, 4-5 Pt-Pt interactions were observed consistent with the presence of a NP. Roughly two Pt-O/N interactions were detected which are likely due to coordination with the encapsulating dendrimer (Table 2.4, entry 5). An oxidation state of nearly +0 was detected. Pt-Pt* was similar qualitatively to a Pt-foil standard (see Chapter 2 Appendix for spectra), and further validate the presence of a nanoparticle. After treatment of this reduced NP with PhICl₂, we were surprised to see no Pt-Pt interactions and an increase in Pt-O/N interactions to 3-4. Pt-Cl interactions were around two and the oxidation state increased to +4 (entry 6). This could suggest that, after oxidative treatment, the NP is completely falling apart and complexing with amine functional groups in the dendrimer as PtCl_x species, or that the Cl atoms are being incorporated into the NP structure to form a more amorphous solid with predominately Cl bridged Pt-Cl-Pt interactions. Due to the lack of Pt-Pt bonds, the NP as originally synthesized are definitely no longer present, but the exact nature of the change is not clear. We do know that Pt-Cl bonds are being formed concomitant with an increase in the overall Pt oxidation state, as expected from literature precedent^{28,29} and empirical results. Pt-Pt/Cl* appear to be similar, qualitatively, to PtCl₄ and Zeise's dimer standards, indicating that the Pt atoms from the NP are still in close proximity to each other and the oxidation state decreased to roughly zero (see Chapter 2 Appendix). If the catalyst is recovered and re-reduced (H₂, 100°C, 24 h), it reverts to the same structure it had initially (Table 2.4, entry 7). If this recycled and reduced NP catalyst is retreated with oxidant, a species very similar to that seen after initial oxidation is formed (entry 8).

For the samples described above, PhICl_2 was allowed to react and oxidize the NPs for 45 minutes before sample preparation. As a comparison to the actual reaction conditions, **2.4** was added with PhICl_2 in toluene, and the mixture was reacted at 100°C for 15 h as per the standard conditions. Gratifyingly, after a reaction with a new batch of $\text{Pt}_{40}/\text{G4OH}/\text{SBA-15}$, fitting of the EXAFS data indicated a similar structure to that found after simple oxidation (Table 2.4, entry 9). In this case, the overall oxidation was not as high with an average value between +2 and +4, which may indicate a gradual reduction of the NP during the reaction, but the Pt-O/N and Pt-Cl interactions did not show a marked difference from only oxidatively treated NPs. The reversibility of the oxidation process and thus the recycling ability of the catalyst was also demonstrated since NPs, recovered and re-reduced after a full reaction, returned to the original NP state (entry 10). Resubmission of these NPs to a new solution of **2.4** and PhICl_2 generated the same sample structure as observed after the first reaction (entry 11).

Taken as a whole, the fitting results reinforce the idea that an amorphous solid species is formed after treatment with PhICl_2 and remains encapsulated within the dendrimer. Reduction with H_2 reforms the NP original structure as evidenced by the number of Pt-Pt and Pt-O/N first shell as well as Pt-Pt second shell interactions. The NPs undergo can undergo this cycle multiple times as supported by XAS experiments and hydroaloxylation reactions run with recycled NP catalysts. This indicates that the changes that result from oxidative treatment are reversible and do not damage the NP catalyst.

During the course of this research program, we have additionally designed and synthesized several different types of nanoparticles, larger in size and utilizing a PVP polymer capping agent. With respect to the electrophilic catalysis generated by PhICl_2 oxidation, we have found that the activity and, to some extent, selectivity of the catalysts can be affected by these parameters. Thus, by obtaining XAS data for a range of nanoparticles we can hope to understand the basis of these differences. Analyzed spectra of 2.9 nm Pt/PVP/SBA-15 NPs indicate a predominance of Pt(0) for the reduced, untreated catalyst with 7-8 Pt-Pt interactions in the first shell (2.75 Å) and 1-2 Pt-Pt* interactions (3.58 Å). No Pt-Cl interactions were detected (Table 2.5, entry 2). This compares favorably to a Pt foil standard where 9-10 Pt-Pt interactions first shell interactions were seen at a bond distance of 2.76 Å (entry 1). After treatment and oxidation with PhICl_2 , only a slight increase in overall oxidation state of the NP was observed relative to the untreated NP (entry 3). The oxidation state was still noticeably less than Pt(+2) as compared with PtCl_2 , K_2PtCl_4 and Zeise's dimer standards. This corresponds favorably with XPS measurements that indicated approximately 25% of the Pt is oxidized. A decrease in Pt-Pt first shell interactions was observed (5-6 at 2.76 Å) with a concomitant weak Pt-Cl interaction (1 at 2.32 Å). The number of Pt-Pt* interactions remained 1-2 (3.56 Å). The relatively fewer surface Pt atoms on this larger NP provide the reasoning for a lower average Pt-Cl interaction count. The decrease in Pt-Pt first shell interactions is larger than would be expected if new Pt-Cl interactions only provided the explanation and thus warrants further investigation.

Table 2.5. XAS Analysis and Fitting Results for 2.9 nm Pt/PVP/SBA-15 NP Catalyst.

Entry	Catalyst	Conditions ^b	Oxid. State	Pt-Pt (Å)	Pt-O/N (Å)	Pt-Cl (Å)	Pt-Pt/Cl* (Å)	Pt-Pt/Cl* (Å)
1	Pt Foil	---	+0	9-10 (2.76)	0	0	0 (3.78)	NC
2	Pt PVP	Reduced	+0	7-8 (2.76)	0	0	1-2 (3.58)	NC
3	Pt PVP	Reduced then Oxidized	+0 to +1	5-6 (2.76)	0	1 (2.32)	1-2 (3.56)	NC

^a Pt PVP = Pt (2.9 nm)/PVP/SBA-15 NPs. ^b Reduced = H₂, 100°C, 24 h; Oxidized = PhICl₂ (3 equiv.-total metal basis), toluene, 100°C, 20 min.; All manipulations performed under Ar atmosphere.; NC = Not Calculated.

The significant amount of Pt(0) present relative to Pt(+2 and +4) in the oxidized Pt/PVP NPs reinforces the hypothesis that larger sized NPs are less likely to become oxidized due to their preference and increased stability in lower oxidation states.³⁴ This is based on a comparison to Pt₄₀/G4OH where an equivalent amount of PhICl₂ oxidant generates predominantly Pt(+4). Therefore, the deactivation of these NPs can be rationalized by the propensity of 2.9 nm Pt/PVP NPs to revert to a Pt(0) oxidation state, which is supported by the XPS and now also the XAS data. However, in order to obtain a better understanding for the poor recycling ability of the catalyst, a series of XAS experiments similar to those performed on the Pt₄₀/G4OH/SBA-15 NPs must be completed. From this information, it may be possible to understand why the PVP-capped NP behaves differently from the dendrimer-capped and how this affects the observed activity. While the possibility remains that catalyst leaching explains the observed lack of recyclability, detailed XAS studies that show the variation in Pt-Pt and Pt-Cl interactions as well as overall oxidation state over multiple reaction cycles will provide an additional layer of information to aid our understanding.

Future Directions: Flow Reactor

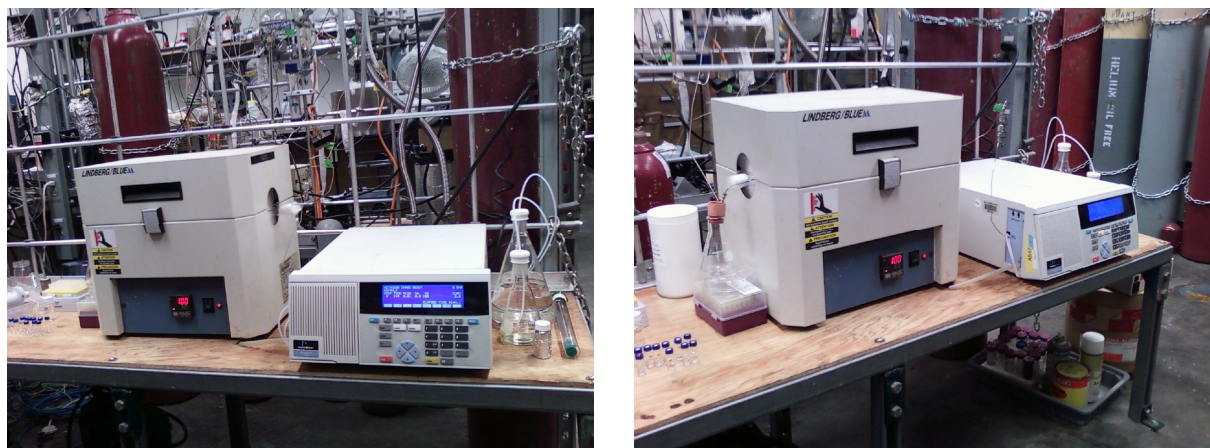
A common and highly useful application of heterogeneous catalysts is the flow reactor. In this system, a solution of reactants and reagents is pushed through a column of catalyst. At a research laboratory scale, an HPLC pump and typical HPLC fittings and tubing can be used. A column of the desired length is simply packed with the catalyst. In this way, multiple solvents and solutions can be pumped through the column with ratios varied as desired via the HPLC pump controller. When the solution exits the column, it has completely reacted to product (or to the extent desired), and more reactant will continuously flow through the column and react until the catalyst loses activity. In reactions where multiple steps are possible with one catalyst species, the flow rate and concentration of reactants can dictate the rate of progression through these synthetic steps. Just as with batch reactions, the temperature can be controlled, as can the concentration, catalyst loading and multiple other variables. With a flow system, however, even more control can be attained relative to batch. For example, depending on the exact reactor setup, not only is it possible to vary the concentration and relative ratio of reactants/reagents/solvents over time, but the catalyst column can also be at different temperatures at various points along the column. Additionally, the catalyst is completely mixed with the reactants, as in batch reactions, but no separation step is required to remove the catalyst.

Flow reactors have superior heat transfer and reactant/catalyst mixing properties and allow for higher pressures and temperatures to be used than in a batch reactor. Furthermore, any

air-sensitive starting materials, intermediates or products and any unstable intermediates will be more stable and significantly less likely to degrade in a flow system as the entire system is closed, and any intermediates formed exist in small quantities for a short duration. Also, because of the continuous nature of the system in conjunction with the ease of altering reaction conditions, optimization of any process can be done in significantly less time and with less effort than with a batch reactor.

Clearly, the degree of control attained with flow reactors in cooperation with their multiple other advantages justifies their use. While at this initial stage we cannot yet take full advantage of the versatility of flow reactors, we have simply sought to determine whether our catalyst system is amenable to this technology. Our main concern was the longevity of the catalyst after oxidative treatment with PhICl_2 . To probe this issue, we designed and set up a simple reactor. A stock solution of toluene, a solution of **2.4** in toluene and a solution of PhICl_2 in toluene were prepared. A 50 x 4.5 mm (inner diameter) HPLC column was filled with 0.75 wt% $\text{Pt}_{40}/\text{G4OH}/\text{SBA-15}$ which corresponds to 220 mg (0.008 mmol) of catalyst. An HPLC pump was then attached to the column. The column was placed in a tube oven set at 100°C and the outlet tube drained into sampling vials (Figure 2.19). In the future, an automatic fraction collector could be used. To the tube connecting the pump to the column, a 90° valve was attached. This valve allowed us to switch between H_2 gas and solution from the pump.

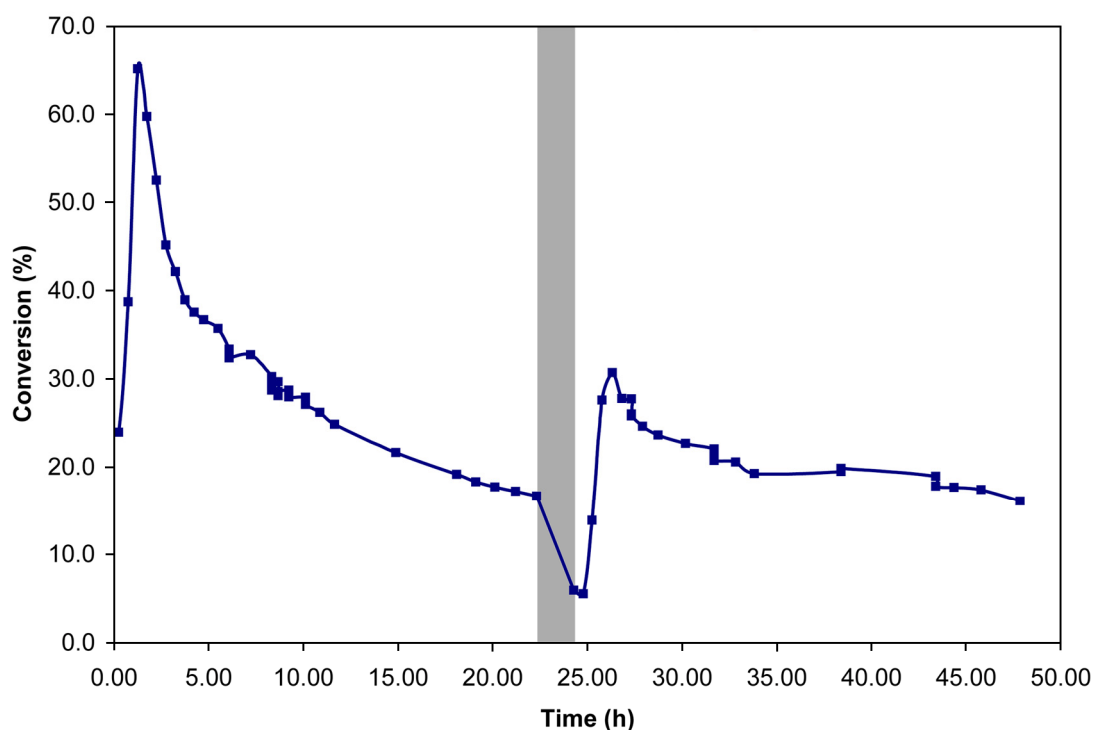
Figure 2.19. Photographs of the Flow Reactor.



To begin our experiment, we flowed H_2 gas through the column at 100°C for 36 h. Then, the valve was rotated and pure toluene was pumped through the column to wet the catalyst. Next, the solution of PhICl_2 in toluene was slowly pumped through the catalyst also at 100°C . The amount of oxidant was three equivalents based on total Pt metal in the column, just as is done for batch reactions with the NPs. After the oxidant solution had passed through the column, the solution of **2.4** was introduced. The flow rate and solution concentration were based on the approximate TOF for the batch reactor and were expected to give around 50% yield. We then could change the concentration (by changing the pure toluene:reactant solution ratio via the pump controls) and flow rate as desired. However, we initially only wanted to get a catalyst activity profile, so no variation of flow rate and concentration was applied. As seen in Figure 2.20, an initial spike in activity is observed, followed by a sharp drop. If the catalyst were ideal with no deactivation observed, we would expect to see a flat line, after the initial equilibration,

indicative of a constant rate of conversion. As time progresses for our system, the catalyst does stabilize and the rate of deactivation slows. After 23 h, we flushed the system with toluene, flowed another three equivalents of oxidant (based on total metal) through the column, flushed briefly with toluene (indicated by the gray region), and switched back to substrate. We observed a slight increase in activity and the resulting deactivation was noticeably less pronounced than before.

Figure 2.20. Plot of Catalyst Activity (Conversion) vs Time for Flow System.



This experiment demonstrates that our electrophilic Pt NPs can be used in a flow reactor. Also, there is a clear effect of oxidant on the catalyst activity that we are only now seeing in detail due to the instantaneous and continuous nature of the information collected by analyzing fractions of solution exiting the column, signifying yet another advantage of flow reactors. It is expected that future investigations will focus on recycling the catalyst in the HPLC column with the hope that new columns will not have to be prepared, and catalyst columns can be reused multiple times. Also, rather than just pre-treating the catalyst with oxidant, as was done above, pretreatment can be followed by (or replaced by) flowing a solution of oxidant through the column in addition to the substrate solution. This is easily accomplished with our flow system, as the HPLC pump can accommodate two solutions flowing in, and can vary the ratios internally. Detailed temperature studies can be accomplished, and, eventually, a set of conditions will be developed that will generate complete conversion to product for prolonged periods of time until the catalyst has to be regenerated.

Flow reactors are a powerful way of both investigating and optimizing a process as well as generating a product with maximum efficiency. We have only begun to scratch the surface of this technology with respect to our developed catalyst, and hope to use this technique to further our understanding and application of its reactivity. This reactor can also be used for other

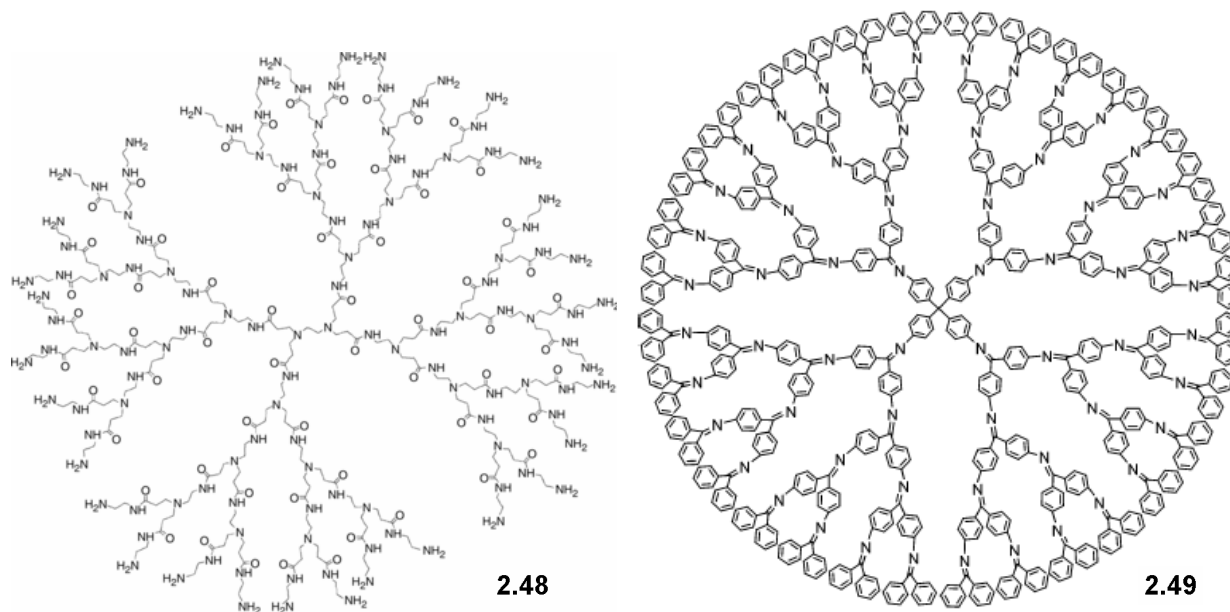
reactions and with other heterogeneous metal NP catalysts to both gain information about the process and provide support for the utility of continuous flow systems.

Future Directions: New Dendrimer Capping Materials

As previously discussed, the use of dendrimers as stabilizing encapsulating agents for nanoparticle synthesis is both common and highly effective. Poly(amidoamine) dendrimers (PAMAM) are currently the most utilized,^{4,10,13,23,27} and depending on the generation of dendrimer, nanoparticles with 10 or more metal atoms can be obtained, corresponding to sizes of <1 nm and higher. Dendrimers also do not have to be removed after nanoparticle synthesis, and thus their presence can affect the reactivity of the nanoparticles via electronic interactions with heteroatoms in the dendrimer, or sterically. They can also provide stability to the nanoparticle and prevent aggregation or other degradation due in part to placement of the nanoparticle in the inner pocket of the dendrimer.^{4,10,13,23,27} Typical requirements for an effective dendrimer capping agent are: 1) nitrogen or other coordinating atoms that can complex with metal ion species prior to nanoparticle formation, 2) steric bulk that provides a pocket of protection for the formed nanoparticle, 3) porosity of the dendrimer at the periphery so that reagents can access the nanoparticle surface, and 4) stability under the reaction conditions. Note that the number of coordinating atoms must be a reasonable ratio with the available space for the nanoparticle to exist in the dendrimer. These sites will serve as a limit on the number of metal atoms that can be incorporated into the dendrimer and thus will control the size of the nanoparticles. More specifically, the dendrimer undergoes sequential complexation from the inner coordinating groups to the outer ones, allowing for precise control of the number of metal atoms encapsulated in the dendrimer that will become the nanoparticle after reduction.^{23,64} In PAMAM dendrimers, tertiary amines act as the requisite coordinating groups.

A recent publication from Yamamoto *et al.* details efforts to build upon the success of PAMAM dendrimers with an alternative structural class of dendrimer.⁶⁵ The tetraphenylmethane-poly(phenylazomethine) (TPM-PPAM) dendrimer synthesized (Figure 2.21, 2.49) has several potential advantages over PAMAM.

Figure 2.21. Structure of PAMAM G3 (**2.48**) and TMP-PPAM G4 (**2.49**) Dendrimer.

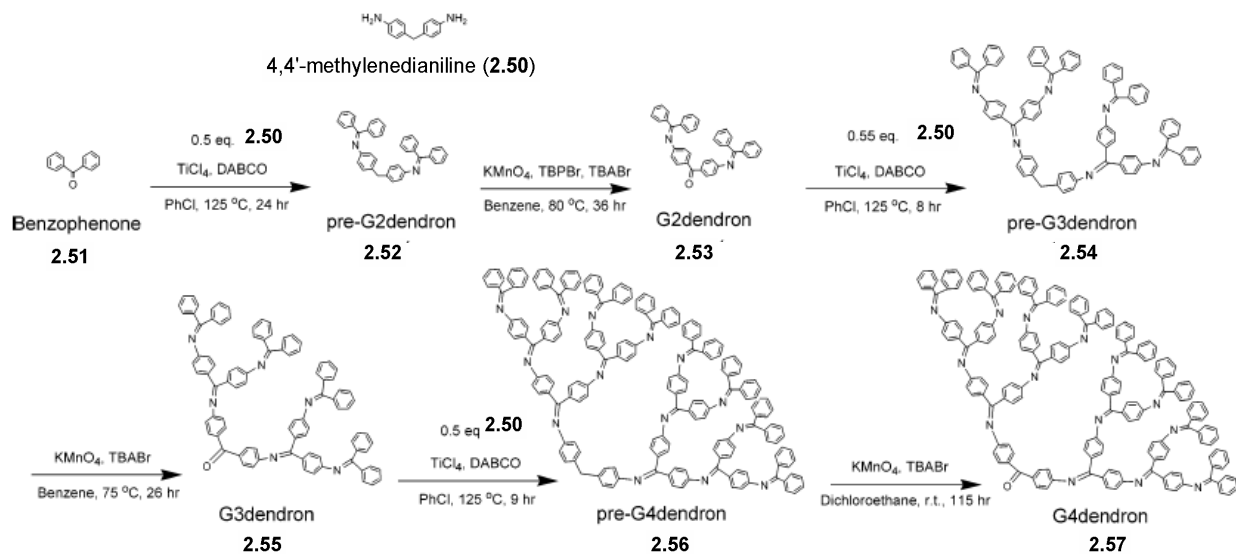


For example, the tetrahedral TPM core of the dendrimer structurally dictates the creation of an omnidirectional shell for any dendrimer generation, as compared to the ‘thick pancake’ shape lower generations of PAMAM dendrimer can form. The further use of benzene rings and planar azomethine linkers creates a very high level of structural rigidity that can create an inner cavity with a strong shell effect based on dense-shell packing.⁶⁵ The steric bulk that results provides excellent protection against aggregation, and these molecules are also stable to much higher temperatures than PAMAM dendrimers. While PAMAM dendrimers utilize tertiary amines for metal ion complexation, the imine groups in **2.49** act as the coordinating atoms. Yamamoto also claims that the chemical structure of the dendrimer allows for better control of ion loading than PAMAM dendrimers, and thus smaller, subnanometer NPs can be formed.⁶⁵ In addition, **2.49** is hydrophobic compared to the hydrophilic PAMAM and will have different electronic interactions with the NP due to the different chemical environment around the NP.

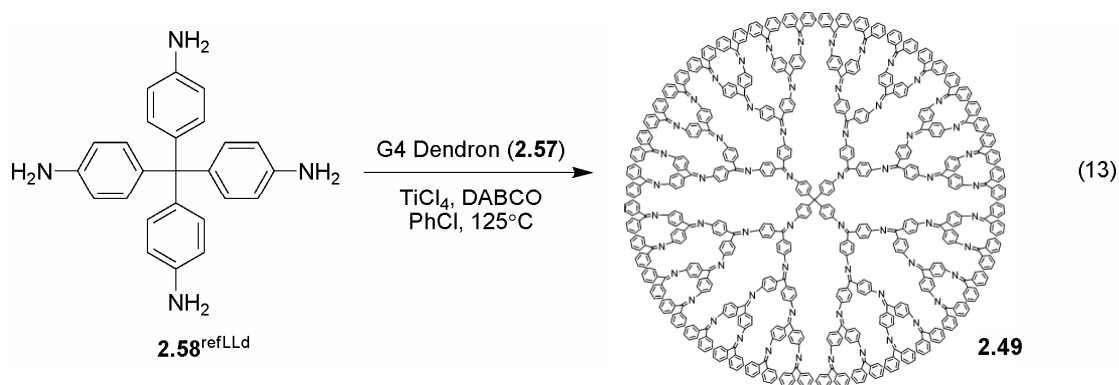
We set about synthesizing **2.49** with the hope that once Pt NPs were formed with this new capping agent, the effect of dendrimers on reactivity for our oxidatively modified NP catalyst system could be studied. Just as was suggested by Yamamoto, the steric environment around that nanoparticle could directly impact the selectivity for reactions like the hydroarylation to form **2.13**. Smaller sized NPs could be generated with the goal of increasing the stability of the NP after oxidation by PhICl_2 . In addition, the different electronic environment around the NP might have an effect on overall reactivity. Without a doubt, the range of questions that could be addressed with this alternative class of NP are significant.

Our synthesis of the TPM-PPAM proceeded as detailed in a set of publications from Yamamoto’s laboratories.⁶⁵ The dendron precursor to the dendrimer was increased in generation via a stepwise manner (Scheme 2.9).

Scheme 2.9. Synthetic Method to Generate Poly(phenylazomethine) Dendron.^{65b}



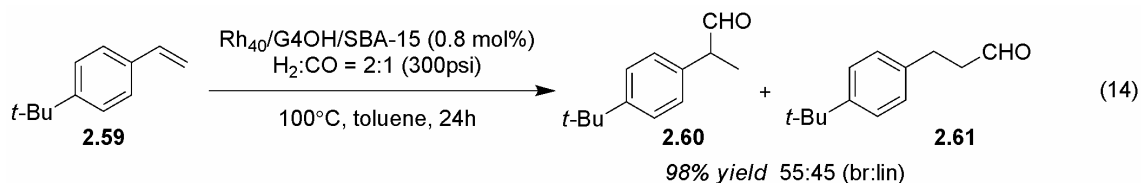
When the pre-fourth generation dendron **2.56** was obtained, recycling size exclusion/gel permeation chromatography (SEC/GPC) was required to effectively separate the desired product. Standard chromatography and recrystallization methods were still necessary, but insufficient to obtain the necessary purity. In order to generate the desired dendrimer, purified 4th generation dendron **2.57** was then subjected to conditions to attach it to the tetraphenylmethane core (eq. 13). Unfortunately, we were unable to successfully form dendrimer **2.49**.



Despite reacting for 24 h at 125 °C with large excesses of TiCl₄ and DABCO, only a small amount of product was detected by MALDI-TOF mass spectroscopy (the only effective means to characterize the molecules of this size). SEC failed to purify the reaction mixture, likely due to the small amount of product and large range of molecular weights of the side products. What would be the equivalent of an inseparable mixture or ‘streak’ in thin-layer chromatography was obtained from the SEC. We did observe, however, in the mixture of decomposition and side products, the presence of incomplete formation of TPM-PPAM dendrimer **2.49**, in which only one to three dendrons coupled to the TPM core. This indicates that alternative and potentially more forcing conditions are required to generate **2.49** and allow for it to be successfully purified.

Future Directions: Different Reactions and Metals

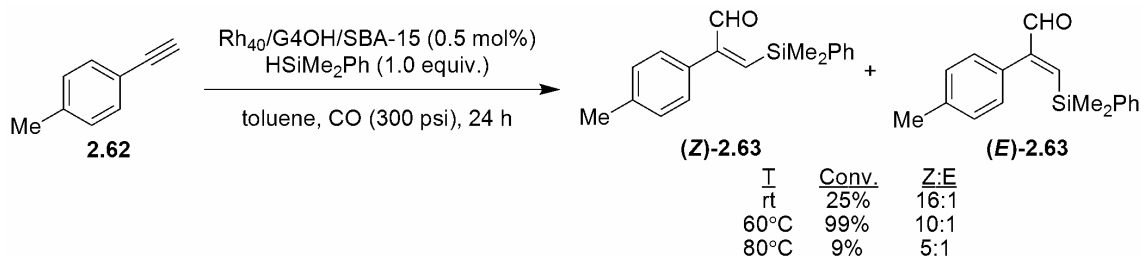
In order to build on our understanding of Pt NP catalysis and the successful results obtained thus far, we have begun to investigate the use of other late metals in alternative forms of reactivity. For example, hydroformylation is a necessary and interesting reaction industrially and utilizes many known catalyst systems. However, nanoparticle catalysts for this chemistry are rare, and heterogeneous systems with similar efficiency as homogeneous catalysts do not exist.^{14,15} In light of this fact, we investigated the use of Rh nanoparticles supported on SBA-15. We found that, under a blended H₂/CO atmosphere, both the branched and linear products derived from **2.59** were formed in an approximately 1:1 ratio regardless of catalyst employed (eq. 14).



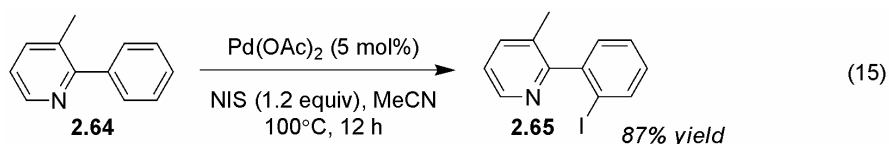
In addition, a survey of Rh nanoparticle catalysts also revealed that the conversion decreases as the particle size increases. The effects of pressure, temperature and H₂/CO ratio have yet to be sufficiently studied. It is likely that a reactor that allows for sampling under pressure will need to be constructed to obtain detailed information regarding the precise effects of these conditions on the reaction.

We also utilized Rh₄₀/G4OH/SBA-15 NPs for a related silylformylation reaction of arylalkyne **2.62**. Initial results indicate that, as expected, reaction selectivity decreases as temperature increases, while some heat is necessary to obtain satisfactory yields (Scheme 2.10).

Scheme 2.10. Silylformylation Reaction with Rh₄₀/G4OH/SBA-15 NPs.



We sought to extend the capabilities of NP catalysts to the important class of reactions proceeding through C-H bond activation utilizing our knowledge of Pt NP catalysts in combination with our ability to utilize NPs in solution. To this end, most of the known C-H bond activation reactions utilize metals other than Pt and are abundant in homogeneous catalysis. Most common of the late transition-metals used are Pd and Rh.⁶⁶ To obtain initial data regarding C-H activation with late-metal NPs, we synthesized Pd NPs with 4th generation PAMAM dendrimer capping agents to utilize for the C-H activation reaction of substituted phenylpyridine **2.64** discovered by Sanford *et al* (eq. 15).⁶⁷



As shown in Table 2.6, we were able to catalyze C-I bond formation to generate **2.65** using *N*-iodosuccinimide (NIS) or $\text{PhI}(\text{OAc})_2/\text{I}_2$ as the iodine source with pre-reduced (H_2 , 100 °C, 24 h) Pd NPs (entries 1 and 3). Unfortunately, recycling of the catalyst (with re-reduction after recovery) resulted in a low yield of **2.65** with either halogen source (entries 2 and 4).

Table 2.6. C-H Activation Reaction of **2.64** using $\text{Pd}_{40}/\text{G4OH}/\text{SBA-15}$ NP Catalyst.

entry	catalyst	halogen source	yield
1	$\text{Pd}_{40}/\text{G}_4\text{OH}/\text{SBA-15}$	NIS	60%
2	$\text{Pd}_{40}/\text{G}_4\text{OH}/\text{SBA-15}^b$	NIS	32%
3 ^c	$\text{Pd}_{40}/\text{G}_4\text{OH}/\text{SBA-15}$	$\text{PhI}(\text{OAc})_2/\text{I}_2$	99%
4 ^c	$\text{Pd}_{40}/\text{G}_4\text{OH}/\text{SBA-15}^b$	$\text{PhI}(\text{OAc})_2/\text{I}_2$	7%

^a All yields determined by NMR vs mesitylene internal standard.

^b Recycled catalyst. ^c Iodinated internal standard was observed.

An alternative benzoquinoline substrate **2.66**, which was reactive under the Sanford conditions,⁶⁸ was unreactive with Pd NPs (Scheme 2.11). The poor recycling for the Pd NPs is a reminder that the existence of leaching must be ruled out before results with these different metal NPs can be trusted.

Table 2.7. C-H Activation Reaction of Benzoquinoline using $\text{Pd}_{40}/\text{G4OH}/\text{SBA-15}$ NPs.

entry	halogen source	X	solvent	temp	yield
1	$\text{PhI}(\text{OAc})_2$	OAc	MeCN	90°C	NR
2	$\text{PhI}(\text{OAc})_2$	OH	MeOH	90°C	NR
3	NCS	Cl	MeCN	90°C	NR
4	PhICl_2	Cl	toluene	90°C	NR
5	NIS	I	MeCN	100°C	NR
6	$\text{PhI}(\text{OAc})_2/\text{I}_2$	I	MeCN	100°C	NR

^a All yields determined by NMR vs mesitylene internal standard. NR = No Reaction

As detailed earlier in this work, it is postulated that edge and corner surface features are the location of the active sites on the NP and thus have a direct impact on the overall catalytic activity of a given NP. Furthermore, the relative presence of different crystal lattice structures

on the NP faces (eg. Pt(110)) can dictate activity and selectivity. Changing the shape of a NP is the easiest and most direct way to alter the relative presence of these features in a known and characterizable fashion.^{8c,h} Thus, studying the shape effects of NPs for all reactions developed would allow for information regarding the effect of surface structure on reactivity. However, it is important to realize that our ability to control the shape of a NP is limited to larger sized NPs in which enough metal atoms are present to allow for this three dimensional structure to exist. Due to the steric constraints and small number of atoms present, dendrimer encapsulated NPs cannot be shape controlled. Most shaped NPs currently known are capped by a polymer such as PVP, and, in our hands, PVP capped NPs have shown good activity and as such should be amenable to these future studies.

Conclusion

We have contributed to the larger goal of bridging the gap between homo- and heterogeneous catalysis with a strategy for developing catalytically active NPs capable of performing reactions previously in the exclusive purview of homogeneous chemistry. To this end, we have successfully designed and synthesized novel electrophilic Pt NPs which catalyze a range of π -bond activation reactions with equivalent or superior yields and selectivities relative to reported homogeneous variants. Instrumental to this success were NP structural analyses and mechanistic insights that uncovered the importance of treatment with the hypervalent iodine oxidizing agent PhICl_2 . Moreover, reaction kinetic analysis confirmed the capability of tuning nanoparticle size and capping agent to improve catalytic ability. Multiple experimental results indicate the heterogeneity of the dendrimer encapsulated NP catalyst supported on SBA-15.

These discoveries, most notably the oxidative modification, illustrate the ability to obtain new reactivity from existing NP systems, and, in some cases, divergent reaction pathways are accessible. In a larger sense, this concept represents a significant advancement in the solution phase applications of supported NPs, and further application with other metals and treatment methods may facilitate the development of heterogeneous catalysts with novel activity or selectivity in an even larger array of chemical reactions. Collection and analysis of XAS data for the Pt NP systems has allowed us to further understand the nature of the oxidation and its effect on the NP structure. In addition, verification of the oxidation state changes that occur was obtained, and the excellent recyclability of the $\text{Pt}_{40}/\text{G4OH}/\text{SBA-15}$ catalyst was corroborated. A continuous flow system was designed, constructed and used with success for the hydroalkoxylation reaction utilizing electrophilic Pt NPs. Future studies will move beyond traditional homogeneous ligand control and utilize NP shape or dendrimer composition to provide opportunities for selective solution-phase reactions.

Experimental Section

General Information. Unless otherwise noted, all commercial materials were used without further purification. All reactions, unless otherwise noted, were conducted using standard high-vacuum or Schlenk techniques. Triethylamine was purified by passing through a column of alumina under argon. Unless otherwise noted, all other solvents were used as received.

TLC analysis of reaction mixtures was performed on Merck silica gel 60 F₂₅₄ TLC plates. Flash chromatography was carried out on Sorbent Technologies 40-63 D 60 Å silica gel. ¹H and ¹³C NMR spectra were recorded with Bruker AVB-400, AV-500, DRX-500 or AV-600 spectrometers and were referenced to residual ¹H and ¹³C signals of the deuterated solvents relative to TMS, respectively. GC-MS data were obtained via a HP 8690 Series Gas Chromatograph with a 5973 Series Mass Selective Detector. IR spectra were recorded on a Nicolet MAGNA-IR 850 spectrometer as thin films on a NaCl disc. High resolution mass spectral data were obtained via the Micro-Mass/Analytical Facility operated by the College of Chemistry, University of California at Berkeley. MALDI-TOF-MS spectra obtained via an Applied Biosystems 4700 Proteomics Analyzer in the positive ion mode, courtesy of the Molecular Foundry, Lawrence Berkeley National Laboratory. ICP-MS data were obtained via Galbraith Laboratories, Inc., Knoxville, TN. Sonication was performed on a VWR ultrasonic cleaner, 75T, 120 W, 45 kHz. Centrifugation was performed on a Thermo Scientific IEC Centra[®] CL2. Preparative scale gel permeation chromatography was performed on a Japan Analytical Industry Co., Ltd. LC-9101 recycling preparative HPLC with JAIGEL-2.5H columns with chloroform as the eluent and a model 3702 UV Detector. Size exclusion chromatography measurements were performed using a Viscotek GPCmax VE 2001 GPC solvent/sample module with THF as the eluent. The system is equipped with UV, refractive index, viscosity and light scattering detectors (Viscotek model 2501 UV detector and TDA 302 triple detector array).

PhICl₂ was prepared according to the method of Skulski *et al.*⁶⁹ All homogeneous catalysts were purchased from Strem Chemical Co. and used as received. Hydroxylamine **2.18**⁴⁵ was prepared and characterized by Jane Wang. **2.20**⁴⁶ was prepared and characterized by Pascal Dube. **2.22** was prepared according to the procedure of Berg *et al.*⁴⁷ **2.24** was prepared by the method of Hiroya *et al.*⁴⁸ **2.26** was prepared by the method of Yasuhara *et al.*⁴⁹ **2.30** was prepared according to the procedure of Sakai *et al.*⁵⁰ 1,6-Enyne **2.33** was prepared by the method of Sher *et al.*^{53,70} **2.37**⁵⁷ was prepared and characterized by David Gorin. **2.60**, **2.61**, and **2.63** were prepared, isolated and characterized by Jack Liu.

The following compounds were not isolated due to low yields, catalyst infeasibility, the preliminary nature of the results, or other factors that precluded further investigation of the transformation in question. They were characterized by comparison of *in situ* NMR spectra with published spectra and found to be consistent: **2.19**,⁴⁵ **2.23**,⁴⁷ **2.28**,⁷¹ **2.38**,⁵⁷ **2.43**,²⁶ **2.65**.⁶⁷

Synthesis of Nanoparticle Catalysts

Dendrimer templated Pt NPs

Dendrimer encapsulated NPs were synthesized following previously published methods^{8j} with some modifications.²³ Generation 4 dendrimers (G4OH) were purchased from Dendritech Inc.

(Midland, MI) as 10.2% (mass) methanol solutions. A dendrimer stock solution (250 μ M) was prepared by adding water to the dendrimer methanol solution. The dendrimer stock solution was mixed with 15-40 mole equivalents of an aqueous solution of 0.01 M K_2PtCl_4 in a 20 mL vial. The vial was purged with Ar for 30 min, tightly sealed with a septum and let sit for 66 h for complexation. Then a 20-fold excess of freshly prepared 0.5 M NaBH_4 (stored at 0°C before use) was injected dropwise into the vial with vigorous stirring. The reaction solution was then stirred for an additional 8 h after which, the reaction solution (10 mL) was purified by dialysis against 2 L of deionized water in cellulose dialysis sacks with a molecular weight cutoff of 12,000 (Sigma-Aldrich, Inc., St. Louis, MO). Dialysis occurred over 24 h with the water changed four times.

$\text{Pt}_{200}/\text{G6OH}$ NPs were synthesized in analogy to this procedure with the proportional increases necessary to obtain 200 atom particles. Generation 6 dendrimer (G6OH) was also purchased from Dendritech Inc. as 10% (mass) methanol solutions.

PVP capped NPs

The Pt NPs capped by PVP were synthesized using established methods.²² Chloroplatinic acid ($\text{H}_2\text{PtCl}_6 \cdot 6\text{H}_2\text{O}$, 99.9% pure on metals basis) and polyvinylpyrrolidone (PVP) with a molecular weight of 29,000 were purchased from Sigma-Aldrich.

For the synthesis of 1.5 nm Pt particles, NaOH was dissolved in ethylene glycol (12.5 mL, 0.5 M). This solution was added to an ethylene glycol solution (12.5 mL) containing $\text{H}_2\text{PtCl}_6 \cdot 6\text{H}_2\text{O}$ (0.25 g, 0.48 mmol). During N_2 purging, this combined solution was heated to 160°C and held for 3 h. The resulting NPs were precipitated with 2 M HCl and dispersed in an ethanol/PVP mixture.

For the synthesis of 2.9 nm Pt particles, aqueous $\text{H}_2\text{PtCl}_6 \cdot 6\text{H}_2\text{O}$ (20 mL of 6.0 mM) was added into 180 mL of methanol. PVP (133 mg) was then dissolved in this mixture and refluxed for 3 h. For the synthesis of 5.0 nm Pt particles, freshly prepared 2.9 nm Pt particles were mixed in a 90% methanol/10% water solution (100 mL). Methanol (90 mL) and a solution of $\text{H}_2\text{PtCl}_6 \cdot 6\text{H}_2\text{O}$ (36.9 mg) in water (10 mL) were added and the combined mixture refluxed for 3 h.

Mesoporous SBA-15 silica

Mesoporous SBA-15 silica was prepared utilizing the conventional method.⁷² Pluronic P123 (6.0 g, BASF) was dissolved in deionized water (45 g) and 2 M HCl (180 g) while stirring at 35°C for 1 h. Tetraethylorthosilicate (12.8 g, Sigma Aldrich, 98%) was then added to the solution and allowed to stir for 20 h. The mixture was then aged at 100°C for 24 h. The mixture was filtered to give a white powder and further purified by washing with ethanol and deionized water. This purified product was dried in air at 100°C and then calcined at 550°C for 12 h. The white powder was stored in a dessicator.

Mesoporous MCF-17 silica

The synthesis of MCF-17 followed the previous reports.⁷³ 1,3,5-trimethylbenzene (4 g) was added to a solution containing triblockcopolymer Pluronic P123 (4 g), HCl (conc., 10 mL) and deionized water (75 mL). The solution was stirred at 40°C for 2 h after which tetraethoxysilane (9.2 mL) was added. After stirring for 5 min, the solution was aged at 40°C for 20 h with no stirring. Then, NH_4F (46 mg) was added to the solution. This solution was transferred to an autoclave and aged at 100°C for an additional 24 h. The precipitate formed was filtered, washed

with deionized water and ethanol and calcined in air at 550°C for 6 h. The white powder obtained was stored in a dessicator.

Preparation of Pt/SBA-15 catalysts

Pt NPs were loaded onto the mesoporous SBA-15 silica prior to the catalytic studies. SBA-15 was added to a colloidal solution of the Pt NPs and the resulting slurry was sonicated for 3 h at room temperature. The NP supported SBA-15 was separated from the solution by centrifuge at 4200 rpm for 6 min. After centrifugation, the solution was clear. The solution was then decanted and the catalyst was dried under ambient conditions and then at 100°C.

PVP encapsulated NPs were loaded to 1.0 wt% Pt. SBA-15 was used for 1.5 and 2.9 nm NPs. MCF-17 was used for 5.0 nm NPs. The larger size mesoporous silica was required for successful loading of the larger sized NPs.

Dendrimer encapsulated NPs were loaded to 0.7 wt% Pt. SBA-15 was used as the support.

For Pd, Au and Rh NPs, an identical procedure was followed. Pd₄₀/G4OH was loaded to 0.35 wt% Pd on SBA-15. Au₅₅/G4OH was loaded to 0.7 wt% Au. Rh₄₀/G4OH was loaded to 0.5 wt% Rh.

Preparation of Pt/SWNT catalyst

A colloidal solution of Pt encapsulated with PVP (1 mg/mL) was diluted by ethanol (final concentration = 0.1 mg / mL). The desired amount of solution (to obtain 0.25 wt. % Pt) was added to carbon nanotube powder (Chevron Research Laboratories) and sonicated for 30 min at room temperature by a commercial ultrasonic cleaner (Branson, 1510R-MT, 70 W, 42 kHz). The black precipitates were separated by centrifugation (3000 rpm, 20 min), thoroughly washed with ethanol two more times, and dried in an oven at 373 K overnight.

Preparation of Pt/mesoporous silica pellet catalyst

For a typical synthesis, P123 (1 g, MW = 5800, Aldrich) was dissolved in a mixture with ethanol (5g) and HCl (0.2 g, aqueous, 1 M), and stirred until a homogeneous solution formed. While the mixture was still stirring, TEOS (2.08 g) was added to the solution, and the mixture was further stirred for 10 min. The solution derived above was then transferred into a ceramic vessel and aged at room temperature for 36 h in air. Then the silica gel was covered with a layer of liquid paraffin in 2-3-mm thickness and heated at 60 °C for 18 h to remove the ethanol completely. The residue liquid paraffin on the surface of the products was removed and cleared by using filter paper. For the removal of the block copolymer, calcination was carried out in an oven at 550 °C in air for 6 h.⁷⁴

For loading the nanoparticles onto the pellet, a Pt₄₀ colloidal solution (10 mL) was concentrated to 1 mL by rotovap at 50°C. The solution was added the pellet of mesoporous support and sonicated for 3 h at rt. The pellet solution was then evaporated at 50°C and the remaining solid was further dried at 100°C for 24 h.

TEM of Pt NPs and supported Pt NP catalysts

Pt NPs were imaged by TEM using a FEI Tecnai G2 S-Twin electron microscope at an accelerating voltage of 200 kV. A representative TEM image of the dendrimer capped Pt₄₀ NPs is shown in the insert of Figure E2.1a. After counting more than 300 NPs, the size distribution of the NPs is shown in Figure E2.1a. The averaged size of the nanoparticle is 1.1 ± 0.3 nm. The averaged diameter of the NPs agrees with calculated size for a 40 atoms Pt cluster assuming a

spherical shape (1.05 nm). For the PVP capped 2.9 nm Pt NPs, the size distribution is shown in Figure E2.1b (diameter is 2.9 ± 0.5 nm). The insert in Figure E2.1b is a representative TEM image for the 2.9 nm Pt NPs.

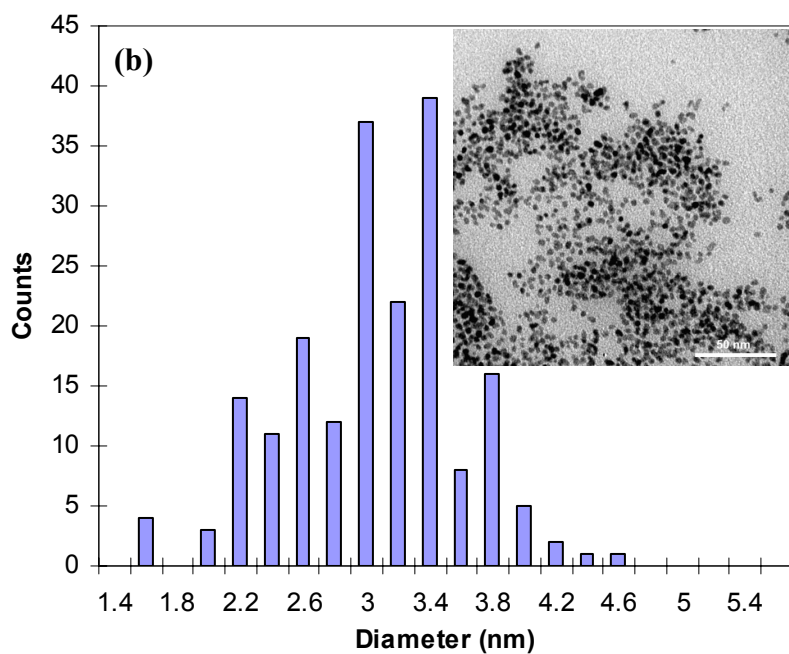
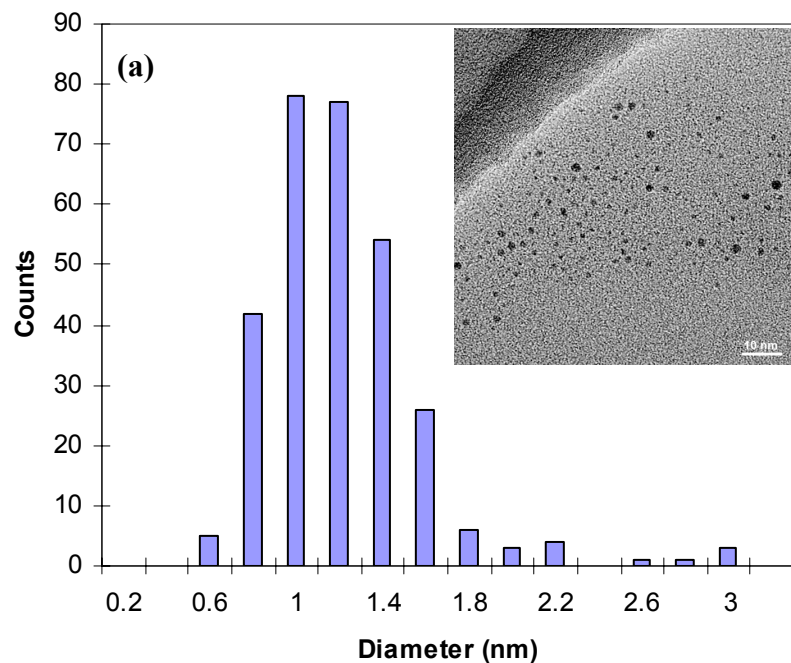


Figure E2.1. Metal particle size distributions obtained by TEM measurements of (a) dendrimer capped Pt₄₀ NPs and (b) PVP capped 2.9 nm Pt NPs. Inserts in (a) and (b) are representative TEM images of Pt₄₀ and 2.9 nm Pt NPs, respectively.

Characterization of Pt/SBA-15 NP catalysts

Characterization results for the dendrimer and PVP capped NPs have been published previously.^{8a,23}

Degradation of PAMAM dendrimer

It is possible that, under the reaction conditions, the dendrimer could decompose. However, the similar, reproducible catalytic activity of the Pt₄₀/G4OH/SBA-15 NP catalyst after recycling, and its divergence from that observed for the PVP capping agent both before and after recycling suggests its continued presence. Furthermore, no aggregation or leaching of the NPs are observed during/after reaction. Recent reports that suggest more harsh conditions are required for complete dendrimer removal.^{27b,31,32} Regardless, if decomposition of the dendrimer is occurring, it does not appear to alter the catalytic activity. For the purposes of this manuscript we will include the capping agent of the nanoparticles in their names as a reference to their origin and initial state.

Synthesis of Pd NPs

Pd NPs^{33,64} were made following the same procedure as Pt with the following exceptions: 1) The dendrimer stock solution was mixed with 15-40 mole equivalents of an aqueous solution of 0.01 M **K₂PdCl₄** in a 20 mL vial. The vial was purged with Ar for 30 min, tightly sealed with a septum and let sit for **1 h** for Pd complexation. 2) For the synthesis of the dendrimer templated NPs, the reaction solution was then stirred for an additional **1 h** after which, the reaction solution (10 mL) was purified by dialysis against 2 L of deionized water in cellulose dialysis sacks with a molecular weight cutoff of 12,000 (Sigma-Aldrich, Inc., St. Louis, MO). 3) Dendrimer encapsulated NPs were loaded to **0.35 wt% Pd**. SBA-15 was used as the support.

Synthesis of Rh NPs

Rh NPs were made following the same procedure as Pt with the following exceptions: 1) The dendrimer stock solution was mixed with 15-40 mole equivalents of an aqueous solution of 0.01 M **RhCl₃ (Rh, 38-40%)** in a 20 mL vial. 2) The complexing process between metal ions and the internal amine groups of the dendrimer was monitored by an UV-Vis spectrometer (Agilent 8453 UV-Vis ChemStation). Since the absorption spectrum only changed slightly after an 18 h exchange under static conditions for the RhCl₃/G4OH solution (66 h for K₂PtCl₄/G4OH solution), we choose 18 h as the complexation time for the RhCl₃/G4OH solution. 3) Dendrimer encapsulated NPs were loaded to **0.5 wt% Rh**. SBA-15 was used as the support.

Synthesis of Au NPs

Au₅₅ NPs were made following the procedure published by Crooks *et al.*⁷⁵ The only exception was the use of G4NH₂ dendrimer rather than Gn-Qp used by the authors. These NPs were synthesized by Wenyu Huang.

Ceria Nanorods

CeO₂ nanorods were prepared by a simple hydrothermal process. Typically, 1 mmol cerium(III) nitrate hexahydrate and 0.01 mmol trisodium phosphate hexahydrate were dissolved in 40 mL distilled water. After stirring at room temperature for 1 h, the mixed solution was transferred into a 50 mL Teflon-lined stainless autoclave and heated at 170 °C for 144 h. Upon leaving the

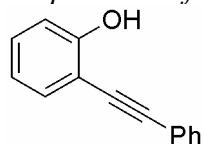
solution cool to room temperature, the precipitates were separated by centrifuging, washed with distilled water and ethanol three times in turn, and then dried at 60 °C for 1 day.

Preparation of Pd₄₀/GAOH/CeO₂ NP catalyst

A colloidal solution of Pt encapsulated with PVP (1 mg/mL) was diluted by ethanol (final concentration = 0.1 mg / mL). The desired amount of solution (to obtain 0.25 wt. % Pt) was added to CeO₂ nanorod powder and sonicated for 30 min at room temperature by a commercial ultrasonic cleaner (Branson, 1510R-MT, 70 W, 42 kHz). The black precipitates were separated by centrifugation (3000 rpm, 20 min), thoroughly washed with ethanol two more times, and dried in an oven at 373 K overnight.

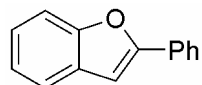
Preparation and Characterization of Organic Substrates and Products

Preparation of 2.4



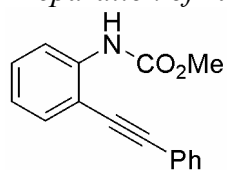
2-(Phenylethynyl)phenol (**2.4**) was prepared by the Pd catalyzed reaction of methoxymethyl protected 2-iodophenol with phenylacetylene followed by deprotection. Spectral data were consistent with the values previously reported.²⁶ ¹H NMR (CDCl₃, 500 MHz): δ 5.87 (s, 1H), 6.94 (td, 1H, *J* = 0.8 and 7.5 Hz), 7.01 (d, 1H, *J* = 8.0 Hz), 7.30 (t, 1H, *J* = 7.5 Hz), 7.39-7.42 (m, 3H), 7.45 (dd, 1H, *J* = 1.5 and 8.0), 7.55-7.59 (m, 2H).

Characterization of 2.5



2-Phenylbenzofuran (**2.5**) was identified by comparison to published characterization data. Spectral data were consistent with the values previously reported.²⁶ ¹H NMR (CDCl₃, 500 MHz): δ 7.06 (s, 1H), 7.23-7.33 (m, 2H), 7.38 (t, 1H, *J* = 7.5 Hz), 7.48 (t, 2H, *J* = 7.3 Hz), 7.55 (d, 1H, *J* = 8.2 Hz), 7.61 (d, 1H, *J* = 7.8 Hz), 7.89 (d, 2H, *J* = 7.0 Hz).

Preparation of 2.6

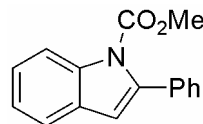


To a dry flask containing 2-iodoaniline (2.65 g, 13.7 mmol, Aldrich) was added pyridine (30 mL, EMD Drisolv[®]) and methyl chloroformate (2 mL, 25.9 mmol, Aldrich) under Ar at 0°C. The reaction mixture was stirred and warmed to room temperature, then allowed to stir for an additional 12 h. At this point, TLC analysis indicated complete consumption of starting material and HCl (30 mL, 1 M) was added to the reaction solution. The resulting mixture was extracted with CH₂Cl₂ (3 x 15 mL, Fisher HPLC grade). The combined organic layers were dried with MgSO₄, filtered and concentrated. Pyridine was removed by toluene azeotrope with a rotary

evaporator. The resulting methyl 2-iodophenylcarbamate (3.63 g, 96%, pale yellow solid) was used in the next step without further purification. ^1H NMR (CDCl_3 , 400 MHz) δ 3.85 (s, 3H), 6.85 (td, 1H, $J = 1.6$ and 7.6 Hz), 7.01 (br s, 1H), 7.38 (t, 1H, $J = 7.2$ Hz), 7.80 (dd, 1H, $J = 1.2$ and 7.6 Hz), 8.10 (d, 1H, $J = 8.0$ Hz).

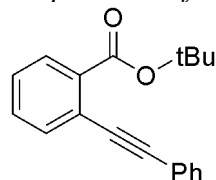
To a dry flask containing dry, degassed triethylamine (20 mL) was added methyl 2-iodophenylcarbamate (2 g, 7.23 mmol) and phenylacetylene (872 μL , 7.94 mmol, Aldrich) under Ar. Then, $\text{Pd}(\text{PPh}_3)_4$ (166 mg, 0.14 mmol, 2 mol%, Strem) and freshly prepared CuI^{76} (69 mg, 0.36 mmol, 5 mol%) was added. The mixture was then stirred for 12 h in the dark under Ar. The reaction mixture was filtered through a plug of silica and the plug was washed with Et_2O (~100 mL, Fisher Anhydrous ACS grade). The filtrate was concentrated and purified by flash chromatography (10% ethyl acetate/hexanes, Fisher ACS grade) to afford methyl 2-(phenylethynyl)phenylcarbamate (**2.6**) as a yellow solid (1.77g, 7.05 mmol, 98%). ^1H NMR (CDCl_3 , 500 MHz): δ 3.816 (s, 3H), 7.04 (t, 1H, $J = 7.5$ Hz), 7.34-7.40 (m, 4H), 7.48 (dd, 2H, $J = 1.5$ and 7.5 Hz), 7.56 (dd, 2 H, $J = 2.5$ and 7.5 Hz), 8.18 (d, 1H, $J = 8.0$ Hz). ^{13}C NMR (CDCl_3 , 125 MHz): δ 52.4, 84.1, 96.2, 111.3, 117.6, 122.3, 122.5, 128.5, 128.8, 129.7, 131.6, 131.7, 138.9, 153.6. IR: 3042, 1742, 1580, 1520, 1491, 1454, 1306, 1281, 1239, 1214, 1103, 1063, 1039, 953 cm^{-1} . HRMS (EI) calc. for $\text{C}_{16}\text{H}_{13}\text{NO}_2$ 251.0950, found 251.0946.

Characterization of **2.7**



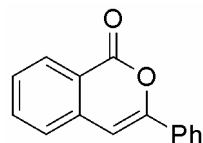
Methyl 2-phenyl-1H-indole-1-carboxylate (**4**). Yellow oil. ^1H NMR (CDCl_3 , 500 MHz): δ 3.82 (s, 3H), 6.63 (s, 1H), 7.29 (t, 1H, $J = 7.5$ Hz), 7.35-7.46 (m, 6H), 7.58 (d, 1H, $J = 7.5$ Hz), 8.18 (d, 1H, $J = 8.5$ Hz). ^{13}C NMR (CDCl_3 , 125 MHz): δ 53.4, 110.8, 115.4, 120.6, 123.3, 124.5, 127.7, 127.8, 128.6, 129.4, 134.1, 137.1, 140.5, 152.2. IR: 1740, 1454, 1439, 1361, 1329, 1266, 1220, 1131, 1050 cm^{-1} . HRMS (EI) calc. for $\text{C}_{16}\text{H}_{13}\text{NO}_2$ 251.0948, found 251.0946.

Preparation of **2.8**



tert-Butyl 2-(phenylethynyl)benzoate (**2.8**) was prepared according to the published procedure. Spectral data were consistent with the values previously reported.⁷⁷ ^1H NMR (CDCl_3 , 500 MHz): δ 1.62 (s, 9H), 7.34-7.39 (m, 4H), 7.45 (td, 1H, $J = 1.6$ and 7.7 Hz), 7.55-7.59 (m, 2H), 7.62 (dd, 1H, $J = 1.1$ and 7.7 Hz), 7.88 (dd, 1H, 1.2 and 7.8 Hz).

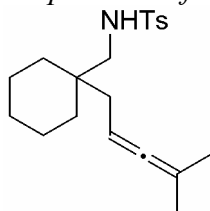
Characterization of **2.9**



3-Phenyl-1H-isochromen-1-one (**2.9**) was identified by comparison to published characterization data. Spectral data were consistent with the values previously reported.⁷⁸ ^1H NMR (CDCl_3 , 500

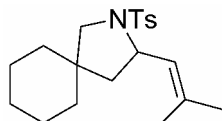
MHz): δ 6.98 (s, 1H), 7.43-7.54 (m, 5H), 7.74 (t, 1H, $J = 7.5$ Hz), 7.90 (d, 2H, $J = 7.3$ Hz), 8.33 (d, 1H, $J = 8.2$ Hz).

Preparation of **2.10**



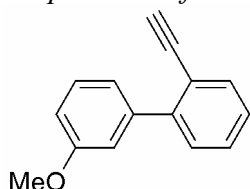
4-Methyl-*N*-((1-(4-methylpenta-2,3-dienyl)cyclohexyl)methyl)benzenesulfonamide (**2.10**) was prepared according to the published procedure. Spectral data were consistent with the values previously reported.⁷⁹ ¹H NMR (toluene-*d*₈, 500 MHz): δ 1.1-1.42 (m, 10H), 1.61 (s, 3H), 1.62 (s, 3H), 1.87 (d, 2H, $J = 8.0$ Hz), 1.95 (s, 3H), 2.80 (d, 2H, 7.0 Hz), 4.82-4.88 (m, 2H), 6.82 (d, 2H, $J = 8.0$ Hz), 7.81 (d, 2H, $J = 8.0$ Hz).

Characterization of **2.11**



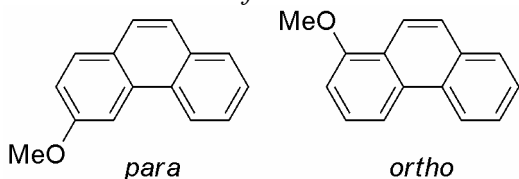
3-(2-Methylprop-1-enyl)-2-tosyl-2-azaspiro[4.5]decane (**2.11**) was identified by comparison to published characterization data. Spectral data were consistent with the values previously reported.⁴¹ ¹H NMR (toluene-*d*₈, 500 MHz): δ 0.8-1.4 (m, 12H), 1.60 (s, 3H), 1.69 (s, 3H), 1.98 (s, 3H), 3.00 (d, 1H, $J = 10.0$ Hz), 3.47 (d, 1H, $J = 10.4$ Hz), 4.41 (q, 1H, $J = 8.8$ Hz), 6.86 (d, 2H, $J = 8.0$ Hz), 7.77 (d, 2H, $J = 8.0$ Hz).

Preparation of **2.12**



2-Ethynyl-3'-methoxybiphenyl (**2.12**) was prepared according to the published procedure. Spectral data were consistent with the values previously reported.⁴² ¹H NMR (CDCl₃, 600 MHz): δ 3.07 (s, 1H), 3.87 (s, 3H), 6.93 (ddd, 1H, $J = 0.6, 2.4$ and 8.4 Hz), 7.17 (m, 2H), 7.31 (td, 1H, $J = 2.4$ and 7.2 Hz), 7.35 (t, 1H, $J = 8.0$ Hz), 7.41 (m, 2H), 7.63 (d, 1H, $J = 8.4$ Hz).

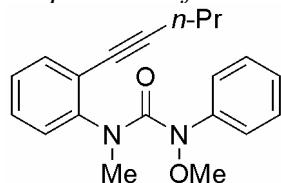
Characterization of **2.13**



3-Methoxyphenanthrene (**2.13**) was identified by comparison to published characterization data. Spectral data were consistent with the values previously reported.⁴² (*para*-**2.13**): ¹H NMR (CDCl₃, 600 MHz): δ 4.04 (s, 3H), 7.26 (dd, 1H, $J = 2.0$ and 8.5 Hz), 7.53-7.67 (m, 3H), 7.69 (d,

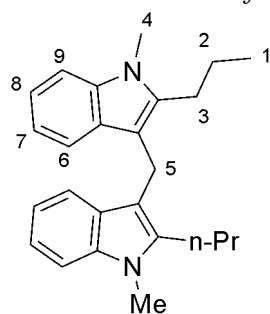
1H, $J = 9.0$ Hz), 7.82 (d, 1H, $J = 9.0$ Hz), 7.89 (d, 1H, $J = 7.2$ Hz), 8.07 (d, 1H, $J = 2.4$ Hz), 8.62 (d, 1H, $J = 8.4$ Hz). (*ortho*-**2.13**): ^1H NMR (CDCl_3 , 600 MHz): δ 4.05 (s, 3H), 7.02 (d, 1H, $J = 7.8$ Hz), 7.58-7.66 (m, 3H), 7.75 (d, 1H, $J = 9.0$ Hz), 7.91 (d, 1H, $J = 9.0$ Hz), 8.25 (d, 1H, $J = 9.0$ Hz), 8.29 (d, 1H, $J = 8.4$ Hz), 8.68 (d, 1H, $J = 8.4$ Hz).

Preparation of **2.14**

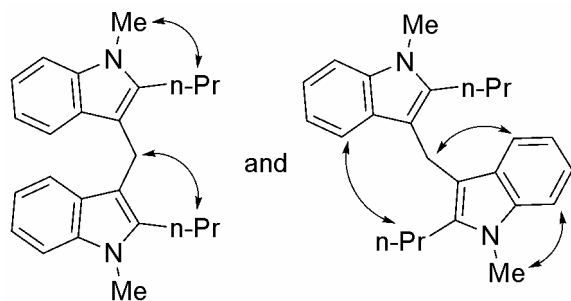


N-Methoxy-*N'*-methyl-*N'*-(2-pent-1-ynyl)phenyl-*N*-phenylurea (**2.14**) was prepared according to the published procedure. Spectral data were consistent with the values previously reported.⁴³ ^1H NMR (CDCl_3 , 500 MHz): δ 1.05 (t, 3H, $J = 7.5$ Hz), 1.62 (q, 2H, $J = 7.3$ Hz), 3.21 (s, 3H), 3.28 (s, 3H), 7.05 (dd, 1H, $J = 1.1$ and 7.9 Hz), 7.14 (t, 2H, $J = 7.8$ Hz), 7.19 (d, 3H, $J = 8.2$ Hz), 7.26 (t, 2H, $J = 7.2$ Hz), 7.38 (dd, 1H, $J = 1.6$ and 7.6 Hz).

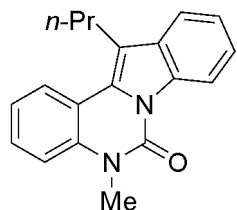
Characterization of **2.15**



Bis(1-methyl-2-propyl-1H-indol-3-yl)methane (**2.15**). Orange oil. ^1H NMR (CDCl_3 , 600 MHz): δ 0.86 (t, 6H, $J = 7.2$ Hz, [1]), 1.47 (p, 4H, $J = 7.6$ Hz, [2]), 2.70 (t, 4H, $J = 7.8$ Hz, [3]), 3.65 (s, 6H, [4]), 4.17 (s, 2H, [5]), 6.96 (t, 2H, $J = 7.2$ Hz, [7]), 7.10 (t, 2H, $J = 7.2$ Hz, [8]), 7.22 (d, 2H, $J = 7.8$ Hz, [9]), 7.40 (d, 2H, $J = 7.8$ Hz, [6]). ^{13}C NMR (CDCl_3 , 150 MHz): δ 13.9 (CH_3), 19.8 (CH_2), 23.1 (CH_2), 26.7 (CH_2), 29.5 (CH_3), 108.4 (CH), 110.4, (C-q), 118.5 (CH), 118.6 (CH), 120.2 (CH), 128.2 (C-q), 136.6 (C-q), 137.2 (C-q). LRMS (EI): $m/z = 358.20$. HSQC correlations (CDCl_3 , 600 and 150 MHz): ^1H 0.86 and ^{13}C 13.9, ^1H 1.47 and ^{13}C 23.1, ^1H 2.70 and ^{13}C 26.7, ^1H 3.65 and ^{13}C 29.5, ^1H 4.17 and ^{13}C 19.8, ^1H 6.96; 7.40 and ^{13}C 118.5; 118.6, ^1H 7.10 and ^{13}C 120.2, ^1H 7.22 and ^{13}C 108.4. All spectra, including HMBC, TOCSY, COSY and DEPT can be found in Chapter 2 Appendix. See below for important nOe correlations:

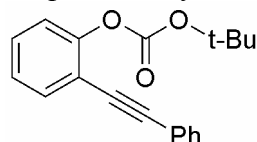


Characterization of **2.16**



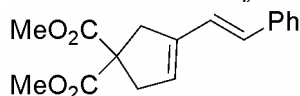
5-Methyl-12-propylindolo[1,2-c]quinazolin-6(5H)-one (**2.16**) was identified by comparison to published characterization data. Spectral data were consistent with the values previously reported.⁴³ ¹H NMR (CDCl₃, 500 MHz): δ 1.11 (t, 3H, $J = 7.2$ Hz), 1.82 (sextet, 2H, $J = 7.5$ Hz), 3.16 (t, 2H, $J = 7.8$ Hz), 3.72 (s, 3H), 7.25-7.32 (m, 2H), 7.38-7.45 (m, 3H), 7.69-7.71 (m, 1H), 8.09 (dd, 1H, $J = 8.4$ Hz and 1.2 Hz), 8.73-8.75 (m, 1H).

Preparation of **2.32**



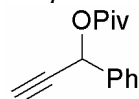
To a dry flask containing dry, degassed triethylamine (15 mL) was added *tert*-butyl 2-iodophenyl carbonate⁸⁰ (1.5 g, 4.72 mmol) and phenylacetylene (570 μ L, 5.19 mmol, Aldrich) under Ar. Then, Pd(PPh₃)₄ (109 mg, 0.09 mmol, 2 mol%, Strem) and freshly prepared CuI⁷⁶ (45 mg, 0.24 mmol, 5 mol%) was added. The mixture was then stirred for 12 h in the dark under Ar. The reaction mixture was filtered through a plug of silica and the plug was washed with Et₂O (~100 mL, Fisher Anhydrous ACS grade). The filtrate was concentrated and purified by flash chromatography (10% ethyl acetate/hexanes, Fisher ACS grade) to afford *tert*-butyl 2-(phenylethynyl)phenyl carbonate (**2.32**) as a yellow solid (1.33 g, 4.53 mmol, 96%). ¹H NMR (CDCl₃, 500 MHz): δ 1.52 (s, 9H), 7.20 (d, 1H, $J = 8.0$ Hz), 7.24 (td, 1H, $J = 7.5$ and 1.0 Hz), 7.35-7.38 (m, 4H), 7.54 (m, 2H), 7.58 (dd, 1H, $J = 7.5$ and 1.5 Hz). ¹³C NMR (CDCl₃, 125 MHz): δ 27.6, 83.7, 83.9, 94.4, 117.6, 122.0, 123.0, 126.0, 128.3, 128.5, 129.5, 131.6, 133.0, 151.3, 151.6. HRMS (EI) calc. for C₁₁H₂₂O₃ 294.1256, found 294.1250.

Characterization of **2.34**



(*E*)-dimethyl 3-styrylcyclopent-3-ene-1,1-dicarboxylate (**2.34**, Pale yellow solid) was identified by comparison to published characterization data. Spectral data were consistent with the values previously reported.⁸¹ ¹H NMR (CDCl₃, 400 MHz): δ 3.21 (br s, 2H), 3.31 (br s, 2H), 3.81 (s, 6H), 5.75 (br s, 1H), 6.52 (d, $J = 16$ Hz, 1H), 6.94 (d, $J = 16$ Hz, 1H), 7.27 (t, $J = 7.2$ Hz, 1H), 7.26 (t, $J = 7.2$ Hz, 2H), 7.44 (d, $J = 7.6$ Hz, 2H).

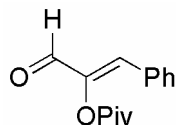
Preparation of **2.35**



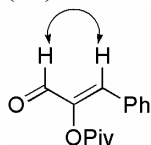
1-phenylprop-2-ynyl pivalate (**2.35**) was prepared via the method of Gulhane *et al.*⁸² as a pale yellow oil (96%). ¹H NMR (CDCl₃, 400 MHz) δ 1.23 (s, 9H), 2.63 (d, $J = 2.4$ Hz, 1H), 6.43 (d, J

= 2.4 Hz, 1H), 7.35-7.42 (m, 3H), 7.52 (dd, $J = 1.8$ and 7.8 Hz, 2H). ^{13}C NMR (CDCl_3 , 75 MHz) δ 27.2, 39.0, 65.3, 75.4, 80.7, 127.6, 128.9, 129.1, 137.1, 177.4. HRMS (EI) calc. for $\text{C}_{14}\text{H}_{16}\text{O}_2$ 216.1153, found 216.1150.

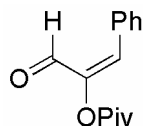
Characterization of **2.36-(Z)**



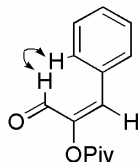
(*Z*)-3-oxo-1-phenylprop-1-en-2-yl pivalate **2.36-(Z)**. Colorless oil. ^1H NMR (CDCl_3 , 500 MHz) δ 1.41 (s, 9H), 7.01 (s, 1H), 7.42-7.44 (m, 3H), 7.65-7.67 (m, 2H), 9.40 (s, 1H). ^{13}C NMR (CDCl_3 , 125 MHz) δ 27.6, 39.6, 129.3, 130.8, 131.2, 132.2, 136.9, 146.9, 175.7, 185.9. HRMS (EI) calc. for $\text{C}_{14}\text{H}_{16}\text{O}_3$ 232.1102, found 232.1099. See below for important nOe correlations:



Characterization of **2.36-(E)**



(*E*)-3-oxo-1-phenylprop-1-en-2-yl pivalate **2.36-(E)**. Colorless oil. ^1H NMR (CDCl_3 , 500 MHz) δ 1.38 (s, 9H), 7.38-7.47 (m, 6H), 9.53 (s, 1H). ^{13}C NMR (CDCl_3 , 125 MHz) δ 27.6, 39.4, 129.2, 130.2, 130.4, 131.6, 137.0, 147.0, 177.0, 184.4. HRMS (FAB) calc. for $\text{C}_{14}\text{H}_{16}\text{O}_3$ 232.1103, found 232.1099. See below for important nOe correlations:



Representative Procedure for Catalytic Reactions

To a dry 10 mL glass reaction tube with stirbar and Teflon screwvalve cap under Ar was added 2-(phenylethynyl)phenol (**2.4**) (20 mg, 0.1025 mmol), Pt(2.9 nm)/PVP/SBA-15 (50 mg, 0.0026 mmol, 2.5 mol%), PhICl_2 (2.1 mg, 0.0077 mmol, 7.5 mol%), mesitylene (15 μL , internal standard, Aldrich) and toluene- d_8 (2 mL, Cambridge Isotopes). The reaction mixture was degassed (freeze/pump method) three times and placed under 1 atm of Ar. The reaction tube was sealed and the mixture heated with stirring to 100°C for 15 hours. The mixture was then cooled to rt and the solid catalyst filtered by glass microfiber filter. The filtrate was transferred to a NMR tube for analysis.

For the Pt₄₀/G4OH/SBA-15 catalyst, prior to addition of all other reaction materials, the catalyst was added to the dry 10 mL glass reaction tube and placed under 1 atm of H₂. The catalyst was then heated to 100°C for 24 hours. After cooling to rt and replacing the H₂ atmosphere with Ar, the reaction setup was continued as discussed above.

2-Phenylbenzofuran (**2.5**) can be isolated in the following manner. The toluene solution containing the product from the catalytic reaction was concentrated and purified by flash chromatography (5% ethyl acetate/hexanes, Fisher ACS grade).

Procedure for Oxidative Rearrangement of Propargyl Pivaloates

The Pt₄₀/G4OH/SBA-15 catalyst (75 mg, 0.0025 mmol, 0.65 wt%, 4 mol%), prior to addition of all other reaction materials, was added to the dry 10 mL glass reaction tube with stirbar and Teflon screwvalve cap and placed under 1 atm of H₂. The catalyst was then heated to 100°C for 24 hours. After cooling to rt the H₂ atmosphere was replaced with Ar.

To the 10 mL glass reaction tube under Ar was added propargyl pivaloate **2.35** (14 mg, 0.625 mmol), PhICl₂ (2.1 mg, 0.0077 mmol, 7.5 mol%), diphenyl sulfoxide (2 equiv, 38 mg, 0.1875 mmol), mesitylene (15 μL, internal standard, Aldrich) and toluene-d₈ (2 mL, Cambridge Isotopes). The reaction mixture was degassed (freeze/pump method) three times and placed under 1 atm of Ar. The reaction tube was sealed and the mixture heated with stirring to 100°C for 15 hours. The mixture was then cooled to rt and the solid catalyst filtered by glass microfiber filter. The filtrate was transferred to a NMR tube for analysis.

Procedure for Cyclopropanation of Propargyl Acetates

With Au NP Catalyst:

The Au₅₅/G4OH/SBA-15 catalyst (70 mg, 0.0025 mmol, 0.7 wt%, 2.5 mol%), prior to addition of all other reaction materials, was added to the dry 10 mL glass reaction tube with stirbar and Teflon screwvalve cap and placed under 1 atm of H₂. The catalyst was then heated to 100°C for 24 hours. After cooling to rt the H₂ atmosphere was replaced with Ar.

To the 10 mL glass reaction tube under Ar was added propargyl acetate **2.37** (13 mg, 0.1 mmol), PhICl₂ (2.1 mg, 0.0077 mmol, 7.5 mol%), styrene (4 equiv, 46 μL, 0.4 mmol), mesitylene (15 μL, internal standard, Aldrich) and MeNO₂-d₃ (2 mL, Cambridge Isotopes). The reaction mixture was degassed (freeze/pump method) three times and placed under 1 atm of Ar. The reaction tube was sealed and the mixture heated with stirring to 100°C for 16 hours. The mixture was then cooled to rt and the solid catalyst filtered by glass microfiber filter. The filtrate was transferred to a NMR tube for analysis.

With homogeneous Au catalyst:

To a 1 dram scintillation vial was added propargyl acetate **2.37** (25.2 mg, 0.2 mmol), styrene (4 equiv., 92 μL, 0.8 mmol), mesitylene (15 μL, internal standard, Aldrich) and MeNO₂-d₃ (1.5 mL, Cambridge Isotopes) followed by catalyst (0.005 mmol, 2.5 mol%). The vial was sealed and the reaction mixture was maintained at room temperature for the 2.5 h. An aliquot of the solution was transferred to a NMR tube for analysis.

Representative Procedure for C-H Activation Reactions

The Pd₄₀/G4OH/SBA-15 catalyst (70 mg, 0.0023 mmol, 0.35 wt%, 3 mol%), prior to addition of all other reaction materials, was added to the dry 10 mL glass reaction tube with stirbar and Teflon screwvalve cap and placed under 1 atm of H₂. The catalyst was then heated to 100°C for 24 hours. After cooling to rt the H₂ atmosphere was replaced with Ar.

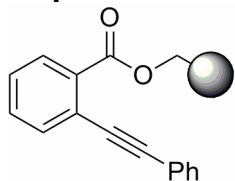
To the 10 mL glass reaction tube under Ar was added 3-methyl-2-phenylpyridine **2.64** (12 μL, 0.08 mmol, TCI America), NIS (1.25 equiv., 25 mg, 0.1 mmol, Acros Organics), mesitylene (15

μL , internal standard, Aldrich) and MeCN-d_3 (2 mL, Cambridge Isotopes). The reaction mixture was degassed (freeze/pump method) three times and placed under 1 atm of Ar. The reaction tube was sealed and the mixture heated with stirring to 100°C for 15 hours. The mixture was then cooled to rt and the solid catalyst filtered by glass microfiber filter. The filtrate was transferred to a NMR tube for analysis.

Representative Procedure for Hydroformylation Reactions

$\text{Rh}_{40}/\text{G4OH}/\text{SBA-15 NP}$ catalyst (50 mg, 0.0024 mmol, 0.5 wt%, 0.8 mol%) was added to a non-stirred, high pressure vessel (Parr Instrument Company Model 4740, 75 mL total volume (1 in. diameter x 5.6 in. depth), maximum pressure @ 350°C = 8500 psi, maximum temperature 540°C , screw cap closure with flexible graphite gasket, Model 4316 gauge block assembly – max pressure 3000 psi) with glass sleeve and stir bar. Toluene- d_8 (3 mL, Cambridge Isotopes), methyl benzoate (15 μL , internal standard) and *tert*-butyl styrene (55 μL , 0.3 mmol, Aldrich) was added. The vessel was sealed and pressurized to 300 psi with H_2/CO gas mixture (2:1 ratio $\text{H}_2:\text{CO}$). The vessel was then bled out and repressurized to 300 psi two times. After the vessel was pressurized for the third time, the bottom of the vessel was placed in a 100°C oil bath and stirred moderately. After 24 h, the vessel was cooled to rt, depressurized and the solution filtered by glass microfiber filter. The filtrate was transferred to a NMR tube for analysis. Note that the NPs were *not* pre-reduced for this reaction.

Preparation of Wang Resin-Bound Benzoate 2.39



To a 30 mL polypropylene Spe-ed cartridge with 70μ PE frit was added Wang resin (1.25 g, 1.13 mmol, NovaBioChem). CH_2Cl_2 (15 mL, Fisher HPLC grade) was then added and the resin swelled for 30 min. Then, 2-(phenylethynyl)benzoic acid⁸³ (1.25 g, 5.63 mmol), diisopropylcarbodiimide (0.876 mL, 5.63 mmol) and dimethylaminopyridine (137 mg, 1.13 mmol) was added. The cartridge was capped and shaken for 100 h. The CH_2Cl_2 was then removed, and the resin washed with dimethylformamide (3 x 10 mL, Fisher), tetrahydrofuran (3 x 10 mL, Fisher ACS grade), methanol (3 x 10 mL, Fisher ACS grade), tetrahydrofuran (3 x 10 mL, Fisher ACS grade) and then CH_2Cl_2 (3 x 10 mL, Fisher HPLC grade). The mixture was allowed to sit for 2 minutes after each addition of solvent before the solvent was removed. The resin was then dried *in vacuo* for 24 h at rt. The Wang resin-bound 2-(phenylethynyl)benzoate (**2.39**) was transferred to a polypropylene bottle and stored at -20°C when not in use.

To determine the percent loading of substrate on the resin, the following procedure was employed. A solution of CH_2Cl_2 (9 mL, Fisher HPLC grade), trifluoroacetic acid (0.95 mL, Aldrich), H_2O (0.025 mL, deionized), and triisopropylsilane (0.025 mL, Aldrich). To a 6 mL polypropylene Spe-ed cartridge with 70μ PE frit was added Wang resin-bound 2-(phenylethynyl)benzoate (**2.39**) (300 mg) and 5 mL of the previously described solution. The cartridge was capped and shaken for 2 h. The solution was then collected and the resin washed with an additional 5 mL of the previously described solution. The resin was further washed with CH_2Cl_2 (3 x 5 mL, Fisher HPLC grade). All wash solutions were collected and combined with the first solution and concentrated. The residue was purified by flash chromatography (30%-

50% ethyl acetate/hexanes (Fisher HPLC grade)) to yield 26 mg of 2-(phenylethynyl)benzoic acid. This correlates to a loading of 43% on the resin.

Representative Procedure for 3-Phase Test

To a dry 10 mL glass reaction tube with stirbar and Teflon screwvalve cap under Ar was added Wang resin-bound 2-(phenylethynyl)benzoate (**2.39**) (20 mg, 0.1025 mmol), Pt(2.9 nm)/PVP/SBA-15 (50 mg, 0.0026 mmol, 2.5 mol%), PhICl_2 (2.1 mg, 0.0077 mmol, 7.5 mol%), mesitylene (15 μL , internal standard, Aldrich) and toluene- d_8 (2 mL, Cambridge Isotopes). The reaction tube was sealed and the mixture heated with stirring to 100°C for 15 hours. The mixture was then cooled to rt and the solid catalyst and resin-bound starting material filtered by glass microfiber filter. The filtrate was transferred to a NMR tube for analysis.

For the $\text{Pt}_{40}/\text{G4OH}/\text{SBA-15}$ catalyst, prior to addition of all other reaction materials, the catalyst was added to a dry 10 mL glass reaction tube and placed under 1 atm of H_2 . The catalyst was then heated to 100°C for 24 hours. After cooling to rt, the reaction setup was continued as discussed above.

Procedure for Mercury Test

The mercury test procedure is identical to that for the standard reaction detailed above with the following exception: after the reaction tube was heated to 100°C for 10 min, it was removed from the oil bath and the stirring stopped. Under a positive pressure of Ar, the screw cap was removed and ~100 mg (3 equivalents) of Hg(0) was added. The mercury was preweighed in a 1 dram vial and the bead of mercury was poured from the vial into the reaction tube. The tube was then resealed with the Teflon screw cap and resubmerged in the 100°C oil bath and stirred for 15 h.

Procedure for Reaction with NP Pellet

The $\text{Pt}_{40}/\text{G4OH}/\text{mesoporous silica}$ pellet catalyst (190 mg, 0.007 mmol, 6 mol%, 0.7 wt%) was added to a dry 10 mL glass Schlenk reaction tube with stirbar and placed under 1 atm of H_2 . The catalyst was then heated to 100°C for 24 hours. After cooling to rt, the catalyst was placed under vacuum followed by Ar. Then, 2-(phenylethynyl)phenol (**2.4**) (21.9 mg, 0.113 mmol), hexamethylbenzene (18 mg, internal standard, Aldrich), 3.5 mL of toluene (HPLC, Fisher) and PhICl_2 (5.6 mg, 0.020 mmol, 12 mol%) was added. The catalyst mixture was degassed (freeze/pump method) three times and placed under 1 atm of Ar. The reaction was then heated with stirring to 100°C. The mixture was monitored by removal of aliquots via syringe, dilution and submission to GC-MS. After 42% yield was obtained, the solution was transferred via cannula to a second dry 10 mL glass Schlenk reaction tube with stirbar under a positive pressure of Ar at 100°C. Then, a fresh, degassed (freeze/pump method) solution of 2-(phenylethynyl)phenol (**2.4**) (21.9 mg, 0.0897 mmol), hexamethylbenzene (18 mg, internal standard, Aldrich) and 3.5 mL of toluene (HPLC, Fisher) was added via cannula to the original 10 mL glass Schlenk reaction tube under Ar at 100°C. The solution was then stirred under Ar at 100°C. Both reaction tubes now containing solution were monitored by removal of aliquots via syringe, dilution and submission to GC-MS.

Recycling Data

After isolation by filtration of the supported NP catalyst, the catalyst was washed with CH_2Cl_2 (2 x 1 mL) and dried *in vacuo*. The catalyst was then added to a dry 10 mL glass reaction tube with

stirbar and Teflon screwvalve cap and reduced under 1 atm of H₂ at 100°C for 24 hours. The catalytic reaction was then carried out as described above.

Recycling results (with retreatment):

Initial: 96% conversion, 92% yield

1x: >99% conversion, 96% yield

2x: >99% conversion, 98% yield

3x: >99% conversion, 98% yield

4x: >99% conversion, 97% yield

For recycling without retreatment, after reaction at 100°C, the mixture was cooled to rt and centrifuged (3 min, 8000 rpm). The supernatant was removed and toluene (1.0 mL) was added. Sonication was then used to redisperse the solid catalyst in toluene. The catalyst suspension was then added to a solution of starting material, mesitylene and toluene (1.0 mL) in a dry 10 mL glass reaction tube with stirbar and Teflon screwvalve cap under Ar. The reaction mixture was degassed (freeze/pump method) three times and placed under 1 atm of Ar. The catalytic reaction was then carried out as described above.

XPS Data

NPs were deposited onto a silicon wafer. Experiments were performed on a Perkin-Elmer PHI 5300 XPS spectrometer with a positron-sensitive detector and a hemispherical energy analyzer in an ion-pumped chamber (evacuated to 2×10^{-9} Torr). The Al K_α ($BE = 1486.6$ eV) X-ray source of the XPS spectrometer was operated at 300 W with 15 kV acceleration voltage.

Treatment conditions: To a dry 10 mL glass reaction tube with stirbar and Teflon screwvalve cap under Ar was added Pt(1.5 nm)/PVP/SBA-15 (4 wt%) (50 mg, 0.0103 mmol), PhICl₂ (8.5 mg, 0.0307 mmol), mesitylene (15 μL, internal standard, Aldrich) and toluene (2 mL, Fisher HPLC grade). The reaction mixture was degassed (freeze/pump method) three times and placed under 1 atm of Ar. The reaction tube was sealed and the mixture heated with stirring to 100°C for 15 hours. After cooling to rt a sample was deposited on a silicon wafer and quickly transferred to the XPS vacuum chamber.

Monitoring of Reaction Yield vs Time for Cyclization of 2.4 to 2.5.

Reactions were conducted at a larger scale but as described above, except with hexamethylbenzene as internal standard. Aliquots of reaction were filtered by glass microfiber filter, diluted with ethyl acetate (Fisher HPLC grade) and analyzed by GC-MS. All catalysts treated *in situ* with PhICl_2 (3 cat. equiv.) unless otherwise stated.

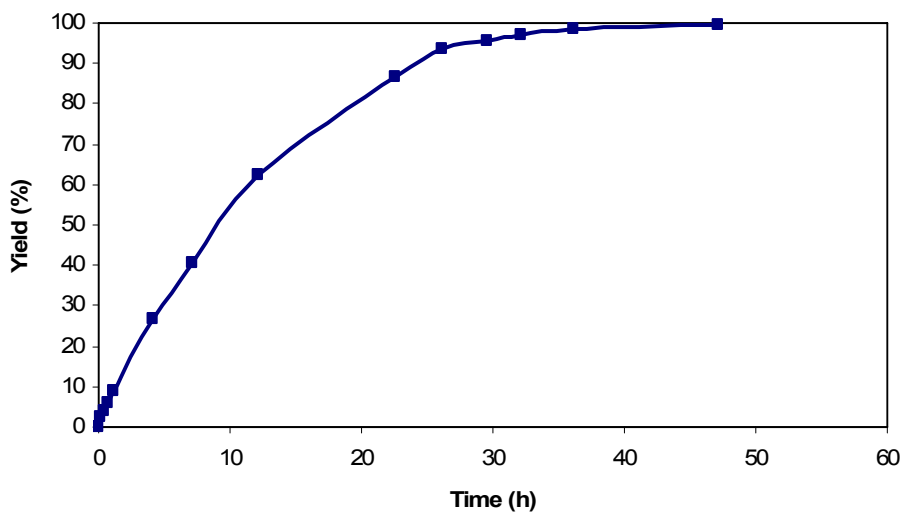
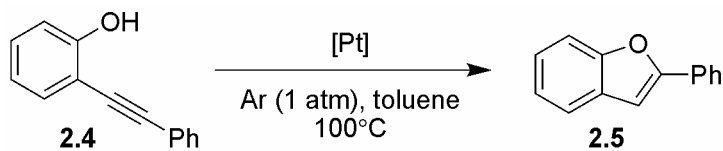


Figure E2.2. $\text{Pt}_{40}/\text{G4OH}/\text{SBA-15}$ (3 mol%). Initial use of catalyst.

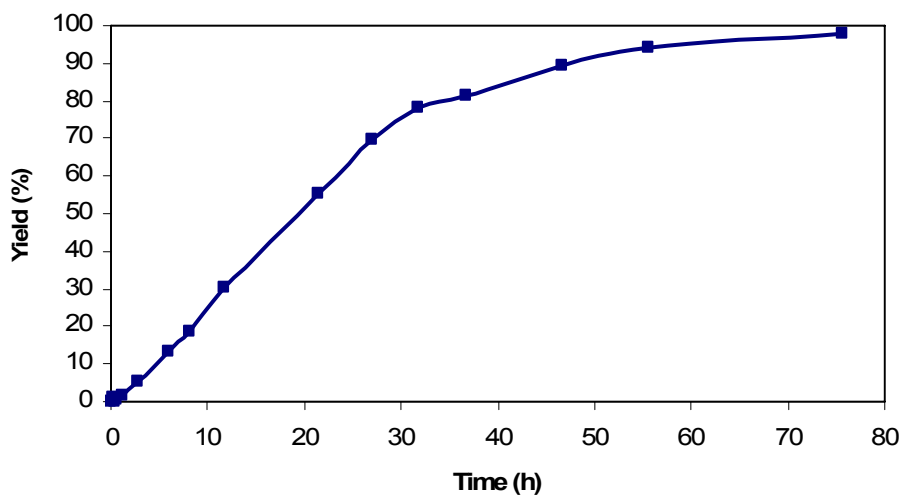


Figure E2.3. $\text{Pt}_{40}/\text{G4OH}/\text{SBA-15}$ (3 mol%). Recycle of catalyst *without* reduction/retreatment.

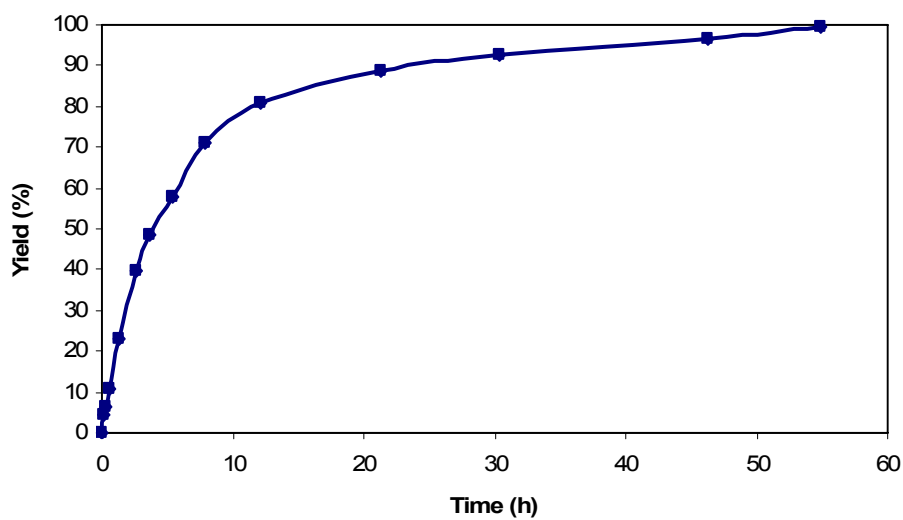


Figure E2.4. Pt₄₀/G4OH/SBA-15 (3 mol%). Recycle of catalyst *with* reduction/retreatment.

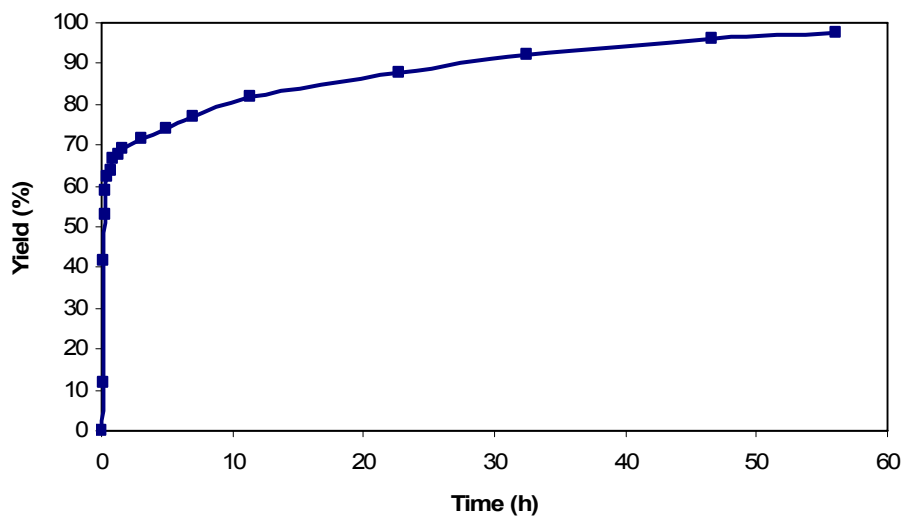


Figure E2.5. Pt (1.5 nm)/PVP/SBA-15 (1 mol%). Initial use of catalyst.

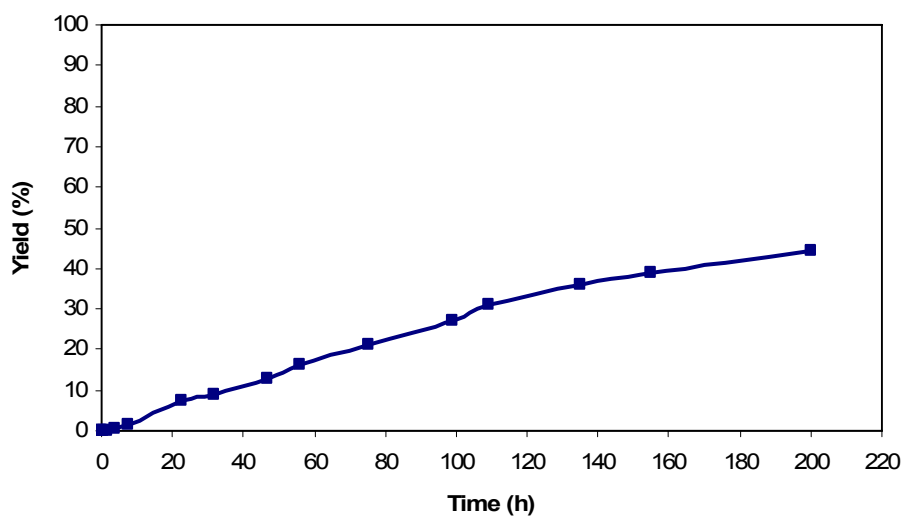


Figure E2.6. Pt (1.5 nm)/PVP/SBA-15 (1 mol%). Recycle of catalyst *without* reduction/retreatment.

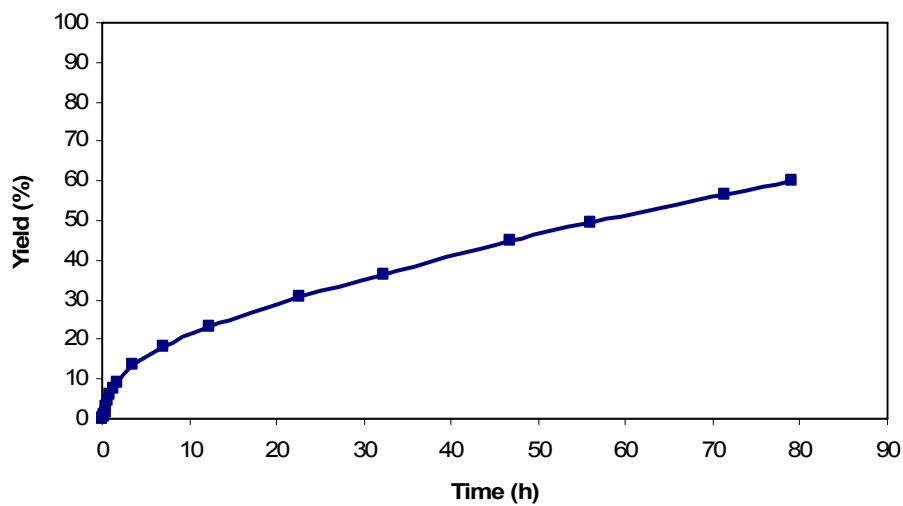


Figure E2.7. Pt (1.5 nm)/PVP/SBA-15 (1 mol%). Recycle of catalyst *with* reduction/retreatment.

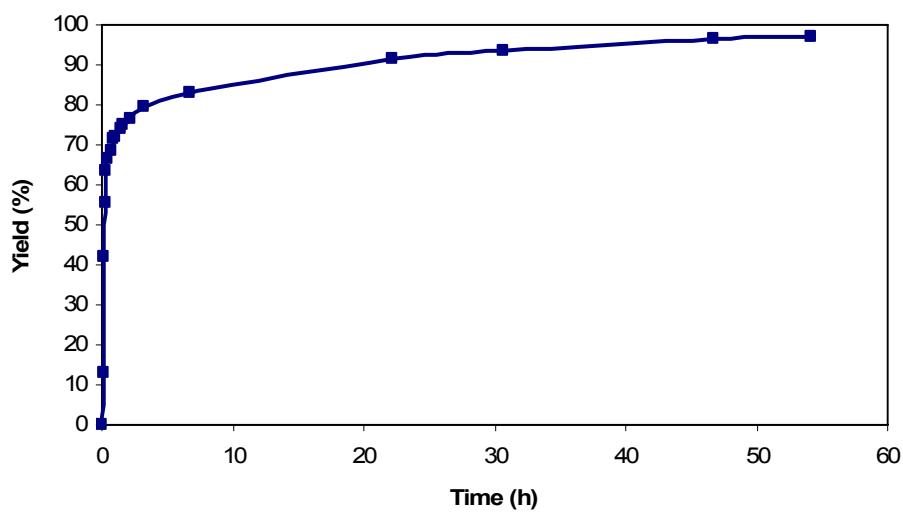


Figure E2.8. Pt (2.9 nm)/PVP/SBA-15 (1 mol%). Initial use of catalyst.

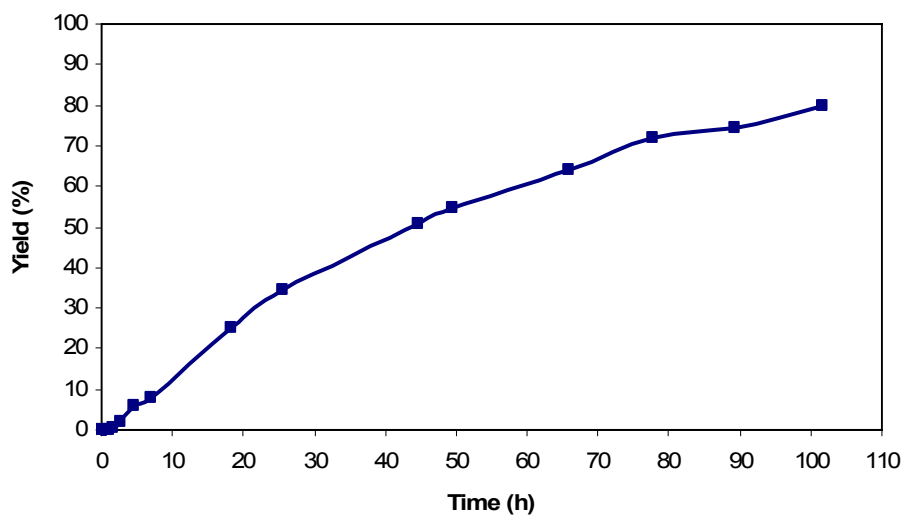


Figure E2.9. Pt (2.9 nm)/PVP/SBA-15 (1 mol%). Recycle of catalyst *without* reduction/retreatment.

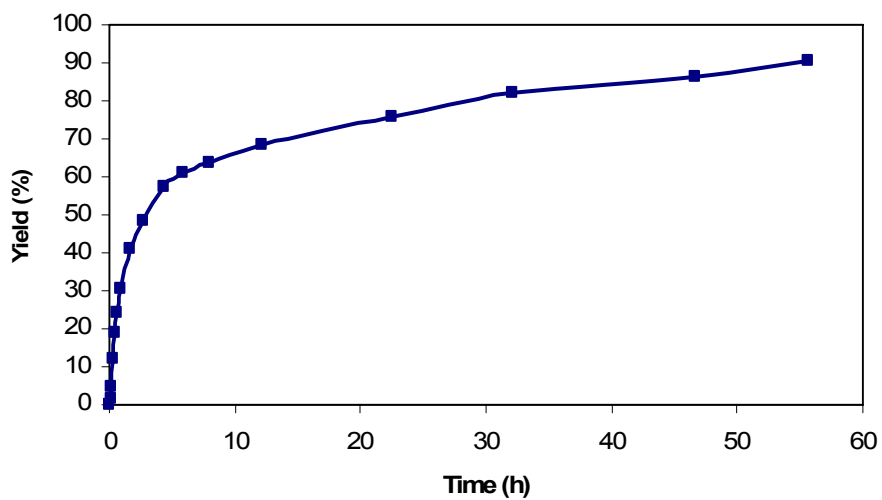


Figure E2.10. Pt (2.9 nm)/PVP/SBA-15 (1 mol%). Recycle of catalyst *with* reduction/retreatment.

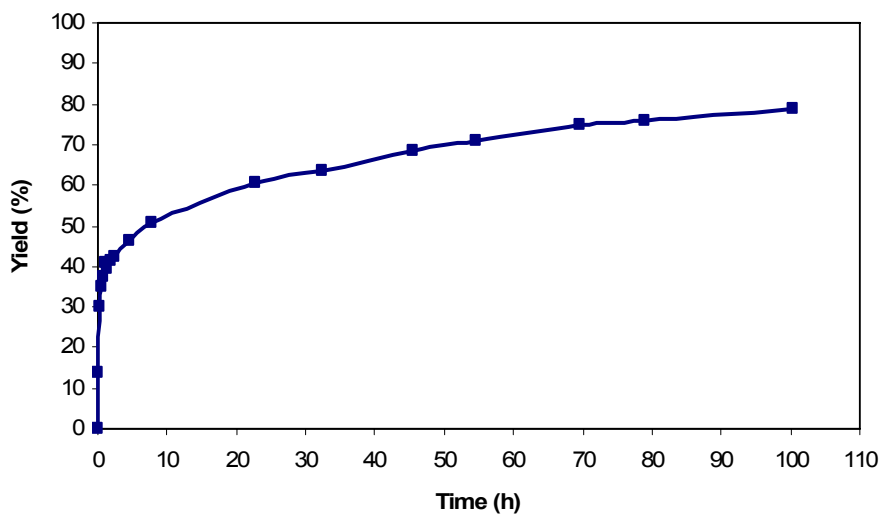


Figure E2.11. Pt (5.0 nm)/PVP/SBA-15 (2 mol%). Initial use of catalyst.

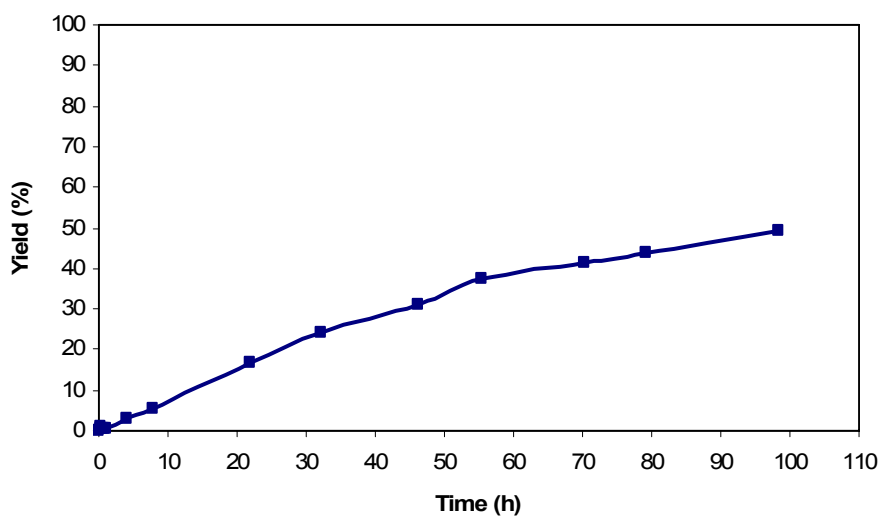


Figure E2.12. Pt (5.0 nm)/PVP/SBA-15 (2 mol%). Recycle of catalyst *without* reduction/retreatment.

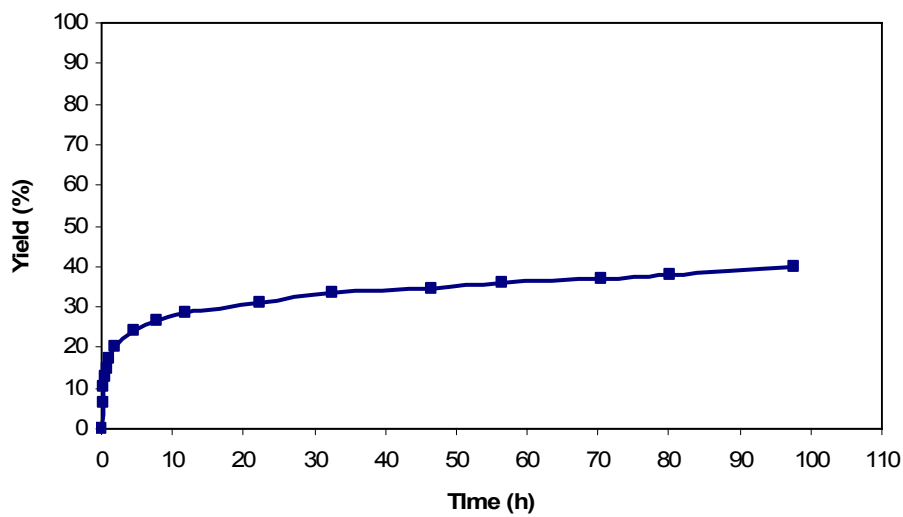


Figure E2.13. Pt (5.0 nm)/PVP/SBA-15 (2 mol%). Recycle of catalyst *with* reduction/retreatment.

ICP-MS Data

Method: GLI Procedure ME-70

Analysis: Platinum

Before reaction Pt₄₀/G4OH/SBA-15: 0.610% (basis: dried)

After reaction Pt₄₀/G4OH/SBA-15: 0.662% (basis: dried)

Centrifuged solution with Pt₄₀/G4OH/SBA-15 removed (after treatment with PhICl₂): 1.7 ppm (basis: as received) (det. limit: 1 ppm)

Filtered solution (glass microfiber filter) with Pt₄₀/G4OH/SBA-15 removed (after treatment with PhICl₂): <1.0 ppm (basis: as received) (det. limit: 1 ppm)

Flow System Protocol

A 50 x 4.5 mm (inner diameter) HPLC column was filled with 0.75 wt% Pt₄₀/G4OH/SBA-15 which corresponds to 220 mg (0.008 mmol) of catalyst. An HPLC pump was then attached to the column. The column was placed in a tube oven set at 100°C and the outlet tube drained into sampling vials. To the tube connecting the pump to the column, a 90° valve was attached. This valve allowed us to switch between H₂ gas and solution from the pump.

To initially reduce the catalyst, H₂ was flowed through the column at 10 mL/min (17 psi) while the column was at 100°C in the oven for 35 h. The 90° valve was then rotated to allow solution from the HPLC pump to flow through the column.

Toluene (dry, degassed) was then pumped through the column (100°C) for 0.5 h at a flow rate of 0.2 mL/min. The pump was then switched to the PhICl₂ solution (0.022 mmol, 6 mL dry degassed toluene) which flowed through the catalyst column (still at 100°C) for 0.5 h, which is the approximate length of time 6 mL takes to flow through the entire system at 0.2 mL/min. The total volume of the system from inlet flask to the catalyst column was 4-5 mL. The pump was then switched to the solution of **2.4** and hexamethylbenzene internal standard in dry, degassed toluene (0.05 M, C₆Me₆ equimolar to **2.4**). This solution was pumped through the catalyst column (100°C) at 0.01 mL/min, which was the flow necessary at the solution concentration to obtain approximately 50% conversion. At this point, we began to collect fractions of the effluent from the system into GC or 1 dram vials, depending on the expected volume of the fraction. Sampling frequency started at 30 min intervals which eventually became longer as the system equilibrated.

There are two types of fractions that were collected. When the sampling frequency was 30 min, the solution collected was roughly 300 µL, which was diluted 10x with ethyl acetate to create a solution for analysis by GC-MS. When the frequency became multiple hours, two types of fractions were collected. The first represents an average data point in that an aliquot of the multi-hour fraction was taken and diluted for analysis. For the second type, every 2-3 hours a fresh vial would be placed under the effluent tube for 10 min to collect 100 µL of solution. This sample would be diluted 10x for GC analysis and corresponds to a precise data point.

When additional PhICl₂ solution was passed through the column, it was prewashed with pure toluene at 100°C for 1 h at 0.2 mL/min. The new PhICl₂ solution (which was identical to the initial solution) was pumped through the catalyst at 0.2 mL/min for 0.5 h. The substrate solution was then passed through the column at 0.01 mL/min as before. It is important to note that when the flow rate is decreased from 0.2 mL/min to 0.01 mL/min it takes 10-15 minutes for this change to propagate through the system.

XAS Specifications and Procedure

Preparation of Samples for XAS Analysis

The samples consisted of Pt nanoparticles (40 atom clusters; approx. 1nm in diameter) that are encapsulated in 4th generation polyaminoamine (PAMAM) dendrimers and supported on SBA-15 mesoporous silica at a loading of 5wt% to allow for sufficient sample concentration and thus signal strength. The powder is suspended in toluene, degassed and placed under argon atmosphere. The samples are then treated and/or reacted as desired. The resulting suspensions are syringed into 1.5mm quartz capillary tubes (Charles Supper Company) and sealed with epoxy. The tubes are centrifuged to compact the sample to the bottom of the tube and are then ready for analysis.

X-Ray Absorption Measurements

Pt L_{III} edge XAS spectra were measured at the Advanced Light Source and Stanford Synchrotron Radiation Lightsource. ALS beamline 10.3.2 and SSRL beamline 4-1. The ALS beamline utilized a bend magnet with the energy range of 11.35 to 12.3 keV. A Si(111) two crystal, constant exit monochromator was used with a seven-element Ge solid-state detector. SSRL beamline 4-1 is a 20-pole, 2.0 Tesla Wiggler, 0.75 mrad, side station beamline with a flat, bent vertically collimating, 1 m, Si(220), Rh-coated, cutoff 9-23 keV, LN₂-cooled monochromator. Energy range was also 11.35 to 12.3 keV with transmission and Lytle detectors.

XANES and EXAFS Data Analysis

All analysis were performed on the IFEFFIT 1.2.11d software package. All scans for a particular sample were normalized and averaged in Sixpack/SamView. Athena was used for background removal and XANES analysis with the following parameters:

Rbkg = 1

k-weight = 3

Background removal: Pre-edge range, normalization range, spline range and edge step determined by program

Forward fourier transform:

k-range = 1 to 12.0

dk = 0.5

window type = Kaiser-bessel

Backward fourier transform:

R-range = 1 to 3

dr = 0.1

window type = Kaiser-bessel

Artemis was used for EXAFS fitting and analysis with the following parameters:

k range = 1 to 12.5

R range = 1 to 4.6 (3.2 for first shell only)

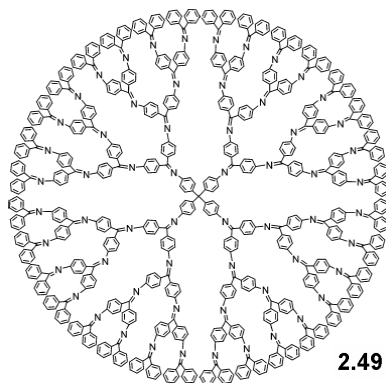
dk = 0.5

dr = 0.1

Fit k-weights = 3

R and k window is Kaiser-bessel for first shell fit only, Hanning for first and second shell combined fitting.

Preparation and Characterization of Intermediates in the Synthesis of Dendrimer 2.49



Pre-G2dendron **2.52** was prepared according to the published procedure. Spectral data were consistent with the values previously reported.^{65b} ¹H NMR (CDCl₃, 600 MHz) δ 3.75 (s, 2H), 6.62 (d, 4H, *J* = 8.4 Hz), 6.86 (d, 4H, *J* = 8.4 Hz), 7.10 (d, 4H, *J* = 7.2 Hz), 7.24-7.30 (m, 6H), 7.40 (t, 4H, *J* = 7.8 Hz), 7.45 (t, 2H, *J* = 7.2 Hz), 7.72 (d, 4H, *J* = 7.8 Hz).

G2dendron **2.53** was prepared according to the published procedure. Spectral data were consistent with the values previously reported.^{65b,e} ¹H NMR (CDCl₃, 600 MHz) δ 6.77 (d, 4H, *J* = 9.0 Hz), 7.12 (d, 4H, *J* = 7.2 Hz), 7.24-7.30 (m, 6H), 7.43 (t, 4H, *J* = 7.8 Hz), 7.50 (t, 2H, *J* = 7.2 Hz), 7.58 (d, 4H, *J* = 8.4 Hz), 7.76 (d, 4H, *J* = 7.2 Hz).

Pre-G3dendron **2.54** was prepared according to the published procedure. Spectral data were consistent with the values previously reported.^{65b} ¹H NMR (CDCl₃, 600 MHz) δ 3.82 (s, 2H), 6.55 (q, 8H, *J* = 4.2 Hz), 6.70 (d, 4H, *J* = 8.4 Hz), 6.83 (d, 4H, *J* = 8.4 Hz), 6.87 (d, 4H, *J* = 8.4 Hz), 7.02 (d, 4H, *J* = 7.2 Hz), 7.14 (d, 4H, *J* = 6.6 Hz), 7.18 (t, 4H, *J* = 7.8 Hz), 7.23-7.31 (m, 8H), 7.38-7.49 (m, 16H), 7.73 (q, 8H, *J* = 7.8 Hz).

G3dendron **2.55** was prepared according to the published procedure. Spectral data were consistent with the values previously reported.^{65b,e} ¹H NMR (CDCl₃, 600 MHz) δ 6.56 (d, 4H, *J* = 7.8 Hz), 6.69 (d, 4H, *J* = 8.4 Hz), 6.75 (d, 4H, *J* = 8.4 Hz), 6.86 (d, 4H, *J* = 8.4 Hz), 6.98 (d, 4H, *J* = 7.2 Hz), 7.15 (br t, 10H, *J* = 6.6 Hz), 7.29 (br q, 6H, *J* = 7.2 Hz), 7.35-7.49 (m, 12H), 7.52 (d, 4H, *J* = 7.8 Hz), 7.58 (d, 4H, *J* = 8.4 Hz), 7.69 (d, 4H, *J* = 7.2 Hz), 7.75 (d, 4H, *J* = 7.8 Hz).

Pre-G4dendron **2.56** was prepared according to the published procedure. Spectral data were consistent with the values previously reported.^{65b} ¹H NMR (CDCl₃, 600 MHz) δ 3.76 (s, 2H), 6.5-7.8 (m, 136H). Conclusive characterization was difficult, material carried on to next step with likely impurities.

G4dendron **2.57** was prepared according to the published procedure.^{65b} MALDI-TOF-MS (Matrix: Dithranol): Calcd: 2690.11 $[M+H]^+$, Found: 2689.99. Sample purified by recycling gel permeation chromatography, representative process trace obtained by UV-Vis detector at 450 nm seen below. Fractions collected were analyzed by MALDI-TOF-MS to determine purity. See Chapter 2 Appendix for MALDI-TOF-MS spectra of purified **2.57**.

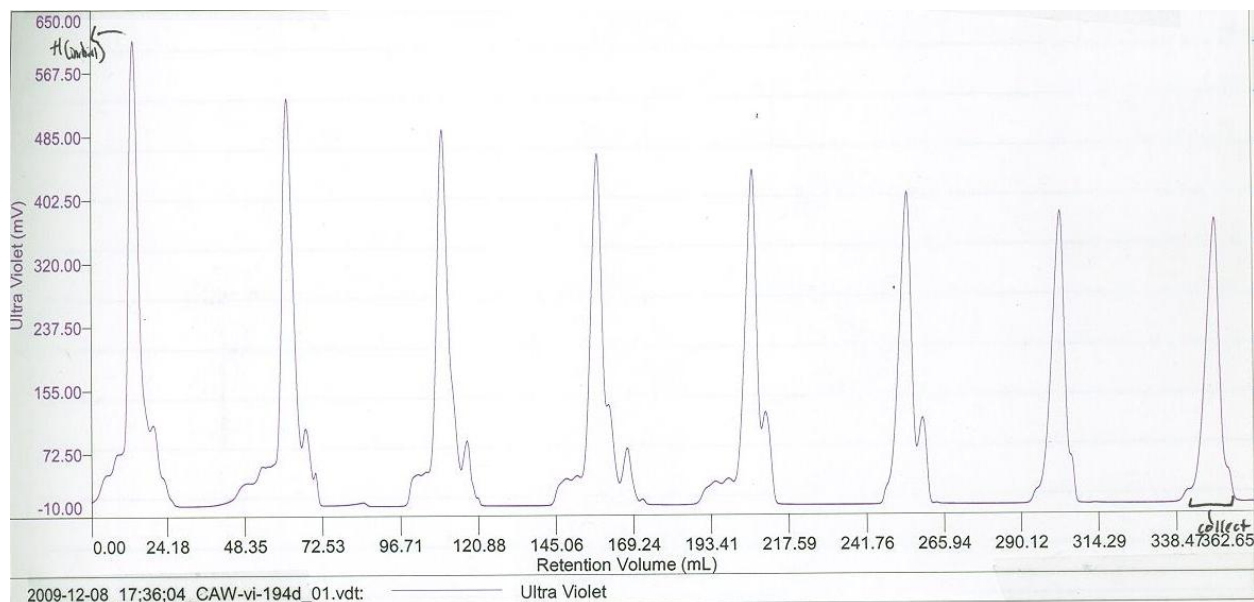


Figure E2.14. Recycling Preparative Gel Permeation Chromatography Trace

Tetraphenylmethane **2.58** was prepared according to the published procedure. Spectral data were consistent with the values previously reported.^{65d} ^1H NMR (DMSO- d_6 , 500 MHz) δ 4.92 (s, 8H), 6.37 (d, 8H, $J = 8.5$ Hz), 6.65 (d, 8H, $J = 8.5$ Hz).

TPM-PPAM dendrimer **2.49** was unsuccessfully synthesized utilizing a published procedure^{65c} with multiple modifications tried, typically involving longer reaction times or increased equivalents of reagents. For MALDI-TOF-MS spectrum of crude mixture, see Chapter 2 Appendix. Recycling gel permeation chromatography unsuccessful at purification of material, see Chapter 2 text.

References

- (1) (a) Corma, A.; Garcia, H. *Top. Catal.* **2008**, *48*, 8. (b) Tada, M.; Motokura, K.; Iwasawa, Y. *Top. Catal.* **2008**, *48*, 32. (c) Hutchings, G. J. *Top. Catal.* **2008**, *48*, 55. (d) Narayanan, R.; Tabor, C.; El-Sayed, M. A. *Top. Catal.* **2008**, *48*, 60. (e) Adamczyk, A.; Xu, Y.; Walaszek, B.; Roelofs, F.; Pery, T.; Pelzer, K.; Philippot, K.; Chaudret, B.; Limbach, H.-H.; Breitzke, H.; Buntkowsky, G. *Top. Catal.* **2008**, *48*, 75. (f) Colacot, T. J. *Top. Catal.* **2008**, *48*, 91. For a review see (g) Astruc, D., Lu, F.; Aranzas, J. R. *Angew. Chem. Int. Ed.* **2005**, *44*, 7852.
- (2) Durán Pachón, L.; Rothenberg, G. *Appl. Organometal. Chem.* **2008**, *22*, 288.
- (3) Astruc, D.; Lu, F.; Ruiz Aranzas, J.R. *Angew. Chem. Int. Ed.* **2005**, *44*, 7852.
- (4) Jesús, E.; Flores, J.C. *Ind. Eng. Chem. Res.* **2008**, *47*, 7968.
- (5) (a) Corma, A.; Garcia, H. *Top. Catal.* **2008**, *48*, 8 and references therein. (b) Tada, M.; Motokura, K.; Iwasawa, Y. *Top. Catal.* **2008**, *48*, 32.
- (6) Pham-Huu, C.; Ersen, O.; Ledoux, M.-J. Carbon and Silicon Carbide Nanotubes Containing Catalysts. In *Nanoparticles and Catalysis*. Astruc, D., Ed.; Wiley-VCH: Weinheim, **2008**, Ch. 7, p. 219-252 and references therein.
- (7) Chandler, B. D.; Gilbertson, J. D. PAMAM Dendrimer Templated Nanoparticle Catalysts. In *Nanoparticles and Catalysis*. Astruc, D., Ed.; Wiley-VCH: Weinheim, **2008**, Ch. 4, p. 129-160 and references therein.
- (8) (a) Kuhn, J.N.; Huang, W.; Tsung, C.-K.; Zhang, Y.; Somorjai, G.A. *J. Am. Chem. Soc.* **2008**, *130*, 14026. (b) Bhattacharjee, S.; Dotzauer, D.M.; Bruening, M.L. *J. Am. Chem. Soc.* **2009**, *131*, 3601. (c) Lee, I.; Delbecq, F.; Morales, R.; Albitzer, M.A.; Zaera, F. *Nature Materials* **2009**, *8*, 132. (d) Tian, N.; Zhou, Z.-Y.; Sun, S.-G.; Ding, Y.; Wang, Z.L. *Science (Washington, D.C.)* **2007**, *316*, 732. (e) Mahmoud, M.A.; Tabor, C.E.; El-Sayed, M.A.; Ding, Y.; Wang, Z.L. *J. Am. Chem. Soc.* **2008**, *130*, 4590. (f) Narayanan, R.; El-Sayed, M.A. *Nano Lett.* **2004**, *4*, 1343. (g) Lee, H. Habas, S. E.; Kweskin, S.; Butcher, D.; Somorjai, G. A.; Yang, P. *Angew. Chem. Int. Ed.* **2006**, *45*, 7824. (g) Rioux, R.M.; Song, H.; Grass, M.; Habas, S.; Niesz, K.; Hoefelmeyer, J. D.; Yang, P.; Somorjai, G. A. *Top. Catal.* **2006**, *39*, 167. (h) Tsung, C.-K. Kuhn, J. N.; Huang, W.; Aliaga, C.; Hung, L.-I.; Somorjai, G.A.; Yang, P. *J. Am. Chem. Soc.* **2009**, *131*, 5816. (i) Delbecq, F.; Zaera, F. *J. Am. Chem. Soc.* **2008**, *130*, 14924. (j) Scott, R.W.J.; Wilson, O.M.; Crooks R.M. *J. Phys. Chem. B* **2005**, *109*, 692.
- (9) For a review of supported NPs and their applications see: Campelo, J. M.; Luna, D.; Luque, R.; Marinas, J. M.; Romero, A. A. *ChemSusChem* **2009**, *2*, 18.
- (10) (a) Bernechea, M.; de Jesús, E.; López-Mardomingo, C.; Terreros, P. *Inorg. Chem.* **2007**, *48*, 4491. (b) Zhang, X.; Corma, A. *Angew. Chem. Int. Ed.* **2008**, *47*, 4358. (c) Han, J.; Liu, Y.; Guo, R. *J. Am. Chem. Soc.* **2009**, *131*, 2060. (d) Li, Y.; Hong, X.M.; Collard, D.M.; El-Sayed, M.A. *Org. Lett.* **2000**, *2*, 2385. (e) Moreno-Maas, M.; Pleixats, R. *Acc. Chem. Res.* **2003**, *36*, 638. (f) Thathagar, M.B.; ten Elshof, J.E.; Rothenberg, G. *Angew. Chem. Int. Ed.* **2006**, *45*, 2886. (g) Neațu, F.; Li, Z.; Richards, R.; Toullec, P. Y.; Genêt, J.-P.; Dumbuya, K.; Gottfried, J. M.; Steinrück, H.-P.; Pârvulescu, V. I.; Michelet, V. *Chem. Eur. J.* **2008**, *14*, 9412. (h) Ooe, M.; Murata, M.; Mizugaki, T.; Ebitani, K.; Kaneda, K. *J. Am. Chem. Soc.* **2004**, *126*, 1604. (i) Li, Y.; El-Sayed, M. A. *J. Phys. Chem. B* **2001**, *105*, 8938.

- (11) Djakovitch, L.; Köhler, K.; de Vries, J.G. The role of Palladium Nanoparticles as Catalysts for Carbon-Carbon Coupling Reactions. In *Nanoparticles and Catalysis*. Astruc, D., Ed.; Wiley-VCH: Weinheim, **2008**, ch. 10, p. 303-348 and references therein.
- (12) Corma, A.; Garcia, H. Supported Gold Nanoparticles as Oxidation Catalysts. In *Nanoparticles and Catalysis*. Astruc, D., Ed.; Wiley-VCH: Weinheim, **2008**, ch. 12, p. 389-426 and references therein.
- (13) For reviews see: (a) Moreno-Mañas, M.; Pleixats, R. *Acc. Chem. Res.* **2003**, *36*, 638. (b) Astruc, D. *Inorg. Chem.* **2007**, *46*, 1884. (c) Durand, J.; Teuma, E.; Gomez, M. *Eur. J. Inorg. Chem.* **2008**, *23*, 3577.
- (14) (a) Han, D.; Li, X.; Zhang, H.; Liu, Z.; Hu, G.; Li, C. *J. Mol. Catal. A: Chemical* **2008**, *283*, 15. (b) Axet, M. R.; Castellón, S.; Claver, C.; Philippot, K.; Lecante, P.; Chaudret, B. *Eur. J. Inorg. Chem.* **2008**, 3460. (c) Bruss, A. J.; Gelesky, M. A.; Machado, G.; Dupont, J. *J. Mol. Catal. A: Chemical* **2006**, *252*, 212.
- (15) Roucoux, A.; Nowicki, A.; Philippot, K. Rhodium and Ruthenium Nanoparticles in Catalysis. In *Nanoparticles and Catalysis*. Astruc, D., Ed.; Wiley-VCH: Weinheim, **2008**, ch. 11, p. 349-388 and references therein.
- (16) Gopidas, K. R.; Whitesell, J. K.; Fox, M. A. *Nano Lett.* **2003**, *3*, 1757.
- (17) Li, Y.; El-Sayed, M. A. *J. Phys. Chem. B* **2001**, *105*, 8938.
- (18) Han, J.; Liu, Y.; Guo, R. *J. Am. Chem. Soc.* **2009**, *131*, 2060.
- (19) Tsunoyama, H.; Sakurai, H.; Negishi, Y.; Tsukuda, T. *J. Am. Chem. Soc.* **2005**, *127*, 9374.
- (20) Widegren, J. A.; Finke, R. G. *J. Mol. Catal. A: Chemical* **2003**, *198*, 317.
- (21) For review see: Chianese, A. R.; Lee, S. J.; Gagné, M. R. *Angew. Chem. Int. Ed.* **2007**, *46*, 4042.
- (22) (a) Rioux, R.M.; Song, H.; Hoefelmeyer, J.D.; Yang, P.; Somorjai, G.A. *J. Phys. Chem. B* **2005**, *109*, 2192. (b) Wang, Y.; Ren, J.; Deng, K.; Gui, L.; Tang, Y. *Chem. Mater.* **2000**, *12*, 1622. (c) Teranishi, T.; Hosoe, M.; Tanaka, T.; Miyake, M. *J. Phys. Chem. B* **1999**, *103*, 3818. (d) Song, H.; Rioux, R. M.; Hoefelmeyer, J. D.; Komor, R.; Neisz, K.; Grass, M.; Yang, P.; Somorjai, G. A. *J. Am. Chem. Soc.* **2006**, *128*, 3027.
- (23) (a) Crooks, R.M.; Mingqi, Z.; Sun, L.; Checkhik, V.; Yeung, L.K. *Acc. Chem. Res.* **2001**, *34*, 181. (b) Huang, W.; Kuhn, J. N.; Tsung, C.-K.; Zhang, Y.; Habas, S. E.; Yang, P.; Somorjai, G. A. *Nano Lett.* **2008**, *8*, 2027.
- (24) Huang, W.; Somorjai, G. A. *Unpublished Results*.
- (25) Consistent with gas phase reactivity, see Reference 23.
- (26) Fürstner, A.; Davies, P.W. *J. Am. Chem. Soc.* **2005**, *127*, 15024.
- (27) (a) Knecht, M. R.; Weir, M. G.; Myers, V. S.; Pyrz, W. D.; Ye, H.; Petkov, V.; Buttrey, D. J.; Frenkel, A. I.; Crooks, R. M. *Chem. Mater.* **2008**, *20*, 5218. (b) Ozturk, O.; Black, T. J.; Perrine, K.; Pizzolato, K.; Williams, C. T.; Parsons, F. W.; Ratliff, J. S.; Gao, J.; Murphy, C. J.; Xie, H.; Ploehn, H. J.; Chen, D. A. *Langmuir* **2005**, *21*, 3998. (c) Ye, H.; Scott, R.W.J.; Crooks, R.M. *Langmuir* **2004**, *20*, 2915.
- (28) Doná, E.; Cordin, M.; Deisl, C.; Bertel, E.; Franchini, C.; Zucca, R.; Redinger, J. *J. Am. Chem. Soc.* **2009**, *131*, 2827.
- (29) Whitfield, S.R.; Sanford, M.S. *J. Am. Chem. Soc.* **2007**, *129*, 15142.
- (30) Other oxidants were used, although with fewer equivalents and with a different 1,6-enyne substrate. The include I₂, Br₂ and HBr. None gave the product in a yield above 10% and often halogenation of the alkyne was observed, especially with higher amounts of oxidant.

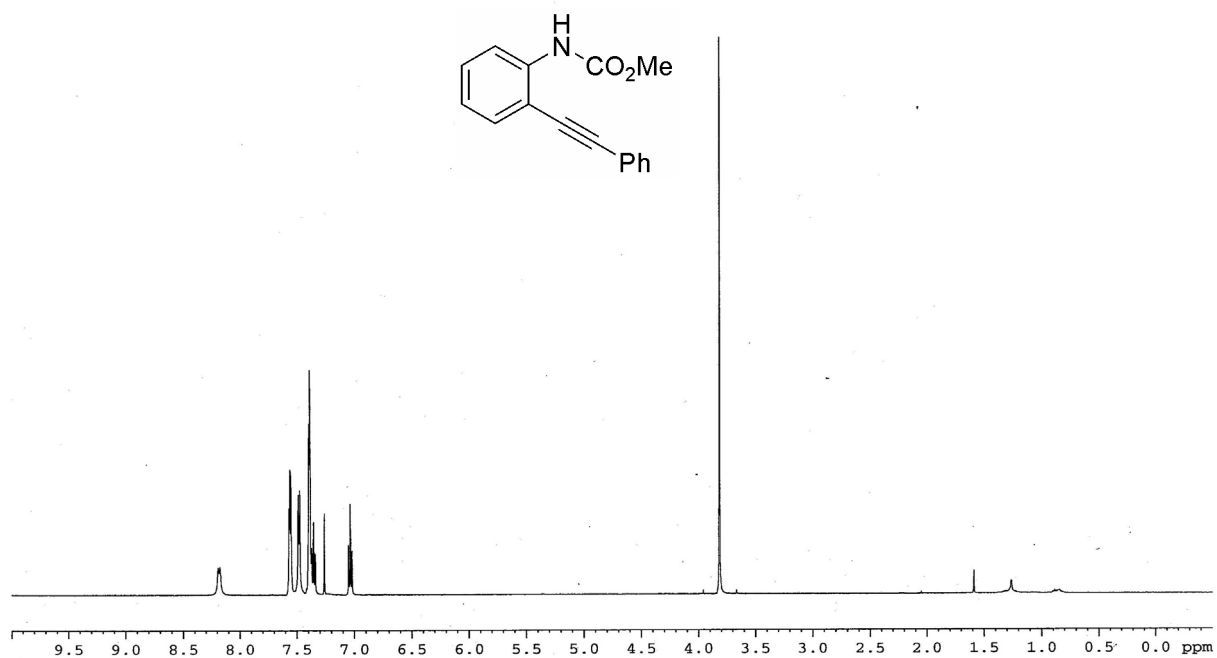
- (31) Deutsch, D. S.; Siani, A.; Fanson, P. T.; Hirata, H.; Matsumoto, S.; Williams, C. T.; Amiridis, M. D. *J. Phys. Chem. C* **2007**, *111*, 4246.
- (32) Lang, H.; May, R.A.; Iversen, B.L.; Chandler, B.D. *J. Am. Chem. Soc.* **2003**, *125*, 14832.
- (33) Niu, Y.; Yeung, L. K.; Crooks, R. M. *J. Am. Chem. Soc.* **2001**, *123*, 6840.
- (34) (a) Cai, W.; Zhong, H.; Zhang, L. *J. Appl. Phys.* **1998**, *83*, 1705. (b) *Smithells Metal Reference Book*. 6th Ed.; Brandes, E.A., Ed.; London; Boston: Butterworths, 1983. (c) Bond, G.C. *Chem. Soc. Rev.* **1991**, *20*, 441.
- (35) (a) Perenboom, J. A. A. J.; Wyder, P.; Meier, F. *Phys. Rep.* **1981**, *78*, 173. (b) Halperin, W. *P. Rev. Mod. Phys.* **1986**, *58*, 533. (c) DiCenzo, S. B.; Berry, S. D.; Hartford, E. H. *Phys. Rev. B* **1988**, *38*, 8465. (d) Lee, S. T.; Apai, G.; Manson, M. G.; Benbow, R.; Hurych, Z. *Phys. Rev. B* **1997**, *23*, 505. (e) Boyen, H. G.; Herzog, T.; Kästle, G.; Weigl, F.; Ziemann, P.; Spatz, J. P.; Möller, M.; Wahrenberg, R.; Garnier, M. G.; Oelhafen, P. *Phys. Rev. B* **2002**, *65*, 075412. (f) Guo, Q.; Luo, K.; Davis, K. A.; Goodman, D. W. *Surf. Interface Anal.* **2001**, *32*, 161. (g) Vinod, C. P.; Kulkarni, G. U.; Rao, C. N. R. *Chem. Phys. Lett.* **1998**, *289*, 329. (h) Stievano, L.; Santucci, S.; Lozzi, L.; Calogero, S.; Wagner, F. E. *J. Non-Cryst. Solids* **1998**, *232*, 644. (i) Paulus, P. M.; Goossens, A.; Thiel, R. C.; Kraan, A. M. V. D.; Schmid, G.; Jongh, L. J. D. *Phys. Rev. B* **2001**, *64*, 205418. (j) Lin, M. E.; Reifenger, R.; Ramachandra, A.; Andres, R. P. *Phys. Rev. B* **1992**, *46*, 15498.
- (36) Valden, M.; Lai, X.; Goodman, D. W. *Science* **1998**, *281*, 1647.
- (37) Thibault-Starzyk, F.; Daturi, M.; Bazin, P.; Marie, O. NO Heterogeneous Catalysis Viewed from the Angle of Nanoparticles. In *Nanoparticles and Catalysis*. Astruc, D., Ed.; Wiley-VCH: Weinheim, **2008**, ch. 16, p. 521 and references therein.
- (38) A control experiment verified that PtCl₂ with SBA-15 would catalyze the reaction, but recycling significantly decreased the activity of the solid catalyst, and the supernatant also showed continued activity for the transformation. This indicates the NP catalyst is more stable to recycling and that PtCl₂ continues to be homogeneous to some degree.
- (39) (a) Nagai, Y.; Hirabayashi, T.; Dohmae, K.; Takagi, N.; Minami, T.; Shinjoh, H.; Matsumoto, S. *J. Catal.* **2006**, *242*, 103. (b) Bunluesin, T.; Gorte, R. J.; Graham, G. W. *App. Catal. B: Environmental*, **1998**, *15*, 107. (c) Carrettin, S.; Concepción, P.; Corma, A.; López Nieto, J. M.; Puentes, V. F. *Angew. Chem. Int. Ed.* **2004**, *43*, 2538. (d) Duarte de Farias, A. M.; Nguyen-Thanh, D.; Fraga, M. A. *App. Catal. B: Environmental* **2010**, *93*, 250.
- (40) Barluenga, J.; Trincado, M.; Rubio, E.; González, J. M. *Angew. Chem. Int. Ed.* **2003**, *42*, 2406.
- (41) LaLonde, R. L.; Sherry, B. D.; Kang, E. J.; Toste, F. D. *J. Am. Chem. Soc.* **2007**, *129*, 2452.
- (42) Fürstner, A.; Mamane, V. *J. Org. Chem.* **2002**, *67*, 6264.
- (43) Nakamura, I.; Sato, Y.; Terada, M. *J. Am. Chem. Soc.* **2009**, *131*, 4198.
- (44) Many more reactions of various classes were tried with Pt NP catalysis. However, due to the limited results obtained, they are not discussed here. More studies should be done before any conclusion is reached. The relevant experiments can be found in Cole Witham's lab notebooks, volumes IV-VI.
- (45) LaLonde, R. L.; Wang, Z. J.; Mba, M.; Lackner, A. D.; Toste, F. D. *Angew. Chem. Int. Ed.* **2010**, *49*, 598.
- (46) Dube, P.; Toste, F. D. *J. Am. Chem. Soc.* **2006**, *128*, 12062-12063.
- (47) Berg, T. C.; Bakken, V.; Gundersen, L.-L.; Petersen, D. *Tetrahedron* **2006**, *62*, 6121.
- (48) Hiroya, K.; Itoh, S.; Sakamoto, T. *J. of Org. Chem.* **2004**, *69*, 1126.

- (49) Yasuhara, A.; Kanamori, Y.; Kaneko, M.; Numata, A.; Kondo, Y.; Sakamoto, T. *J. Chem. Soc., Perk. Trans. 1: Org. and Bio-Org. Chem.* **1999**, *4*, 529.
- (50) (a) Sakai, H.; Tsutsumi, K.; Morimoto, T.; Kakiuchi, K.. *Adv. Syn. Catal.* **2008**, *350*, 2498. (b) Iritani, K.; Matsubara, S.; Uchimoto, K.. *Tetrahedron Lett.* **1988**, *29*, 1799.
- (51) (a) Nieto-Oberhuber, C.; Muñoz, M. P.; López, S.; Jiménez-Núñez, E.; Nevado, C.; Herrero-Gómez, E.; Raducan, M.; Echavarren, A. M. *Chem. Eur. J.* **2006**, *12*, 1677. (b) Amijs, C. H. M.; Ferrer, C.; Echavarren, A. M. *Chem. Comm.* **2007**, 698. (c) Jiménez-Núñez, E.; Claverie, C. K.; Nieto-Oberhuber, C.; Echavarren, A. M. *Angew. Chem. Int. Ed.* **2006**, *45*, 5452. (d) Nieto-Oberhuber, C.; López, S.; Muñoz, M. P.; Jiménez-Núñez, E.; Buñuel, E.; Cárdenas, D. J.; Echavarren, A. M. *Chem. Eur. J.* **2006**, *12*, 1694. (e) Mamane, V.; Gress, T.; Krause, H.; Fürstner, A. *J. Am. Chem. Soc.* **2004**, *126*, 8654.
- (52) (a) Nieto-Oberhuber, C.; López, S.; Jiménez-Núñez, E.; Echavarren, A. M. *Chem. Eur. J.* **2006**, *12*, 5916. (b) Cabello, N.; Jiménez-Núñez, E.; Buñuel, E.; Cárdenas, D. J.; Echavarren, A. M. *Eur. J. Org. Chem.* **2007**, 4217.
- (53) (a) López, S.; Herrero-Gómez, E.; Pérez-Galán, P.; Nieto-Oberhuber, C.; Echavarren, A. M. *Angew. Chem. Int. Ed.* **2006**, *45*, 6029. (b) Nieto-Oberhuber, C.; Muñoz, M. P.; Buñuel, E.; Nevado, C.; Cárdenas, D. J.; Echavarren, A. M. *Angew. Chem., Int. Ed.* **2004**, *43*, 2402. (c) Nieto-Oberhuber, C.; López, S.; Echavarren, A. M. *J. Am. Chem. Soc.* **2005**, *127*, 6178.
- (54) García-Mota, M.; Cabello, N.; Maseras, F.; Echavarren, A. M.; Pérez-Ramírez, J.; Lopez, N. *ChemPhysChem* **2008**, *9*, 1624.
- (55) Witham, C. A.; Mauleón, P.; Shapiro, N. D.; Sherry, B. D.; Toste, F. D. *J. Am. Chem. Soc.* **2007**, *129*, 5838.
- (56) The yield shown is obtained utilizing the standard conditions for NP catalysis (toluene, Ar, 100°C). This transformation is known with homogeneous Pd catalysis, but under different conditions: Liang, Y.; Tang, S.; Zhang, X.-D.; Mao, L.-Q.; Xie, Y.-X.; Li, J.-H. *Org. Lett.* **2006**, *8*, 3017.
- (57) Johansson, M. J.; Gorin, D. J.; Staben, S. T.; Toste, F. D. *J. Am. Chem. Soc.* **2005**, *127*, 18002.
- (58) (a) Davies, I.W.; Matty, L.; Hughes, D.L.; Reider, P.J. *J. Am. Chem. Soc.* **2001**, *123*, 10139. (b) Dahan, A.; Portnoy, M. *J. Am. Chem. Soc.* **2007**, *129*, 5860.
- (59) We attempted to attach either **2.40** and **2.41** to Wang resin and 4-aminophenyl resin utilizing a range of conditions. Poor results were consistently obtained with <20% loading onto the resin.
- (60) (a) Whitesides, G. M.; Hackett, M.; Brainard, R. L.; Lavalleye, J.-P. P. M.; Sowinski, A. F.; Izumi, A. N.; Moore, S. S.; Brown, D. W.; Staudt, E. M. *Organometallics* **1985**, *4*, 1819. (b) Dyson, P. J. *Dalton Trans.* **2003**, 2964. (c) Schmidt, A. F.; Al-Halalqa, A.; Smirnov, V. V. *Kinetics and Catalysis* **2008**, *49*, 395.
- (61) For excellent review of XAS spectroscopy see: Kelly, S.D.; Hesterberg, D.; Ravel, B. Analysis of Soils and Minerals Using X-ray Absorption Spectroscopy. In *Methods of Soil Analysis. Part 5 – Mineralogical Methods*. Ulery, A.L.; Drees, R., Eds.; Soil Science Society of America, Inc., **2008**, ch. 14, p. 387-464 and references therein.
- (62) (a) Ayala, R.; Marcos, E. S.; Díaz-Moreno, S.; Solé, A.; Muñoz-Páez, A. *J. Phys. Chem. B* **2001**, *105*, 7588. (b) Dunaev, A. V.; Arkhangelsky, I. V.; Zubavichus, Y. V.; Avdeev, V. V. *Carbon* **2008**, *46*, 788.
- (63) Boag, N. M.; Ravetz, M. S. *Acta. Cryst.* **2007**, *E63*, m3103.
- (64) Scott, R. W. J.; Ye, H.; Henriquez, R. R.; Crooks, R. M. *Chem. Mater.* **2003**, *15*, 3873.

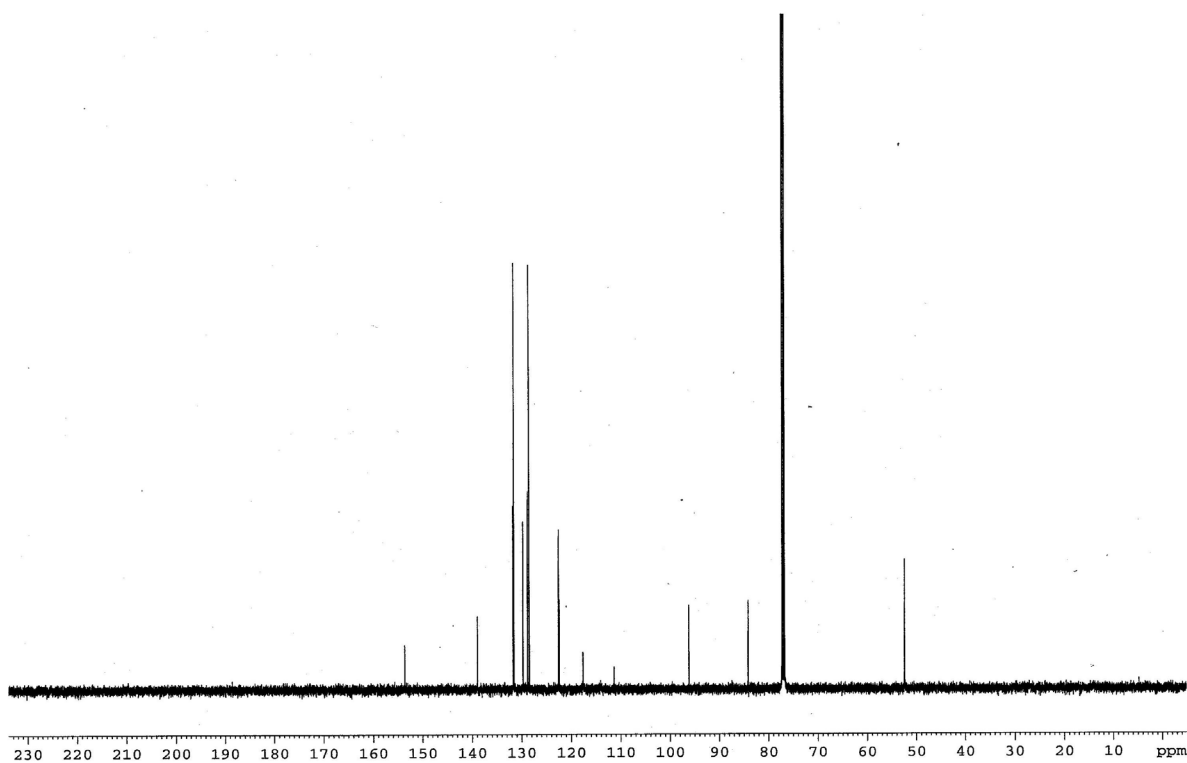
- (65) (a) Yamamoto, K.; Imaoka, T.; Chun, W.-J.; Enoki, O.; Katoh, H.; Takenaga, M.; Sono, A. *Nature Chemistry* **2009**, *1*, 397. (b) Takanashi, K.; Chiba, H.; Higuchi, M.; Yamamoto, K. *Org. Lett.* **2004**, *6*, 1709. (c) Enoki, O.; Katoh, H.; Yamamoto, K. *Org. Lett.* **2006**, *8*, 569. (d) Laliberté, D.; Maris, T.; Wuest, J. D. *Can. J. Chem.* **2004**, *82*, 386. (e) Higuchi, M.; Shiki, S.; Yamamoto, K. *Org. Lett.* **2000**, *2*, 3079.
- (66) Accounts of these types of reactions are abundant and will not be further discussed here. More than 180 reviews exist in the literature at the time of publication of this dissertation. For some of the more recent reviews see: (a) Ahmet, G.; Theopold, K. H. *Chem. Rev.* **2010**, *110*, 1060. (b) Sun, C.-L.; Li, B.-J.; Shi, Z.-J. *Chem. Comm.* **2010**, *46*, 677. (c) Mkhali, I. A. I.; Barnard, J. H.; Marder, T. B.; Murphy, J. M.; Hartwig, J. F. *Chem. Rev.* **2010**, *110*, 890. (d) Giri, R.; Shi, B.-F.; Engle, K. M.; Maugel, N.; Yu, J.-Q. *Chem. Soc. Rev.* **2009**, *38*, 3242.
- (67) (a) Kalyani, D.; Dick, A. R.; Anani, W. Q.; Sanford, M. S. *Tetrahedron* **2006**, *62*, 11483. (b) Kalyani, D.; Dick, A. R.; Anani, W. Q.; Sanford, M. S. *Org. Lett.* **2006**, *8*, 2523.
- (68) (a) Dick, A. R.; Hull, K. L.; Sanford, M. S. *J. Am. Chem. Soc.* **2004**, *126*, 2300. (b) Hull, K. L.; Sanford, M. S. *J. Am. Chem. Soc.* **2007**, *129*, 11904. (c) Hull, K. L.; Sanford, M. S. *J. Am. Chem. Soc.* **2009**, *131*, 9651.
- (69) Zielinska, A.; Skulski, L. *Tetrahedron Lett.* **2004**, *45*, 1087.
- (70) Chatani, N.; Morimoto, T.; Muto, S.; Murai, J. *J. Am. Chem. Soc.* **1994**, *116*, 6049.
- (71) Sakai, N.; Kimiyoshi, A.; Takeo, K. *Org. Lett.* **2004**, *6*, 1527.
- (72) Zhao, D.; Huo, Q.; Feng, J.; Chmelka, B. F.; Stucky, G. D. *J. Am. Chem. Soc.* **1998**, *120*, 6024.
- (73) (a) Han, Y.; Lee, S. S.; Ying, J. Y. *Chem. Mater.* **2007**, *19*, 2292. (b) Schmidt-Winkel, P.; Lukens, W. W.; Yang, P. D.; Margolese, D. I.; Lettow, J. S.; Ying, J. Y.; Stucky, G. D. *Chem. Mater.* **2000**, *12*, 686.
- (74) Yang, H.; Shi, Q.; Tian, B.; Xie, S.; Zhang, F.; Yan, Y.; Tu, B.; Zhao, D. *Chem. Mater.* **2003**, *15*, 536.
- (75) Kim, Y.-G.; Oh, S.-K.; Crooks, R. M. *Chem. Mater.* **2004**, *16*, 167.
- (76) Amarego, W.; Chai, L. F.; Christina, L. L. In *Purification of Laboratory Chemicals*, 5th Ed. Elsevier, **2003**.
- (77) Yao, T.; Larock, R. C. *J. Org. Chem.* **2003**, *68*, 5936.
- (78) Uchiyama, M.; Ozawa, H.; Takuma, K.; Matsumoto, Y.; Yonehara, M.; Hiroya, K.; Sakamoto, T. *Org. Lett.* **2006**, *8*, 5517.
- (79) Zhang, Z.; Liu, C.; Kinder, R. E.; Han, X.; Qian, H.; Widenhoefer, R. A. *J. Am. Chem. Soc.* **2006**, *128*, 9066.
- (80) Anderson, S.; Taylor, P. N.; Verschoor, G. L. B. *Chem. Eur. J.* **2004**, *10*, 518.
- (81) Nieto-Oberhuber, C.; Muñoz, M. P.; López, S.; Jiménez-Núñez, E.; Nevado, C.; Herrero-Gómez, E.; Raducan, M.; Echavarren, A. M. *Chem. Eur. J.* **2006**, *12*, 1677.
- (82) Chakraborti, A. K.; Sharma, L.; Gulhane, R. *Tetrahedron* **2003**, *59*, 7661.
- (83) Zhang, Q.; Shi, C.; Zhang, H.-R.; Wang, K. K. *J. Org. Chem.* **2000**, *65*, 7977.

Chapter 2 Appendix. Selected Spectral Data.

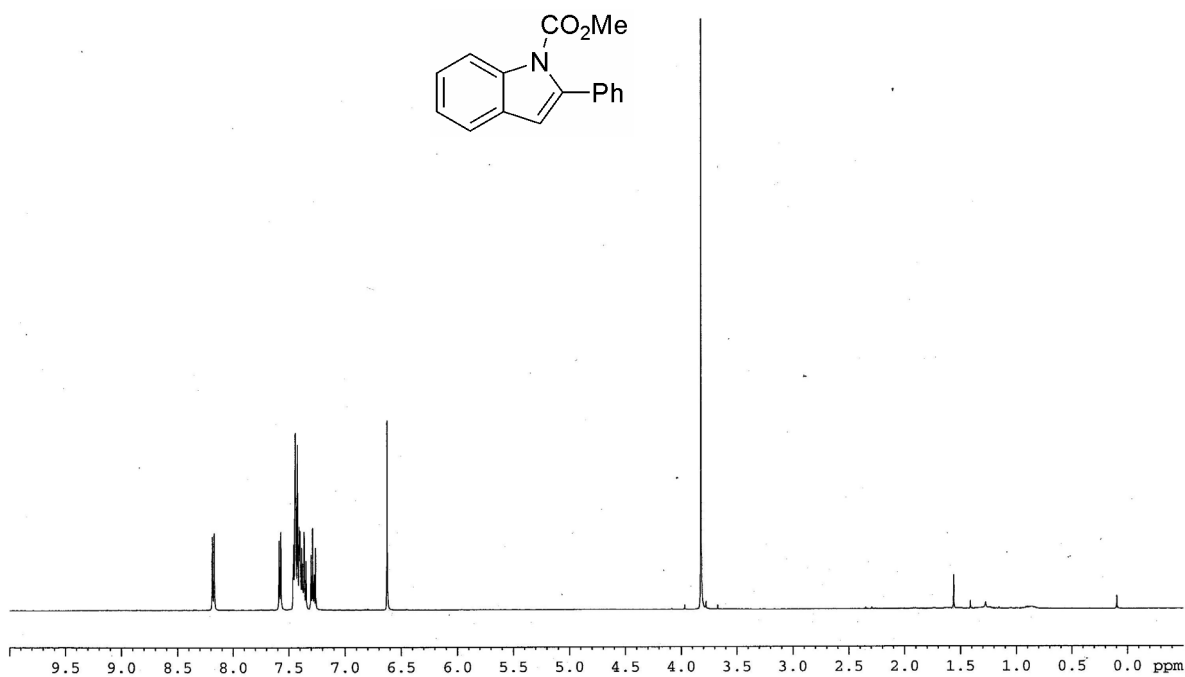
^1H NMR (CDCl_3 , 500 MHz) for **2.6**



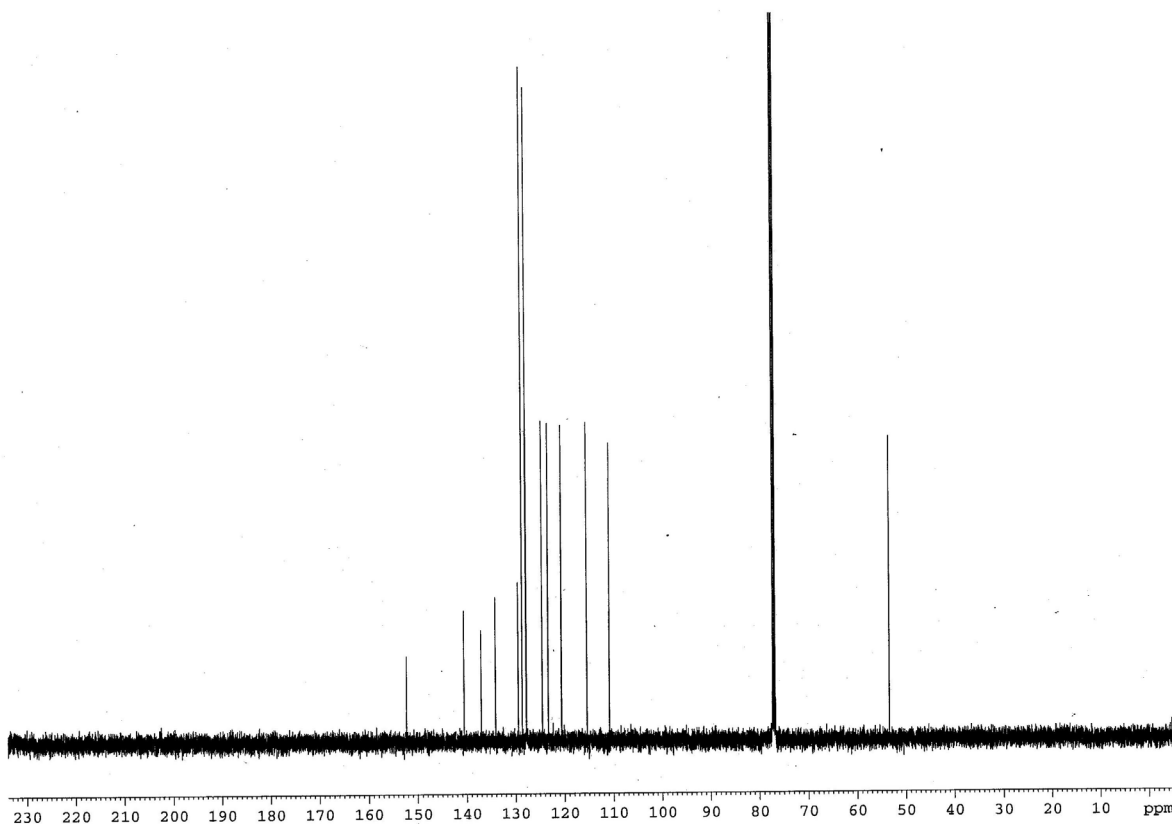
^{13}C NMR (CDCl_3 , 125 MHz) for **2.6**



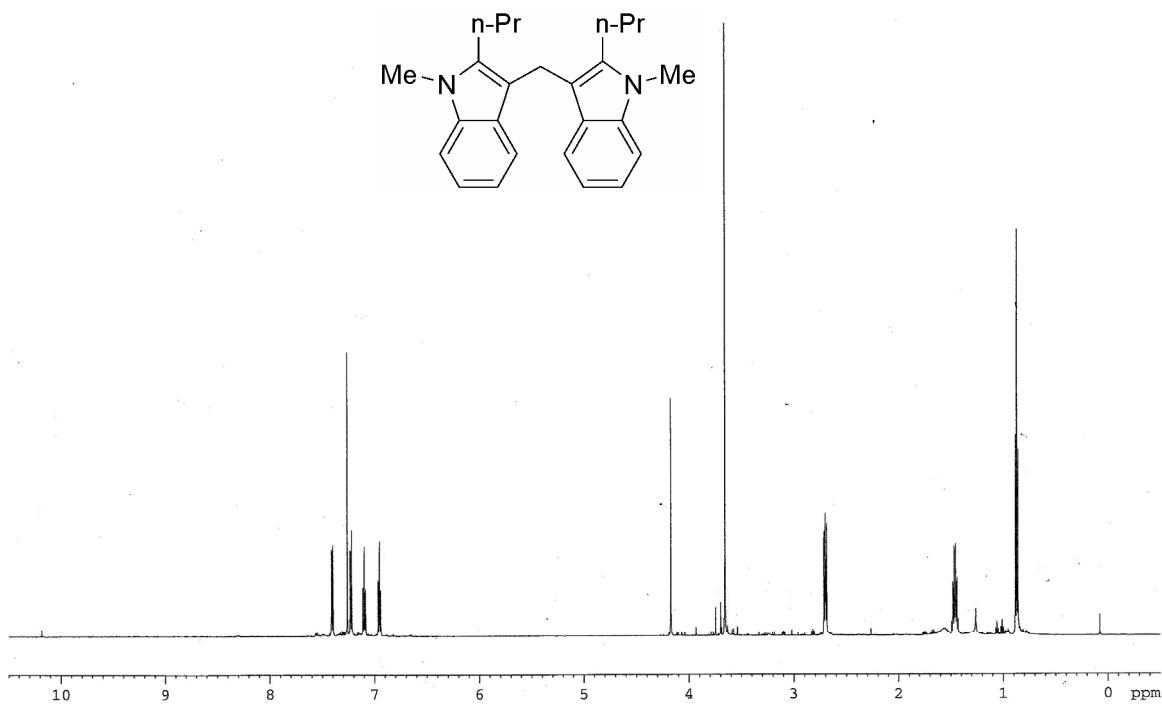
^1H NMR (CDCl_3 , 500 MHz) for **2.7**



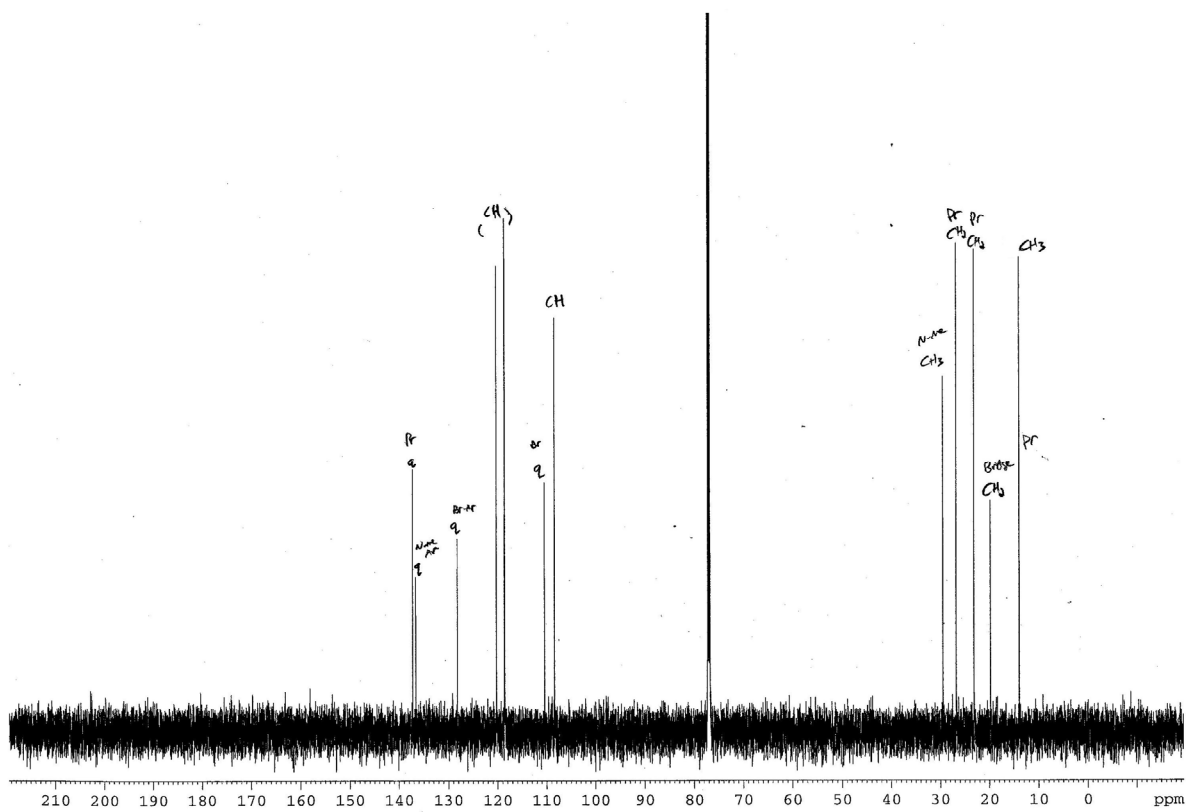
^{13}C NMR (CDCl_3 , 125 MHz) for **2.7**



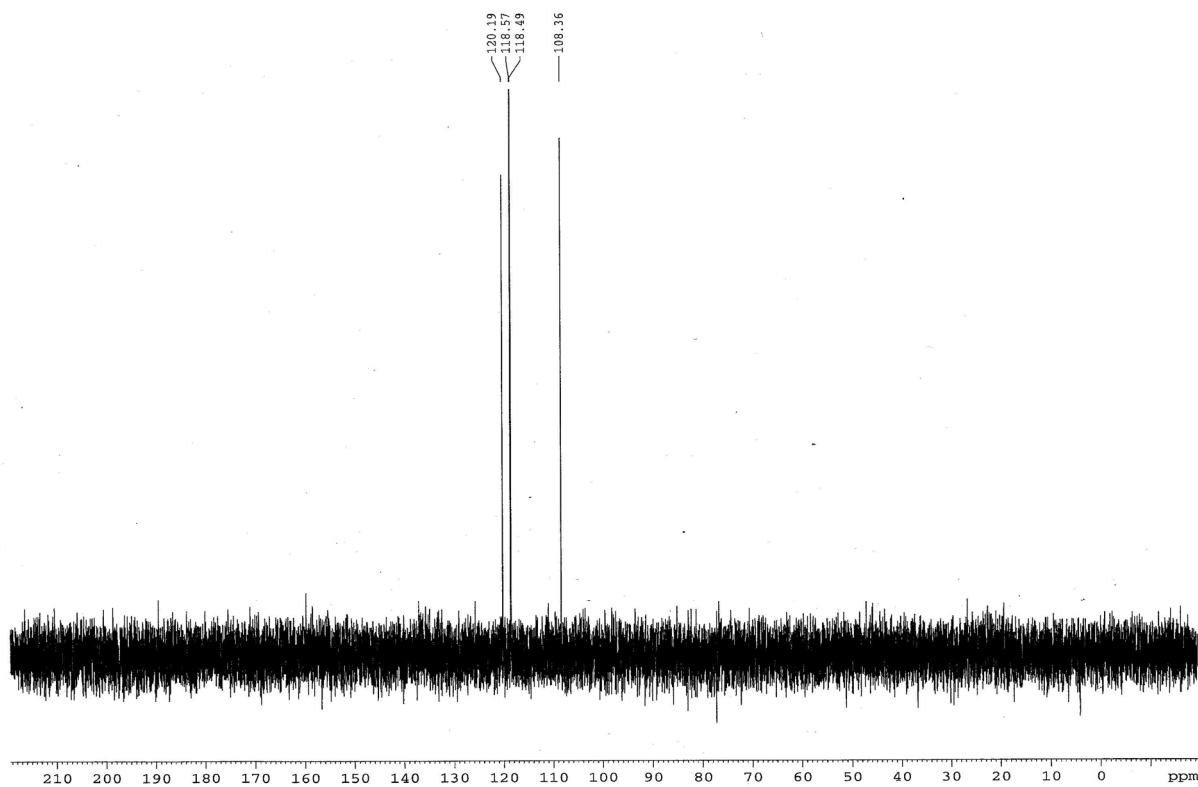
^1H NMR (CDCl_3 , 600 MHz) for **2.15**



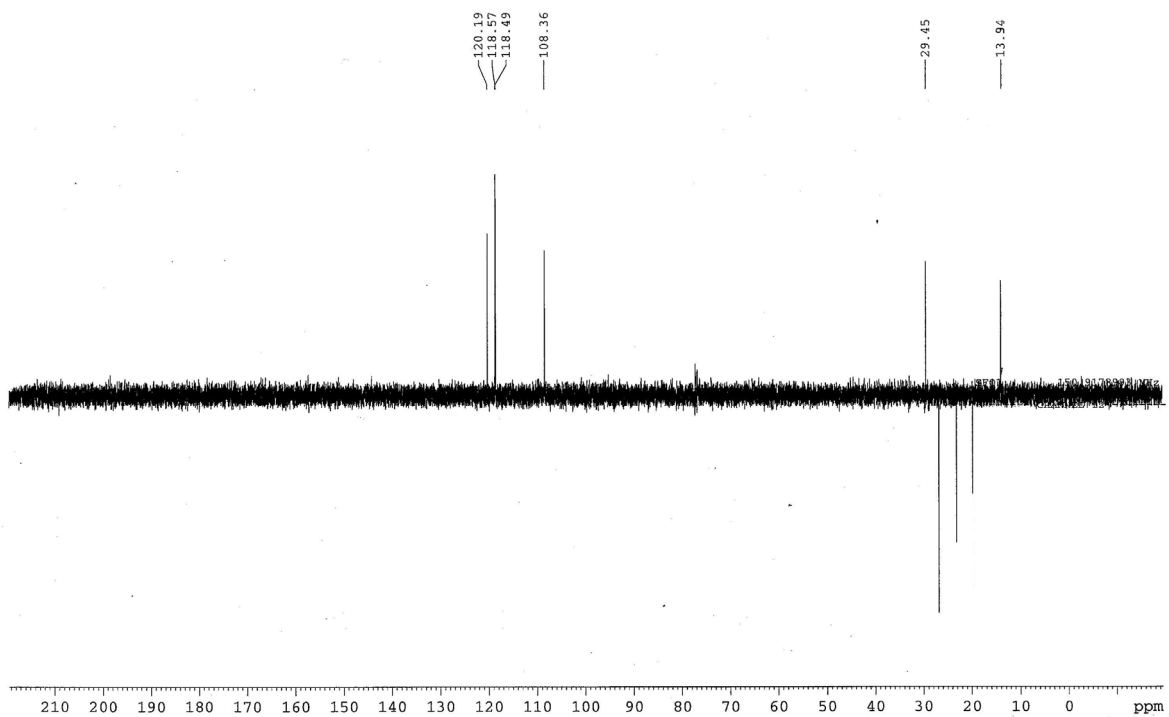
^{13}C NMR (CDCl_3 , 150 MHz) for **2.15**



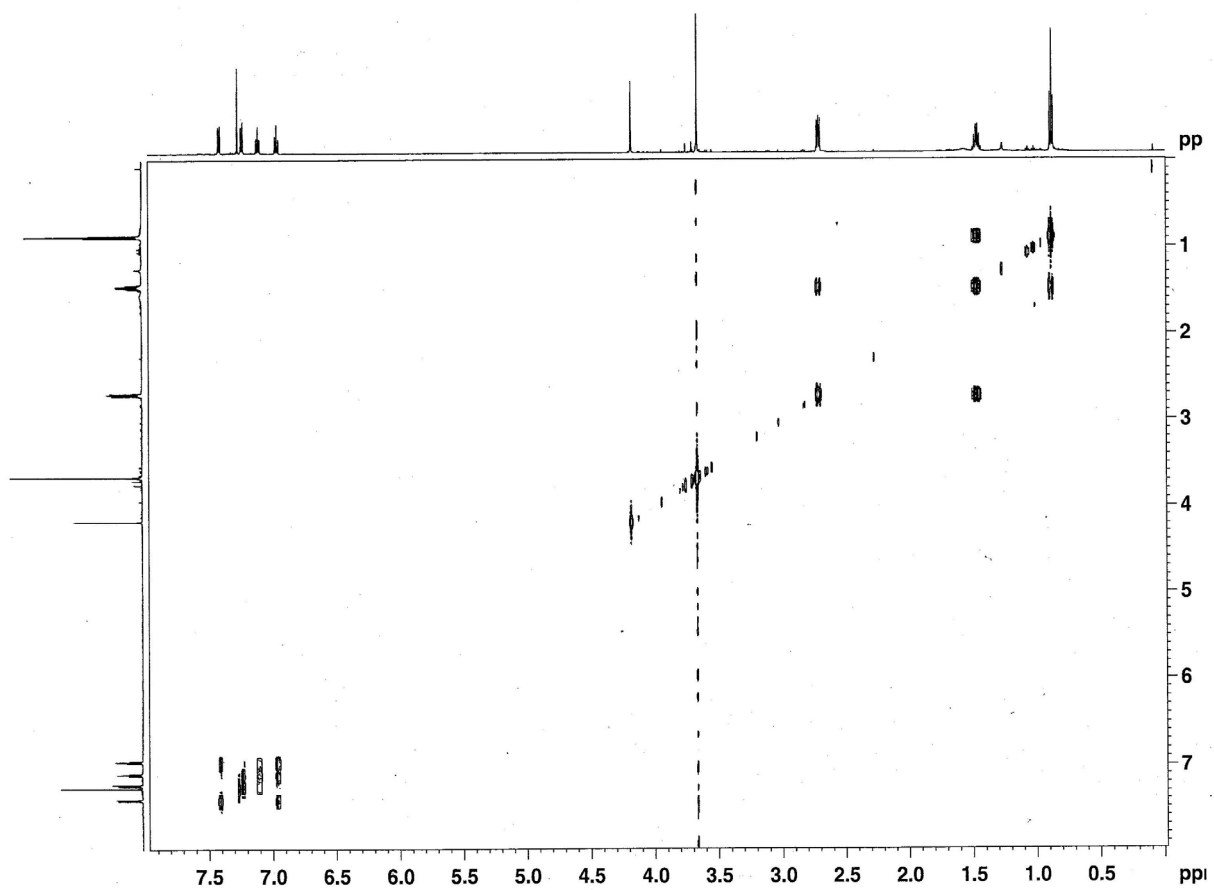
DEPT90 NMR (CDCl₃, 150 MHz) for **2.15**



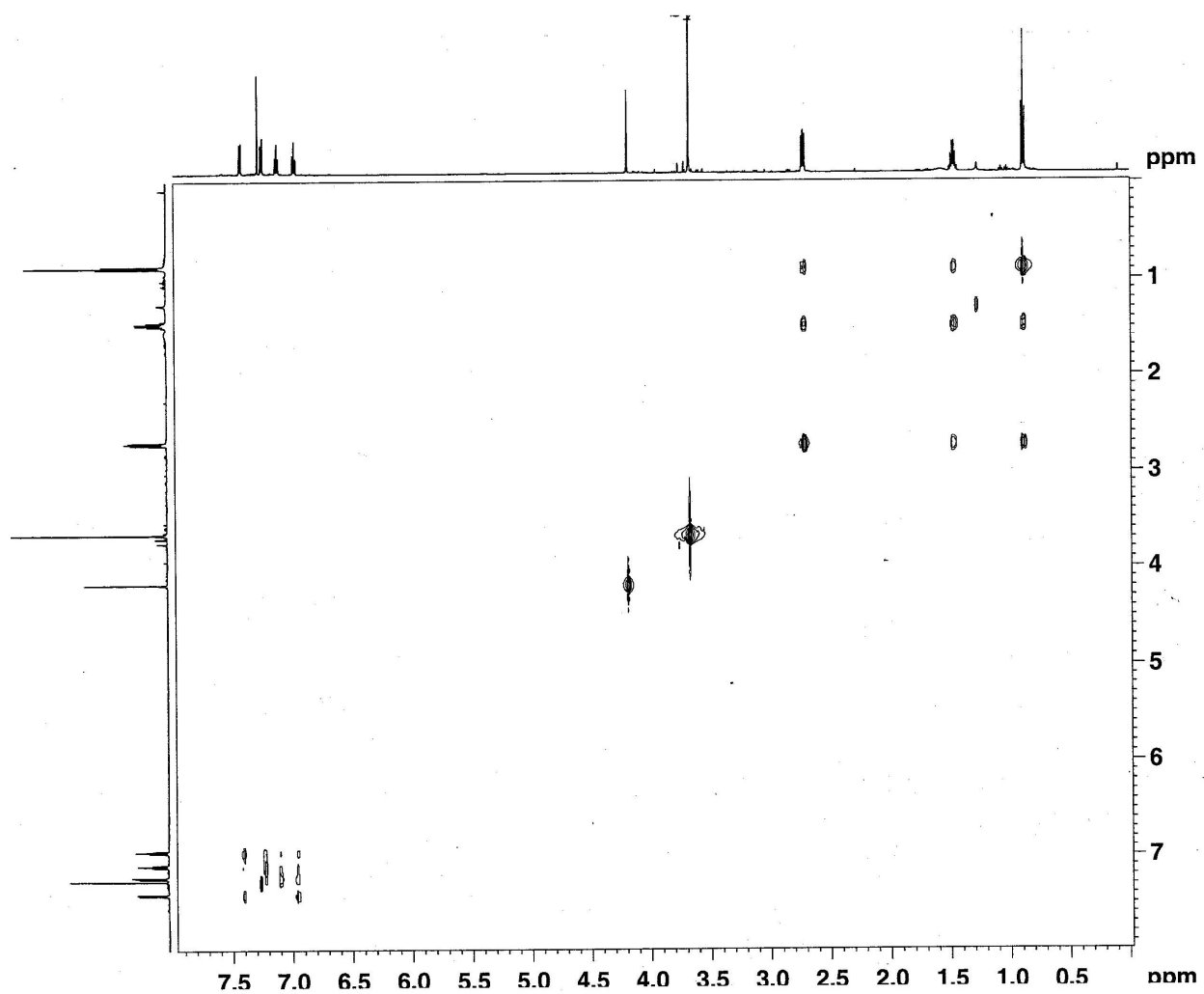
DEPT135 NMR (CDCl₃, 150 MHz) for **2.15**



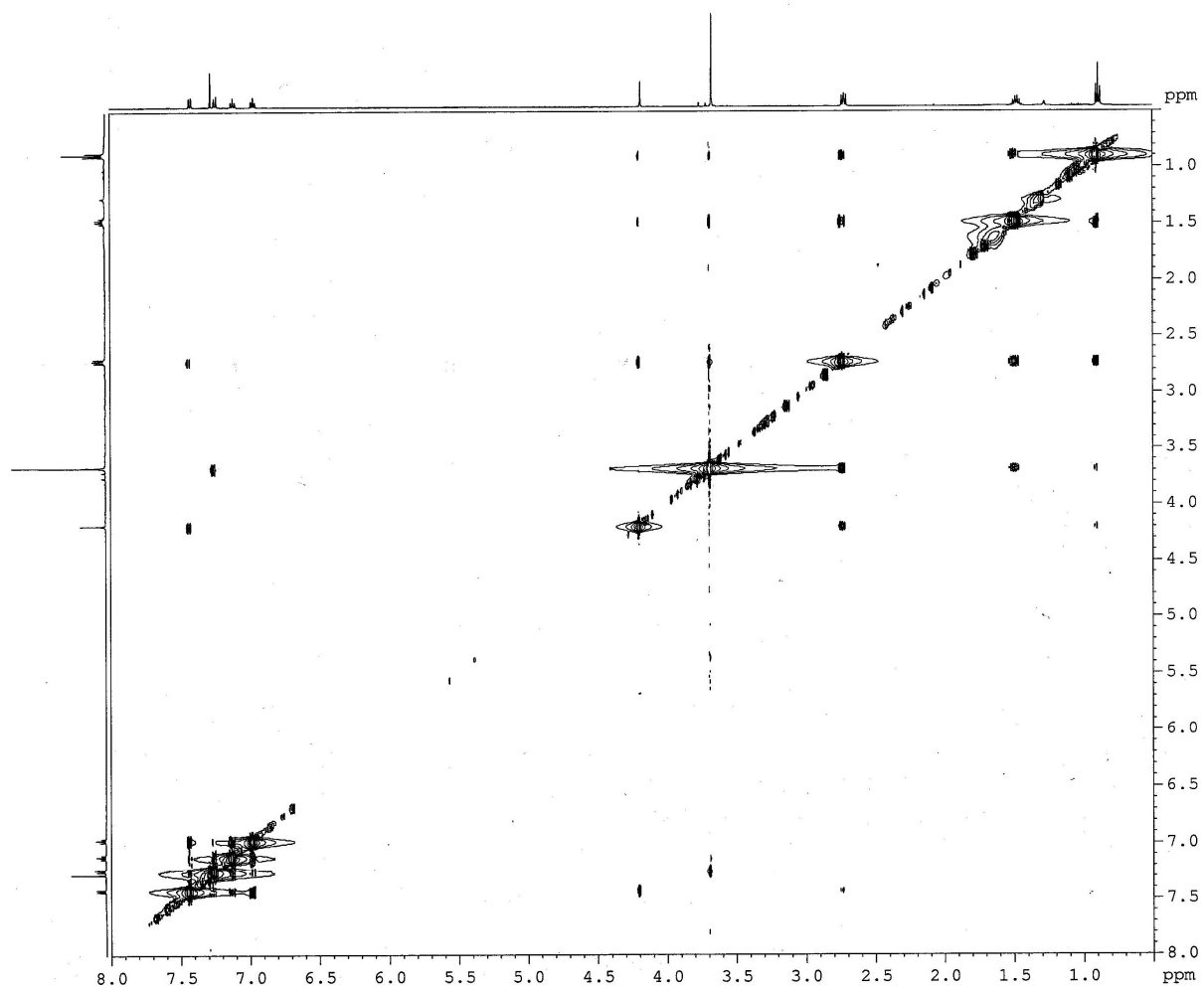
COSY NMR (CDCl₃, 600 MHz) for **2.15**



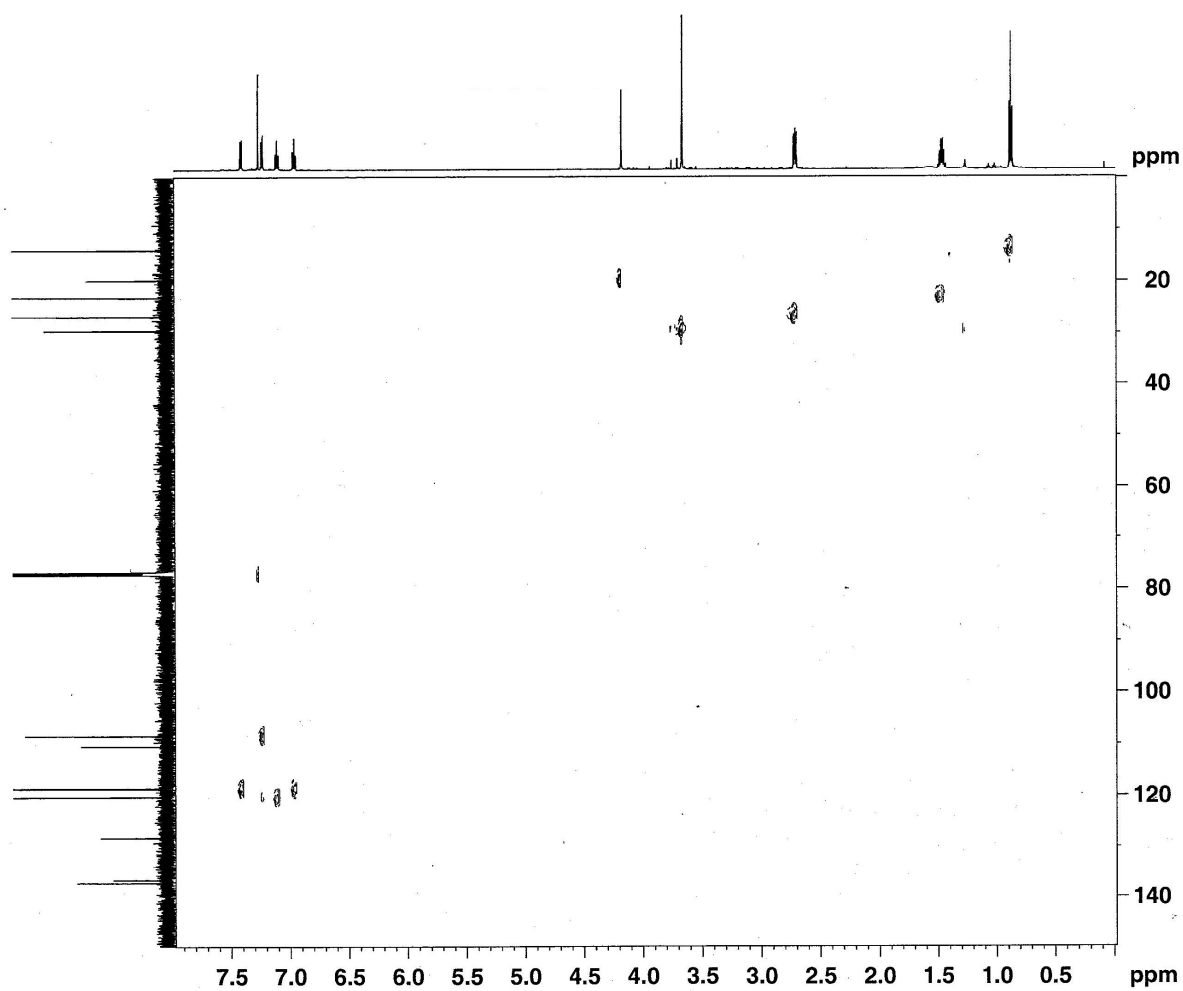
TOCSY NMR (CDCl₃, 600 MHz) for **2.15**



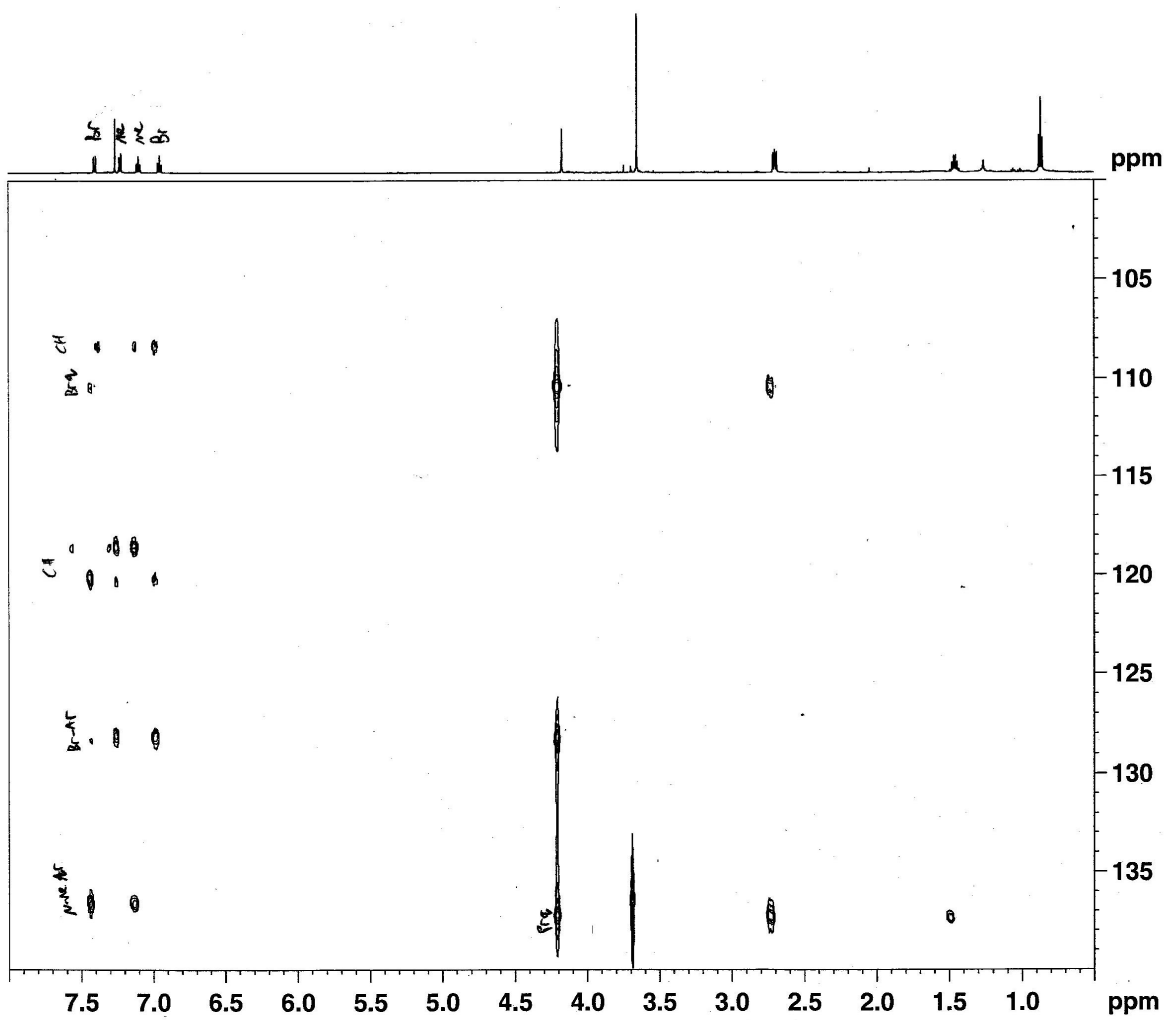
NOESY NMR (CDCl₃, 500 MHz) for 2.15



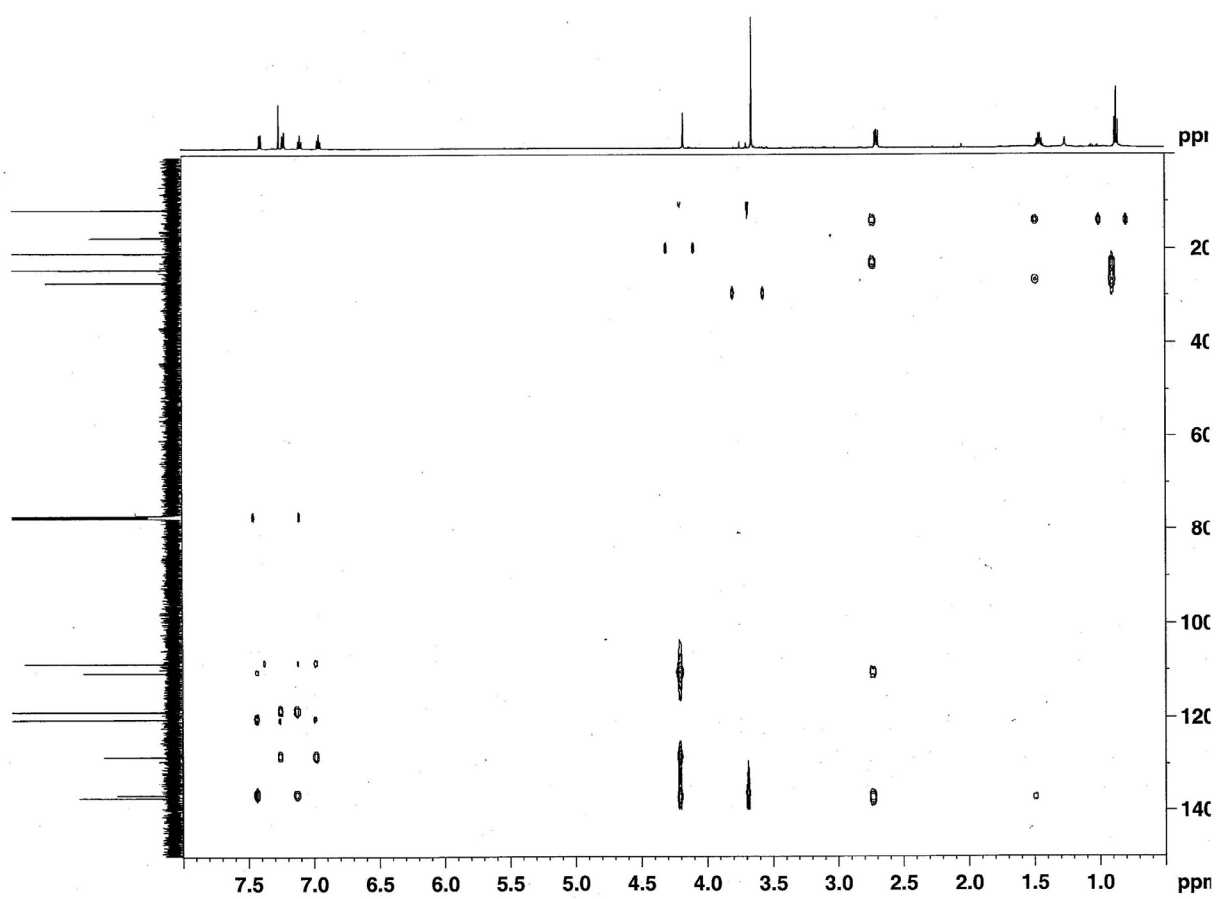
HSQC NMR (CDCl₃, 600 MHz) for **2.15**



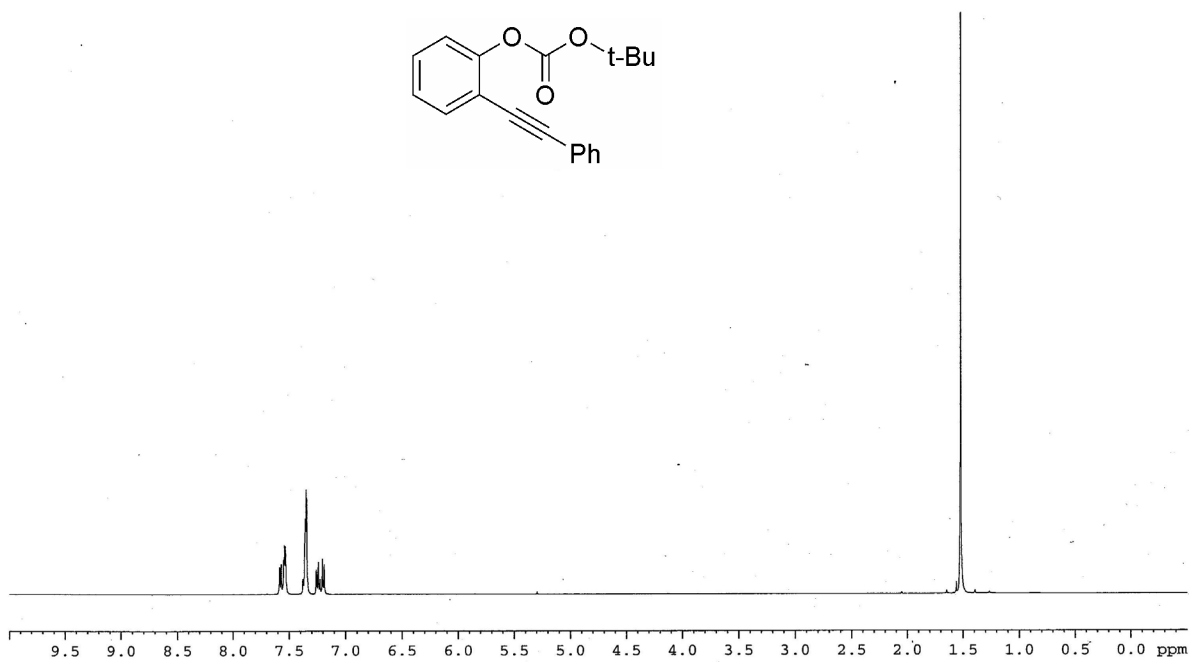
HMBC NMR (CDCl₃, 600 MHz) for 2.15



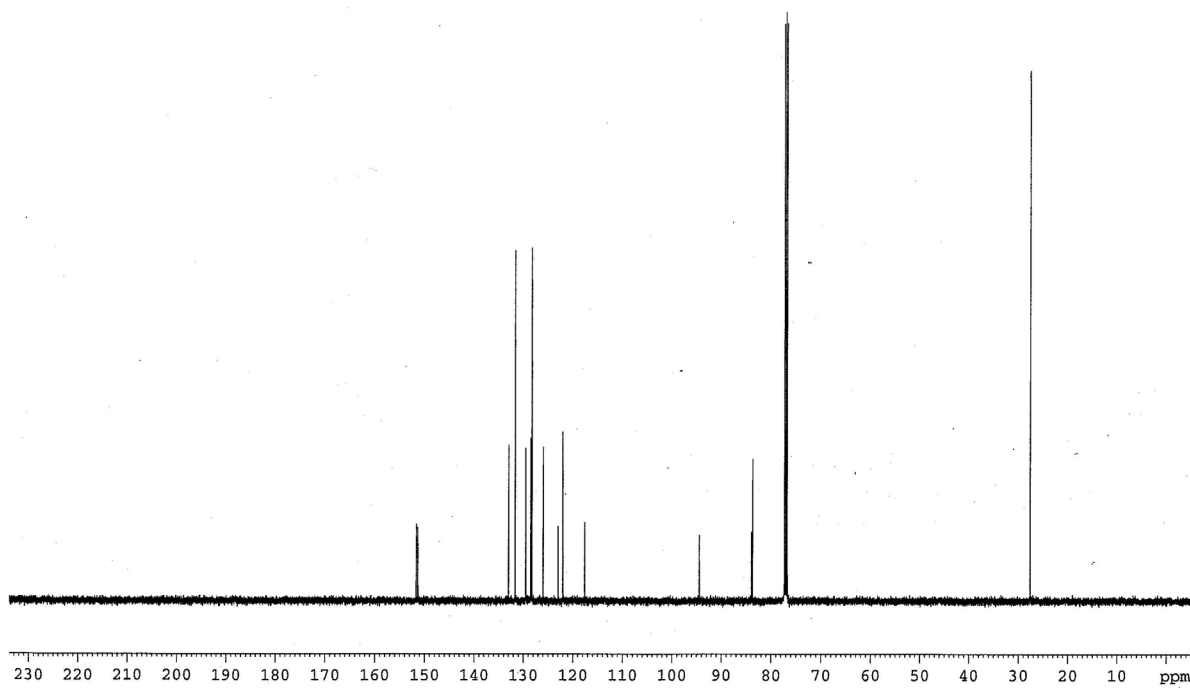
HMBC NMR (CDCl₃, 600 MHz) for 2.15



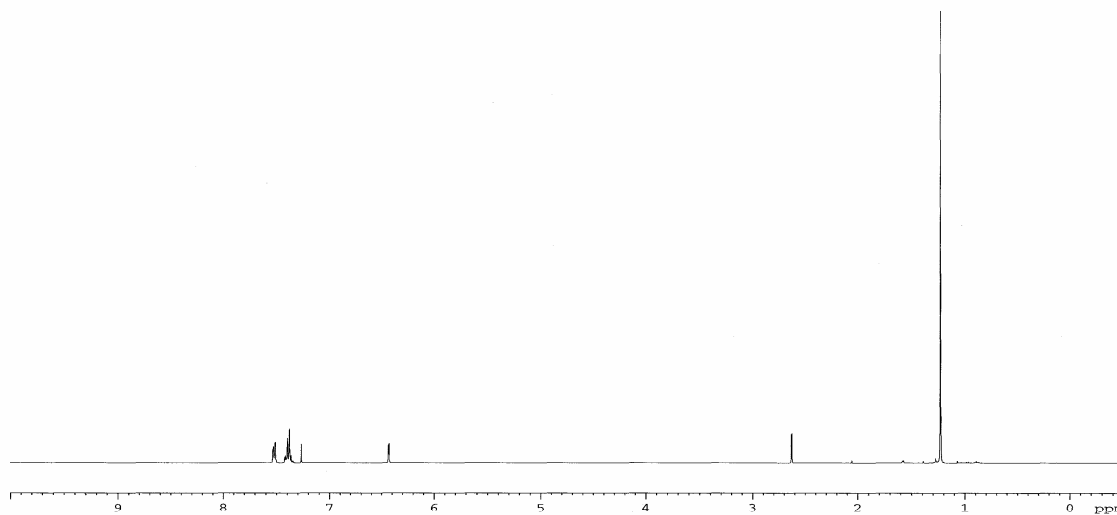
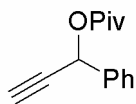
^1H NMR (CDCl_3 , 500 MHz) for **2.32**



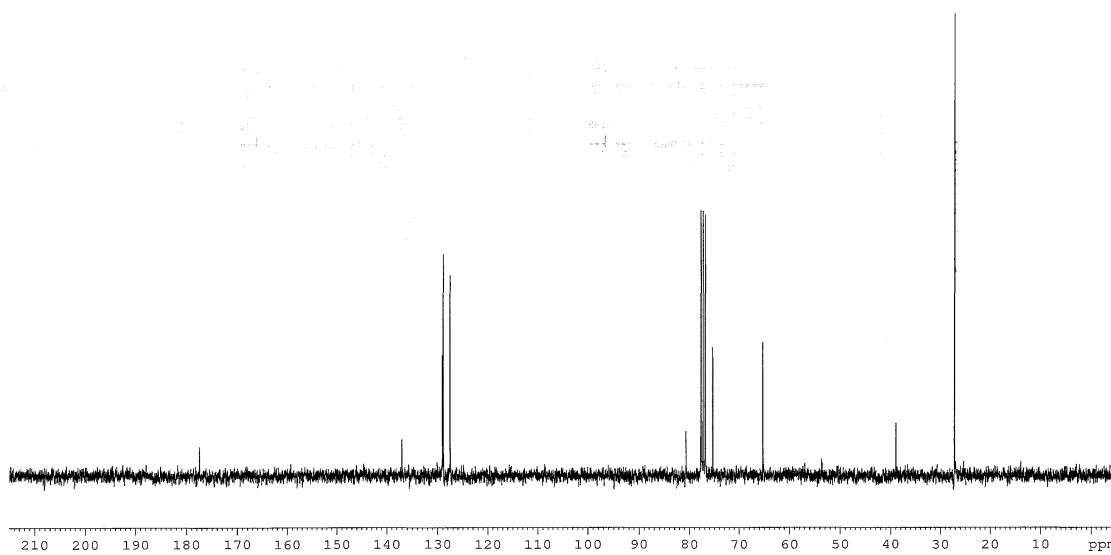
^{13}C NMR (CDCl_3 , 125 MHz) for **2.32**



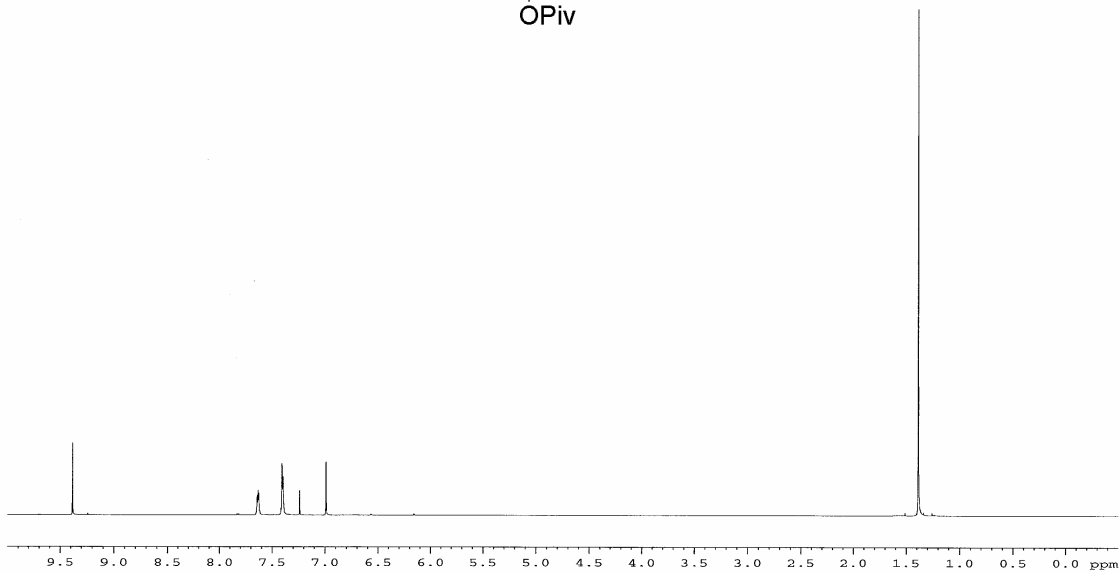
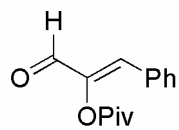
^1H NMR (CDCl_3 , 400 MHz) for **2.35**



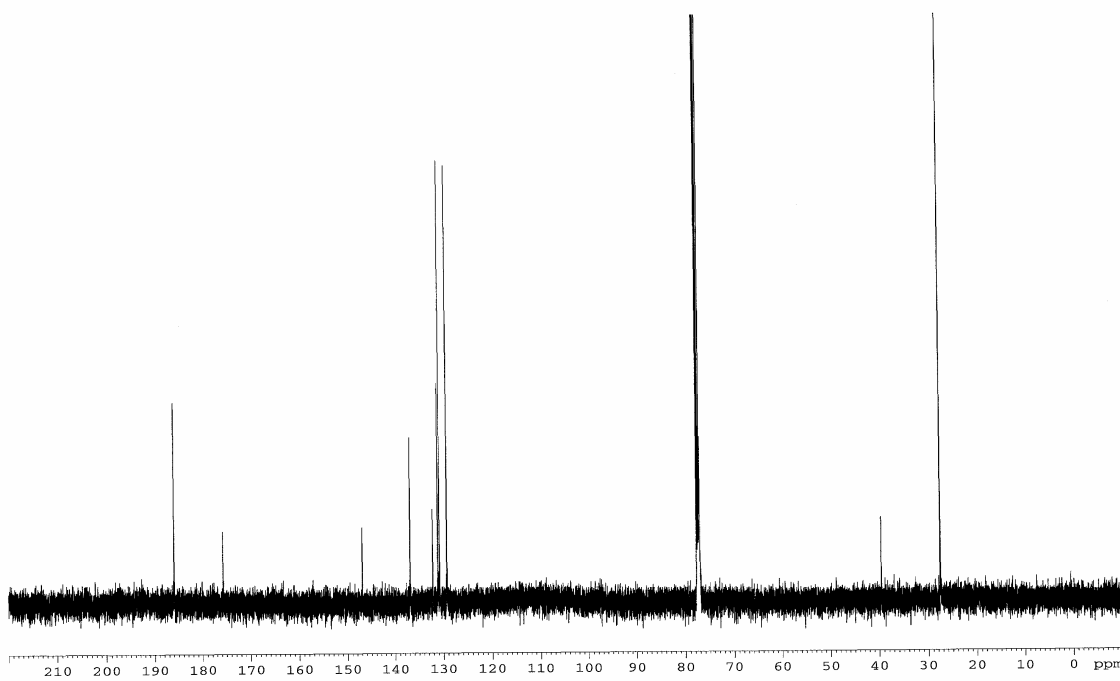
^{13}C NMR (CDCl_3 , 75 MHz) for **2.35**



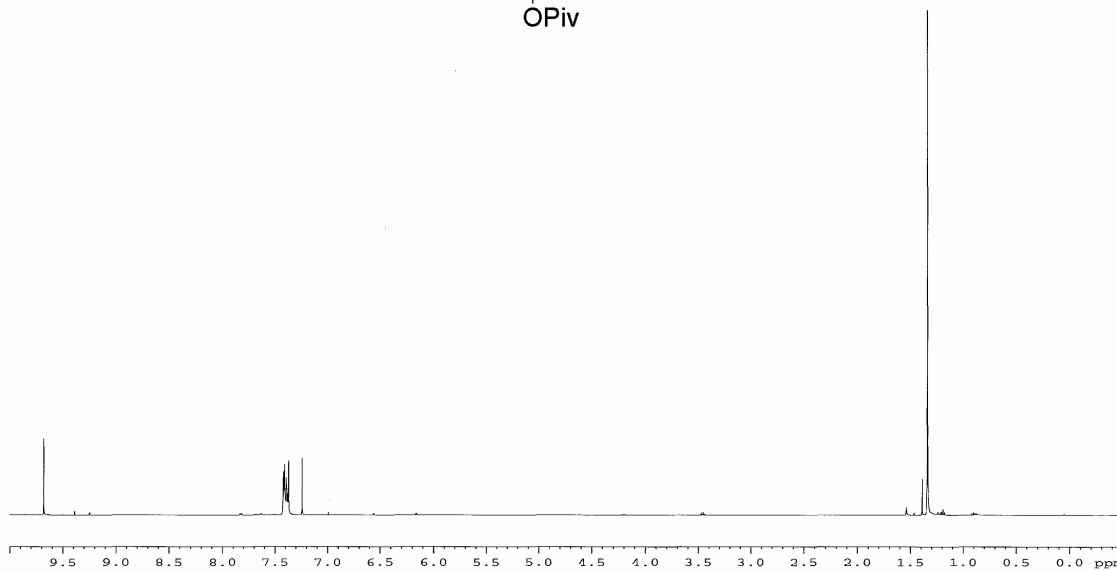
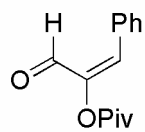
^1H NMR (CDCl_3 , 500 MHz) for **2.36-(Z)**



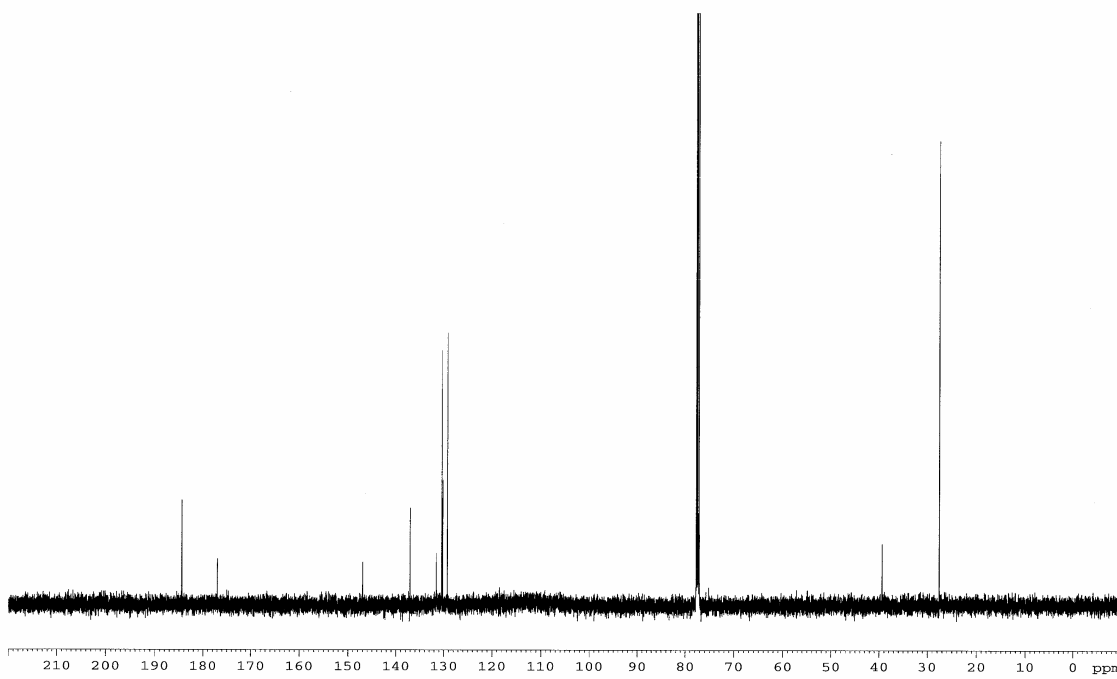
^{13}C NMR (CDCl_3 , 125 MHz) for **2.36-(Z)**



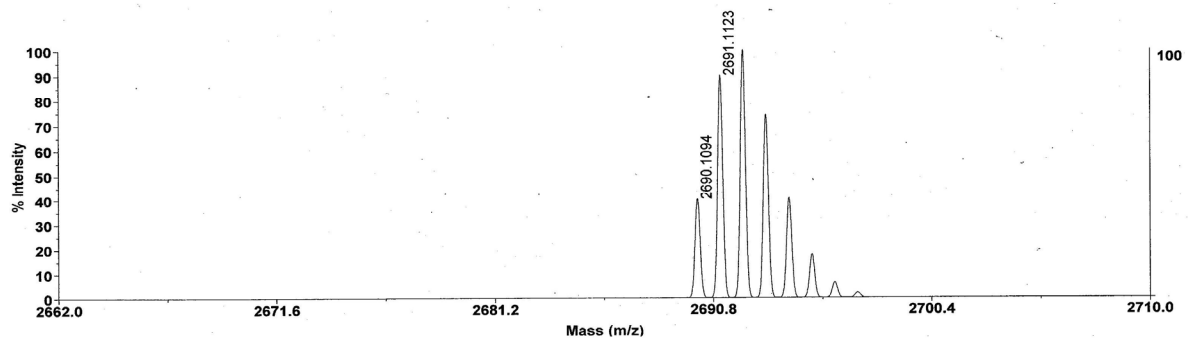
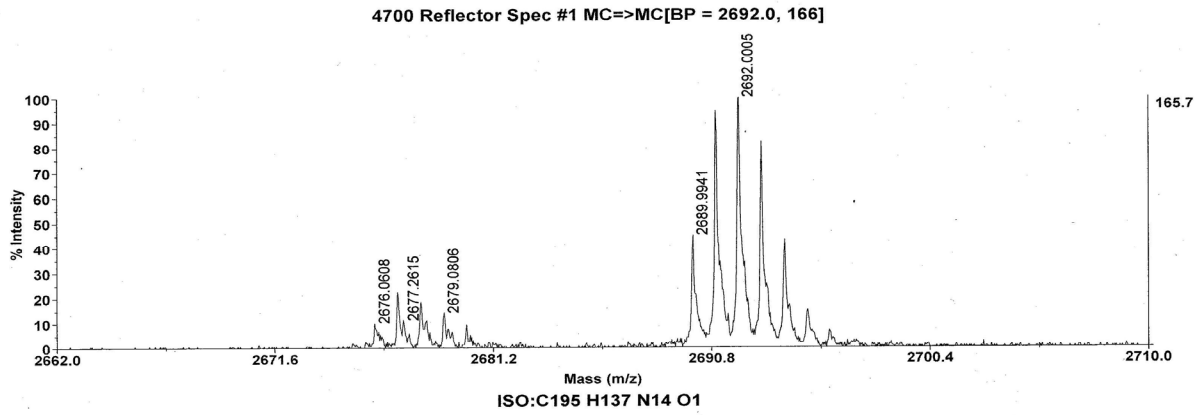
^1H NMR (CDCl_3 , 500 MHz) for **2.36-(E)**



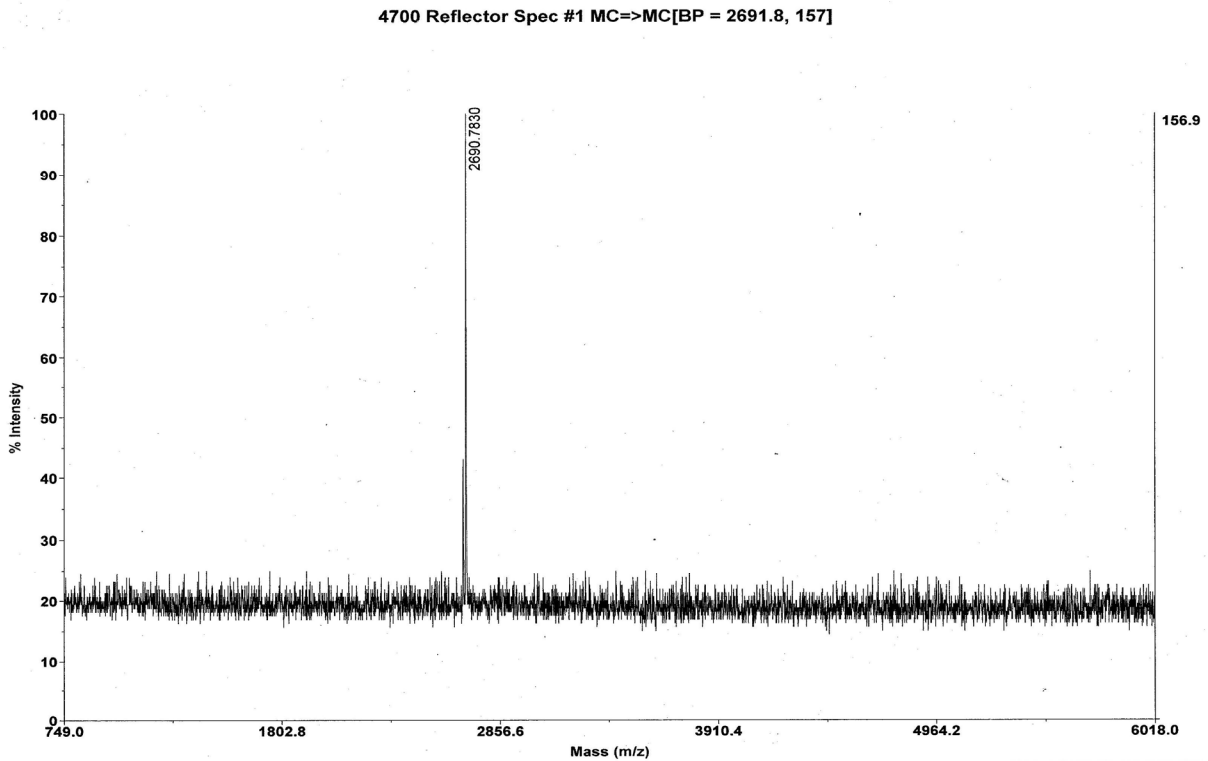
^{13}C NMR (CDCl_3 , 125 MHz) for **2.36-(E)**



High Resolution MALDI-TOF-MS for 2.57

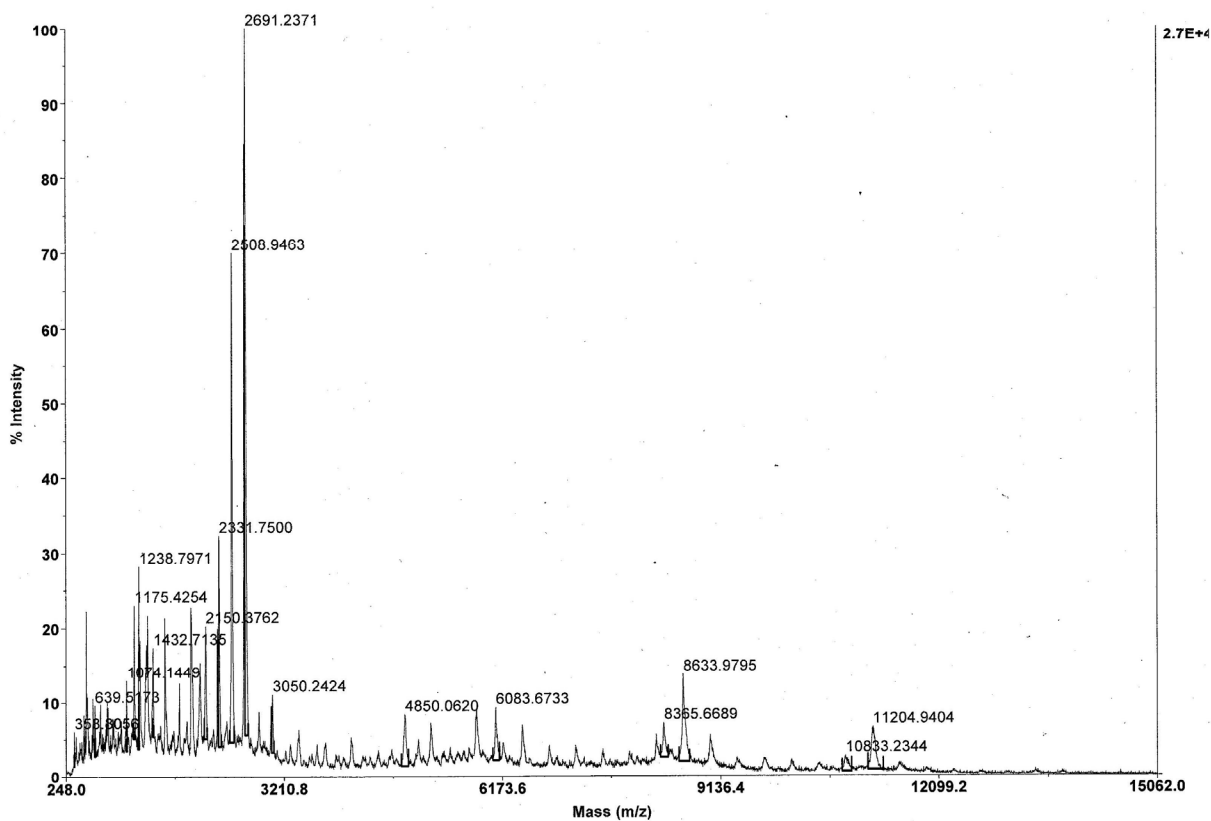


Full Spectrum MALDI-TOF-MS for 2.57



Crude Mixture MALDI-TOF-MS from 2.49 Synthesis

4700 Linear Spec #1 MC=>MC[BP = 2692.3, 27468]



XAS Data

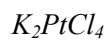
Reduced = H₂, 100°C, 24 h

Oxidized = PhICl₂, toluene, 100°C

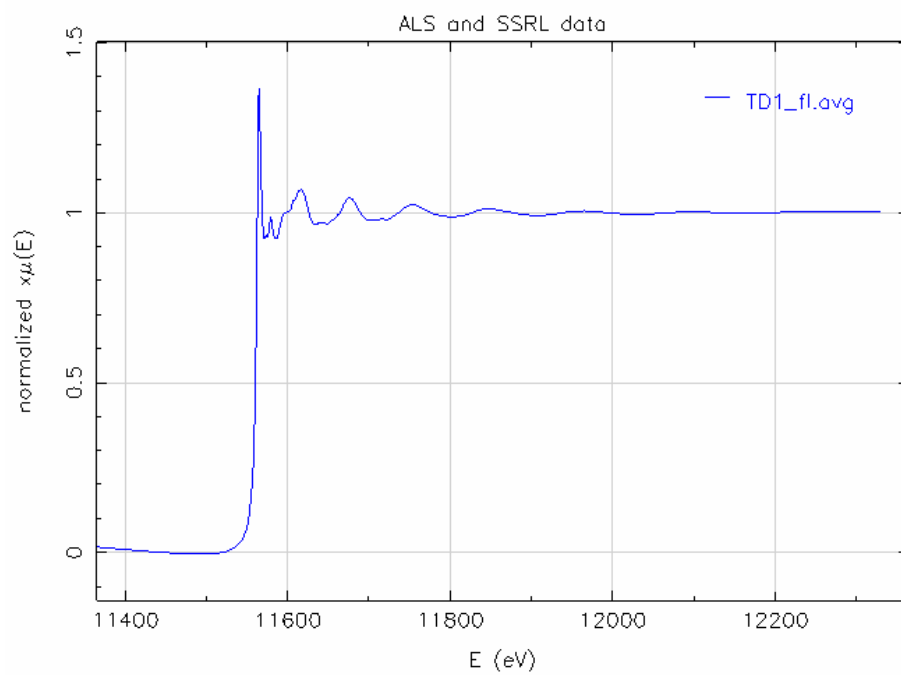
Recovered/Recycled = catalyst filtered, isolated and dried

Reaction = PhICl₂, 2.4, 100°C, toluene

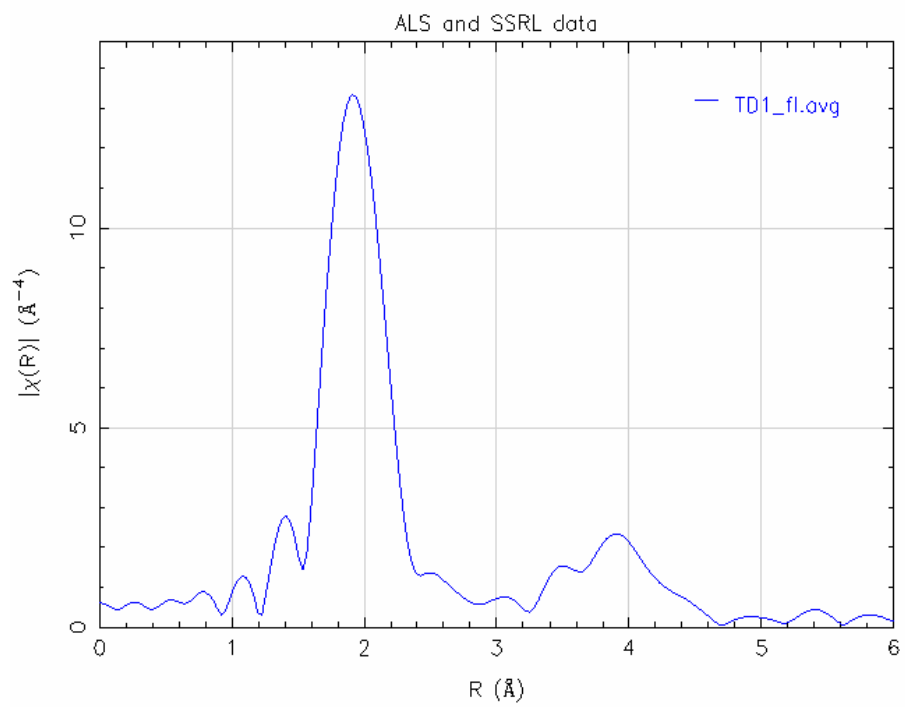
Continued on next page...



E-Space

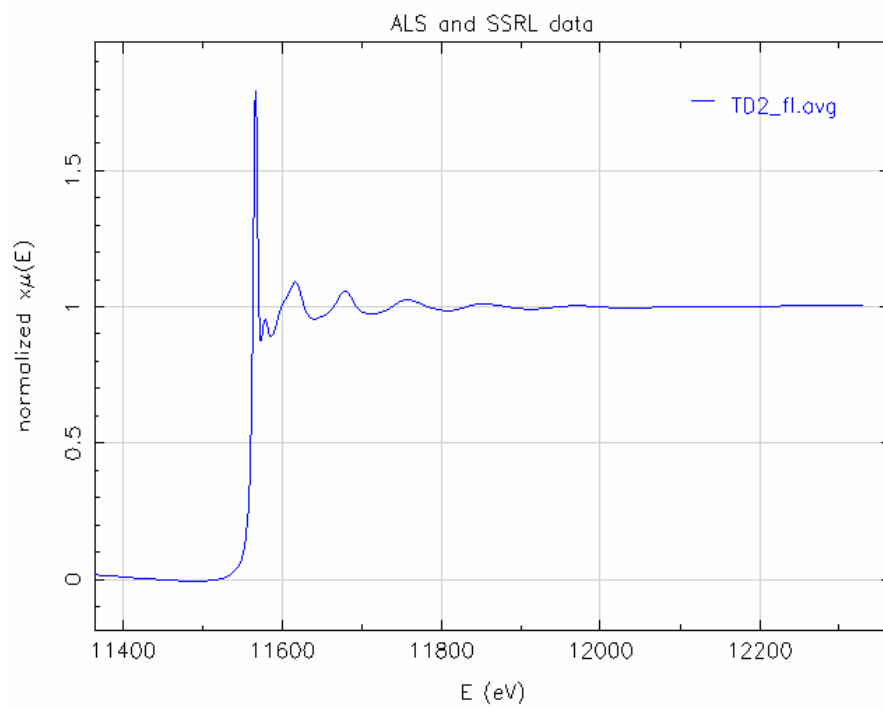


R-Space

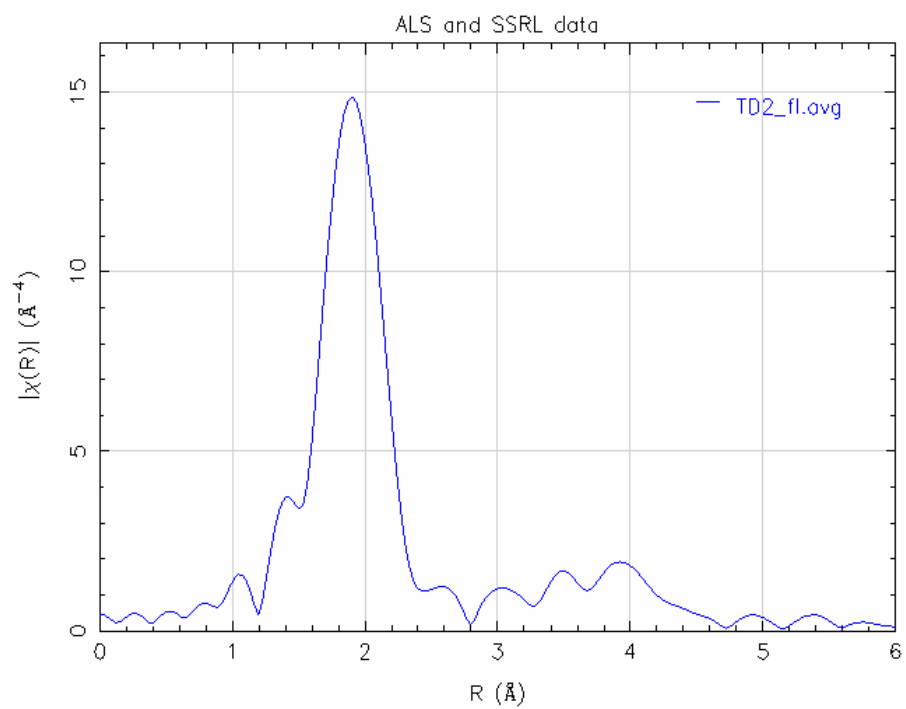




E-Space

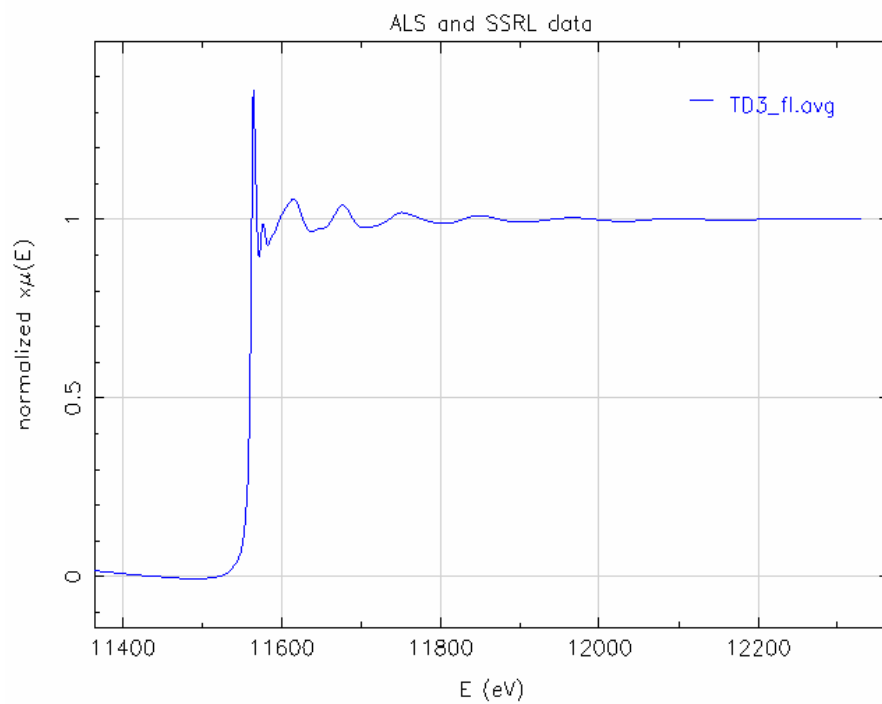


R-Space

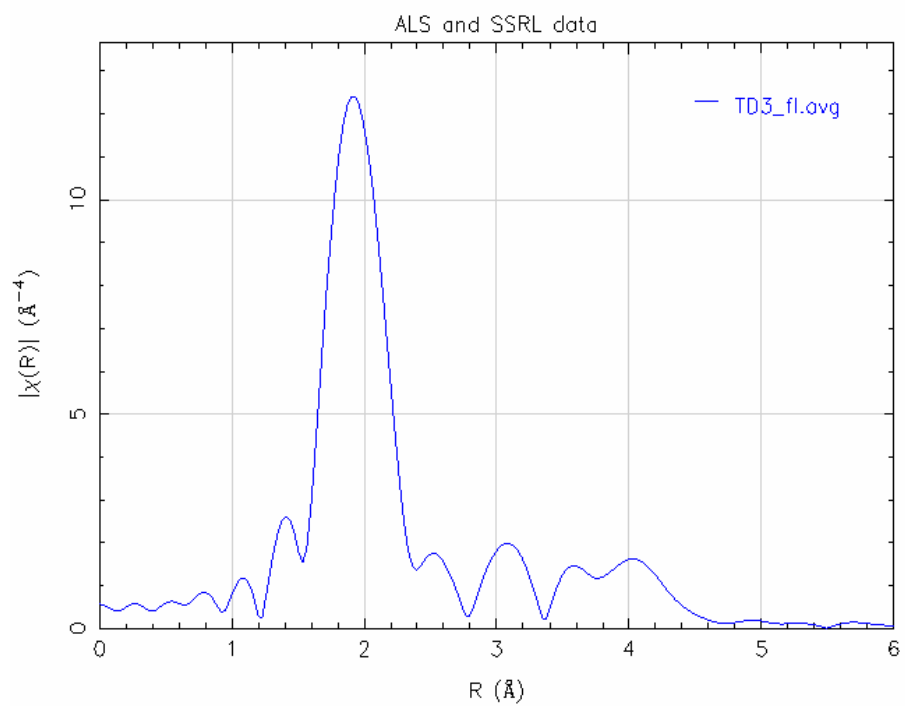


$PtCl_2$

E-Space

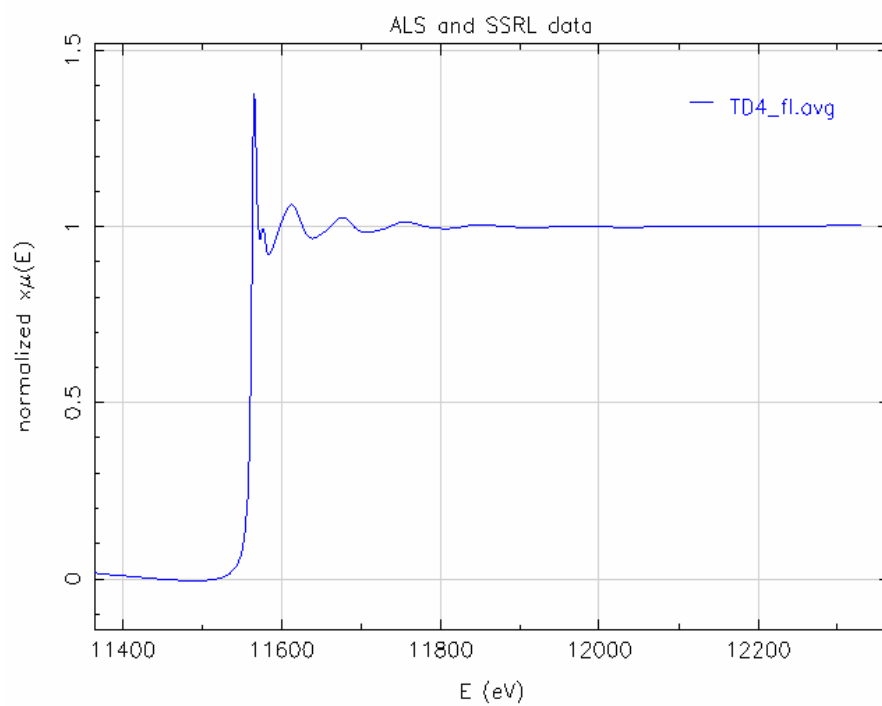


R-Space

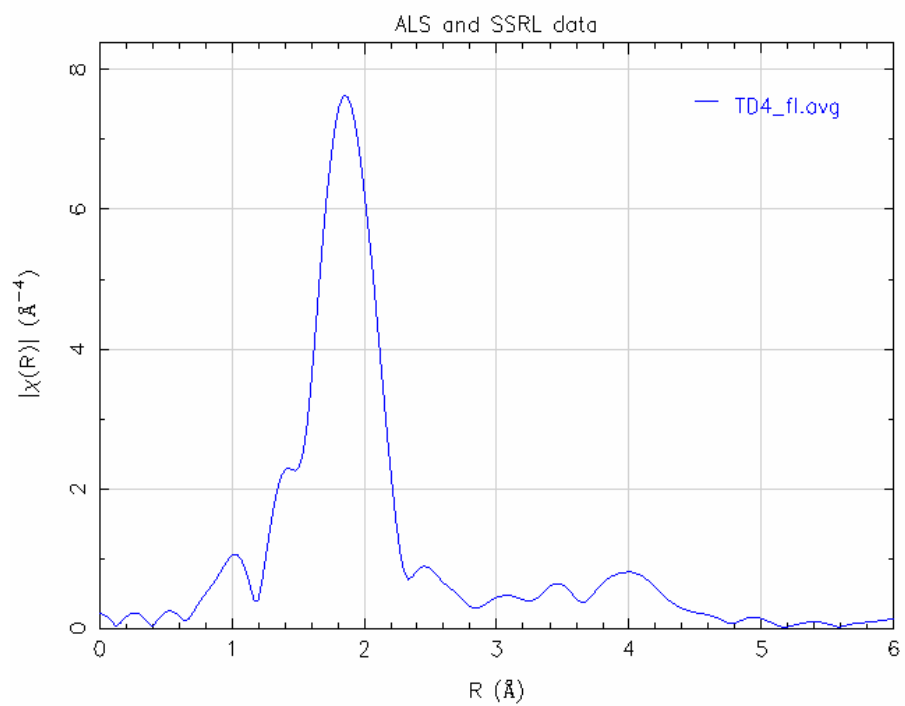


Zeise's Dimer

E-Space

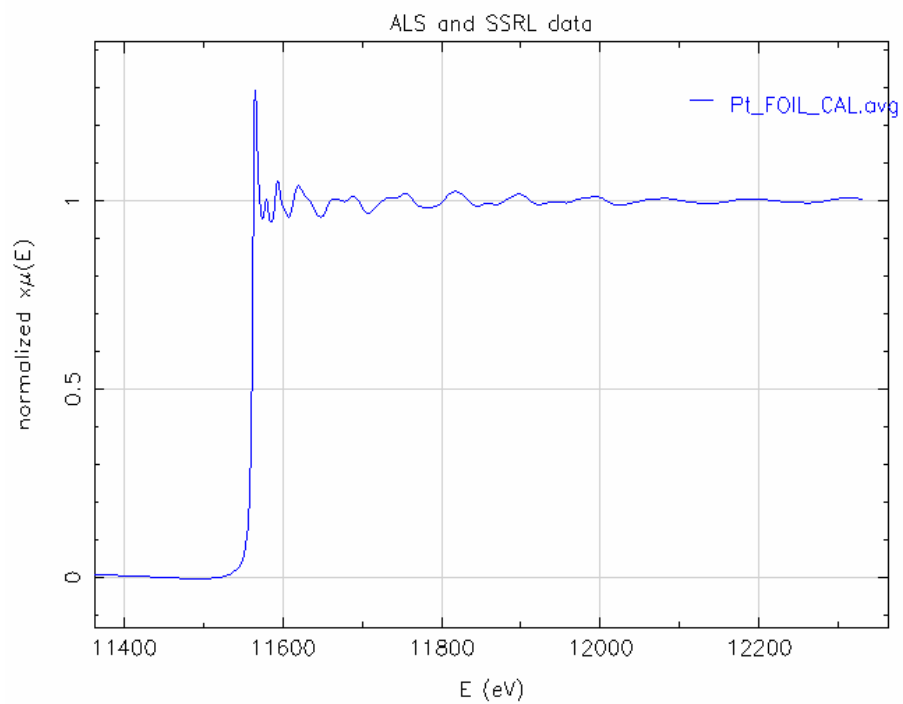


R-Space

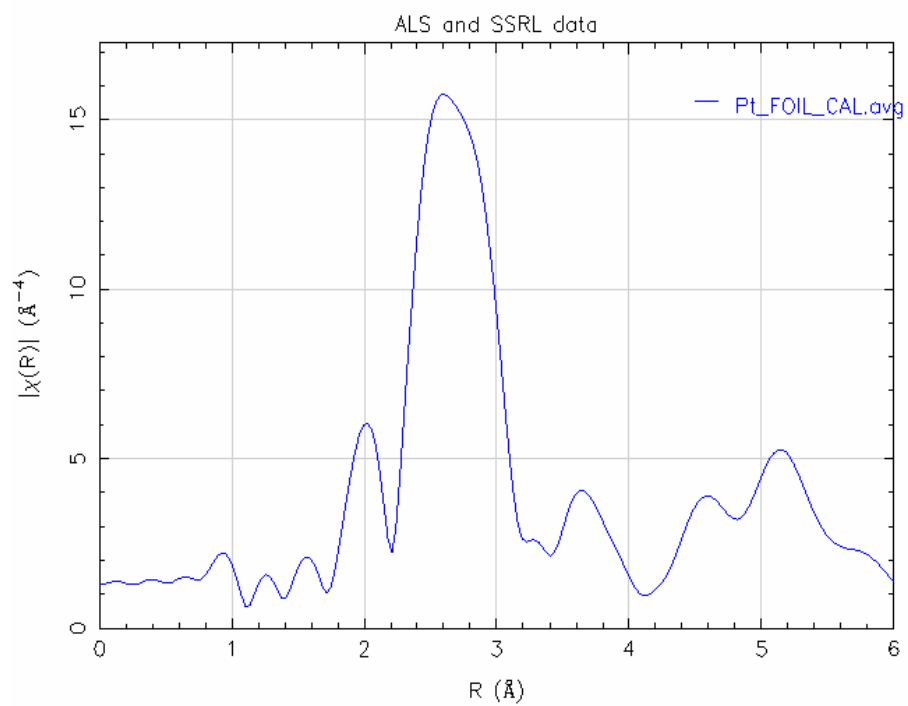


PtFoil

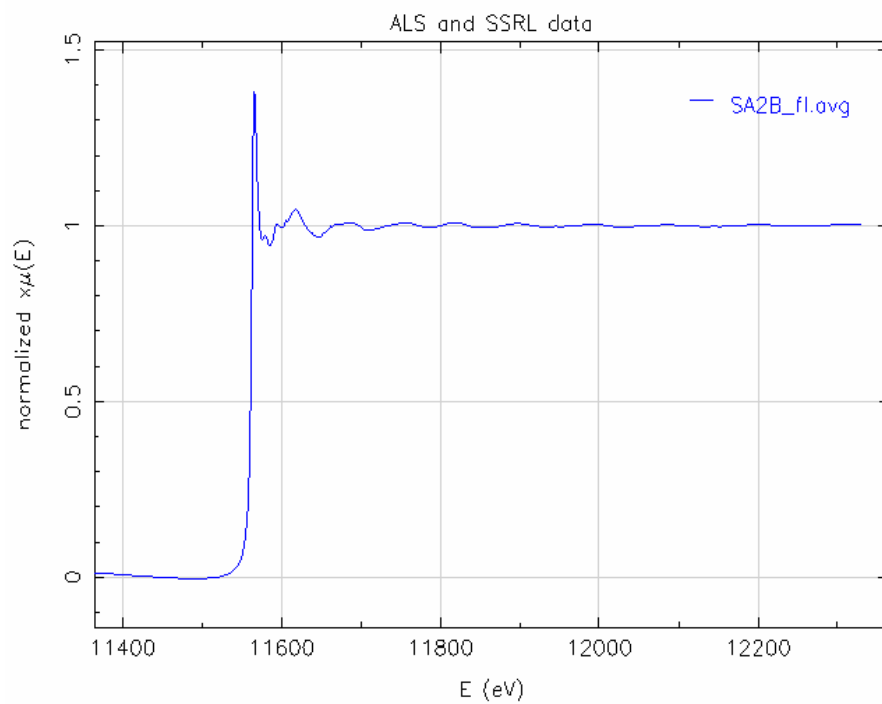
E-Space



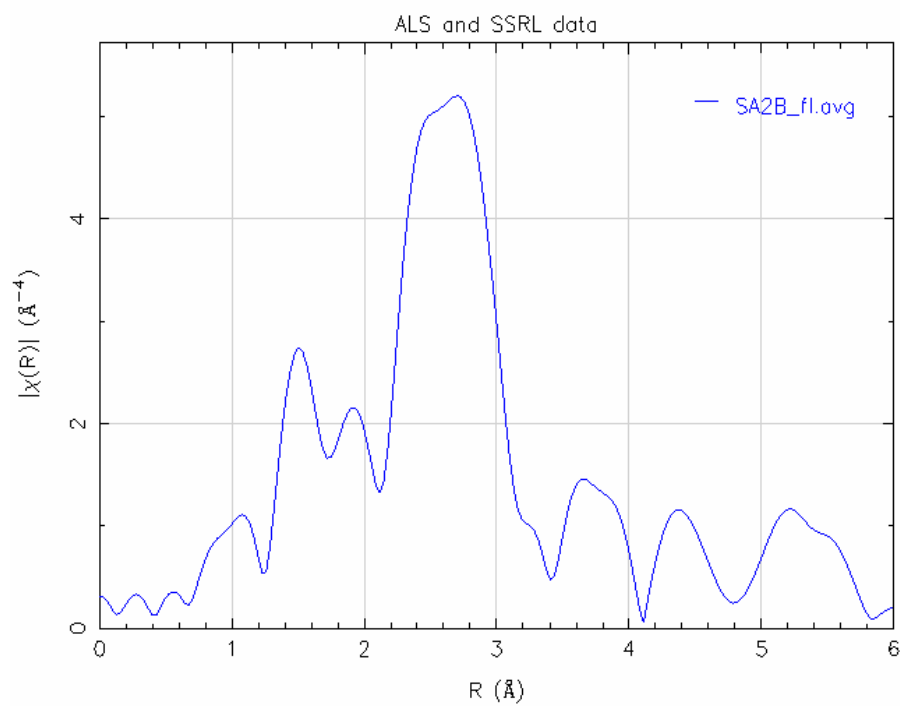
R-Space



E-Space

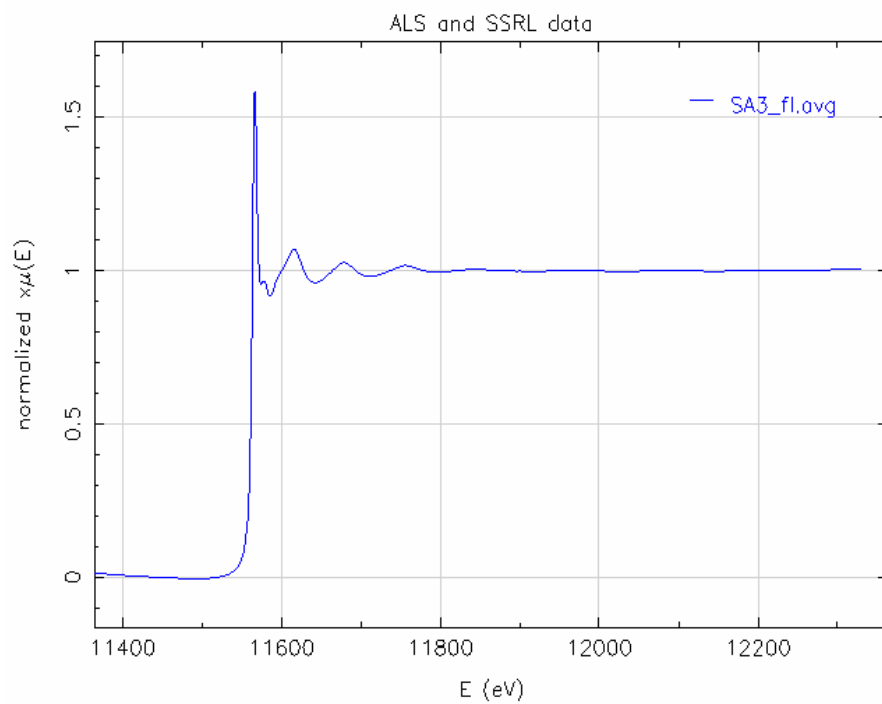


R-Space

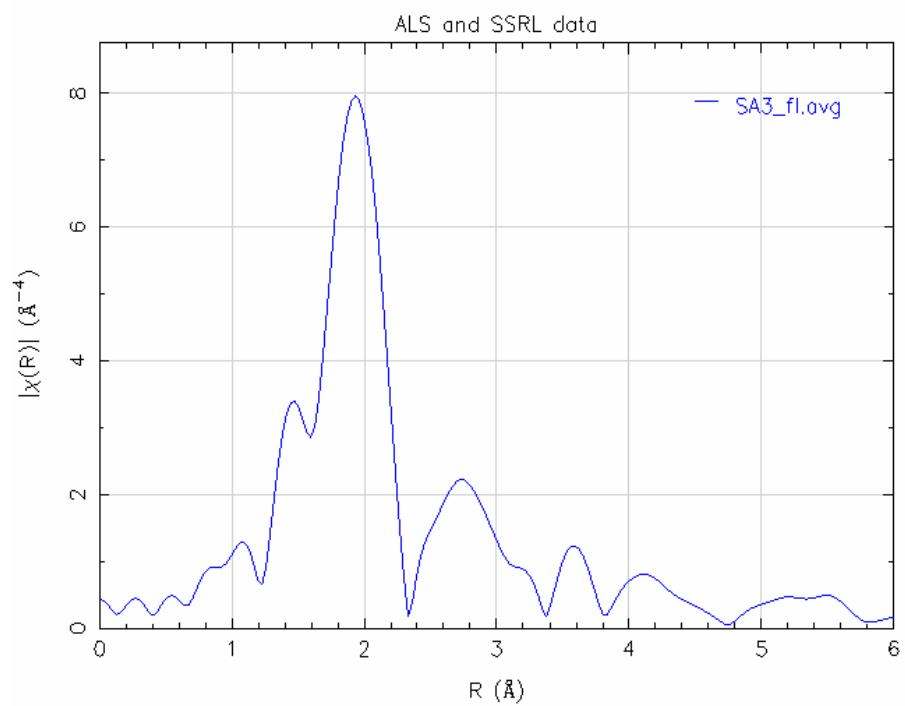


Pt₄₀/G4OH/SBA-15 – reduced then oxidized

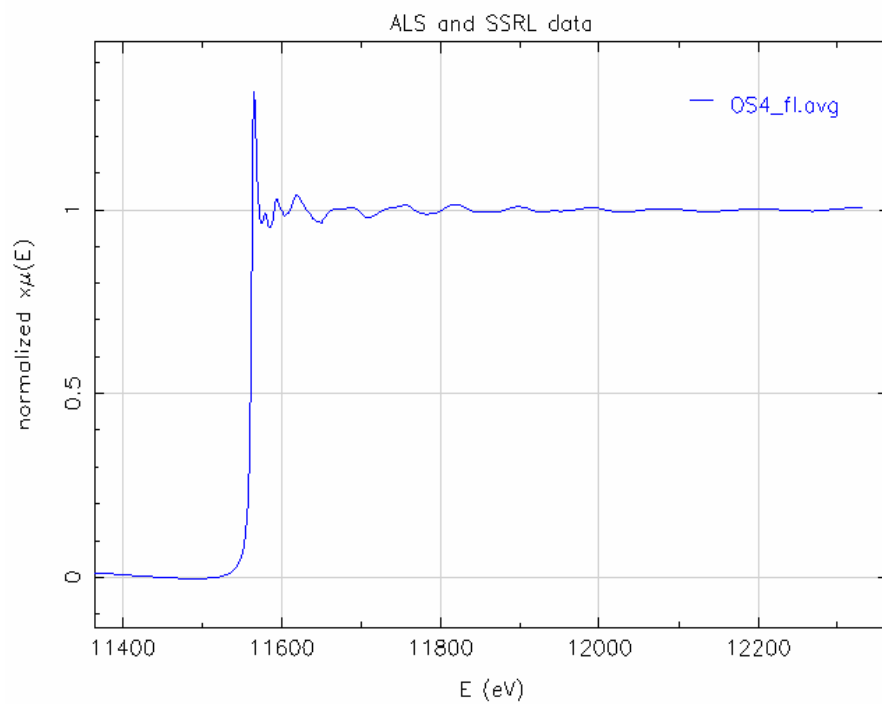
E-Space



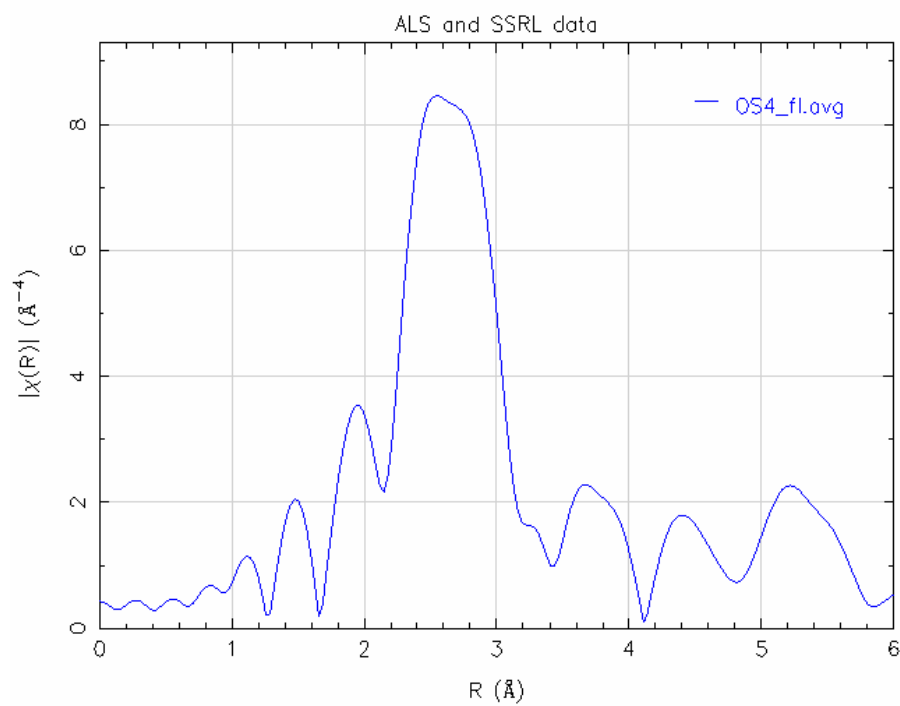
R-Space



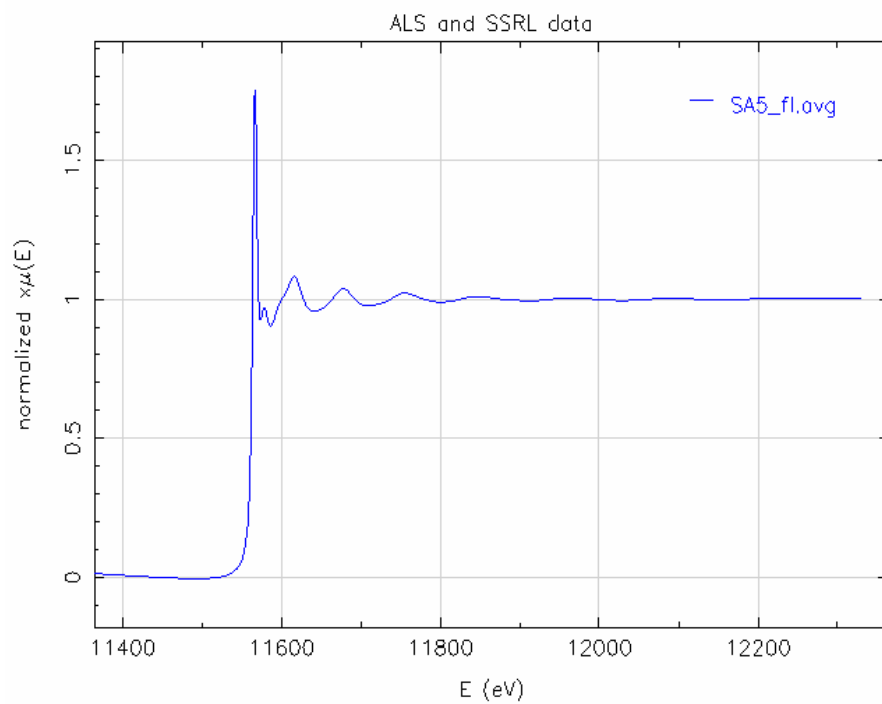
E-Space



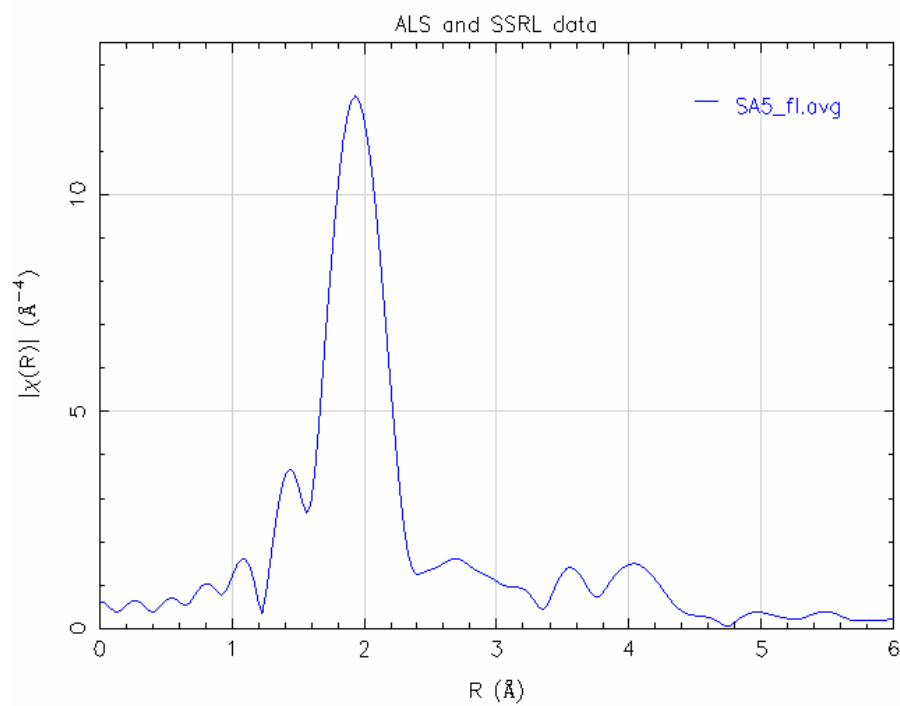
R-Space



E-Space

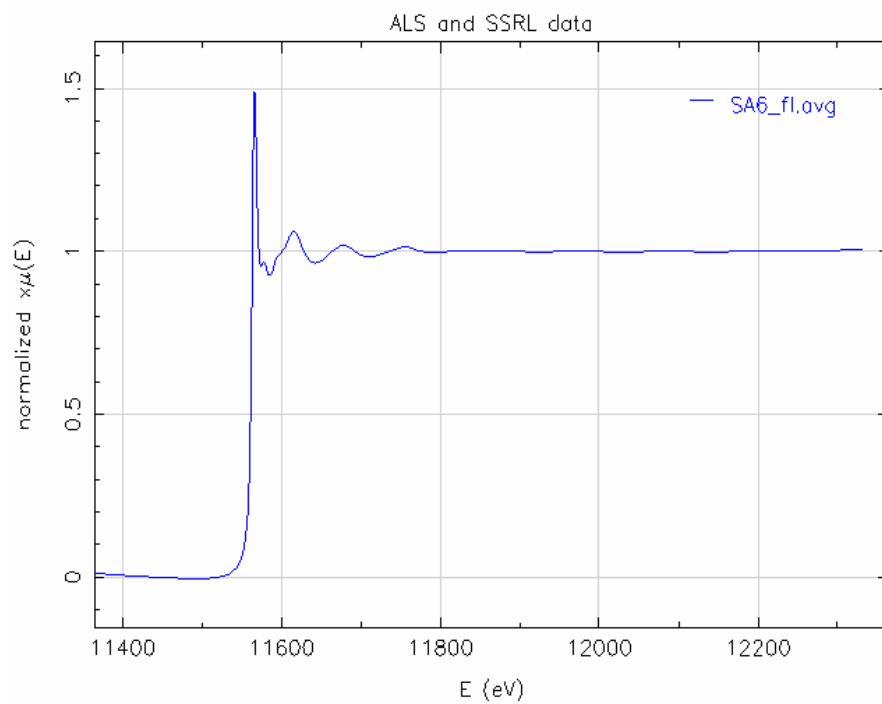


R-Space

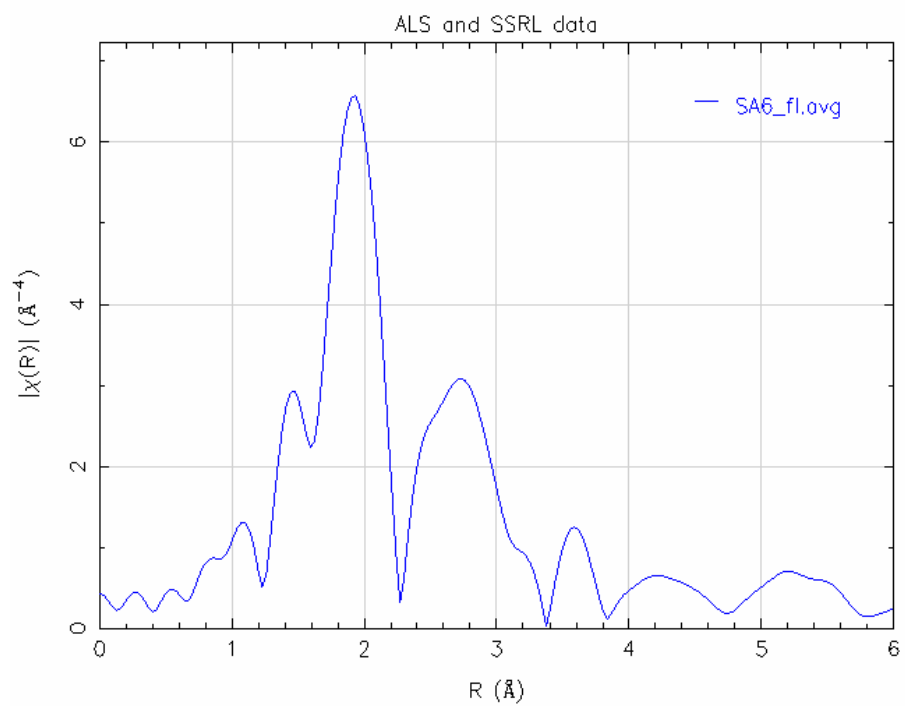


Pt₄₀/G4OH/SBA-15 – reduced then reaction

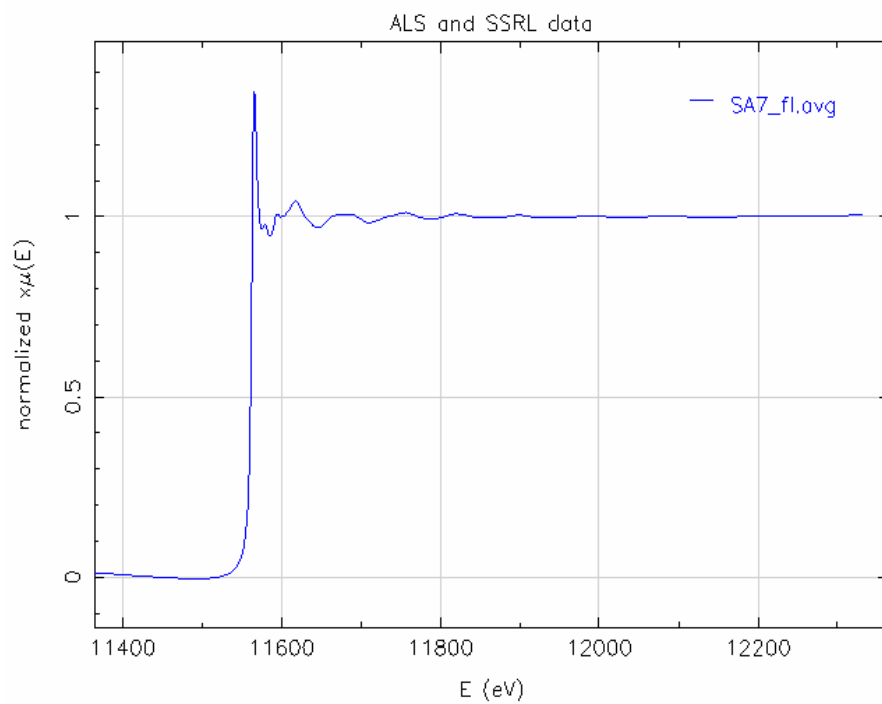
E-Space



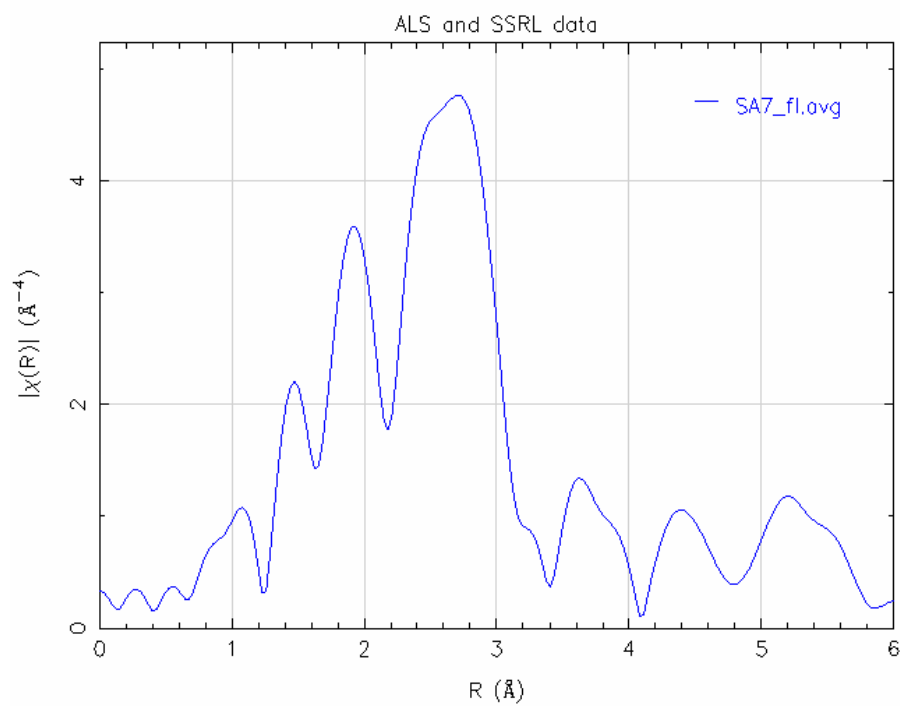
R-Space



E-Space

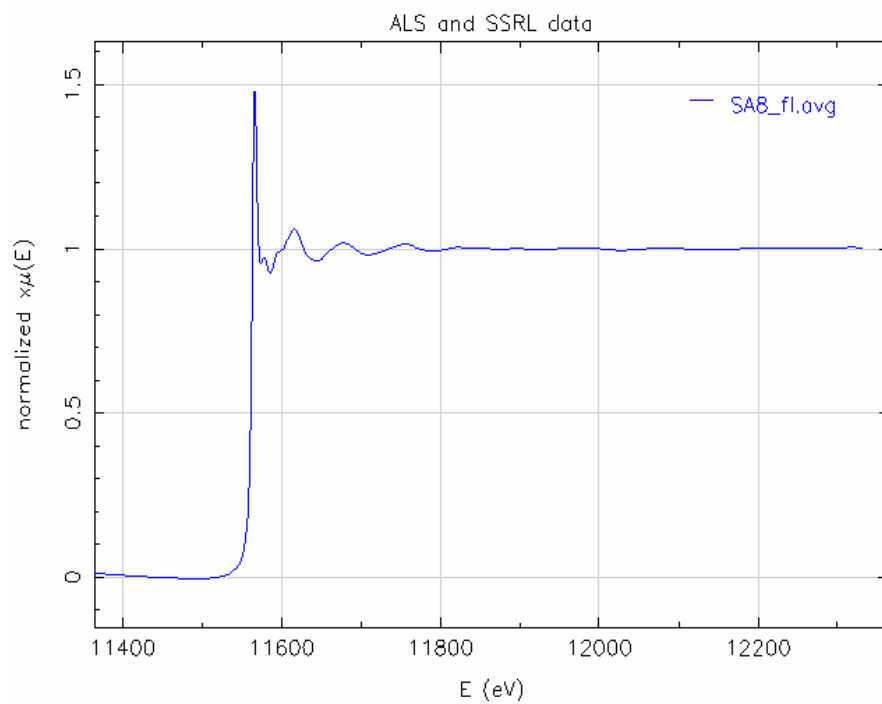


R-Space

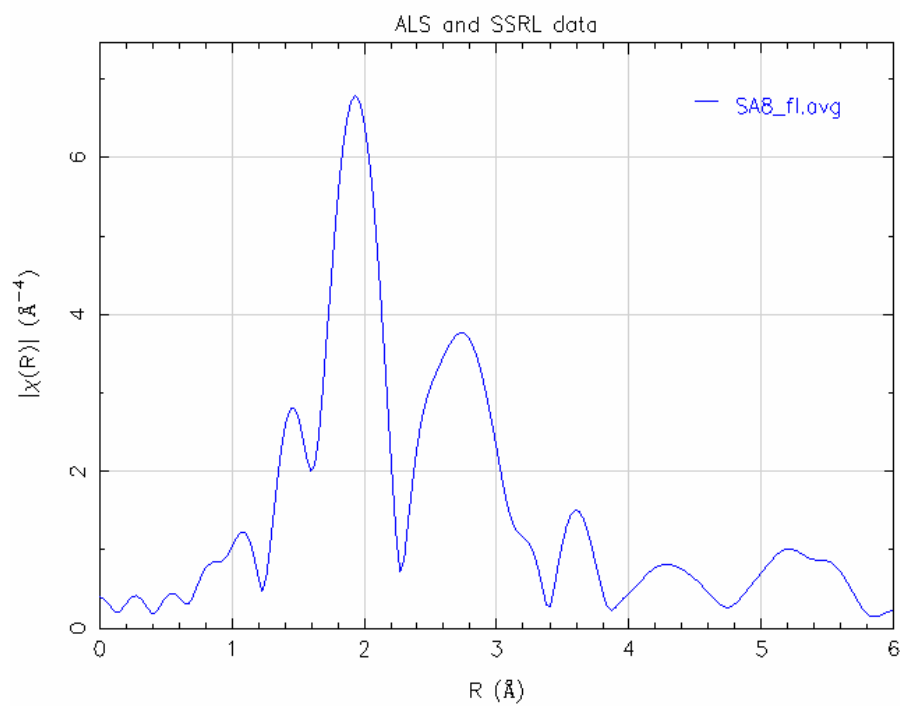


Pt₄₀/G4OH/SBA-15 – reduced, reaction, recover/recycle and re-reduce then reaction again

E-Space

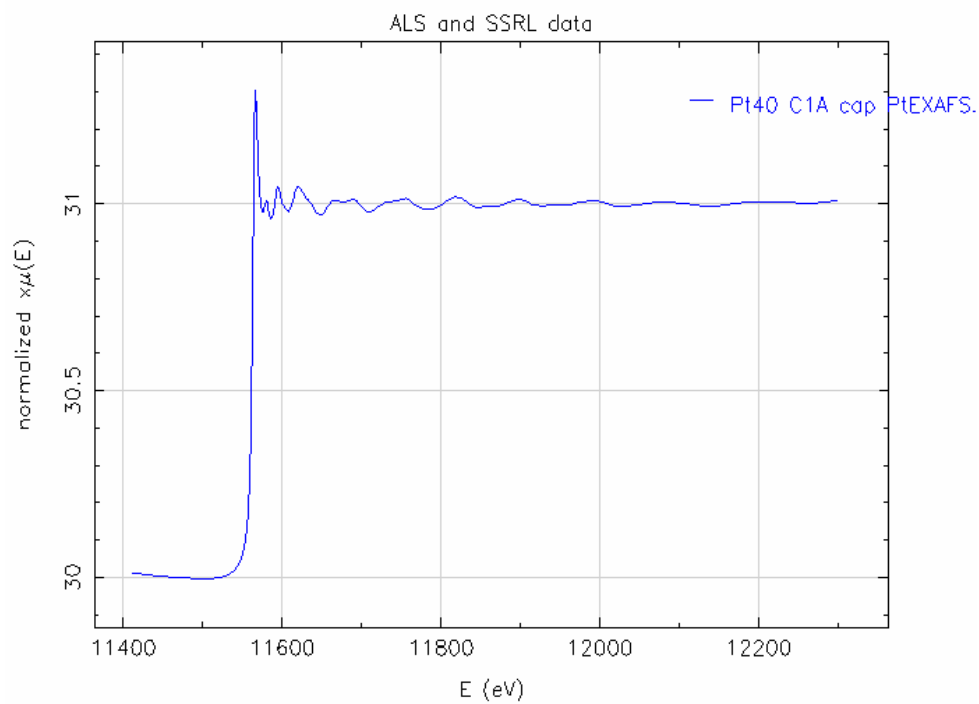


R-Space

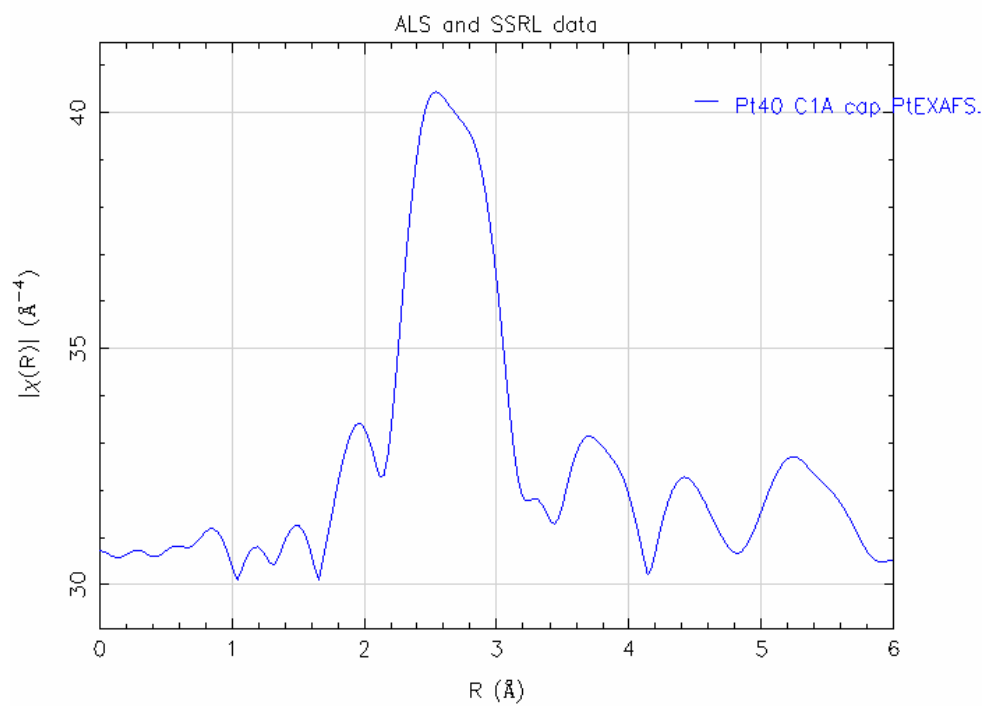


2.9 nm Pt/PVP/SBA-15 – reduced only

E-Space

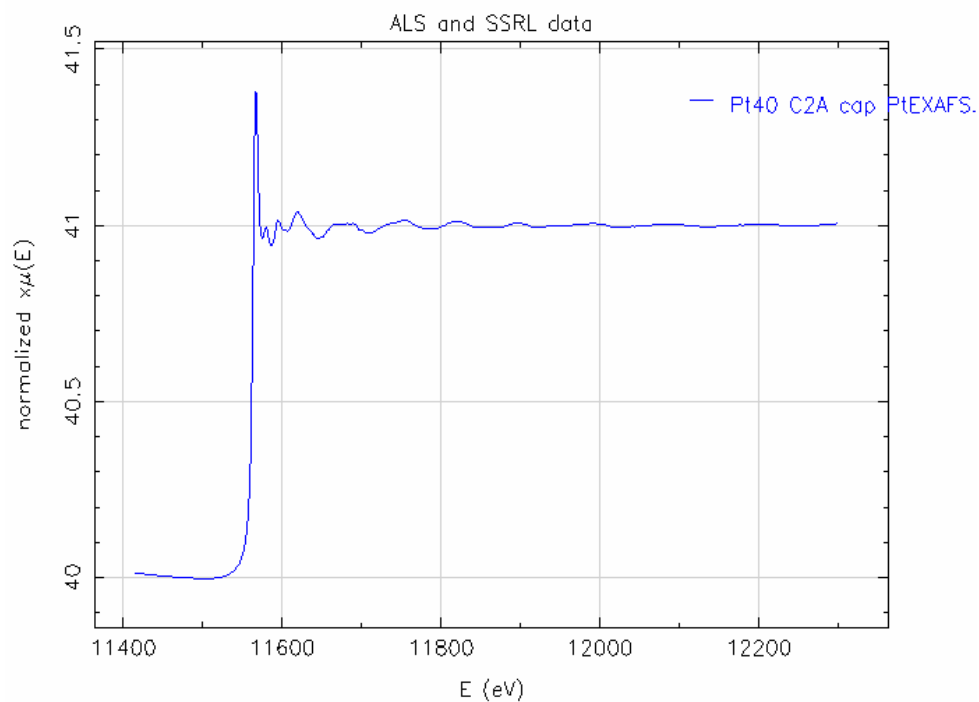


R-Space



2.9 nm Pt/PVP/SBA-15 – reduced then oxidized

E-Space



R-Space

